Luminescence-based methods for the investigation of ligand binding and GRK2 recruitment to GPCRs

Dissertation

zur Erlangung des Doktorgrades der Naturwissenschaften (Dr. rer. nat.)
an der Fakultät für Chemie und Pharmazie
der Universität Regensburg

vorgelegt von

Lukas Grätz

aus Arnstorf

im Jahr 2021

Die vorliegende Arbeit entstand im Zeitraum von Dezember 2016 bis Januar 2021 unter der Anleitung von Prof. Dr. Armin Buschauer, Prof. Dr. Günther Bernhardt und PD Dr. Max Keller an der Fakultät für Chemie und Pharmazie der Universität Regensburg.

Das Promotionsgesuch wurde eingereicht im Januar 2021.

Tag der mündlichen Prüfung: 16. März 2021

Vorsitzender des Prüfungsausschusses:	Prof. Dr. Sigurd Elz
Erstgutachter:	PD Dr. Max Keller
Zweitgutachter:	Prof. Dr. Joachim Wegener
Drittprüfer:	Prof. Dr. Pierre Koch

Acknowledgments

An dieser Stelle möchte ich allen Personen Danke sagen, die zum Entstehen dieser Arbeit beigetragen haben und die mich über die Jahre der Promotion begleitet haben. Insbesondere möchte ich mich bedanken bei:

Herrn Prof. Dr. Armin Buschauer für die Aufnahme in seinen Arbeitskreis und die Vergabe dieses enorm interessanten und herausfordernden Themas. Leider konnte er nur noch die ersten Resultate dieser Arbeit sehen;

Herrn Prof. Dr. Günther Bernhardt für seine Betreuung, seine Korrekturen über die letzten Jahre und seine zahlreichen wissenschaftlichen Ratschläge;

Herrn PD Dr. Max Keller für die Bereitschaft, meine Betreuung mit zu übernehmen, auch wenn die Arbeit nicht direkt in sein Themengebiet fällt, für seine stete Hilfe, unabhängig davon, wie viel er zu tun hatte, für die Durchsicht dieser Arbeit und für das Erstellen des Erstgutachtens;

Herrn Prof. Dr. Joachim Wegener für die Bereitschaft, das Zweitgutachten dieser Arbeit zu erstellen;

Herrn Prof. Dr. Pierre Koch für die Teilnahme an der Promotionsprüfung als Drittprüfer;

Herrn Prof. Dr. Sigurd Elz für die Unterstützung der Finanzierung meiner Promotion und für die Übernahme des Vorsitzes der Promotionsprüfung;

Herrn Dr. Timo Littmann, dafür, dass er sich mit einer enormen Geduld und Ruhe immer die Zeit genommen hat, mich in sämtliche biochemischen/molekularbiologischen Methoden einzuarbeiten, ehrlich mit mir über meine Ergebnisse und Ideen zu diskutieren und alle meine fachlichen Fragen zu beantworten, egal, wie banal sie auch waren. Zusätzlich möchte ich ihm für seine Hilfe bei dem Projekt aus Kapitel 4 danken;

Herrn Dr. Steffen Pockes für seine vielseitige Unterstützung über die Jahre meiner Promotion, für die gute und unterhaltsame Zusammenarbeit in verschiedenen Projekten und für sein stetes Interesse am Fortschritt meiner Arbeit;

Herrn Prof. Dr. Ago Rinken für die Möglichkeit, meinen Auslandsaufenthalt in seiner Arbeitsgruppe an der Universität Tartu zu absolvieren. In diesem Zusammenhang möchte ich mich auch bei Herrn Tõnis Laasfeld für die Einarbeitung und Beantwortung sämtlicher Fragen zum Prinzip der Fluoreszenzanisotropie bedanken;

allen Co-Autoren für die angenehme und produktive Zusammenarbeit. Insbesondere bedanke ich mich bei Frau Katharina Tropmann, Frau Dr. Sabrina Biselli, Frau Dr. Edith Bartole, Herrn Dr. Andrea Pegoli, Frau Corinna Gruber, Herrn PD Dr. Max Keller, Herrn Christoph Müller und Herrn Dr. Jonas Buschmann, ohne deren Fluoreszenzliganden diese Arbeit von vornherein nicht entstehen hätte können;

Frau Maria Beer-Krön, Frau Brigitte Wenzl, Frau Susanne Bollwein, Frau Elvira Schreiber und Frau Lydia Schneider für die hervorragende Unterstützung bei verschiedenen Experimenten und für die Organisation des Laboralltags;

Herrn Peter Richthammer für seine alltägliche gute Laune und seine Hilfe bei technischen Problemen;

Frau Dr. Laura Humphrys for proofreading Chapter 3 and improving my English skills (hopefully :D);

meinen Pharmazie-Wahlpflichtpraktikanten Frau Lea Schödel und Herrn Petar Rusev für ihre Unterstützung bei einigen Experimenten aus Kapitel 5;

der Deutschen Forschungsgemeinschaft für die finanzielle Unterstützung während meiner Promotion im Rahmen des Graduiertenkollegs GRK1910 „Medicinal Chemistry of Selective GPCR Ligands“. In diesem Zusammenhang geht auch ein Dankeschön an alle Mitglieder des GRK1910 für die interessanten Workshops und Retreats;

Frau Lisa Schindler für den gemeinsamen frühmorgendlichen Arbeitsbeginn und die Mittagspausen :D. Ganz besonders möchte ich mich aber dafür bedanken, dass du immer für einen da bist. Danke, dass ich mit dir über alle möglichen Themen reden kann und du mir immer wieder durch „Rat und Tat“ hilfst ;) ;

Frau Carina Höring für die schöne gemeinsame Zeit im Büro (und für das Mithochnehmen des Morgenkaffees xD) und für die vielzähligen (fachlichen) Gespräche. Danke, dass du es (häufig :D) geschafft hast, meine Stimmung zu heben, wenn es mal schlechter lief;

Frau Ulla Seibel für die schöne Zeit, die vielen Unterhaltungen und das Ausrichten mehrerer lustiger Silvesterabende. Danke auch dafür, dass du mich zu meinem ersten Halbmarathon „überredet“ und mich des Öfteren zum kombinierten „Kondi“ und Zirkeltraining mitgeschleift hast, selbst wenn die/meine Motivation mal nicht so hoch war :D;

meinen ersten Laborkollegen Herrn Christoph Müller und Herrn Dr. Jonas Buschmann für ihre große Hilfe bei allen anfänglichen Problemen, wodurch sie mir den Einstieg in die Promotion enorm erleichtert haben. Vielen Dank, Jonas, auch für die Unterstützung bei meiner einzigen (und dann auch noch erfolgreichen) Synthese :D;

allen ehemaligen und aktuellen Mitgliedern des LS Buschauer und „AK Pockes“ für die angenehme Arbeitsatmosphäre und die lustige Zeit. So manche (abendliche) Unternehmung und Aktion der letzten Jahre wird mir sicher noch lange im Gedächtnis bleiben :D.

Zu guter Letzt, aber ganz besonders möchte ich meiner Familie danken, die mich auf meinem bisherigen Weg immer begleitet, mich bei Allem unterstützt und mir Rückhalt gegeben hat: meinen Eltern Thomas und Corinna, und meiner Schwester Lena. Ohne sie wäre diese Arbeit nicht möglich gewesen.

Publications, presentations and professional training

Publications (peer-reviewed articles)

(published prior to the submission of this thesis)

Grätz, L., Laasfeld, T., Allikalt, A., Gruber, C. G., Pegoli, A., Tahk, M.-J., Tsernant M.-L., Keller, M. & Rinken, A. BRET- and fluorescence anisotropy-based assays for real-time monitoring of ligand binding to M_2 muscarinic acetylcholine receptors. *Biochim. Biophys. Acta Mol. Cell Res.* **1868**, 118930, doi:10.1016/j.bbamcr.2020.118930 (2021).

Grätz, L., Tropmann, K., Bresinsky, M., Müller, C., Bernhardt, G. & Pockes, S. NanoBRET binding assay for histamine H_2 receptor ligands using live recombinant HEK293T cells. *Sci. Rep.* **10**, 13288, doi:10.1038/s41598-020-70332-3 (2020).

Bartole, E.[#], Grätz, L.[#], Littmann, T., Wifling, D., Seibel, U., Buschauer, A. & Bernhardt, G. UR-DEBa242: a Py-5-labeled fluorescent multipurpose probe for investigations on the histamine H_3 and H_4 receptors. *J. Med. Chem.* **63**, 5297-5311, doi:10.1021/acs.jmedchem.0c00160 (2020) ([#]: equal contribution)

Höring, C., Seibel, U., Tropmann, K., Grätz, L., Mönnich, D., Pitzl, S., Bernhardt, G., Pockes, S. & Strasser, A. A dynamic, split-luciferase-based mini-G protein sensor to functionally characterize ligands at all four histamine receptor subtypes. *Int. J. Mol. Sci.* **21**, 8440, doi:10.3390/ijms21228440 (2020).

Forster, L., Grätz, L., Mönnich, D., Bernhardt, G. & Pockes, S. A split luciferase complementation assay for the quantification of β-arrestin2 recruitment to dopamine D_2-like receptors. *Int. J. Mol. Sci.* **21**, 6103, doi:10.3390/ijms21176103 (2020).

Gruber, C. G., Pegoli, A., Müller, C., Grätz, L., She, X. & Keller, M. Differently fluorescence-labelled dibenzodiazepinone-type muscarinic acetylcholine receptor ligands with high M_2R affinity. *RSC Med. Chem.* **11**, 823-832, doi:10.1039/d0md00137f (2020).

Oral presentations

Comparison of differently fluorescence-labelled muscarinic M_2 receptor ligands in a BRET-based binding assay. *Research Day of the Emil Fischer Graduate School* (2019, Erlangen, Germany)

BRET-based binding assays: Pyrylium-labeled histamine receptor ligands allow for the determination of binding constants at equilibrium and in real time. *48th Meeting of the European Histamine Research Society* (2019, Krakow, Poland)

Bioluminescence meets fluorescent ligands: BRET-based assays as an alternative to classic radioligand binding assays. *Christmas Colloquium of the Department of Organic Chemistry* (2018, Regensburg, Germany)

Pyrylium-labeled ligands enable the determination of GPCR ligand binding in NanoBRET assays. *9th Summer School in Medicinal Chemistry* (2018, Regensburg, Germany)

Poster presentations

(only contributions as presenting author are listed)

Grätz, L.; Littmann, T.; Müller, C.; Buschmann, J.; Keller, M.; Buschauer, A. & Bernhardt, G. Insertion of NanoLuc into extracellular loops enables BRET-based binding assays at the neuropeptide Y Y_1 and Y_2 receptor. *Conference of the German Pharmaceutical Society (DPhG)* (2019, Heidelberg, Germany)

Grätz, L.; Littmann, T.; Bartole, E.; Biselli, S.; Pegoli, A.; Tropmann, K.; Keller, M.; Buschauer, A. & Bernhardt, G. A BRET-based assay to determine GPCR ligand binding using pyrylium-labeled fluorescent tracers. *4th German Pharm-Tox Summit* (2019, Stuttgart, Germany)

Grätz, L.; Littmann, T.; Bartole, E.; Biselli, S.; Pegoli, A.; Keller, M.; Bernhardt, G. & Buschauer, A. Pyrylium-labelled GPCR ligands enable the determination of equilibrium binding constants and binding kinetics in NanoBRET assays. *9th Summer School in Medicinal Chemistry* (2018, Regensburg, Germany)

Grätz, L.; Littmann, T.; Biselli, S.; Bartole, E.; Pegoli, A.; Keller, M.; Bernhardt, G. & Buschauer, A. NanoBRET-based determination of GPCR binding using pyrylium-labeled fluorescent ligands. *Frontiers in Medicinal Chemistry* (2018, Jena, Germany)

Professional training

Since 12/2016:	Member of the Research Training Group GRK1910 “Medicinal Chemistry of Selective GPCR Ligands” funded by the Deutsche Forschungsgemeinschaft
Since 12/2016:	Member of the Emil Fischer Graduate School of Pharmaceutical Sciences and Molecular Medicine, Regensburg and Erlangen
03/2017:	Fortbildung für Projektleiter und Beauftragte für Biologische Sicherheit (§§ 15 und 17 Gentechniksicherheitsverordnung), Regensburg

Contents

1. General introduction

1.1 G protein-coupled receptors (GPCRs)

G protein-coupled receptors (GPCRs) represent the largest family of membrane proteins in the human genome with more than 800 encoded members.[1] They are responsible for mediating the cellular response to many diverse extracellular stimuli, including the recognition of neurotransmitters, lipids, peptides and even photons.[2,3] Consequently, GPCRs play an important role in the regulation of various (patho)physiological processes and represent one of the most attractive family of biological targets for drugs used for therapy.[3,4] In general, GPCRs share a similar basic receptor architecture with seven membrane-spanning α-helices, which are connected by three extracellular and three intracellular loops.[5,6] Their N-terminus is located at the extracellular side and their C-terminus at the intracellular side of the plasma membrane.[5] Phylogenetically, vertebrate GPCRs are subdivided into five main families: the *Rhodopsin* receptor family (class A), which represents the largest family comprising approximately 670 receptors,[7] the *Secretin* receptor family (class B), the *Adhesion* receptor family, the *Glutamate* receptor family (class C) and the *Frizzled* family (class F).[8]

GPCRs are capable of transducing signals via different pathways, one of them being mediated by G proteins (guanine nucleotide-binding proteins), which bind to the intracellular side of the receptor.[9] G proteins consist of an α subunit, a β-subunit and a γ-subunit, constituting an inactive heterotrimer when the Gα subunit is bound to GDP.[10,11] Upon activation (e.g. binding of an agonist), GPCRs promote the guanine nucleotide exchange from GDP to GTP in the receptor-bound Gα subunit.[11-13] This process leads to conformational changes, which result in the dissociation of the G protein from the receptor and its disruption into a GTP-bound Gα subunit and a Gβγ dimer.[9,14] The Gα subunit, as long as it is bound to GTP, can interact with different effector proteins, such as adenylate cyclases, phospholipase C-β or Rho guanine nucleotide exchange factors.[13,15] The exact interaction profile thereby depends on the type or isoform of the activated α subunit.[13] The Gβγ dimer can address effector proteins as well, e.g. ion channels or G protein-coupled receptor kinases (GRKs).[13,16] Finally, the intrinsic GTPase activity within the Gα subunit leads to the hydrolysis of GTP to GDP, and consequently to the reformation of the inactivated heterotrimeric G protein complex, which is now capable of entering a new activation cycle.[9,13]

Apart from “switching on” G proteins, receptor activation also results in the phosphorylation of the receptor at its intracellular loops and its C-terminus, e.g. by second messenger-dependent kinases or GRKs.[17] This process represents an important step in the regulation of GPCR signaling.[18] In particular, GRK-phosphorylated receptors show an increased affinity for β-arrestins, which block the G protein binding site at the receptor and thus interrupt G protein-dependent signaling.[19]

Besides preventing the interaction between GPCR and G protein, β-arrestins play a multifaceted role[20-22]: for example, β-arrestins can initiate receptor internalization by directing receptors into clathrin-coated pits.[23,24] Additionally, they are involved in signaling cascades themselves by promoting the action of other proteins such as MAP kinases.[19,25]

1.2 Bioluminescence and its application in GPCR research

Bioluminescence has been long known as the naturally occurring phenomenon of light emission by living organisms.[26,27] The first detailed description dates back to the ancient Greek philosopher Aristotle and the Roman natural philosopher Pliny the Elder, who provided the first comprehensive descriptions of bioluminescent organisms.[26,28] Since then, bioluminescence has been observed in a plethora of different organisms (over 700 genera), including insects, marine organisms, bacteria and fungi.[29-31] The generation of light by living organisms serves various purposes, e.g. attracting mates, luring prey or repelling predators.[26,29,32] Bioluminescence is generated through an enzymatic biochemical reaction, in the most cases mediated by specific enzymes called luciferases.[26,27,33] Despite the large structural diversity of luciferases and their substrates (luciferins, for selected structures see Figure 1.1),[34,35] bioluminescent reactions follow a similar mechanism: the luciferase catalyzes the generation of a high-energy intermediate state of its substrate (luciferin) in the presence of oxygen. Subsequent relaxation of the luciferin to its ground state causes the emission of light.[35,36]

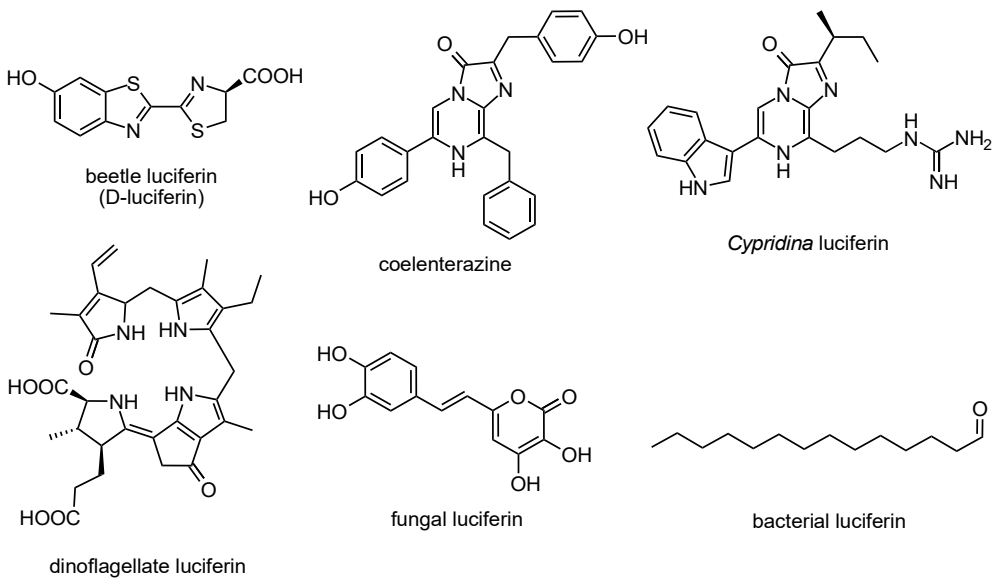

Figure 1.1: Selected structures of luciferins from various organisms.

Since the cloning and first expression of the firefly luciferase in mammalian cells in the 1980s,[37] bioluminescence-producing enzymes have become increasingly popular in biochemical research, as bioluminescence-based techniques offer some distinct advantages, such as a high sensitivity or a simple and rapid detectability.[33,38,39] In the last decades, advances in molecular biology further led to a large variety of genetically encoded luciferases and potential applications of bioluminescence in biochemistry.[27,33,39] Some of the most prominent luciferases used for the investigation of membrane-bound receptors, including GPCRs, originate from beetles (e.g. fireflies or click beetles) or marine organisms (e.g. the sea pansy *Renilla reniformis* or the copepod *Gaussia princeps*). More information about selected luciferases is given in the following section.

1.2.1 Overview over luciferases commonly used for the investigation of GPCRs

1.2.1.1 D-Luciferin-dependent luciferases

One of the most widely employed group of luciferases utilizes D-luciferin as a substrate and is found in various beetles.[27,40,41] Their bioluminescent reactions further depend on the presence of Mg^{2+} and ATP as co-factors (see Scheme 1.1).[33,40,41] Therefore, such bioluminescence systems are often applied as ATP indicators, e.g. for the measurement of cell viability or the activity of kinases.[42,43]

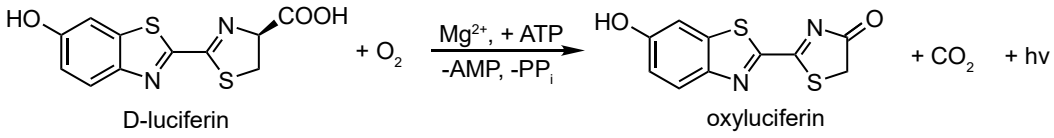

Scheme 1.1: Bioluminescent reaction catalyzed by D-luciferin-dependent luciferases. The oxidative decarboxylation of D-luciferin to oxyluciferin depends on the presence of Mg^{2+} cations and ATP, which is decomposed to AMP and pyrophosphate.

The first luciferase gene in general was cloned from the North American firefly *Photinus pyralis* (FLuc),[37,44] which still represents the best and most extensively studied luciferase. It has a size of approx. 61 kDa and shows a typical yellow-green light emission ($\lambda_{max} \approx 560$ nm) under standard conditions[40] (note: all indicated maximal emission wavelengths (λ_{max}) refer to the light emission detected under usage of the respective standard substrate). Notably, the emission wavelength and quantum yield (defined as the ratio of the number of emitted photons by the number of reacted molecules of luciferin[45,46]) of FLuc bioluminescence vary strongly with changing pH and temperature or in the presence/absence of metal ions.[47,48] However, various FLuc variants with higher thermostability could be generated by random or site-directed mutagenesis.[49,50]

As the amino acid environment in the active site was found to be crucial for the “color” of the emitted light, mutagenesis was also applied to shift the emission maxima of beetle luciferases.[51-54] Preferably, mutants with red-shifted spectra were generated, as light with longer wavelengths is less absorbed by biological tissues,[55] facilitating *in vivo* bioluminescence imaging. Another successfully applied strategy to induce a bathochromic shift of the bioluminescence spectra of beetle luciferases was the use of chemically modified D-luciferin derivatives.[56-59]
The kinetics of FLuc bioluminescence vary with the experimental conditions.[60,61] In the presence of lower concentrations of substrates and co-factors (D-luciferin, Mg^{2+}, ATP), the light emission is rather stable over a long period of time. In contrast, when using high concentrations of substrate, the reaction starts with an intense initial light emission followed by a rapid decay to a plateau at 5-10% of the maximal signal, which is stable for hours or even days.[45] The rapid decrease in signal intensity most likely occurs due to product inhibition, as some products of side reactions (e.g. dehydroluciferin) were reported to act as inhibitors of the “light-producing” reaction depicted in Scheme 1.1.[41,45,62]

Besides FLuc, the next most popular class of D-luciferin-dependent luciferases is derived from different click beetles.[27] Compared to FLuc, these luciferases exhibit a higher thermostability and are more robust against changes in pH.[40,63-65] Furthermore, engineered click beetle luciferases are available in a variety of “colors” covering the range from green (e.g. emerald luciferase (ELuc), $\lambda_{max} \approx 538$ nm[66]; or click beetle green luciferase (CBG), $\lambda_{max} \approx 540$ nm[63]) to red (e.g. click beetle red luciferase (CBR), $\lambda_{max} \approx 615$ nm[63,67]) light.

1.2.1.2 Luciferases and photoproteins from marine organisms

Apart from insects, bioluminescence is abundantly found in organisms of the sea.[29,32] Many of these “marine” luciferases share coelenterazine as a common luciferin (see Scheme 1.2)[29,30] and tend to have their emission maximum in the blue part of the visible spectrum.[32] In contrast to beetle luciferases, most of their bioluminescent reactions require neither Mg^{2+} nor ATP as cofactors.[68-71] In terms of kinetics, coelenterazine-dependent luciferases typically belong to the “flash-type” luciferases, i.e. the signal reaches a very bright and immediate peak right after substrate addition followed by a rapid decay.[30,71,72] On one hand, these flash kinetics limit the duration of the experiment, but on the other hand enable a remarkably high sensitivity shortly after addition of the substrate.[73]

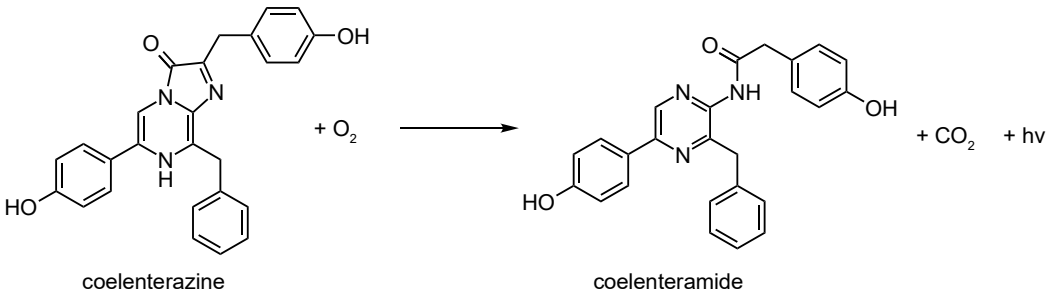

coelenterazine coelenteramide

Scheme 1.2: Bioluminescent reaction catalyzed by coelenterazine-dependent luciferases, which are present in marine organisms. In contrast to beetle luciferases, the reaction is independent of Mg^{2+} and ATP.

A very prominent marine luciferase is found in the sea pansy *Renilla reniformis* (RLuc, 36 kDa, λ_{max} ≈ 480 nm).[70,74] However, native RLuc is rapidly inactivated in serum[75] and has a comparatively low light output.[70,76] These limitations could be overcome by developing improved RLuc mutants, such as RLuc8.[75]

In 2005, the luciferase from the copepod *Gaussia princeps* (GLuc, λ_{max} ≈ 480 nm) could be efficiently expressed in mammalian cells after codon optimization for the first time.[71] GLuc is one of the smallest known luciferases (19.9 kDa) and exhibits high stability with respect to changes in pH or temperature.[71] The bioluminescence of GLuc shows a very rapid decay after an initial and bright peak,[71] which limits its applications as a reporter protein and requires the addition of the substrate via an injector.[69] Again, genetic engineering gave access to GLuc variants exhibiting more stable signals.[77,78] In contrast to all above-described luciferases, GLuc is naturally secreted.[71] The group of secreted luciferases also includes the luciferase from the ostracod *Cypridina noctiluca* (CLuc, λ_{max} ≈ 465 nm), which uses a luciferin structurally similar to coelenterazine (see Figure 1.1).[79] These luciferases offer the opportunity to measure the luminescence response in cell culture media without the need to affect the cells, or even in blood or urine samples in the course of *in vivo* studies.[80,81]

A quite recent extension of the portfolio of bioluminescent proteins is the NanoLuc® (NLuc), which is derived from the luciferase of the deep-sea shrimp *Oplophorus gracilirostris*[82] and represents one of the brightest luciferases described so far with an emission peak at approx. 460 nm.[69] The native enzyme is a heteromeric complex consisting of two 35 kDa and two 19 kDa subunits.[82] Although the 19 kDa subunit was found to be responsible for the catalytic activity, it seemed to require the 35 kDa subunit as a stabilizing partner and for sufficient expression.[82] By multiple mutagenesis steps, the 19 kDa subunit was optimized in terms of high activity in the absence of the 35 kDa subunit, light output and pH-/temperature-stability (stable up to 55 °C), finally resulting in NLuc.[69] In parallel, the coelenterazine derivative furimazine was developed to increase the overall luminescence of NLuc, and to decrease the autoluminescence of the substrate.[69]

The small size and the high brightness of NLuc have made it a very popular choice for different applications in all fields of biochemistry.[28,83] NLuc was also inserted into endogenous loci utilizing modern genome editing techniques, such as CRISPR/Cas9, giving access to luciferase-tagged proteins expressed under endogenous promotion.[84-87]

Marine luciferases are generally limited in their use for *in vivo* imaging as their blue bioluminescence is strongly absorbed by tissue.[55,88] Their suitability could be improved by generating luciferase variants with an increased light output (e.g. the mentioned RLuc8[75] and NLuc[69,89]) or with an emission shifted to longer wavelengths (e.g. RLuc8.6-535[90]). Another approach to make “blue-emitting” luciferases more feasible for *in vivo* imaging is based on the principle of BRET (bioluminescence resonance energy transfer), which is described below in detail.[91,92] For this purpose, the luciferase is fused to a fluorescent protein with a red-shifted emission. The occurring intramolecular energy transfer from the luciferase to the fluorescent protein leads to an increase in light intensity and shifts the light emission to longer wavelengths.[93-97]

Besides the classical luciferases, other naturally occurring photoproteins, which are able to generate bioluminescence in the presence of coelenterazine, are used in biochemical research, e.g. aequorin[98,99] or obelin.[100,101] In contrast to luciferases, an oxygen-activated coelenterazine is already bound tightly to the active site of the apoprotein (e.g. apoaequorin).[102] For most photoproteins, the binding of Ca^{2+} ions induces a conformational change within the protein, which allows the reaction of the bound coelenterazine to an excited coelenteramide anion and CO_2. Upon relaxation of the coelenteramide anion, blue light is emitted (note: the exact wavelength depends on the type of photoprotein).[33,102] As the intensity of the bioluminescent reaction depends on the concentration of Ca^{2+}, these photoproteins have been widely used as Ca^{2+} probes,[103] e.g. for the investigation of GPCR-mediated Ca^{2+} signaling.[104,105]

1.2.2 Advantages of bioluminescence-based methods

Bioluminescence-based techniques are widely popular for *in vitro* investigations in different fields of biochemical research for the following reasons: first, they do not depend on the use of radioactive isotopes and therefore do not require special safety and handling regulations.[33] Moreover, the low background due to the absence of an external light source, as opposed to fluorescence-based detection, and the efficiency of bioluminescent reactions result in a wide dynamic range and an exceptional sensitivity.[27,39,42] In conjunction with technological advancements, which allow the detection of very low light intensities,[106] these properties have made bioluminescence also feasible for *in vivo* imaging studies.[39,91,92,107] Since luciferases with different characteristics are available, bioluminescence-based methods offer large flexibility in the assay configuration, as the setup can be adapted according to the specific research question. Furthermore, different luciferases can potentially be combined in multiplex assays, e.g. by applying suitable filters and mathematical corrections.[63,108-111]

Besides the classical application of luciferases as reporter genes,[112] e.g. to detect altered gene transcription as a consequence of a change in the intracellular cAMP level,[113,114] two of the most common bioluminescence-based techniques in GPCR research, described in the following, are based on the phenomena of resonance energy transfer (RET) and split protein complementation.

1.2.3 Bioluminescence resonance energy transfer (BRET)

The first experimental observation of RET was made in 1922, when Cario and Franck postulated the presence of an energy transfer in a vapor consisting of mercury and thallium atoms.[115] Despite increasing experimental evidence, it took around 25 additional years until Theodor Förster was able to complete the theoretical framework behind the observations.[115,116] RET is defined as the phenomenon of a non-radiative energy transfer from an excited donor chromophore to an acceptor chromophore in its ground state through dipole-dipole coupling.[117,118] The efficiency of this energy transfer is proportional to the degree of overlap between the donor emission spectrum and the acceptor absorbance spectrum.[119,120] Additionally, it strongly depends on the distance (r) of the donor and acceptor ($\sim 1/r^6$, efficient RET occurs at distances between 1 and 10 nm), which led to its use as a “spectroscopic ruler”,[121] and the proper orientation of the transition dipoles of the chromophores.[122]

These properties, in combination with the possibility to follow dynamic processes, have made RET a widely used technique in various studies on protein-protein interactions in living cells as well.[122]

Therefore, a suitable donor and acceptor (note: spectral overlap is a requirement) are fused to the proteins of interest. Upon interaction of the two proteins, donor and acceptor come into close proximity leading to RET, provided they are in the correct orientation (see Figure 1.2). In the case of a fluorescent donor (e.g. a fluorescent protein), the occurring process is called FRET (Förster or "fluorescence" resonance energy transfer).[118,123] The main limitation of FRET in cell-based assays is the need for a light source to excite the donor, which can result in high autofluorescence, photobleaching and phototoxic effects on the cells.[123,124] These disadvantages can be avoided using a bioluminescence-based variant of RET, called BRET, where luciferases are used as donors (see Figure 1.2).[123-125] BRET is not only an artificial phenomenon, but also occurs in nature, e.g. in the jellyfish *Aequorea victoria*, where BRET from the photoprotein aequorin to the *Aequorea* green fluorescent protein is responsible for the emission of bluish-green light.[33,99]

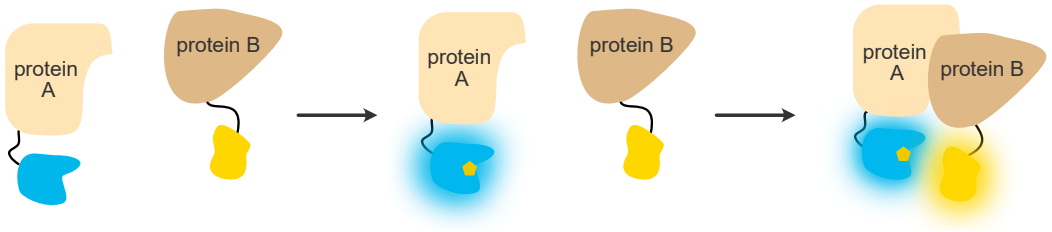

Figure 1.2: Schematic illustration of the principle of BRET-based monitoring of protein-protein interactions. The luciferase (in blue) and the fluorescent acceptor (here: a fluorescent protein in yellow) are fused (in most cases via flexible linkers) to the proteins, which are expected to interact. After addition of the luciferase substrate (yellow pentagon), the bioluminescent reaction occurs under emission of light (blue glow). When the two fusion proteins interact, the donor and the acceptor come into close proximity (approx. < 10 nm for efficient BRET), resulting in an increase in acceptor fluorescence by the non-radiative energy transfer from the donor to the acceptor.

The first experimental application of BRET was reported in 1999, when Xu *et al.* used the BRET pair RLuc and yellow fluorescent protein (YFP) (later called BRET^1 as it was the first used BRET system) to detect interactions between circadian clock proteins.[126] Since then, many different combinations of BRET donors and fluorescent acceptors have been used in biochemical research.[73,127]

The most commonly used luciferases (BRET donors) have been RLuc (or its variants),[93,94,128,129] FLuc,[130,131] and in recent years also NLuc.[132,133] The brightness of NLuc leads to ultra-high sensitivity in so-called NanoBRET experiments and its small size is advantageous in terms of maintaining the function of the protein it is attached to.[127,133,134] BRET experiments with flash-type luciferases, such as RLuc, potentially suffer from a limited duration of the experiments because of the rapid signal decay. To some extent, this problem can be solved by using chemically protected substrates, which are slowly released by intracellular esterases.[135]

In terms of BRET acceptors, fluorescent proteins have traditionally been the fluorescent acceptors of choice as they allow for convenient labeling of the protein of interest by genetic modification.[73] Additionally, they are rarely cytotoxic[136] and are available in various colors.[137] Other possible BRET acceptors are fluorescent nanoparticles, e.g. quantum dots,[138,139] or organic dyes.[73,131,140] The latter have become especially popular in NanoBRET systems[132] involving a self-labeling HaloTag,[141,142] which facilitates site-specific labeling of proteins with organic dyes, or in BRET-based receptor binding assays.[143]

1.2.4 Split luciferase complementation

Another very commonly used bioluminescence-based technique for monitoring protein-protein interactions is based on split luciferase complementation. For this approach, the functional luciferase is split into two catalytically inactive fragments, which are genetically fused to the two proteins of interest. When these interact, the luciferase fragments come into close proximity, resulting in their association and reversible restoration of the enzymatic activity of the luciferase (see Figure 1.3).[144,145] In contrast, the related method of split luciferase reconstitution depends on the intein-mediated irreversible formation of the mature luciferase.[146,147] Split luciferase complementation assays, being based on bioluminescence, are highly sensitive.[145,148] They can be used to monitor dynamic processes in living cells as the fragments, in contrast to other split protein complementation approaches, such as assays based on split fluorescent proteins,[149] have a rather short folding time after complementation and interact in a reversible manner.[148,150-152] One of the main challenges in setting up such assays lies in finding the best dissection site for the luciferase to ensure high luminescence activity after complementation and reduce unspecific self-complementation, which would result in an increased background signal.[153-155] However, many of the above-described luciferases with different characteristics have been successfully "dissected" for the use in split protein complementation assays, including FLuc,[155-157] RLuc,[154,158-160] GLuc[153,161,162] and click beetle luciferases.[152,163,164]

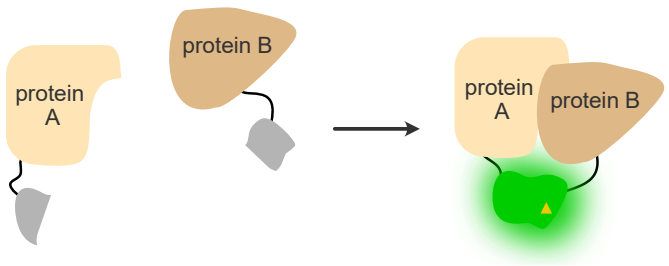

Figure 1.3: Schematic illustration of the split luciferase complementation principle. A luciferase is split into two catalytically inactive fragments, which are genetically fused to two potentially interacting proteins. Upon interaction of the two proteins, the luciferase fragments come into close proximity, leading to their association and the reversible recovery of the enzymatic activity. The latter can be measured as bioluminescence after addition of the luciferase substrate (yellow triangle).

In 2015, a NLuc-based split luciferase complementation system (NanoBiT®) was reported, which benefits from the advantages of NLuc (e.g. high brightness).[150] The luciferase was dissected into two unequally sized fragments, comprising 159 amino acids (18 kDa) and only 11 amino acids (1.3 kDa), thus minimizing sterical hindrance of the host protein by the smaller fragment. Furthermore, the auto-affinity of the two fragments, which would lead to self-complementation, was reduced by mutagenesis of the smaller fragment, thus lowering the background signal.[150] Depending on the aim of a study, the low-affinity 1.3 kDa fragment can be exchanged by another equally sized fragment called HiBiT, which shows an extraordinarily high affinity towards the 18 kDa luciferase fragment.[165] Thus, also the investigation of marginally occurring protein-protein interactions is possible. However, the higher tendency for self-complementation must be considered for their interpretation.

Worth mentioning, the diversity of available split luciferases with different characteristics offers the opportunity of combining them to study more than one protein-protein interaction in a single assay (multiparametric assays).[63,109,166,167]

1.2.5 Application of BRET and split luciferase complementation in GPCR research

Both aforementioned methods, BRET and split luciferase complementation, have been extensively applied for the investigation of biological processes involving GPCRs:

BRET, for example, was used to study GPCR oligomerization[168-170] or to detect conformational changes within these receptors.[171,172] Furthermore, BRET has been used for the investigation of GPCR signal transduction, such as measuring the formation of second messengers[173,174] or monitoring the interaction of GPCRs with G proteins,[175,176] β-arrestins[86,128,177] or GRKs.[178,179]

Recently, it was demonstrated by Stoddart *et al.* that BRET-based techniques can be used to investigate ligand binding to GPCRs in living cells.[143] For this purpose, the small and very bright luciferase NLuc (λ_{max} ≈ 460 nm)[69] was fused to the extracellular N-terminus of the investigated receptor as a BRET donor. Upon binding of a fluorescent ligand and addition of the bioluminogenic substrate, BRET occurs between the luciferase and the bound fluorescent ligand (see Figure 1.4), provided that the prerequisites of efficient BRET (short distance, favorable orientation, spectral overlap) are fulfilled. Importantly, the extent of energy transfer can be correlated with the amount of bound ligand.[134] Notably, non-specific interactions of the fluorescent ligand, which can be substantial,[134,180] are basically not measured in BRET binding assays, as mainly the fraction of receptor-bound fluorescent ligand can be detected due to the distance constraints of BRET.[134] This contributes to high signal-to-background ratios in such binding assays.

Besides the possibility of assessing receptor affinities of fluorescently labeled ligands (saturation binding) and also unlabeled ligands (competition binding), BRET-based binding assays allow for the investigation of binding kinetics in real time without the need of removing unbound fluorescent ligand.[134]

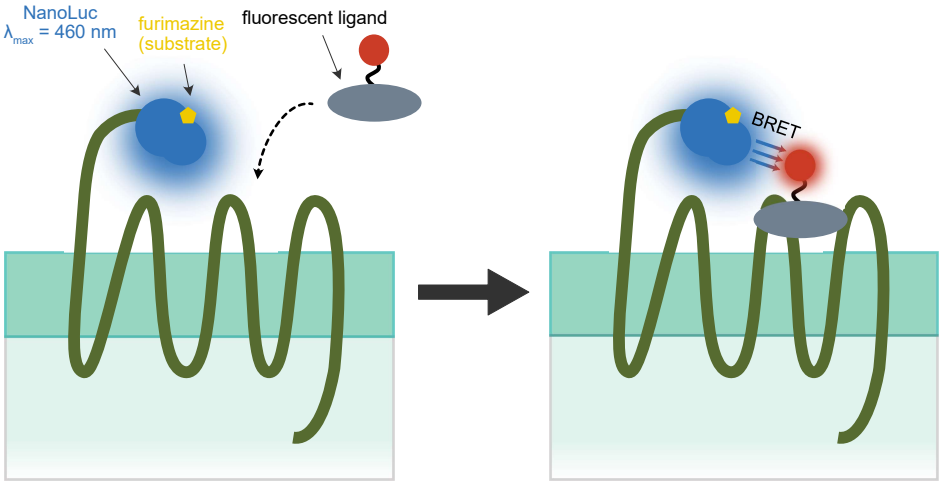

Figure 1.4: Schematic illustration of the BRET-based GPCR binding assay described by Stoddart *et al.*. The GPCR of interest is N-terminally tagged with NLuc (BRET donor), which is capable of catalyzing a bioluminescent reaction after addition of the substrate. Binding of a fluorescent ligand (BRET acceptor) brings it in close proximity to NLuc resulting in BRET.

Similarly to BRET, there are also various applications of the split luciferase complementation principle to detect PPIs in the context of GPCR research, such as probing the recruitment of G protein surrogates[181-183] or β-arrestins[67,151,164] to the receptor, or measuring GPCR oligomerization.[184-186]

1.3 Scope and aim of the thesis

For more than half a century, radioligand binding assays have played a pivotal role in studying ligand binding to GPCRs.[187] Despite the unquestionable high sensitivity and robustness of this method, radiochemical assays are associated with several drawbacks, especially in terms of safety precautions and waste disposal. Furthermore, there is a very limited number of commercial suppliers, not least being the reason for the high acquisition costs of radioligands. During the last decades, fluorescence-based techniques emerged as complementary methods and gained significant importance in the field of GPCR research.[188,189] In contrast to radioligand binding assays, most binding assays using fluorescent ligands allow measuring ligand binding under homogeneous assay conditions, not requiring the separation of bound and unbound ligand.[134,190,191] Furthermore, some fluorescence-based techniques enable monitoring of ligand binding in real time, which can improve the understanding of binding kinetics.

The primary aim of this thesis was the development of BRET-based binding assays for different GPCRs as an alternative or complementary method to the routinely used radioligand binding assays at the institute. To achieve this, the principle of BRET-based GPCR binding assays recently described by Stoddart *et al.*[143] had to be applied to various GPCRs, including peptidergic and aminergic receptors. The reported BRET-based binding assay makes use of the bright and small luciferase NanoLuc® (NLuc, λ_{max} ≈ 460 nm)[69] as a BRET donor, which is fused to the extracellularly located N-terminus of the receptor of interest. When a fluorescent ligand, showing a spectral overlap with the luciferase, binds to the receptor in a manner, which leads to a short distance and an appropriate orientation of the ligand relative to the NLuc-tagged N-terminus of the receptor, BRET can occur.[134] The energy transfer, being proportional to the amount of receptor-bound ligand, can be measured and quantified in real time.[134,189]

One subproject of this thesis had to be dedicated to the development of whole-cell BRET-based binding assays for the human histamine H_2 receptor and the human muscarinic acetylcholine M_2 receptor, using fluorescent ligands developed by other members of the research group. The fluorescent probes had to be characterized by saturation binding, kinetic binding studies and competition binding with unlabeled receptor ligands. The M_2 receptor BRET binding assay had to be directly compared with a fluorescence anisotropy-based M_2 receptor binding assay, using the same fluorescent probes. A particular focus in these studies had to be put on binding kinetics.

Furthermore, the applicability of the originally described method (N-terminal fusion of NLuc to the receptor)[143] to GPCRs with longer N-termini (> 40 amino acids) had to be explored, as the increased distance between the N-terminally attached NLuc and the bound fluorescent ligand might result in very low BRET signals. In these studies, the neuropeptide Y Y_1 receptor (Y_1R) (N-terminus: 44 amino acids), which represents an intensely studied biological target in our

research group, and the neurotensin receptor 1 (NTS_1R) (N-terminus: 67 amino acids) had to be included. N-terminal attachment of NLuc, potentially resulting in low signal-to-background ratios, had to be compared with alternative strategies, i.e. shortening of the N-terminus or insertion of NLuc into an extracellular loop of the receptor.

Finally, first steps towards multiparametric luminometric assays, measuring fluorescent ligand binding and the activation or recruitment of an intracellular effector in one cell population (requires bioluminescent proteins with different emission wavelengths and an appropriate combination of optical filters), had to be undertaken. For this purpose, a split luciferase-based assay for the assessment of the recruitment of the G protein-coupled receptor kinase 2 (GRK2) to different GPCRs had to be developed.

1.4 References

1. Fredriksson, R., Lagerström, M. C., Lundin, L.-G. & Schiöth, H. B. The G-protein-coupled receptors in the human genome form five main families. Phylogenetic analysis, paralogon groups, and fingerprints. *Mol. Pharmacol.* **63**, 1256-1272, doi:10.1124/mol.63.6.1256 (2003).

2. Katritch, V., Cherezov, V. & Stevens, R. C. Structure-function of the G protein-coupled receptor superfamily. *Annu. Rev. Pharmacol. Toxicol.* **53**, 531-556, doi:10.1146/annurev-pharmtox-032112-135923 (2013).

3. Wacker, D., Stevens, R. C. & Roth, B. L. How ligands illuminate GPCR molecular pharmacology. *Cell* **170**, 414-427, doi:10.1016/j.cell.2017.07.009 (2017).

4. Hauser, A. S., Attwood, M. M., Rask-Andersen, M., Schiöth, H. B. & Gloriam, D. E. Trends in GPCR drug discovery: new agents, targets and indications. *Nat. Rev. Drug Discov.* **16**, 829-842, doi:10.1038/nrd.2017.178 (2017).

5. Katritch, V., Cherezov, V. & Stevens, R. C. Diversity and modularity of G protein-coupled receptor structures. *Trends Pharmacol. Sci.* **33**, 17-27, doi:10.1016/j.tips.2011.09.003 (2012).

6. Rosenbaum, D. M., Rasmussen, S. G. & Kobilka, B. K. The structure and function of G-protein-coupled receptors. *Nature* **459**, 356-363, doi:10.1038/nature08144 (2009).

7. Lagerström, M. C. & Schiöth, H. B. Structural diversity of G protein-coupled receptors and significance for drug discovery. *Nat. Rev. Drug Discov.* **7**, 339-357, doi:10.1038/nrd2518 (2008).

8. Alexander, S. P. H., Christopoulos, A., Davenport, A. P., Kelly, E., Mathie, A., Peters, J. A., Veale, E. L., Armstrong, J. F., Faccenda, E., Harding, S. D., Pawson, A. J., Sharman, J. L., Southan, C., Davies, J. A. & CGTP Collaborators. The concise guide to pharmacology 2019/20: G protein-coupled receptors. *Br. J. Pharmacol.* **176**, S21-S141, doi:10.1111/bph.14748 (2019).

9. Hilger, D., Masureel, M. & Kobilka, B. K. Structure and dynamics of GPCR signaling complexes. *Nat. Struct. Mol. Biol.* **25**, 4-12, doi:10.1038/s41594-017-0011-7 (2018).

10. Hepler, J. R. & Gilman, A. G. G proteins. *Trends Biochem. Sci.* **17**, 383-387, doi:10.1016/0968-0004(92)90005-t (1992).

11. Offermanns, S. G-proteins as transducers in transmembrane signalling. *Prog. Biophys. Mol. Biol.* **83**, 101-130, doi:10.1016/s0079-6107(03)00052-x (2003).

12. Gilman, A. G. G proteins: transducers of receptor-generated signals. *Annu. Rev. Biochem* **56**, 615-649, doi:10.1146/annurev.bi.56.070187.003151 (1987).

13. Milligan, G. & Kostenis, E. Heterotrimeric G-proteins: a short history. *Br. J. Pharmacol.* **147**, S46-S55, doi:10.1038/sj.bjp.0706405 (2006).

14. Oldham, W. M. & Hamm, H. E. Heterotrimeric G protein activation by G-protein-coupled receptors. *Nat. Rev. Mol. Cell Biol.* **9**, 60-71, doi:10.1038/nrm2299 (2008).

15. Kristiansen, K. Molecular mechanisms of ligand binding, signaling, and regulation within the superfamily of G-protein-coupled receptors: molecular modeling and mutagenesis approaches to receptor structure and function. *Pharmacol. Ther.* **103**, 21-80, doi:10.1016/j.pharmthera.2004.05.002 (2004).

16. Smrcka, A. V. G protein βγ subunits: central mediators of G protein-coupled receptor signaling. *Cell. Mol. Life Sci.* **65**, 2191-2214, doi:10.1007/s00018-008-8006-5 (2008).

17. Tobin, A. B. G-protein-coupled receptor phosphorylation: where, when and by whom. *Br. J. Pharmacol.* **153**, S167-S176, doi:10.1038/sj.bjp.0707662 (2008).

18. Patwardhan, A., Cheng, N. & Trejo, J. Post-translational modifications of G protein–coupled receptors control cellular signaling dynamics in space and time. *Pharmacol. Rev.* **73**, 120-151, doi:10.1124/pharmrev.120.000082 (2021).

19. DeWire, S. M., Ahn, S., Lefkowitz, R. J. & Shenoy, S. K. β-Arrestins and cell signaling. *Annu. Rev. Physiol.* **69**, 483-510, doi:10.1146/annurev.physiol.69.022405.154749 (2007).

20. Shenoy, S. K. & Lefkowitz, R. J. Multifaceted roles of β-arrestins in the regulation of seven-membrane-spanning receptor trafficking and signalling. *Biochem. J.* **375**, 503-515, doi:10.1042/bj20031076 (2003).

21. Lohse, M. J. & Klenk, C. Blocking them all: β-arrestins inhibit cellular signaling. *Mol. Cell* **31**, 619-621, doi:10.1016/j.molcel.2008.08.015 (2008).

22. Kendall, R. T. & Luttrell, L. M. Diversity in arrestin function. *Cell. Mol. Life Sci.* **66**, 2953-2973, doi:10.1007/s00018-009-0088-1 (2009).

23. Marchese, A., Chen, C., Kim, Y.-M. & Benovic, J. L. The ins and outs of G protein-coupled receptor trafficking. *Trends Biochem. Sci.* **28**, 369-376, doi:10.1016/S0968-0004(03)00134-8 (2003).

24. Moore, C. A. C., Milano, S. K. & Benovic, J. L. Regulation of receptor trafficking by GRKs and arrestins. *Annu. Rev. Physiol.* **69**, 451-482, doi:10.1146/annurev.physiol.69.022405.154712 (2007).

25. Luttrell, L. M. & Gesty-Palmer, D. Beyond desensitization: physiological relevance of arrestin-dependent signaling. *Pharmacol. Rev.* **62**, 305-330, doi:10.1124/pr.109.002436 (2010).

26. Kahlke, T. & Umbers, K. D. L. Bioluminescence. *Curr. Biol.* **26**, R313-R314, doi:10.1016/j.cub.2016.01.007 (2016).

27. Kaskova, Z. M., Tsarkova, A. S. & Yampolsky, I. V. 1001 lights: luciferins, luciferases, their mechanisms of action and applications in chemical analysis, biology and medicine. *Chem. Soc. Rev.* **45**, 6048-6077, doi:10.1039/c6cs00296j (2016).

28. England, C. G., Ehlerding, E. B. & Cai, W. NanoLuc: a small luciferase is brightening up the field of bioluminescence. *Bioconjug. Chem.* **27**, 1175-1187, doi:10.1021/acs.bioconjchem.6b00112 (2016).

29. Haddock, S. H. D., Moline, M. A. & Case, J. F. Bioluminescence in the sea. *Ann. Rev. Mar. Sci.* **2**, 443-493, doi:10.1146/annurev-marine-120308-081028 (2010).

30. Markova, S. V. & Vysotski, E. S. Coelenterazine-dependent luciferases. *Biochemistry (Moscow)* **80**, 714-732, doi:10.1134/S0006297915060073 (2015).

31. Widder, E. A. & Falls, B. Review of bioluminescence for engineers and scientists in biophotonics. *IEEE J. Sel. Top. Quantum Electron.* **20**, 232-241, doi:10.1109/JSTQE.2013.2284434 (2014).

32. Widder, E. A. Bioluminescence in the ocean: origins of biological, chemical, and ecological diversity. *Science* **328**, 704-708, doi:10.1126/science.1174269 (2010).

33. Scott, D., Dikici, E., Ensor, M. & Daunert, S. Bioluminescence and its impact on bioanalysis. *Annu. Rev. Anal. Chem.* **4**, 297-319, doi:10.1146/annurev-anchem-061010-113855 (2011).

34. Hastings, J. W. Biological diversity, chemical mechanisms, and the evolutionary origins of bioluminescent systems. *J. Mol. Evol.* **19**, 309-321, doi:10.1007/BF02101634 (1983).

35. Wilson, T. & Hastings, J. W. Bioluminescence. *Annu. Rev. Cell Dev. Biol.* **14**, 197-230, doi:10.1146/annurev.cellbio.14.1.197 (1998).

36. Vacher, M., Fdez. Galván, I., Ding, B.-W., Schramm, S., Berraud-Pache, R., Naumov, P., Ferré, N., Liu, Y.-J., Navizet, I., Roca-Sanjuán, D., Baader, W. J. & Lindh, R. Chemi- and bioluminescence of cyclic peroxides. *Chem. Rev.* **118**, 6927-6974, doi:10.1021/acs.chemrev.7b00649 (2018).

37. de Wet, J. R., Wood, K. V., DeLuca, M., Helinski, D. R. & Subramani, S. Firefly luciferase gene: structure and expression in mammalian cells. *Mol. Cell. Biol.* **7**, 725-737, doi:10.1128/mcb.7.2.725 (1987).

38. Roda, A., Guardigli, M., Pasini, P. & Mirasoli, M. Bioluminescence and chemiluminescence in drug screening. *Anal. Bioanal. Chem.* **377**, 826-833, doi:10.1007/s00216-003-2096-6 (2003).

39. Roda, A., Guardigli, M., Michelini, E. & Mirasoli, M. Bioluminescence in analytical chemistry and in vivo imaging. *Trends Anal. Chem.* **28**, 307-322, doi:10.1016/j.trac.2008.11.015 (2009).

40. Wood, K. V., Lam, Y. A. & McElroy, W. D. Introduction to beetle luciferases and their applications. *J. Biolumin. Chemilumin.* **4**, 289-301, doi:10.1002/bio.1170040141 (1989).

41. Viviani, V. R. The origin, diversity, and structure function relationships of insect luciferases. *Cell. Mol. Life Sci.* **59**, 1833-1850, doi:10.1007/PL00012509 (2002).

42. Fan, F. & Wood, K. V. Bioluminescent assays for high-throughput screening. *Assay Drug Dev. Technol.* **5**, 127-136, doi:10.1089/adt.2006.053 (2007).

43. Klumpp, M., Boettcher, A., Becker, D., Meder, G., Blank, J., Leder, L., Forstner, M., Ottl, J. & Mayr, L. M. Readout technologies for highly miniaturized kinase assays applicable to high-throughput screening in a 1536-well format. *J. Biomol. Screen.* **11**, 617-633, doi:10.1177/1087057106288444 (2006).

44. de Wet, J. R., Wood, K. V., Helinski, D. R. & DeLuca, M. Cloning of firefly luciferase cDNA and the expression of active luciferase in Escherichia coli. *Proc. Natl. Acad. Sci. U.S.A.* **82**, 7870-7873, doi:10.1073/pnas.82.23.7870 (1985).

45. Fraga, H. Firefly luminescence: a historical perspective and recent developments. *Photochem. Photobiol. Sci.* **7**, 146-158, doi:10.1039/b719181b (2008).

46. Seliger, H. H. & McElroy, W. D. Quantum yield in the oxidation of firefly luciferin. *Biochem. Biophys. Res. Commun.* **1**, 21-24, doi:10.1016/0006-291X(59)90082-8 (1959).

47. Ando, Y., Niwa, K., Yamada, N., Enomoto, T., Irie, T., Kubota, H., Ohmiya, Y. & Akiyama, H. Firefly bioluminescence quantum yield and colour change by pH-sensitive green emission. *Nat. Photonics* **2**, 44-47, doi:10.1038/nphoton.2007.251 (2008).

48. Seliger, H. H. & McElroy, W. D. The colors of firefly bioluminescence: enzyme configuration and species specificity. *Proc. Natl. Acad. Sci. U.S.A.* **52**, 75-81, doi:10.1073/pnas.52.1.75 (1964).

49. Branchini, B. R., Ablamsky, D. M., Murtiashaw, M. H., Uzasci, L., Fraga, H. & Southworth, T. L. Thermostable red and green light-producing firefly luciferase mutants for bioluminescent reporter applications. *Anal. Biochem.* **361**, 253-262, doi:10.1016/j.ab.2006.10.043 (2007).

50. Pozzo, T., Akter, F., Nomura, Y., Louie, A. Y. & Yokobayashi, Y. Firefly luciferase mutant with enhanced activity and thermostability. *ACS Omega* **3**, 2628-2633, doi:10.1021/acsomega.7b02068 (2018).

51. Branchini, B. R., Ablamsky, D. M., Davis, A. L., Southworth, T. L., Butler, B., Fan, F., Jathoul, A. P. & Pule, M. A. Red-emitting luciferases for bioluminescence reporter and imaging applications. *Anal. Biochem.* **396**, 290-297, doi:10.1016/j.ab.2009.09.009 (2010).

52. Branchini, B. R., Southworth, T. L., Khattak, N. F., Michelini, E. & Roda, A. Red- and green-emitting firefly luciferase mutants for bioluminescent reporter applications. *Anal. Biochem.* **345**, 140-148, doi:10.1016/j.ab.2005.07.015 (2005).

53. Nishiguchi, T., Yamada, T., Nasu, Y., Ito, M., Yoshimura, H. & Ozawa, T. Development of red-shifted mutants derived from luciferase of Brazilian click beetle Pyrearinus termitilluminans. *J. Biomed. Opt.* **20**, 101205, doi:10.1117/1.jbo.20.10.101205 (2015).

54. Viviani, V. R., Uchida, A., Viviani, W. & Ohmiya, Y. The influence of Ala243 (Gly247), Arg215 and Thr226 (Asn230) on the bioluminescence spectra and pH-sensitivity of railroad worm, click beetle and firefly luciferases. *Photochem. Photobiol.* **76**, 538-544, doi:10.1562/0031-8655(2002)076<0538:tioaga>2.0.co;2 (2002).

55. Weissleder, R. A clearer vision for in vivo imaging. *Nat. Biotechnol.* **19**, 316-317, doi:10.1038/86684 (2001).

56. Hall, M. P., Woodroofe, C. C., Wood, M. G., Que, I., van't Root, M., Ridwan, Y., Shi, C., Kirkland, T. A., Encell, L. P., Wood, K. V., Löwik, C. & Mezzanotte, L. Click beetle luciferase mutant and near infrared naphthyl-luciferins for improved bioluminescence imaging. *Nat. Commun.* **9**, 132, doi:10.1038/s41467-017-02542-9 (2018).

57. Kuchimaru, T., Iwano, S., Kiyama, M., Mitsumata, S., Kadonosono, T., Niwa, H., Maki, S. & Kizaka-Kondoh, S. A luciferin analogue generating near-infrared bioluminescence achieves highly sensitive deep-tissue imaging. *Nat. Commun.* **7**, 11856, doi:10.1038/ncomms11856 (2016).

58. Mofford, D. M., Reddy, G. R. & Miller, S. C. Aminoluciferins extend firefly luciferase bioluminescence into the near-infrared and can be preferred substrates over D-luciferin. *J. Am. Chem. Soc.* **136**, 13277-13282, doi:10.1021/ja505795s (2014).

59. Conley, N. R., Dragulescu-Andrasi, A., Rao, J. & Moerner, W. E. A selenium analogue of firefly D-luciferin with red-shifted bioluminescence emission. *Angew. Chem. Int. Ed.* **51**, 3350-3353, doi:10.1002/anie.201105653 (2012).

60. Fontes, R., Dukhovich, A., Sillero, A. & Sillero, M. A. G. Synthesis of dehydroluciferin by firefly luciferase: effect of dehydroluciferin, coenzyme A and nucleoside triphosphates on the luminescent reaction. *Biochem. Biophys. Res. Commun.* **237**, 445-450, doi:10.1006/bbrc.1997.7161 (1997).

61. DeLuca, M., Wannlund, J. & McElroy, W. D. Factors affecting the kinetics of light emission from crude and purified firefly luciferase. *Anal. Biochem.* **95**, 194-198, doi:10.1016/0003-2697(79)90204-5 (1979).

62. Thorne, N., Inglese, J. & Auld, D. S. Illuminating insights into firefly luciferase and other bioluminescent reporters used in chemical biology. *Chem. Biol.* **17**, 646-657, doi:10.1016/j.chembiol.2010.05.012 (2010).

63. Villalobos, V., Naik, S., Bruinsma, M., Dothager, R. S., Pan, M.-H., Samrakandi, M., Moss, B., Elhammali, A. & Piwnica-Worms, D. Dual-color click beetle luciferase heteroprotein fragment complementation assays. *Chem. Biol.* **17**, 1018-1029, doi:10.1016/j.chembiol.2010.06.018 (2010).

64. Viviani, V. R. & Bechara, E. J. H. Bioluminescence of brazilian fireflies (Coleoptera: Lampyridae): spectral distribution and pH effect on luciferase-elicited colors. Comparison with elaterid and phengodid luciferases. *Photochem. Photobiol.* **62**, 490-495, doi:10.1111/j.1751-1097.1995.tb02373.x (1995).

65. Oliveira, G. & Viviani, V. R. Comparison of the thermostability of recombinant luciferases from Brazilian bioluminescent beetles: Relationship with kinetics and bioluminescence colours. *Luminescence* **33**, 282-288, doi:10.1002/bio.3411 (2018).

66. Nakajima, Y., Yamazaki, T., Nishii, S., Noguchi, T., Hoshino, H., Niwa, K., Viviani, V. R. & Ohmiya, Y. Enhanced beetle luciferase for high-resolution bioluminescence imaging. *PLoS One* **5**, e10011, doi:10.1371/journal.pone.0010011 (2010).

67. Takakura, H., Hattori, M., Takeuchi, M. & Ozawa, T. Visualization and quantitative analysis of G protein-coupled receptor−β-arrestin interaction in single cells and specific organs of living mice using split luciferase complementation. *ACS Chem. Biol.* **7**, 901-910, doi:10.1021/cb200360z (2012).

68. Yeh, H.-W., Xiong, Y., Wu, T., Chen, M., Ji, A., Li, X. & Ai, H.-W. ATP-independent bioluminescent reporter variants to improve in vivo imaging. *ACS Chem. Biol.* **14**, 959-965, doi:10.1021/acschembio.9b00150 (2019).

69. Hall, M. P., Unch, J., Binkowski, B. F., Valley, M. P., Butler, B. L., Wood, M. G., Otto, P., Zimmerman, K., Vidugiris, G., Machleidt, T., Robers, M. B., Benink, H. A., Eggers, C. T., Slater, M. R., Meisenheimer, P. L., Klaubert, D. H., Fan, F., Encell, L. P. & Wood, K. V. Engineered luciferase reporter from a deep sea shrimp utilizing a novel imidazopyrazinone substrate. *ACS Chem. Biol.* **7**, 1848-1857, doi:10.1021/cb3002478 (2012).

70. Matthews, J. C., Hori, K. & Cormier, M. J. Purification and properties of Renilla reniformis luciferase. *Biochemistry* **16**, 85-91, doi:10.1021/bi00620a014 (1977).

71. Tannous, B. A., Kim, D.-E., Fernandez, J. L., Weissleder, R. & Breakefield, X. O. Codon-optimized Gaussia luciferase cDNA for mammalian gene expression in culture and in vivo. *Mol. Ther.* **11**, 435-443, doi:10.1016/j.ymthe.2004.10.016 (2005).

72. Bhaumik, S. & Gambhir, S. S. Optical imaging of Renilla luciferase reporter gene expression in living mice. *Proc. Natl. Acad. Sci. U.S.A.* **99**, 377-382, doi:10.1073/pnas.012611099 (2002).

73. Weihs, F. & Dacres, H. Red-shifted bioluminescence resonance energy transfer: improved tools and materials for analytical in vivo approaches. *Trends Anal. Chem.* **116**, 61-73, doi:10.1016/j.trac.2019.04.011 (2019).

74. Lorenz, W. W., McCann, R. O., Longiaru, M. & Cormier, M. J. Isolation and expression of a cDNA encoding Renilla reniformis luciferase. *Proc. Natl. Acad. Sci. U.S.A.* **88**, 4438-4442, doi:10.1073/pnas.88.10.4438 (1991).

75. Loening, A. M., Fenn, T. D., Wu, A. M. & Gambhir, S. S. Consensus guided mutagenesis of Renilla luciferase yields enhanced stability and light output. *Protein Eng. Des. Sel.* **19**, 391-400, doi:10.1093/protein/gzl023 (2006).

76. Inouye, S. & Shimomura, O. The use of Renilla luciferase, Oplophorus luciferase, and apoaequorin as bioluminescent reporter protein in the presence of coelenterazine analogues as substrate. *Biochem. Biophys. Res. Commun.* **233**, 349-353, doi:10.1006/bbrc.1997.6452 (1997).

77. Degeling, M. H., Bovenberg, M. S., Lewandrowski, G. K., de Gooijer, M. C., Vleggeert-Lankamp, C. L., Tannous, M., Maguire, C. A. & Tannous, B. A. Directed molecular evolution reveals Gaussia luciferase variants with enhanced light output stability. *Anal. Chem.* **85**, 3006-3012, doi:10.1021/ac4003134 (2013).

78. Maguire, C. A., Deliolanis, N. C., Pike, L., Niers, J. M., Tjon-Kon-Fat, L. A., Sena-Esteves, M. & Tannous, B. A. Gaussia luciferase variant for high-throughput functional screening applications. *Anal. Chem.* **81**, 7102-7106, doi:10.1021/ac901234r (2009).

79. Nakajima, Y., Kobayashi, K., Yamagishi, K., Enomoto, T. & Ohmiya, Y. cDNA cloning and characterization of a secreted luciferase from the luminous Japanese ostracod, Cypridina noctiluca. *Biosci. Biotechnol. Biochem.* **68**, 565-570, doi:10.1271/bbb.68.565 (2004).

80. Tannous, B. A. Gaussia luciferase reporter assay for monitoring biological processes in culture and in vivo. *Nat. Protoc.* **4**, 582-591, doi:10.1038/nprot.2009.28 (2009).

81. Tannous, B. A. & Teng, J. Secreted blood reporters: insights and applications. *Biotechnol. Adv.* **29**, 997-1003, doi:10.1016/j.biotechadv.2011.08.021 (2011).

82. Inouye, S., Watanabe, K., Nakamura, H. & Shimomura, O. Secretional luciferase of the luminous shrimp Oplophorus gracilirostris: cDNA cloning of a novel imidazopyrazinone luciferase. *FEBS Lett.* **481**, 19-25, doi:10.1016/S0014-5793(00)01963-3 (2000).

83. Biewenga, L., Rosier, B. & Merkx, M. Engineering with NanoLuc: a playground for the development of bioluminescent protein switches and sensors. *Biochem. Soc. Trans.* **48**, 2643-2655, doi:10.1042/bst20200440 (2020).

84. White, C. W., Caspar, B., Vanyai, H. K., Pfleger, K. D. G. & Hill, S. J. CRISPR-mediated protein tagging with Nanoluciferase to investigate native chemokine receptor function and conformational changes. *Cell Chem. Biol.* **27**, 499-510, doi:10.1016/j.chembiol.2020.01.010 (2020).

85. White, C. W., Johnstone, E. K. M., See, H. B. & Pfleger, K. D. G. NanoBRET ligand binding at a GPCR under endogenous promotion facilitated by CRISPR/Cas9 genome editing. *Cell. Signal.* **54**, 27-34, doi:10.1016/j.cellsig.2018.11.018 (2019).

86. White, C. W., Vanyai, H. K., See, H. B., Johnstone, E. K. M. & Pfleger, K. D. G. Using nanoBRET and CRISPR/Cas9 to monitor proximity to a genome-edited protein in real-time. *Sci. Rep.* **7**, 3187, doi:10.1038/s41598-017-03486-2 (2017).

87. Basu, S., Adams, L., Guhathakurta, S. & Kim, Y.-S. A novel tool for monitoring endogenous alpha-synuclein transcription by NanoLuciferase tag insertion at the 3'end using CRISPR-Cas9 genome editing technique. *Sci. Rep.* **8**, 45883-45883, doi:10.1038/srep45883 (2017).

88. Zhao, H., Doyle, T., Coquoz, O., Kalish, F., Rice, B. & Contag, C. Emission spectra of bioluminescent reporters and interaction with mammalian tissue determine the sensitivity of detection in vivo. *J. Biomed. Opt.* **10**, 041210, doi:10.1117/1.2032388 (2005).

89. Stacer, A. C., Nyati, S., Moudgil, P., Iyengar, R., Luker, K. E., Rehemtulla, A. & Luker, G. D. NanoLuc reporter for dual luciferase imaging in living animals. *Mol. Imaging* **12**, 457-469, doi:10.2310/7290.2013.00062 (2013).

90. Loening, A. M., Wu, A. M. & Gambhir, S. S. Red-shifted Renilla reniformis luciferase variants for imaging in living subjects. *Nat. Methods* **4**, 641-643, doi:10.1038/nmeth1070 (2007).

91. Mezzanotte, L., van 't Root, M., Karatas, H., Goun, E. A. & Löwik, C. W. G. M. In vivo molecular bioluminescence imaging: new tools and applications. *Trends Biotechnol.* **35**, 640-652, doi:10.1016/j.tibtech.2017.03.012 (2017).

92. Xu, T., Close, D., Handagama, W., Marr, E., Sayler, G. & Ripp, S. The expanding toolbox of in vivo bioluminescent imaging. *Front. Oncol.* **6**, 150, doi:10.3389/fonc.2016.00150 (2016).

93. De, A., Ray, P., Loening, A. M. & Gambhir, S. S. BRET3: a red-shifted bioluminescence resonance energy transfer (BRET)-based integrated platform for imaging protein-protein interactions from single live cells and living animals. *FASEB J.* **23**, 2702-2709, doi:10.1096/fj.08-118919 (2009).

94. Dragulescu-Andrasi, A., Chan, C. T., De, A., Massoud, T. F. & Gambhir, S. S. Bioluminescence resonance energy transfer (BRET) imaging of protein-protein interactions within deep tissues of living subjects. *Proc. Natl. Acad. Sci. U.S.A.* **108**, 12060-12065, doi:10.1073/pnas.1100923108 (2011).

95. Chu, J., Oh, Y., Sens, A., Ataie, N., Dana, H., Macklin, J. J., Laviv, T., Welf, E. S., Dean, K. M., Zhang, F., Kim, B. B., Tang, C. T., Hu, M., Baird, M. A., Davidson, M. W., Kay, M. A., Fiolka, R., Yasuda, R., Kim, D. S., Ng, H. L. & Lin, M. Z. A bright cyan-excitable orange fluorescent protein facilitates dual-emission microscopy and enhances bioluminescence imaging in vivo. *Nat. Biotechnol.* **34**, 760-767, doi:10.1038/nbt.3550 (2016).

96. Schaub, F. X., Reza, M. S., Flaveny, C. A., Li, W., Musicant, A. M., Hoxha, S., Guo, M., Cleveland, J. L. & Amelio, A. L. Fluorophore-NanoLuc BRET reporters enable sensitive in vivo optical imaging and flow cytometry for monitoring tumorigenesis. *Cancer Res.* **75**, 5023-5033, doi:10.1158/0008-5472.can-14-3538 (2015).

97. Yeh, H. W., Karmach, O., Ji, A., Carter, D., Martins-Green, M. M. & Ai, H. W. Red-shifted luciferase-luciferin pairs for enhanced bioluminescence imaging. *Nat. Methods* **14**, 971-974, doi:10.1038/nmeth.4400 (2017).

98. Inouye, S., Noguchi, M., Sakaki, Y., Takagi, Y., Miyata, T., Iwanaga, S., Miyata, T. & Tsuji, F. I. Cloning and sequence analysis of cDNA for the luminescent protein aequorin. *Proc. Natl. Acad. Sci. U.S.A.* **82**, 3154-3158, doi:10.1073/pnas.82.10.3154 (1985).

99. Shimomura, O., Johnson, F. H. & Saiga, Y. Extraction, purification and properties of aequorin, a bioluminescent protein from the luminous hydromedusan, Aequorea. *J. Cell. Comp. Physiol.* **59**, 223-239, doi:10.1002/jcp.1030590302 (1962).

100. Markova, S. V., Vysotski, E. S., Blinks, J. R., Burakova, L. P., Wang, B. C. & Lee, J. Obelin from the bioluminescent marine hydroid Obelia geniculata: cloning, expression, and comparison of some properties with those of other Ca^{2+}-regulated photoproteins. *Biochemistry* **41**, 2227-2236, doi:10.1021/bi0117910 (2002).

101. Illarionov, B. A., Bondar, V. S., Illarionova, V. A. & Vysotski, E. S. Sequence of the cDNA encoding the Ca^{2+}-activated photoprotein obelin from the hydroid polyp Obelia longissima. *Gene* **153**, 273-274, doi:10.1016/0378-1119(94)00797-V (1995).

102. Vysotski, E. S., Markova, S. V. & Frank, L. A. Calcium-regulated photoproteins of marine coelenterates. *Mol. Biol.* **40**, 355-367, doi:10.1134/S0026893306030022 (2006).

103. Chiesa, A., Rapizzi, E., Tosello, V., Pinton, P., de Virgilio, M., Fogarty, K. E. & Rizzuto, R. Recombinant aequorin and green fluorescent protein as valuable tools in the study of cell signalling. *Biochem. J.* **355**, 1-12, doi:10.1042/0264-6021:3550001 (2001).

104. Konieczny, A., Braun, D., Wifling, D., Bernhardt, G. & Keller, M. Oligopeptides as neuropeptide Y Y_4 receptor ligands: identification of a high-affinity tetrapeptide agonist and a hexapeptide antagonist. *J. Med. Chem.* **63**, 8198-8215, doi:10.1021/acs.jmedchem.0c00426 (2020).

105. Lukasheva, V., Devost, D., Le Gouill, C., Namkung, Y., Martin, R. D., Longpré, J.-M., Amraei, M., Shinjo, Y., Hogue, M., Lagacé, M., Breton, B., Aoki, J., Tanny, J. C., Laporte, S. A., Pineyro, G., Inoue, A., Bouvier, M. & Hébert, T. E. Signal profiling of the β_1AR reveals coupling to novel signalling pathways and distinct phenotypic responses mediated by β_1AR and β_2AR. *Sci. Rep.* **10**, 8779, doi:10.1038/s41598-020-65636-3 (2020).

106. Massoud, T. F. & Gambhir, S. S. Molecular imaging in living subjects: seeing fundamental biological processes in a new light. *Genes Dev.* **17**, 545-580, doi:10.1101/gad.1047403 (2003).

107. Contag, C. H., Spilman, S. D., Contag, P. R., Oshiro, M., Eames, B., Dennery, P., Stevenson, D. K. & Benaron, D. A. Visualizing gene expression in living mammals using a bioluminescent reporter. *Photochem. Photobiol.* **66**, 523-531, doi:10.1111/j.1751-1097.1997.tb03184.x (1997).

108. Gammon, S. T., Leevy, W. M., Gross, S., Gokel, G. W. & Piwnica-Worms, D. Spectral unmixing of multicolored bioluminescence emitted from heterogeneous biological sources. *Anal. Chem.* **78**, 1520-1527, doi:10.1021/ac051999h (2006).

109. Hida, N., Awais, M., Takeuchi, M., Ueno, N., Tashiro, M., Takagi, C., Singh, T., Hayashi, M., Ohmiya, Y. & Ozawa, T. High-sensitivity real-time imaging of dual protein-protein interactions in living subjects using multicolor luciferases. *PLoS One* **4**, e5868, doi:10.1371/journal.pone.0005868 (2009).

110. Nakajima, Y., Kimura, T., Sugata, K., Enomoto, T., Asakawa, A., Kubota, H., Ikeda, M. & Ohmiya, Y. Multicolor luciferase assay system: one-step monitoring of multiple gene expressions with a single substrate. *Biotechniques* **38**, 891-894, doi:10.2144/05386st03 (2005).

111. Sarrion-Perdigones, A., Chang, L., Gonzalez, Y., Gallego-Flores, T., Young, D. W. & Venken, K. J. T. Examining multiple cellular pathways at once using multiplex hextuple luciferase assaying. *Nat. Commun.* **10**, 5710, doi:10.1038/s41467-019-13651-y (2019).

112. Hill, S. J., Baker, J. G. & Rees, S. Reporter-gene systems for the study of G-protein-coupled receptors. *Curr. Opin. Pharmacol.* **1**, 526-532, doi:10.1016/s1471-4892(01)00091-1 (2001).

113. Kuhn, K. K., Ertl, T., Dukorn, S., Keller, M., Bernhardt, G., Reiser, O. & Buschauer, A. High affinity agonists of the neuropeptide Y (NPY) Y_4 receptor derived from the C-terminal pentapeptide of human pancreatic polypeptide (hPP): synthesis, stereochemical discrimination, and radiolabeling. *J. Med. Chem.* **59**, 6045-6058, doi:10.1021/acs.jmedchem.6b00309 (2016).

114. Nordemann, U., Wifling, D., Schnell, D., Bernhardt, G., Stark, H., Seifert, R. & Buschauer, A. Luciferase reporter gene assay on human, murine and rat histamine H_4 receptor orthologs: correlations and discrepancies between distal and proximal readouts. *PLoS One* **8**, e73961, doi:10.1371/journal.pone.0073961 (2013).

115. Deal, J., Pleshinger, D. J., Johnson, S. C., Leavesley, S. J. & Rich, T. C. Milestones in the development and implementation of FRET-based sensors of intracellular signals: a biological perspective of the history of FRET. *Cell. Signal.* **75**, 109769, doi:10.1016/j.cellsig.2020.109769 (2020).

116. Förster, T. Zwischenmolekulare Energiewanderung und Fluoreszenz. *Ann. Phys.* **437**, 55-75, doi:10.1002/andp.19484370105 (1948).

117. Ciruela, F. Fluorescence-based methods in the study of protein-protein interactions in living cells. *Curr. Opin. Biotechnol.* **19**, 338-343, doi:10.1016/j.copbio.2008.06.003 (2008).

118. Pfleger, K. D. & Eidne, K. A. Monitoring the formation of dynamic G-protein-coupled receptor-protein complexes in living cells. *Biochem. J.* **385**, 625-637, doi:10.1042/bj20041361 (2005).

119. Haugland, R. P., Yguerabide, J. & Stryer, L. Dependence of the kinetics of singlet-singlet energy transfer on spectral overlap. *Proc. Natl. Acad. Sci. U.S.A.* **63**, 23-30, doi:10.1073/pnas.63.1.23 (1969).

120. Wu, P. & Brand, L. Resonance energy transfer: methods and applications. *Anal. Biochem.* **218**, 1-13, doi:10.1006/abio.1994.1134 (1994).

121. Stryer, L. & Haugland, R. P. Energy transfer: a spectroscopic ruler. *Proc. Natl. Acad. Sci. U.S.A.* **58**, 719-726, doi:10.1073/pnas.58.2.719 (1967).

122. Lohse, M. J., Nuber, S. & Hoffmann, C. Fluorescence/bioluminescence resonance energy transfer techniques to study G-protein-coupled receptor activation and signaling. *Pharmacol. Rev.* **64**, 299-336, doi:10.1124/pr.110.004309 (2012).

123. Boute, N., Jockers, R. & Issad, T. The use of resonance energy transfer in high-throughput screening: BRET versus FRET. *Trends Pharmacol. Sci.* **23**, 351-354, doi:10.1016/S0165-6147(02)02062-X (2002).

124. Bacart, J., Corbel, C., Jockers, R., Bach, S. & Couturier, C. The BRET technology and its application to screening assays. *Biotechnol. J.* **3**, 311-324, doi:10.1002/biot.200700222 (2008).

125. Eidne, K. A., Kroeger, K. M. & Hanyaloglu, A. C. Applications of novel resonance energy transfer techniques to study dynamic hormone receptor interactions in living cells. *Trends Endocrinol. Metab.* **13**, 415-421, doi:10.1016/S1043-2760(02)00669-0 (2002).

126. Xu, Y., Piston, D. W. & Johnson, C. H. A bioluminescence resonance energy transfer (BRET) system: application to interacting circadian clock proteins. *Proc. Natl. Acad. Sci. U.S.A.* **96**, 151-156, doi:10.1073/pnas.96.1.151 (1999).

127. El Khamlichi, C., Reverchon-Assadi, F., Hervouet-Coste, N., Blot, L., Reiter, E. & Morisset-Lopez, S. Bioluminescence resonance energy transfer as a method to study protein-protein interactions: application to G protein coupled receptor biology. *Molecules* **24**, 537, doi:10.3390/molecules24030537 (2019).

128. Bertrand, L., Parent, S., Caron, M., Legault, M., Joly, E., Angers, S., Bouvier, M., Brown, M., Houle, B. & Ménard, L. The BRET2/arrestin assay in stable recombinant cells: a platform to screen for compounds that interact with G protein-coupled receptors (GPCRs). *J. Recept. Signal Transduct. Res.* **22**, 533-541, doi:10.1081/rrs-120014619 (2002).

129. De, A., Loening, A. M. & Gambhir, S. S. An improved bioluminescence resonance energy transfer strategy for imaging intracellular events in single cells and living subjects. *Cancer Res.* **67**, 7175-7183, doi:10.1158/0008-5472.can-06-4623 (2007).

130. Arai, R., Nakagawa, H., Kitayama, A., Ueda, H. & Nagamune, T. Detection of protein-protein interaction by bioluminescence resonance energy transfer from firefly luciferase to red fluorescent protein. *J. Biosci. Bioeng.* **94**, 362-364, doi:10.1016/S1389-1723(02)80178-5 (2002).

131. Yamakawa, Y., Veda, H., Kitayama, A. & Nagamune, T. Rapid homogeneous immunoassay of peptides based on bioluminescence resonance energy transfer from firefly luciferase. *J. Biosci. Bioeng.* **93**, 537-542, doi:10.1016/S1389-1723(02)80234-1 (2002).

132. Dale, N. C., Johnstone, E. K. M., White, C. W. & Pfleger, K. D. G. NanoBRET: the bright future of proximity-based assays. *Front. Bioeng. Biotechnol.* **7**, 56, doi:10.3389/fbioe.2019.00056 (2019).

133. Machleidt, T., Woodroofe, C. C., Schwinn, M. K., Méndez, J., Robers, M. B., Zimmerman, K., Otto, P., Daniels, D. L., Kirkland, T. A. & Wood, K. V. NanoBRET-a novel BRET platform for the analysis of protein-protein interactions. *ACS Chem. Biol.* **10**, 1797-1804, doi:10.1021/acschembio.5b00143 (2015).

134. Stoddart, L. A., Kilpatrick, L. E. & Hill, S. J. NanoBRET approaches to study ligand binding to GPCRs and RTKs. *Trends Pharmacol. Sci.* **39**, 136-147, doi:10.1016/j.tips.2017.10.006 (2018).

135. Pfleger, K. D., Dromey, J. R., Dalrymple, M. B., Lim, E. M., Thomas, W. G. & Eidne, K. A. Extended bioluminescence resonance energy transfer (eBRET) for monitoring prolonged protein-protein interactions in live cells. *Cell. Signal.* **18**, 1664-1670, doi:10.1016/j.cellsig.2006.01.004 (2006).

136. Zhang, J., Campbell, R. E., Ting, A. Y. & Tsien, R. Y. Creating new fluorescent probes for cell biology. *Nat. Rev. Mol. Cell. Biol.* **3**, 906-918, doi:10.1038/nrm976 (2002).

137. Rodriguez, E. A., Campbell, R. E., Lin, J. Y., Lin, M. Z., Miyawaki, A., Palmer, A. E., Shu, X., Zhang, J. & Tsien, R. Y. The growing and glowing toolbox of fluorescent and photoactive proteins. *Trends Biochem. Sci.* **42**, 111-129, doi:10.1016/j.tibs.2016.09.010 (2017).

138. Kamkaew, A., Sun, H., England, C. G., Cheng, L., Liu, Z. & Cai, W. Quantum dot-NanoLuc bioluminescence resonance energy transfer enables tumor imaging and lymph node mapping in vivo. *Chem. Commun. (Camb.)* **52**, 6997-7000, doi:10.1039/c6cc02764d (2016).

139. So, M.-K., Xu, C., Loening, A. M., Gambhir, S. S. & Rao, J. Self-illuminating quantum dot conjugates for in vivo imaging. *Nat. Biotechnol.* **24**, 339-343, doi:10.1038/nbt1188 (2006).

140. Smirnova, D. V., Samsonova, J. V. & Ugarova, N. N. The bioluminescence resonance energy transfer from firefly luciferase to a synthetic dye and its application for the rapid homogeneous immunoassay of progesterone. *Photochem. Photobiol.* **92**, 158-165, doi:10.1111/php.12556 (2016).

141. England, C. G., Luo, H. & Cai, W. HaloTag technology: a versatile platform for biomedical applications. *Bioconjug. Chem.* **26**, 975-986, doi:10.1021/acs.bioconjchem.5b00191 (2015).

142. Los, G. V., Encell, L. P., McDougall, M. G., Hartzell, D. D., Karassina, N., Zimprich, C., Wood, M. G., Learish, R., Ohana, R. F., Urh, M., Simpson, D., Mendez, J., Zimmerman, K., Otto, P., Vidugiris, G., Zhu, J., Darzins, A., Klaubert, D. H., Bulleit, R. F. & Wood, K. V. HaloTag: A novel protein labeling technology for cell imaging and protein analysis. *ACS Chem. Biol.* **3**, 373-382, doi:10.1021/cb800025k (2008).

143. Stoddart, L. A., Johnstone, E. K. M., Wheal, A. J., Goulding, J., Robers, M. B., Machleidt, T., Wood, K. V., Hill, S. J. & Pfleger, K. D. G. Application of BRET to monitor ligand binding to GPCRs. *Nat. Methods* **12**, 661-663, doi:10.1038/nmeth.3398 (2015).

144. Azad, T., Tashakor, A. & Hosseinkhani, S. Split-luciferase complementary assay: applications, recent developments, and future perspectives. *Anal. Bioanal. Chem.* **406**, 5541-5560, doi:10.1007/s00216-014-7980-8 (2014).

145. Hattori, M. & Ozawa, T. Split luciferase complementation for analysis of intracellular signaling. *Anal. Sci.* **30**, 539-544, doi:10.2116/analsci.30.539 (2014).

146. Ozawa, T., Kaihara, A., Sato, M., Tachihara, K. & Umezawa, Y. Split luciferase as an optical probe for detecting protein−protein interactions in mammalian cells based on protein splicing. *Anal. Chem.* **73**, 2516-2521, doi:10.1021/ac0013296 (2001).

147. Paulmurugan, R., Umezawa, Y. & Gambhir, S. S. Noninvasive imaging of protein–protein interactions in living subjects by using reporter protein complementation and reconstitution strategies. *Proc. Natl. Acad. Sci. U.S.A.* **99**, 15608-15613, doi:10.1073/pnas.242594299 (2002).

148. Wehr, M. C. & Rossner, M. J. Split protein biosensor assays in molecular pharmacological studies. *Drug Discov. Today* **21**, 415-429, doi:10.1016/j.drudis.2015.11.004 (2016).

149. Magliery, T. J., Wilson, C. G., Pan, W., Mishler, D., Ghosh, I., Hamilton, A. D. & Regan, L. Detecting protein-protein interactions with a green fluorescent protein fragment reassembly trap: scope and mechanism. *J. Am. Chem. Soc.* **127**, 146-157, doi:10.1021/ja046699g (2005).

150. Dixon, A. S., Schwinn, M. K., Hall, M. P., Zimmerman, K., Otto, P., Lubben, T. H., Butler, B. L., Binkowski, B. F., Machleidt, T., Kirkland, T. A., Wood, M. G., Eggers, C. T., Encell, L. P. & Wood, K. V. NanoLuc complementation reporter optimized for accurate measurement of protein interactions in cells. *ACS Chem. Biol.* **11**, 400-408, doi:10.1021/acschembio.5b00753 (2016).

151. Littmann, T., Buschauer, A. & Bernhardt, G. Split luciferase-based assay for simultaneous analyses of the ligand concentration- and time-dependent recruitment of β-arrestin2. *Anal. Biochem.* **573**, 8-16, doi:10.1016/j.ab.2019.02.023 (2019).

152. Littmann, T., Ozawa, T., Hoffmann, C., Buschauer, A. & Bernhardt, G. A split luciferase-based probe for quantitative proximal determination of $G\alpha_q$ signalling in live cells. *Sci. Rep.* **8**, 17179, doi:10.1038/s41598-018-35615-w (2018).

153. Kim, S. B., Sato, M. & Tao, H. Split Gaussia luciferase-based bioluminescence template for tracing protein dynamics in living cells. *Anal. Chem.* **81**, 67-74, doi:10.1021/ac801658y (2009).

154. Paulmurugan, R. & Gambhir, S. S. Monitoring protein-protein interactions using split synthetic Renilla luciferase protein-fragment-assisted complementation. *Anal. Chem.* **75**, 1584-1589, doi:10.1021/ac020731c (2003).

155. Paulmurugan, R. & Gambhir, S. S. Firefly luciferase enzyme fragment complementation for imaging in cells and living animals. *Anal. Chem.* **77**, 1295-1302, doi:10.1021/ac0484777 (2005).

156. Luker, K. E., Smith, M. C., Luker, G. D., Gammon, S. T., Piwnica-Worms, H. & Piwnica-Worms, D. Kinetics of regulated protein-protein interactions revealed with firefly luciferase complementation imaging in cells and living animals. *Proc. Natl. Acad. Sci. U.S.A.* **101**, 12288-12293, doi:10.1073/pnas.0404041101 (2004).

157. Ramkumar, K. M., Sekar, T. V., Foygel, K., Elango, B. & Paulmurugan, R. Reporter protein complementation imaging assay to screen and study Nrf2 activators in cells and living animals. *Anal. Chem.* **85**, 7542-7549, doi:10.1021/ac401569j (2013).

158. Hirohama, M., Voet, A. R., Ozawa, T., Saitoh, H., Nakao, Y., Zhang, K. Y., Ito, A. & Yoshida, M. Assay methods for small ubiquitin-like modifier (SUMO)-SUMO-interacting motif (SIM) interactions in vivo and in vitro using a split-luciferase complementation system. *Anal. Biochem.* **448**, 92-94, doi:10.1016/j.ab.2013.12.009 (2014).

159. Kaihara, A., Umezawa, Y. & Furukawa, T. Bioluminescent indicators for Ca^{2+} based on split Renilla luciferase complementation in living cells. *Anal. Sci.* **24**, 1405-1408, doi:10.2116/analsci.24.1405 (2008).

160. Stefan, E., Aquin, S., Berger, N., Landry, C. R., Nyfeler, B., Bouvier, M. & Michnick, S. W. Quantification of dynamic protein complexes using Renilla luciferase fragment complementation applied to protein kinase A activities in vivo. *Proc. Natl. Acad. Sci. U.S.A.* **104**, 16916-16921, doi:10.1073/pnas.0704257104 (2007).

161. Luker, K. E., Mihalko, L. A., Schmidt, B. T., Lewin, S. A., Ray, P., Shcherbo, D., Chudakov, D. M. & Luker, G. D. In vivo imaging of ligand receptor binding with Gaussia luciferase complementation. *Nat. Med.* **18**, 172-177, doi:10.1038/nm.2590 (2011).

162. Remy, I. & Michnick, S. W. A highly sensitive protein-protein interaction assay based on Gaussia luciferase. *Nat. Methods* **3**, 977-979, doi:10.1038/nmeth979 (2006).

163. Kim, S. B., Otani, Y., Umezawa, Y. & Tao, H. Bioluminescent indicator for determining protein−protein interactions using intramolecular complementation of split click beetle luciferase. *Anal. Chem.* **79**, 4820-4826, doi:10.1021/ac0621571 (2007).

164. Misawa, N., Kafi, A. K. M., Hattori, M., Miura, K., Masuda, K. & Ozawa, T. Rapid and high-sensitivity cell-based assays of protein−protein interactions using split click beetle luciferase complementation: an approach to the study of G-protein-coupled receptors. *Anal. Chem.* **82**, 2552-2560, doi:10.1021/ac100104q (2010).

165. Schwinn, M. K., Machleidt, T., Zimmerman, K., Eggers, C. T., Dixon, A. S., Hurst, R., Hall, M. P., Encell, L. P., Binkowski, B. F. & Wood, K. V. CRISPR-mediated tagging of endogenous proteins with a luminescent peptide. *ACS Chem. Biol.* **13**, 467-474, doi:10.1021/acschembio.7b00549 (2018).

166. Kim, S. B., Umezawa, Y., Kanno, K. A. & Tao, H. An integrated-molecule-format multicolor probe for monitoring multiple activities of a bioactive small molecule. *ACS Chem. Biol.* **3**, 359-372, doi:10.1021/cb800004s (2008).

167. Paulmurugan, R., Tamrazi, A., Massoud, T. F., Katzenellenbogen, J. A. & Gambhir, S. S. In vitro and in vivo molecular imaging of estrogen receptor α and β homo- and heterodimerization: exploration of new modes of receptor regulation. *Mol. Endocrinol.* **25**, 2029-2040, doi:10.1210/me.2011-1145 (2011).

168. Angers, S., Salahpour, A., Joly, E., Hilairet, S., Chelsky, D., Dennis, M. & Bouvier, M. Detection of β_2-adrenergic receptor dimerization in living cells using bioluminescence resonance energy transfer (BRET). *Proc. Natl. Acad. Sci. U.S.A.* **97**, 3684-3689, doi:10.1073/pnas.97.7.3684 (2000).

169. Kroeger, K. M., Hanyaloglu, A. C., Seeber, R. M., Miles, L. E. & Eidne, K. A. Constitutive and agonist-dependent homo-oligomerization of the thyrotropin-releasing hormone receptor. Detection in living cells using bioluminescence resonance energy transfer. *J. Biol. Chem.* **276**, 12736-12743, doi:10.1074/jbc.M011311200 (2001).

170. Plach, M., Schäfer, T., Borroto-Escuela, D. O., Weikert, D., Gmeiner, P., Fuxe, K. & Friedland, K. Differential allosteric modulation within dopamine D_2R - neurotensin NTS1R and D_2R - serotonin 5-$HT_{2A}R$ receptor complexes gives bias to intracellular calcium signalling. *Sci. Rep.* **9**, 16312, doi:10.1038/s41598-019-52540-8 (2019).

171. Schihada, H., Ma, X., Zabel, U., Vischer, H. F., Schulte, G., Leurs, R., Pockes, S. & Lohse, M. J. Development of a conformational histamine H_3 receptor biosensor for the synchronous screening of agonists and inverse agonists. *ACS Sensors* **5**, 1734-1742, doi:10.1021/acssensors.0c00397 (2020).

172. Schihada, H., Vandenabeele, S., Zabel, U., Frank, M., Lohse, M. J. & Maiellaro, I. A universal bioluminescence resonance energy transfer sensor design enables high-sensitivity screening of GPCR activation dynamics. *Commun. Biol.* **1**, 105, doi:10.1038/s42003-018-0072-0 (2018).

173. Jiang, L. I., Collins, J., Davis, R., Lin, K. M., DeCamp, D., Roach, T., Hsueh, R., Rebres, R. A., Ross, E. M., Taussig, R., Fraser, I. & Sternweis, P. C. Use of a cAMP BRET sensor to characterize a novel regulation of cAMP by the sphingosine 1-phosphate/G_{13} pathway. *J. Biol. Chem.* **282**, 10576-10584, doi:10.1074/jbc.M609695200 (2007).

174. Hübner, H., Schellhorn, T., Gienger, M., Schaab, C., Kaindl, J., Leeb, L., Clark, T., Möller, D. & Gmeiner, P. Structure-guided development of heterodimer-selective GPCR ligands. *Nat. Commun.* **7**, 12298, doi:10.1038/ncomms12298 (2016).

175. Ayoub, M. A., Maurel, D., Binet, V., Fink, M., Prézeau, L., Ansanay, H. & Pin, J.-P. Real-time analysis of agonist-induced activation of protease-activated receptor 1/$G\alpha_{i1}$ protein complex measured by bioluminescence resonance energy transfer in living cells. *Mol. Pharmacol.* **71**, 1329-1340, doi:10.1124/mol.106.030304 (2007).

176. Galés, C., Van Durm, J. J., Schaak, S., Pontier, S., Percherancier, Y., Audet, M., Paris, H. & Bouvier, M. Probing the activation-promoted structural rearrangements in preassembled receptor-G protein complexes. *Nat. Struct. Mol. Biol.* **13**, 778-786, doi:10.1038/nsmb1134 (2006).

177. Hamdan, F. F., Audet, M., Garneau, P., Pelletier, J. & Bouvier, M. High-throughput screening of G protein-coupled receptor antagonists using a bioluminescence resonance energy transfer 1-based β-arrestin2 recruitment assay. *J. Biomol. Screen.* **10**, 463-475, doi:10.1177/1087057105275344 (2005).

178. Hasbi, A., Devost, D., Laporte, S. A. & Zingg, H. H. Real-time detection of interactions between the human oxytocin receptor and G protein-coupled receptor kinase-2. *Mol. Endocrinol.* **18**, 1277-1286, doi:10.1210/me.2003-0440 (2004).

179. Jorgensen, R., Holliday, N. D., Hansen, J. L., Vrecl, M., Heding, A., Schwartz, T. W. & Elling, C. E. Characterization of G-protein coupled receptor kinase interaction with the neurokinin-1 receptor using bioluminescence resonance energy transfer. *Mol. Pharmacol.* **73**, 349-358, doi:10.1124/mol.107.038877 (2008).

180. Iliopoulos-Tsoutsouvas, C., Kulkarni, R. N., Makriyannis, A. & Nikas, S. P. Fluorescent probes for G-protein-coupled receptor drug discovery. *Expert Opin. Drug Discov.* **13**, 933-947, doi:10.1080/17460441.2018.1518975 (2018).

181. Höring, C., Seibel, U., Tropmann, K., Grätz, L., Mönnich, D., Pitzl, S., Bernhardt, G., Pockes, S. & Strasser, A. A dynamic, split-luciferase-based mini-G protein sensor to functionally characterize ligands at all four histamine receptor subtypes. *Int. J. Mol. Sci.* **21**, 8440, doi:10.3390/ijms21228440 (2020).

182. Pottie, E., Dedecker, P. & Stove, C. P. Identification of psychedelic new psychoactive substances (NPS) showing biased agonism at the 5-HT_{2A}R through simultaneous use of β-arrestin 2 and miniGα_q bioassays. *Biochem. Pharmacol.* **182**, 114251, doi:10.1016/j.bcp.2020.114251 (2020).

183. Wan, Q., Okashah, N., Inoue, A., Nehmé, R., Carpenter, B., Tate, C. G. & Lambert, N. A. Mini G protein probes for active G protein-coupled receptors (GPCRs) in live cells. *J. Biol. Chem.* **293**, 7466-7473, doi:10.1074/jbc.RA118.001975 (2018).

184. Casadó-Anguera, V., Bonaventura, J., Moreno, E., Navarro, G., Cortés, A., Ferré, S. & Casadó, V. Evidence for the heterotetrameric structure of the adenosine A_{2A}–dopamine D_2 receptor complex. *Biochem. Soc. Trans.* **44**, 595-600, doi:10.1042/BST20150276 (2016).

185. Luker, K. E., Gupta, M. & Luker, G. D. Imaging chemokine receptor dimerization with firefly luciferase complementation. *FASEB J.* **23**, 823-834, doi:10.1096/fj.08-116749 (2009).

186. Wouters, E., Marín, A. R., Dalton, J. A. R., Giraldo, J. & Stove, C. Distinct dopamine D_2 receptor antagonists differentially impact D_2 receptor oligomerization. *Int. J. Mol. Sci.* **20**, doi:10.3390/ijms20071686 (2019).

187. Lefkowitz, R. J. Historical review: a brief history and personal retrospective of seven-transmembrane receptors. *Trends Pharmacol. Sci.* **25**, 413-422, doi:10.1016/j.tips.2004.06.006 (2004).

188. Sridharan, R., Zuber, J., Connelly, S. M., Mathew, E. & Dumont, M. E. Fluorescent approaches for understanding interactions of ligands with G protein coupled receptors. *Biochim. Biophys. Acta Biomembr.* **1838**, 15-33, doi:10.1016/j.bbamem.2013.09.005 (2014).

189. Stoddart, L. A., White, C. W., Nguyen, K., Hill, S. J. & Pfleger, K. D. Fluorescence- and bioluminescence-based approaches to study GPCR ligand binding. *Br. J. Pharmacol.* **173**, 3028-3037, doi:10.1111/bph.13316 (2016).

190. Emami-Nemini, A., Roux, T., Leblay, M., Bourrier, E., Lamarque, L., Trinquet, E. & Lohse, M. J. Time-resolved fluorescence ligand binding for G protein–coupled receptors. *Nat. Protoc.* **8**, 1307-1320, doi:10.1038/nprot.2013.073 (2013).

191. Rinken, A., Lavogina, D. & Kopanchuk, S. Assays with detection of fluorescence anisotropy: challenges and possibilities for characterizing ligand binding to GPCRs. *Trends Pharmacol. Sci.* **39**, 187-199, doi:10.1016/j.tips.2017.10.004 (2018).

2. NanoBRET binding assay for histamine H_2 receptor ligands using live recombinant HEK293T cells

Note: Prior to the submission of this thesis, the content of this chapter was published together with additional data (not shown in this thesis) in collaboration with partners:

Grätz, L.; Tropmann, K; Bresinsky, M.; Müller, C.; Bernhardt, G.& Pockes, S. NanoBRET binding assay for histamine H_2 receptor ligands using live recombinant HEK293T cells. *Sci. Rep.* **10**, 13288, doi: 10.1038/s41598-020-70332-3 (2020).

The following experimental work was performed by co-authors:

K. Tropmann:	Synthesis and analytical characterization of the fluorescent ligands **2.1**-**2.3** (not shown); flow cytometric binding experiments and β-arrestin2 recruitment assays with **2.1-2.3**
K. Tropmann & M. Bresinsky:	Radioligand competition binding experiments
C. Müller:	Synthesis of the Py-1 dye used for the synthesis of **2.1** (not shown)

2.1 Introduction

The histamine H_2 receptor (H_2R), which is endogenously activated by the biogenic amine histamine, is a long known member of rhodopsin-like receptors (class A), the largest and best studied group of G protein-coupled receptors (GPCRs).[1-4] It represents an established target for the treatment of gastroesophageal reflux disease and peptic ulcer, for which H_2R antagonists, such as cimetidine, ranitidine and famotidine (for structures, see Appendix Figure A1), representing the first blockbuster drugs on the market, were developed in the 1970s.[5] Current research on CNS-penetrating H_2R ligands, especially focusing on agonists,[6] is ongoing in order to get a better understanding of the physiological role of the H_2R in the brain. Since the H_2R has been described as being expressed in postsynaptic neurons and being involved in cognitive processes, it was proposed that stimulation of neuronal H_2Rs could have similar positive effects on memory and learning as antagonizing the histamine H_3 receptor,[7-9] making the H_2R an interesting target for the development of future drugs addressing the CNS.

One of the first steps in the development of new ligands is the investigation of their binding properties at the putative target. Until now, the characterization of potential ligands in terms of receptor binding has been mostly done performing radioligand binding experiments.[10] Despite the high sensitivity and robustness, the use of radiolabeled substances is usually connected with some drawbacks. In addition to the constantly increasing costs and safety issues,[11] the availability as well as the quality of commercial radioligands often decreases. Furthermore, the management of radioactive waste is becoming increasingly regulated and expensive. To overcome these issues, techniques using fluorescently labeled ligands, such as flow cytometry and the recently described NanoBRET binding assay,[12,13] which has been adapted to several GPCRs by now,[14-25] have gained great importance.[11,26]

For the NanoBRET binding assay, the NanoLuc® (NLuc), a genetically engineered luciferase derived from a deep-sea shrimp,[27] is fused to the N-terminus of the GPCR of interest in the function of a BRET donor.[12] Upon addition of the substrate, the luciferase catalyzes an oxidation reaction, which is accompanied by the emission of blue light ($\lambda_{max} \approx 460$ nm).[27] Once a suitable fluorescent ligand, i.e. its excitation spectrum overlaps with the bioluminescence spectrum of NLuc, binds to the tagged receptor, the ligand fluoresces due to bioluminescence resonance energy transfer (BRET). However, this energy transfer can only occur when the ligand is in close proximity (approx. < 10 nm) and in a favorable orientation to the luciferase,[13] which leads to the observation of low non-specific binding in such assays. The binding process can additionally be followed in real time and not only after equilibrium is reached, which gives deeper insight into the binding behavior of the ligand.

In this study, a BRET-based binding assay was established for the human histamine H_2 receptor (hH_2R) by fusing NLuc to the N-terminus of the receptor (NLuc-H_2R). This fusion protein was stably expressed in live HEK293T cells and three differently fluorescence-labeled ligands (**2.1**-**2.3**, Figure 2.1) were subsequently compared in BRET saturation binding experiments at the NLuc-H_2R. Furthermore, real-time kinetic binding experiments and BRET competition binding experiments with various reported H_2R ligands were conducted using the fluorescent probe **2.1**.

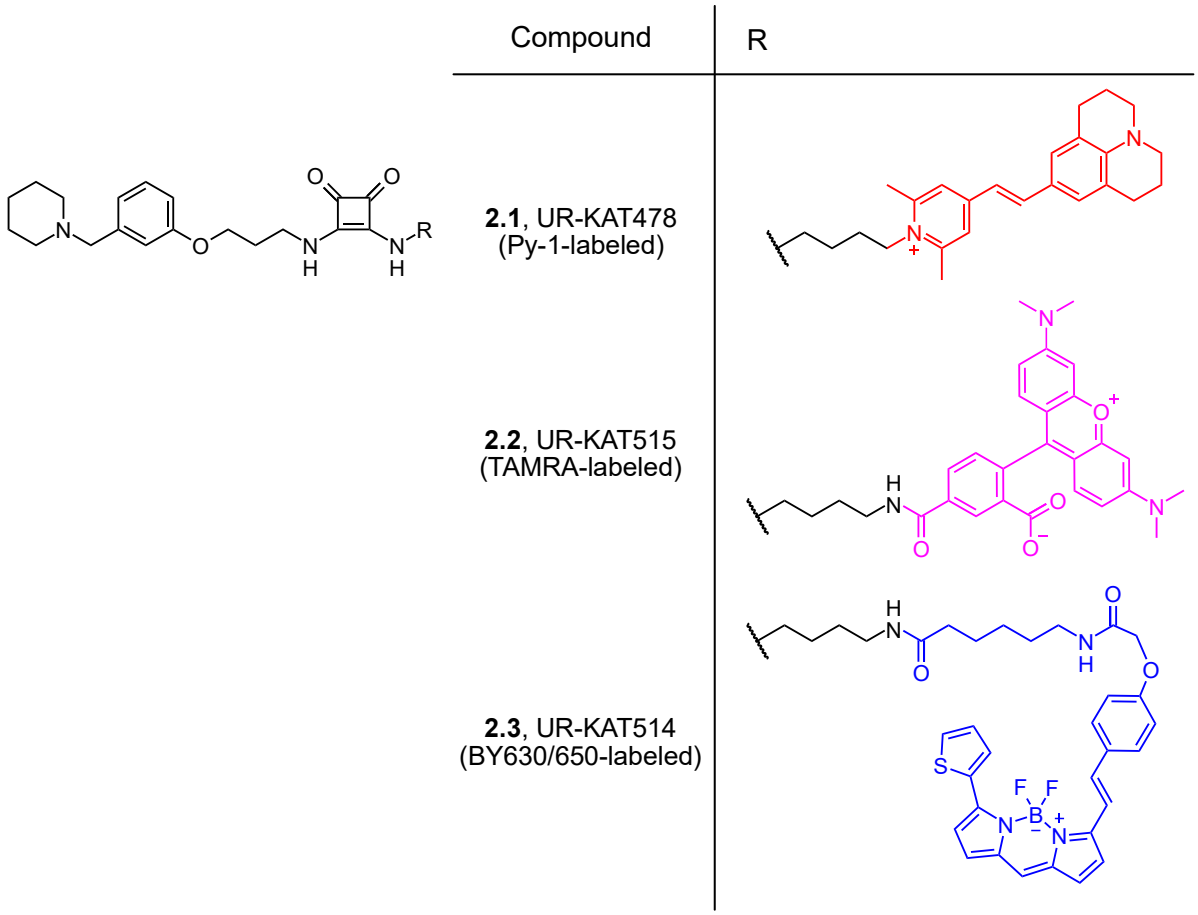

Figure 2.1: Structures of the investigated fluorescent H_2R ligands **2.1**-**2.3**.

2.2 Materials and methods

2.2.1 Materials

Dulbecco's Modified Eagle's Medium (DMEM), L-glutamine and HEPES were purchased from Sigma-Aldrich (Munich, Germany). Leibovitz' L-15 medium (L-15) was from Fisher Scientific (Nidderau, Germany). Fetal calf serum (FCS), geneticin (G418) and trypsin/EDTA (0.05%/0.02%) were from Biochrom (Berlin, Germany). Hygromycin B was purchased from AG Scientific (San Diego, CA, USA), whereas zeocin was obtained from InvivoGen (Toulouse, France). Bovine serum albumin (BSA) was from SERVA Electrophoresis (Heidelberg, Germany). Furimazine (Nano-Glo® Live Cell Substrate) was purchased from Promega (Mannheim, Germany) and the pcDNA3.1 vector was from Thermo Fisher (Nidderau, Germany).

Histamine dihydrochloride was from TCI Chemicals (Tokyo, Japan). Cimetidine was from Sigma-Aldrich (Munich, Germany), whereas famotidine and ranitidine hydrochloride were purchased from Tocris Bioscience (Bristol, UK). The syntheses of UR-Po444 and UR-Po448 were described previously.[6] The synthesis of the radioligand [^{3}H]UR-DE257 was reported elsewhere.[28] Stock solutions of the investigated competitive ligands were prepared in millipore H_2O or DMSO (Merck Millipore, Darmstadt, Germany), whenever the compound was insoluble in H_2O. Stock solutions of the fluorescent ligands **2.1**-**2.3** were prepared in DMSO and stored in aliquots at -80 °C.

2.2.2 Generation of plasmids

The cDNA coding for the human H_2R was purchased from the cDNA Resource Center (Rolla, MO, USA). The plasmid encoding NanoLuc® (NLuc) was kindly provided by Promega (Mannheim, Germany). The sequences of the receptor and the luciferase were amplified using standard PCR techniques, introducing restriction sites at their respective 5' and 3' ends as well as the membrane signal peptide of the murine $5HT_{3A}$ receptor upstream of the luciferase gene. The digested PCR products were subsequently cloned in-frame into the pcDNA3.1 vector backbone to generate the pcDNA3.1 NLuc-H_2R. The luciferase and the receptor were connected by a short and flexible linker sequence consisting of Gly and Ser (-SGGGS-). The quality of the plasmid was verified by sequencing (Eurofins Genomics, Ebersberg, Germany).

2.2.3 Cell culture and generation of stable transfectants

HEK293T cells (kind gift from Prof. Dr. Wulf Schneider, Institute for Medical Microbiology and Hygiene, University Hospital Regensburg, Germany) were routinely cultivated in DMEM, supplemented with 2 mM L-glutamine and 10% FCS (full medium), at 37 °C in a humidified atmosphere containing 5% CO_2. They were regularly monitored for mycoplasma infection using

the Venor GeM Mycoplasma Detection Kit (Minerva Biolabs, Berlin, Germany) and were negative. In order to generate stable transfectants, HEK293T cells were seeded at a density of $3 \cdot 10^5$ cells/mL in a 6-well plate (Sarstedt, Nümbrecht, Germany) one day prior to transfection with 2 µg of the pcDNA3.1 NLuc-H_2R using X-tremeGENE™ HP transfection reagent (Roche Diagnostics, Mannheim, Germany) according to the manufacturer's protocol. After two days of incubation, the transfected cells were detached by trypsinization and centrifuged (500 *g*, 5 min). The cells were seeded on a 150 mm-cell culture dish (Sarstedt, Nümbrecht, Germany) and G418 was added immediately at a final concentration of 1 mg/mL to select for stable transfectants. The medium was exchanged regularly until stable growth of the colonies was observed. For cultivation of the stably transfected cells, the concentration of G418 was reduced to 600 µg/mL.

HEK293T-hH_2R-qs5-HA cells used for flow cytometric binding studies were maintained in full medium, supplemented with 400 µg/mL G418 and 100 µg/mL hygromycin B,[29] whereas HEK293T-ARRB2-H_2R cells, which were used for the β-arrestin2 recruitment assay, were maintained in full medium, supplemented with 600 µg/mL G418 and 400 µg/mL zeocin.[30]

2.2.4 Radioligand competition binding assay

General procedures for the generation of recombinant baculoviruses, culture of Sf9 cells and membrane preparation were described elsewhere.[31] Radioligand competition binding experiments using membrane preparations of Sf9 insect cells expressing the hH_2R-Gsα$_s$ fusion protein were performed according to a described procedure,[32] using [^{3}H]UR-DE257[28] as the radioligand (c = 20 nM, K_d = 11.2 nM). In order to investigate the effect of sodium on the binding of histamine, NaCl was added to the binding buffer (consisting of 12.5 mM $MgCl_2$, 1 mM EDTA and 75 mM Tris/HCl, pH 7.4)[32] at a physiological concentration of 145 mM. The obtained specific binding data were analyzed by a four-parameter logistic fit (GraphPad Prism 8.0, GraphPad Software Inc., San Diego, CA, USA) yielding pIC_{50} values, which were transformed into pK_i values using the Cheng-Prusoff equation.[33] Means and SEMs were calculated for the pK_i values.

2.2.5 Flow cytometric saturation binding assay

Flow cytometric binding studies at HEK293T-hH_2R-qs5-HA cells were performed with a FACSCanto™II flow cytometer (Becton Dickinson, Heidelberg, Germany), equipped with an argon laser (488 nm) and a red diode laser (633 nm). The fluorescence signals were recorded with the following instrument settings:

compound **2.1**, excitation: 488 nm, emission: 670 ± 65 nm (PerCP-Cy5.5 channel), gain: 485 V;
compound **2.2**, excitation: 488 nm, emission: 585 ± 21 nm (PE channel), gain: 420 V;
compound **2.3**, excitation: 633 nm, emission: 660 ± 10 nm (APC channel), gain: 350 V.

All measurements were performed in duplicate and data acquisition was stopped after 10 000 gated events.

Preparation of the HEK293T-hH_2R-qs5-HA cells was performed as described[29] with minor modifications – in detail: on the day of the experiment, HEK293T-hH_2R-qs5-HA cells were detached from the cell culture flasks by trypsinization and centrifuged (500 *g*, 5 min). The cell pellet was resuspended in L-15 containing 1% FCS and the cell density was adjusted to $1 \cdot 10^6$ cells/mL. Serial dilutions of the fluorescent ligands **2.1**-**2.3** and famotidine (non-specific binding) were prepared in DMSO/H_2O (1:1, v/v). All incubation steps were performed in 96-well Primaria™ plates (Corning, NY, USA). 200 µL of the adjusted cell suspension were either added to 2 µL of DMSO/H_2O (1:1, v/v, total binding) or a solution of famotidine (non-specific binding, 300-fold excess over the respective concentration of fluorescent ligand). Incubation was subsequently started after adding 2 µL of a solution of the respective fluorescent ligand in different concentrations (100-fold more concentrated than the final assay concentration). The Primaria™ plate was shaken at rt in the dark for 60 min. Samples were then transferred to 5 mL polystyrol tubes (Sarstedt, Nümbrecht, Germany) and measured immediately. Raw data were processed with FACSDiva™ Software (Becton Dickinson, Heidelberg, Germany) to calculate the geometric mean values of the areas corresponding to the fluorescence signals in the respective channels. The obtained geometric mean values were plotted against the fluorescent ligand concentration. Total and non-specific binding were fitted simultaneously using the "one site-total and nonspecific binding" model (Prism 8.0). Specific binding was analyzed by an equation describing hyperbolic binding ("one site-specific binding", Prism 8.0) yielding K_d values. K_d values were transformed into pK_d values, for which means and SEMs were calculated.

2.2.6 β-arrestin2 recruitment assay

β-arrestin2 recruitment was assessed in a split luciferase-based assay using HEK293T-ARRB2-H_2R cells stably expressing the H_2R-ELucC and ELucN-ARRB2 fusion proteins.[30] The experiments were performed according to a described procedure[30] with slight modifications – in detail: One day before the experiment, the cells were detached by trypsinization and centrifuged (500 *g*, 5 min). The cell pellet was resuspended in L-15 supplemented with 5% FCS and 10 mM HEPES (pH 7.4), and the cell density was adjusted to $1.25 \cdot 10^6$ cells/mL (agonist mode) or $1.4 \cdot 10^6$ cells/mL (antagonist mode). 80 µL (agonist mode) or 70 µL (antagonist mode) of the adjusted cell suspension were seeded into a white 96-well plate (Brand, Wertheim, Germany) and the cells were incubated overnight in a humidified atmosphere (37 °C, no additional CO_2).
For the determination of agonism, 10 µL of a solution of D-luciferin monopotassium salt (Fisher Scientific, Nidderau, Germany) in L-15 with 10 mM HEPES (pH 7.4) (c_{final} = 1 mM) were added per well and bioluminescence was measured for 15 min at 37 °C with an integration time of 1 s

(baseline read) using an EnSpire plate reader (PerkinElmer, Rodgau, Germany). In the meantime, serial dilutions of the investigated compounds (10-fold more concentrated than the final assay concentration) were prepared in L-15 with 10 mM HEPES (pH 7.4) and pre-warmed to 37 °C. After the baseline-read, the dilutions of the test compounds (10 µL/well) were added to the cells. Bioluminescence was measured for 50 min at 37 °C with an integration time of 1 s. The obtained peak luminescence values were normalized to the maximal response induced by 1 mM histamine (100% value) and a negative control (neat buffer, 0% value).

For the determination of antagonism, the dilutions of the test compounds (10 µL/well) were added to the cells directly after the addition of a solution of D-luciferin (10 µL/well, c_{final} = 1 mM) and the baseline was recorded as described for the agonist mode. Subsequently, 10 µL of a solution of histamine (c_{final} = 8 µM) were added per well and bioluminescence was measured for 50 min as described above. Resulting peak luminescence values were normalized to the effect induced by 8 µM histamine (100% value) and a negative control (neat buffer, 0% value). Data were analyzed by a four-parameter logistic equation (Prism 8.0) yielding pIC_{50} values, which were transformed into pK_b values by applying the Cheng-Prusoff equation.[33] Means and SEMs were calculated for the respective pK_b values.

2.2.7 BRET binding assay

HEK293T cells stably expressing the NLuc-H_2R were detached from the cell culture flasks after reaching approx. 80% confluency by trypsinization. After centrifugation (600 *g*, 5 min), the cell pellet was resuspended in L-15 with 5% FCS and 10 mM HEPES (pH 7.4), and $1 \cdot 10^5$ cells were seeded in a volume of 70 µL (saturation and competition binding) or 80 µL (kinetic experiments) per well into white 96-well plates (Brand, Wertheim, Germany). The cells were incubated overnight at 37 °C in a humidified atmosphere (no additional CO_2). All serial dilutions of the fluorescent ligands and competitors (10-fold more concentrated than the final assay concentration) were prepared in L-15 supplemented with 10 mM HEPES (pH 7.4) and 2% BSA (assay buffer).

For saturation binding experiments, 10 µL of the dilutions of the tested fluorescent ligands **2.1**-**2.3** and 10 µL of assay buffer (total binding) or assay buffer containing famotidine (non-specific binding, 300-fold excess over the respective concentration of fluorescent ligand) were added to the cells. After incubating the cells for 60 min at 27 °C, 10 µL of the substrate furimazine (Nano-Glo® Live Cell Substrate), which was diluted according to the manufacturer's protocol beforehand, were added. After 5 minutes of equilibration inside the plate reader (pre-warmed to 27 °C), the measurement was started.

For competition binding experiments, 10 µL of a solution of the tested competitor (varying concentrations) and 10 µL of a solution of **2.1** (one fixed concentration, c_{final} = 50 nM) were added to the cells at the same time. A 100% control containing the fluorescent ligand but no competitor as well as a solvent control (0% value) were included in each experiment for normalization purposes. After incubating the cells at 27 °C for 60 min, the substrate was added and the measurement was started as described above.

Kinetic measurements were performed as follows: 10 µL of assay buffer (for total binding) or a solution of famotidine (non-specific binding, 300-fold excess over the used concentration of **2.1**, c_{final}(famotidine) = 15 µM) were added to the cells. After the addition of 10 µL of the substrate furimazine (Nano-Glo® Live Cell Substrate, pre-diluted according to the manufacturer's instructions), the plate was placed inside the plate reader (pre-warmed to 27 °C) for 5 min to equilibrate. To start the association, 50 µL of a 3-fold concentrated solution (with respect to the final assay concentration) of the fluorescent ligand **2.1** (c_{final} = 50 nM) were added to the cells and the association was measured for 60 min. Dissociation experiments were conducted in wells, which were prepared as described for association experiments (preincubated with **2.1** for 60 min; c_{final} = 50 nM). To initiate dissociation, 50 µL of a 4-fold concentrated solution (with respect to the final concentration) of famotidine (c_{final} = 15 µM) were added to the cells and after the addition of the substrate, dissociation was measured for 4 h (final well volume: 200 µL).

All BRET measurements were performed at 27 °C using a TECAN InfiniteLumi or a TECAN GENiosPro plate reader (TECAN Austria GmbH, Grödig, Austria). The bioluminescence signal was detected using the pre-equipped 460 ± 35 nm (460/35BP, InfiniteLumi) or 460 ± 50 nm band-pass (460/50BP, GENiosPro) filter. The emission of the fluorescent ligand was detected through a 610 nm long-pass (610LP) filter with both plate readers. For equilibrium measurements, the integration time was set to 100 ms for both channels. For kinetic experiments, the integration time was increased to 500 ms for both channels to reduce noise.

"Raw BRET ratios" were calculated by the following equation:

$$raw\ BRET\ ratio = \frac{emission\ (fluorescent\ acceptor, 610\mathrm{LP})}{emission\ (bioluminescent\ donor, 460\mathrm{BP})}$$

For all BRET experiments, "corrected BRET ratios" were obtained by subtracting the BRET ratio of a buffer control.

All data from BRET experiments were analyzed using Prism 8.0. For saturation binding experiments, total and non-specific binding were analyzed simultaneously applying the "one site-total and nonspecific binding" fit (Prism 8.0). Specific binding was analyzed by an equation describing hyperbolic binding ("one site-specific binding", Prism 8.0) yielding K_d values. These were transformed into pK_d values, for which means and SEMs were calculated.

Data from association experiments with the fluorescent ligand **2.1** were analyzed by an equation for monophasic association (Prism 8.0), yielding the observed association rate constant k_{obs}, whereas data from dissociation experiments were analyzed by an equation for monoexponential decay (Prism 8.0) yielding the dissociation rate constant k_{off}. The association rate constant k_{on} was calculated using the following equation:

$$k_{\mathrm{on}} = \frac{k_{\mathrm{obs}} - k_{\mathrm{off}}}{c(ligand)}$$

, where c(ligand) represents the used concentration of the fluorescent ligand (here: c(**2.1**) = 50 nM). The kinetically derived dissociation constant $K_d^{kinetic}$ was calculated as follows:

$$K_{\mathrm{d}}^{\mathrm{kinetic}} = \frac{k_{\mathrm{off}}}{k_{\mathrm{on}}}$$

The obtained $K_d^{kinetic}$ value was then transformed into a $pK_d^{kinetic}$ value.

Error propagation (specific binding, k_{on}, $K_d^{kinetic}$ and $pK_d^{kinetic}$) was performed according to the following formula:

$$\Delta z = \sqrt{\left(\frac{\partial f}{\partial x_1}\right)^2 \Delta x_1^2 + \left(\frac{\partial f}{\partial x_2}\right)^2 \Delta x_2^2 + \cdots}$$

,where f is the function of x_1, x_2,… ($f(x_1, x_2,\ldots) = z$) and Δx_1, Δx_2,… are errors of x_1, x_2,…; Δz consequently represents the propagated error of z.

For competition binding experiments, data were normalized to a solvent control (0% value) and a 100% control solely containing fluorescent ligand but no competitor. The normalized data were then analyzed by a four-parameter logistic fit (Prism 8.0) yielding pIC_{50} values. These were transformed into pK_i values using the Cheng-Prusoff equation.[33] Means and SEMs were calculated for the pK_i values.

2.3 Results and discussion

2.3.1 BRET saturation binding experiments at the NLuc-H_2R

To investigate the suitability of the differently fluorescence-labeled ligands **2.1**-**2.3** for the new binding assay, BRET saturation binding experiments were performed at the NLuc-H_2R, stably expressed in intact HEK293T cells. To prevent the adsorption of the fluorescent ligands to the plate material or plastic vessels during the experiment, the buffer used for all serial dilutions was supplemented with 2% bovine serum albumin (BSA) (see Appendix Figure A2). As depicted in Figure 2.2, binding was saturable for all compounds. The corresponding equilibrium dissociation constants (pK_d values) are listed in Table 2.1. The highest affinity was observed for the BODIPY 630/650-labeled ligand **2.3** (UR-KAT514, pK_d ± SEM = 8.59 ± 0.08) followed by **2.1** (UR-KAT478, Py-1-labeled, pK_d ± SEM = 7.35 ± 0.09) and **2.2** (UR-KAT515, TAMRA-labeled, pK_d ± SEM = 6.84 ± 0.06). These values were in accordance with the results from canonical binding assays, such as radioligand competition binding experiments (see Appendix Figure A3) or flow cytometric saturation binding experiments (see Appendix Figure A4), and with results from a split luciferase-based β-arrestin2 recruitment assay, in which all three fluorescent ligands showed antagonistic behavior (see Appendix Figure A5, cf. Table 2.1).

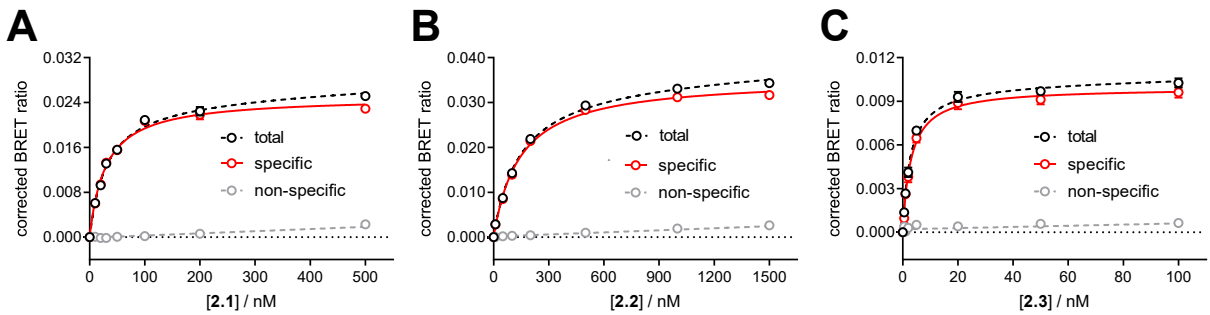

Figure 2.2: Binding isotherms from BRET saturation binding experiments with **2.1** (**A**), **2.2** (**B**) and **2.3** (**C**) at intact HEK293T cells stably expressing the NLuc-H_2R. Non-specific binding was assessed in the presence of an excess of famotidine (300-fold over the respective concentration of fluorescent ligand). Data represent means (total and non-specific binding) or calculated values (specific binding) ± errors of one representative experiment from a set of three independent experiments, each performed in triplicate. Error bars of total and non-specific binding represent the SEM, whereas error bars of specific binding represent propagated errors.

However, **2.3** only showed a moderate signal-to-background ratio (S/B ratio, Figure 2.2C), whereas a higher BRET ratio was observed for ligands **2.1** and **2.2** (Figure 2.2A and 2.2B), which makes them more suitable as BRET acceptors for screening purposes. Due to the higher binding affinity compared to **2.2**, the Py-1-labeled ligand **2.1** was used for further experiments, as it represented the best compromise with respect to S/B ratio and binding affinity in the BRET binding assay.

Table 2.1: Dissociation constants of the fluorescent ligands **2.1**-**2.3** determined in binding and functional assays at the H_2R.

Compound	BRET binding assay		Radioligand comp. binding		Flow cytometry		β-arrestin2 recruitment	
	pK_d[a]	*N*	pK_i[b]	*N*	pK_d[c]	*N*	pK_b[d]	*N*
2.1	7.35 ± 0.09	3	7.62 ± 0.06	3	7.13 ± 0.03	3	7.78 ± 0.15	6
2.2	6.84 ± 0.06	3	7.00 ± 0.10	4	6.25 ± 0.01	3	7.18 ± 0.13	5
2.3	8.59 ± 0.08	3	8.35 ± 0.05	3	7.86 ± 0.14	3	8.09 ± 0.04	3

[a]Determined by BRET saturation binding experiments performed at intact HEK293T cells stably expressing the NLuc-H_2R; data represent means ± SEM from *N* independent experiments, each performed in triplicate. [b]Determined by radioligand competition binding experiments with [^{3}H]UR-DE257 (c = 20 nM, K_d = 11.2 nM) using membrane preparations of Sf9 insect cells expressing the hH_2R-G$s\alpha_s$ fusion protein; data represent means ± SEM from *N* independent experiments, each performed in triplicate. [c]Determined by flow cytometric saturation binding experiments at HEK293T-hH_2R-qs5-HA cells; data represent means ± SEM from *N* independent experiments, each performed in duplicate. [d]Determined by inhibition of the response induced by histamine (c = 8 µM, EC_{50} = 3.8 µM) in a split luciferase-based β-arrestin2 recruitment assay at HEK293T-ARRB2-H_2R cells; data represent means ± SEM from *N* independent experiments, each performed in triplicate.

2.3.2 Kinetic BRET binding experiments with the fluorescent ligand 2.1

For a further characterization of **2.1**, real-time kinetic binding experiments were conducted (Figure 2.3) at intact HEK293T cells stably expressing the NLuc-H_2R. The fluorescent ligand (c(**2.1**) = 50 nM) was fully bound to the receptor after approx. 30 min (see Figure 2.3A). After the cells had been preincubated with **2.1** for 60 min (c = 50 nM), dissociation was initiated by the addition of an excess of famotidine (300-fold excess over the used concentration of **2.1**, c(famotidine) = 15 µM). **2.1** showed a slow dissociation from the receptor (Figure 2.3B) and only a small amount of **2.1** was displaced after 4 h (≈ 35-40%). A similar behavior was reported for the structurally related radioligand [^{3}H]UR-DE257, leading to the assumption that the pharmacological scaffold is responsible for this type of binding kinetics.[28] The kinetic parameters describing the binding of **2.1** to the NLuc-H_2R are summarized in Table 2.2.

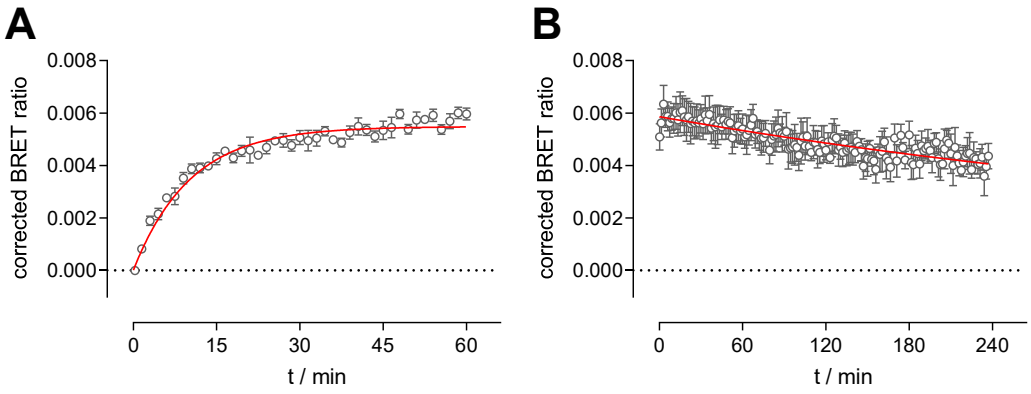

Figure 2.3: Association (**A**) and dissociation (**B**) kinetics of the fluorescent ligand **2.1** obtained from BRET binding experiments at intact HEK293T cells stably expressing the NLuc-H_2R. Association (**A**) was started by the addition of **2.1** (c = 50 nM). Dissociation (**B**) was initiated by the addition of famotidine (300-fold excess over the concentration of **2.1**, c(famotidine) = 15 µM) to cells, which were preincubated with **2.1** (c = 50 nM) for 60 min. Data are shown as means ± propagated errors of one representative experiment from a set of four independent experiments, each performed in triplicate.

Table 2.2: Kinetic constants of the fluorescent ligand **2.1** obtained from BRET binding experiments at the NLuc-H_2R.

Compound	k_{obs} [min^{-1}][a]	k_{off} [min^{-1}][b]	k_{on} [min^{-1} nM^{-1}][c]	p$K_d^{kinetic}$, [d]
2.1	0.093 ± 0.009	0.0023 ± 0.0002	0.0018 ± 0.0002	8.89 ± 0.05

[a-d]Determined by kinetic BRET binding experiments at intact HEK293T cells stably expressing the NLuc-H_2R; data originate from four independent experiments performed in triplicate. [a]Observed association rate constant (k_{obs}) ± SEM describing the association of **2.1** to the NLuc-H_2R (c(**2.1**) =50 nM). [b]Dissociation rate constant (k_{off}) ± SEM. [c]Association rate constant (k_{on}) ± propagated error, calculated using k_{obs}, k_{off} and the used concentration of **2.1** (c = 50 nM) (k_{on} = (k_{obs} - k_{off}) / c(ligand)). [d]Kinetically derived dissociation constant ($K_d^{kinetic}$ = k_{off} / k_{on}; transformed into a p$K_d^{kinetic}$ value) ± propagated error.

2.3.3 BRET competition binding experiments at the NLuc-H_2R

To show the versatility of the presented assay, we performed BRET competition binding experiments with **2.1** (c = 50 nM) and different reported H_2 receptor agonists and antagonists (for structures, see Appendix Figure A1). Despite the slow dissociation kinetics of the fluorescent ligand **2.1**, all competitive ligands were able to displace the fluorescent tracer completely from the NLuc-H_2R (Figure 2.4). Notably, the displacement curves from the experiments with histamine showed a markedly flatter slope (slope ± SEM = -0.55 ± 0.03, N = 5) compared to the displacement curves obtained for the other competitive ligands. The flatter slope might indicate the existence of a second receptor affinity state, which has been described previously for the hH_2R.[34] However, this hypothesis was not supported by the data from competition binding experiments with an extended set of histamine concentrations (see Appendix Figure A6) and monophasic binding was assumed for all investigated compounds. The pK_i values obtained from the BRET competition binding experiments with **2.1** are listed in Table 2.3. The determined pK_i values were in good agreement with literature-described data from radioligand binding experiments using membrane preparations of CHO cells expressing the hH_2R.[34] However, they showed a larger deviation from data acquired using membrane preparations of Sf9 insect cells expressing the hH_2R-Gsα$_s$ fusion protein.[28] It is conspicuous that the investigated agonists (histamine, UR-Po444 and UR-Po448) showed higher affinities at Sf9 membranes, whereas the tested antagonists/inverse agonists (cimetidine, ranitidine and famotidine) exhibited lower affinities (cf. Table 2.3), when compared to the results from the BRET binding assay. A possible explanation for this observation could be the direct fusion of the hH_2R with the Gsα$_s$. Thereby, the receptor is permanently in an active receptor conformation, which favors agonist binding.[35] In contrast, inverse agonists or antagonists have a preference for an inactive receptor conformation or have no preferred receptor state at all. This could lead to the lower apparent affinities of cimetidine, ranitidine and famotidine at the hH_2R-Gsα$_s$, as these ligands were also described as inverse agonists at the hH_2R.[36-38]

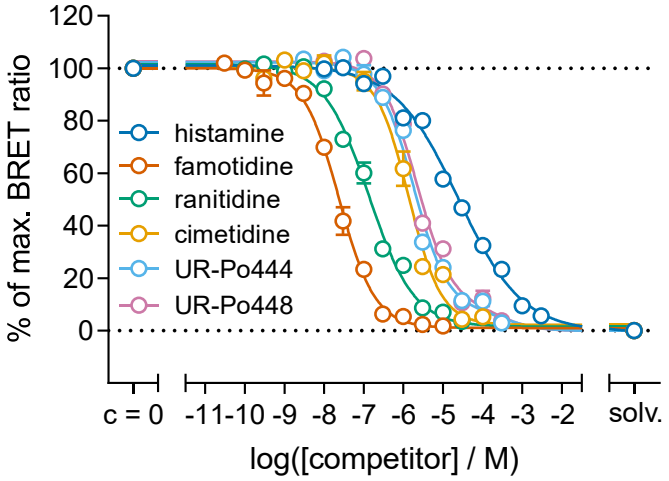

Figure 2.4: Displacement curves from BRET competition binding experiments with **2.1** (c = 50 nM) and reported H_2R ligands. Experiments were performed at intact HEK293T cells stably expressing the NLuc-H_2R. Data are shown as means ± SEM from four to five independent experiments, each performed in triplicate; solv.: solvent control.

Another explanation for the discrepancy in the determined pK_i values, which is particularly evident for histamine, is the allosteric effect of sodium on agonist binding to several GPCRs.[39]

In contrast to the BRET binding assay and the reported radioligand binding experiments at CHO membranes,[34] the buffer routinely used for radioligand binding experiments on membrane preparations of Sf9 cells expressing the hH_2R-G$s\alpha_s$ fusion protein is devoid of sodium ions.[32] To investigate the potential effect of sodium on the apparent binding affinity of histamine at the hH_2R, we changed the assay procedure for radioligand competition binding experiments on Sf9 cell membranes by adding sodium at a physiological concentration (c = 145 mM) to the binding buffer. This modification of the assay procedure resulted in an ≈ 100-fold decrease in affinity for histamine (pK_i ± SEM = 4.37 ± 0.02 (cf. Table 2.3)), which was now in good agreement with the results from the BRET binding assay. This result further suggested that, especially for agonists,[39] the presence or absence of sodium in the used buffer must be considered when comparing data from different binding assays.

Table 2.3: Binding data (pK_i values) of reported H_2R ligands from BRET competition binding experiments with **2.1** at the NLuc-H_2R.

Compound	BRET binding assay		Radioligand comp. binding Sf9 membranes		Radioligand comp. binding CHO membranes
	pK_i[a]	*N*	pK_i	*N*	pK_i[e]
histamine	4.96 ± 0.09	5	6.27[b], 4.37 ± 0.02[d]	3	4.10, 5.69
cimetidine	6.31 ± 0.14	4	5.56 ± 0.14[c]	3	6.18
ranitidine	7.20 ± 0.09	4	5.76[b]	---	7.07
famotidine	7.94 ± 0.04	5	6.87[b]	---	7.80
UR-Po444	6.00 ± 0.09	4	6.60 ± 0.08[c]	3	n.d.
UR-Po448	5.89 ± 0.09	4	6.34 ± 0.04[c]	3	n.d.

[a]Determined by BRET competition binding experiments with **2.1** (c = 50 nM, K_d = 44.8 nM) at intact HEK293T cells stably expressing the NLuc-H_2R; data represent means ± SEM from *N* independent experiments, each performed in triplicate. [b]Baumeister *et al.*[28] [c]Determined by radioligand competition binding experiments with [^{3}H]UR-DE257 (c = 20 nM, K_d = 11.2 nM) using membrane preparations of Sf9 insect cells stably expressing the hH_2R-G$s\alpha_s$ fusion protein; data represent means ± SEM from *N* independent experiments performed in triplicate. [d]Determined in analogy to [c], but with the addition of NaCl (c = 145 mM) to the binding buffer; value represents mean ± SEM from *N* independent experiments performed in triplicate. [e]Leurs *et al.*[34]; data originate from radioligand competition binding experiments with [^{125}I]-iodoaminopotentidine using membrane preparations of CHO cells expressing the hH_2R; the two indicated values for histamine represent the pK_i values for the high- and low-affinity state of the hH_2R, respectively. n.d.: not determined.

2.4 Conclusion

In this study we report the development of a BRET binding assay for the human histamine H_2 receptor. As a homogeneous and live cell-based method, the BRET binding assay allows for the convenient determination of affinity constants of putative H_2R ligands, independent of their quality of action without any washing or separation steps. The results from the presented BRET binding assay, for both fluorescently labeled and unlabeled ligands, compared well with other currently used radioactivity- or fluorescence-based (e.g. flow cytometry) binding assays. It is a prerequisite for the establishment of such assays to have access to suitable fluorescent ligands. Three differently fluorescence-labeled compounds were tested in BRET saturation binding experiments at the NLuc-H_2R and all of them have proven to be generally usable. In this study, the Py-1-labeled compound **2.1** turned out to be the best compromise with respect to binding affinity and S/B ratio and was successfully used for further investigations in kinetic and competition binding experiments. BRET binding assays have hitherto only been described for the $H_{1,3,4}Rs$,[19,21] making this study close the gap of BRET binding assays within the histamine receptor family. Thus, selectivity studies, which are essential for the development of new drug candidates, can be carried out based on the same assay principle, which significantly increases the comparability of results. All in all, this study showed that the BRET binding assay is a valuable test system for the histamine H_2 receptor and provides a novel fluorescence-based alternative to other conventional binding assays.

2.5 References

1. Black, J. W., Duncan, W. A., Durant, C. J., Ganellin, C. R. & Parsons, E. M. Definition and antagonism of histamine H_2-receptors. *Nature* **236**, 385-390, doi:10.1038/236385a0 (1972).

2. Lagerström, M. C. & Schiöth, H. B. Structural diversity of G protein-coupled receptors and significance for drug discovery. *Nat. Rev. Drug Discov.* **7**, 339-357, doi:10.1038/nrd2518 (2008).

3. Panula, P., Chazot, P. L., Cowart, M., Gutzmer, R., Leurs, R., Liu, W. L. S., Stark, H., Thurmond, R. L. & Haas, H. L. International Union of Basic and Clinical Pharmacology. XCVIII. Histamine receptors. *Pharmacol. Rev.* **67**, 601-655, doi:10.1124/pr.114.010249 (2015).

4. Schwartz, J. C., Pollard, H. & Quach, T. T. Histamine as a neurotransmitter in mammalian brain: neurochemical evidence. *J. Neurochem.* **35**, 26-33, doi:10.1111/j.1471-4159.1980.tb12485.x (1980).

5. van der Goot, H. & Timmerman, H. Selective ligands as tools to study histamine receptors. *Eur. J. Med. Chem.* **35**, 5-20, doi:10.1016/s0223-5234(00)00101-x (2000).

6. Pockes, S., Wifling, D., Keller, M., Buschauer, A. & Elz, S. Highly potent, stable, and selective dimeric hetarylpropylguanidine-type histamine H_2 receptor agonists. *ACS Omega* **3**, 2865-2882, doi:10.1021/acsomega.8b00128 (2018).

7. Darras, F. H., Pockes, S., Huang, G., Wehle, S., Strasser, A., Wittmann, H. J., Nimczick, M., Sotriffer, C. A. & Decker, M. Synthesis, biological evaluation, and computational studies of tri- and tetracyclic nitrogen-bridgehead compounds as potent dual-acting AChE inhibitors and hH_3 receptor antagonists. *ACS Chem. Neurosci.* **5**, 225-242, doi:10.1021/cn4002126 (2014).

8. Khan, N., Saad, A., Nurulain, S. M., Darras, F. H., Decker, M. & Sadek, B. The dual-acting H3 receptor antagonist and AChE inhibitor UW-MD-71 dose-dependently enhances memory retrieval and reverses dizocilpine-induced memory impairment in rats. *Behav. Brain Res.* **297**, 155-164, doi:10.1016/j.bbr.2015.10.022 (2016).

9. Sadek, B., Khan, N., Darras, F. H., Pockes, S. & Decker, M. The dual-acting AChE inhibitor and H_3 receptor antagonist UW-MD-72 reverses amnesia induced by scopolamine or dizocilpine in passive avoidance paradigm in rats. *Physiol. Behav.* **165**, 383-391, doi:10.1016/j.physbeh.2016.08.022 (2016).

10. Paton, W. D. & Rang, H. P. The uptake of atropine and related drugs by intestinal smooth muscle of the guinea-pig in relation to acetylcholine receptors. *Proc. R. Soc. Lond. B Biol. Sci.* **163**, 1-44, doi:10.1098/rspb.1965.0058 (1965).

11. Stoddart, L. A., White, C. W., Nguyen, K., Hill, S. J. & Pfleger, K. D. Fluorescence- and bioluminescence-based approaches to study GPCR ligand binding. *Br. J. Pharmacol.* **173**, 3028-3037, doi:10.1111/bph.13316 (2016).

12. Stoddart, L. A., Johnstone, E. K. M., Wheal, A. J., Goulding, J., Robers, M. B., Machleidt, T., Wood, K. V., Hill, S. J. & Pfleger, K. D. G. Application of BRET to monitor ligand binding to GPCRs. *Nat. Methods* **12**, 661-663, doi:10.1038/nmeth.3398 (2015).

13. Stoddart, L. A., Kilpatrick, L. E. & Hill, S. J. NanoBRET approaches to study ligand binding to GPCRs and RTKs. *Trends Pharmacol. Sci.* **39**, 136-147, doi:10.1016/j.tips.2017.10.006 (2018).

14. Christiansen, E., Hudson, B. D., Hansen, A. H., Milligan, G. & Ulven, T. Development and characterization of a potent free fatty acid receptor 1 (FFA1) fluorescent tracer. *J. Med. Chem.* **59**, 4849-4858, doi:10.1021/acs.jmedchem.6b00202 (2016).

15. Conroy, S., Kindon, N. D., Glenn, J., Stoddart, L. A., Lewis, R. J., Hill, S. J., Kellam, B. & Stocks, M. J. Synthesis and evaluation of the first fluorescent antagonists of the human $P2Y_2$ receptor based on AR-C118925. *J. Med. Chem.* **61**, 4272, doi:10.1021/acs.jmedchem.8b00606 (2018).

16. Hansen, A. H., Sergeev, E., Pandey, S. K., Hudson, B. D., Christiansen, E., Milligan, G. & Ulven, T. Development and characterization of a fluorescent tracer for the free fatty acid receptor 2 (FFA2/GPR43). *J. Med. Chem.* **60**, 5638-5645, doi:10.1021/acs.jmedchem.7b00338 (2017).

17. Hoare, B. L., Bruell, S., Sethi, A., Gooley, P. R., Lew, M. J., Hossain, M. A., Inoue, A., Scott, D. J. & Bathgate, R. A. D. Multi-component mechanism of H2 relaxin binding to RXFP1 through NanoBRET kinetic analysis. *iScience* **11**, 93-113, doi:10.1016/j.isci.2018.12.004 (2019).

18. Kozielewicz, P., Bowin, C. F., Turku, A. & Schulte, G. A NanoBRET-based binding assay for Smoothened allows real-time analysis of ligand binding and distinction of two binding sites for BODIPY-cyclopamine. *Mol. Pharmacol.* **97**, 23-34, doi:10.1124/mol.119.118158 (2020).

19. Mocking, T. A. M., Verweij, E. W. E., Vischer, H. F. & Leurs, R. Homogeneous, real-time NanoBRET binding assays for the histamine H_3 and H_4 receptors on living cells. *Mol. Pharmacol.* **94**, 1371-1381, doi:10.1124/mol.118.113373 (2018).

20. Sakyiamah, M. M., Nomura, W., Kobayakawa, T. & Tamamura, H. Development of a NanoBRET-based sensitive screening method for CXCR4 ligands. *Bioconjug. Chem.* **30**, 1442-1450, doi:10.1021/acs.bioconjchem.9b00182 (2019).

21. Stoddart, L. A., Vernall, A. J., Bouzo-Lorenzo, M., Bosma, R., Kooistra, A. J., de Graaf, C., Vischer, H. F., Leurs, R., Briddon, S. J., Kellam, B. & Hill, S. J. Development of novel fluorescent histamine H_1-receptor antagonists to study ligand-binding kinetics in living cells. *Sci. Rep.* **8**, 1572, doi:10.1038/s41598-018-19714-2 (2018).

22. Wang, J. H., Shao, X. X., Hu, M. J., Wei, D., Liu, Y. L., Xu, Z. G. & Guo, Z. Y. A novel BRET-based binding assay for interaction studies of relaxin family peptide receptor 3 with its ligands. *Amino Acids* **49**, 895-903, doi:10.1007/s00726-017-2387-4 (2017).

23. White, C. W., Johnstone, E. K. M., See, H. B. & Pfleger, K. D. G. NanoBRET ligand binding at a GPCR under endogenous promotion facilitated by CRISPR/Cas9 genome editing. *Cell. Signal.* **54**, 27-34, doi:10.1016/j.cellsig.2018.11.018 (2019).

24. Wu, Q. P., Zhang, L., Shao, X. X., Wang, J. H., Gao, Y., Xu, Z. G., Liu, Y. L. & Guo, Z. Y. Application of the novel bioluminescent ligand-receptor binding assay to relaxin-RXFP1 system for interaction studies. *Amino Acids* **48**, 1099-1107, doi:10.1007/s00726-015-2146-3 (2016).

25. Soave, M., Stoddart, L. A., Brown, A., Woolard, J. & Hill, S. J. Use of a new proximity assay (NanoBRET) to investigate the ligand-binding characteristics of three fluorescent ligands to the human β_1-adrenoceptor expressed in HEK-293 cells. *Pharmacol. Res. Perspect.* **4**, e00250, doi:10.1002/prp2.250 (2016).

26. Sridharan, R., Zuber, J., Connelly, S. M., Mathew, E. & Dumont, M. E. Fluorescent approaches for understanding interactions of ligands with G protein coupled receptors. *Biochim. Biophys. Acta Biomembr.* **1838**, 15-33, doi:10.1016/j.bbamem.2013.09.005 (2014).

27. Hall, M. P., Unch, J., Binkowski, B. F., Valley, M. P., Butler, B. L., Wood, M. G., Otto, P., Zimmerman, K., Vidugiris, G., Machleidt, T., Robers, M. B., Benink, H. A., Eggers, C. T., Slater, M. R., Meisenheimer, P. L., Klaubert, D. H., Fan, F., Encell, L. P. & Wood, K. V. Engineered luciferase reporter from a deep sea shrimp utilizing a novel imidazopyrazinone substrate. *ACS Chem. Biol.* **7**, 1848-1857, doi:10.1021/cb3002478 (2012).

28. Baumeister, P., Erdmann, D., Biselli, S., Kagermeier, N., Elz, S., Bernhardt, G. & Buschauer, A. [^{3}H]UR-DE257: development of a tritium-labeled squaramide-type selective histamine H_2 receptor antagonist. *ChemMedChem* **10**, 83-93, doi:10.1002/cmdc.201402344 (2015).

29. Mosandl, J. Radiochemical and luminescence-based binding and functional assays for human histamine receptors using genetically engineered cells, PhD Thesis, University of Regensburg (2009). https://epub.uni-regensburg.de/12335/

30. Felixberger, J. Luciferase complementation for the determination of arrestin recruitment: investigations at histamine and NPY receptors, PhD Thesis, University of Regensburg (2014). https://epub.uni-regensburg.de/31292/

31. Pop, N., Igel, P., Brennauer, A., Cabrele, C., Bernhardt, G. N., Seifert, R. & Buschauer, A. Functional reconstitution of human neuropeptide Y (NPY) Y_2 and Y_4 receptors in Sf9 insect cells. *J. Recept. Signal Transduct. Res.* **31**, 271-285, doi:10.3109/10799893.2011.583253 (2011).

32. Kagermeier, N., Werner, K., Keller, M., Baumeister, P., Bernhardt, G., Seifert, R. & Buschauer, A. Dimeric carbamoylguanidine-type histamine H_2 receptor ligands: a new class of potent and selective agonists. *Bioorg. Med. Chem.* **23**, 3957-3969, doi:10.1016/j.bmc.2015.01.012 (2015).

33. Cheng, Y. & Prusoff, W. H. Relationship between the inhibition constant (K_i) and the concentration of inhibitor which causes 50 per cent inhibition (I_{50}) of an enzymatic reaction. *Biochem. Pharmacol.* **22**, 3099-3108, doi:10.1016/0006-2952(73)90196-2 (1973).

34. Leurs, R., Smit, M. J., Menge, W. M. & Timmerman, H. Pharmacological characterization of the human histamine H_2 receptor stably expressed in Chinese hamster ovary cells. *Br. J. Pharmacol.* **112**, 847-854, doi:10.1111/j.1476-5381.1994.tb13157.x (1994).

35. De Lean, A., Stadel, J. M. & Lefkowitz, R. J. A ternary complex model explains the agonist-specific binding properties of the adenylate cyclase-coupled β-adrenergic receptor. *J. Biol. Chem.* **255**, 7108-7117 (1980).

36. Alewijnse, A. E., Smit, M. J., Hoffmann, M., Verzijl, D., Timmerman, H. & Leurs, R. Constitutive activity and structural instability of the wild-type human H_2 receptor. *J. Neurochem.* **71**, 799-807, doi:10.1046/j.1471-4159.1998.71020799.x (1998).

37. Preuss, H., Ghorai, P., Kraus, A., Dove, S., Buschauer, A. & Seifert, R. Constitutive activity and ligand selectivity of human, guinea pig, rat, and canine histamine H_2 receptors. *J. Pharmacol. Exp. Ther.* **321**, 983-995, doi:10.1124/jpet.107.120014 (2007).

38. Preuss, H., Ghorai, P., Kraus, A., Dove, S., Buschauer, A. & Seifert, R. Mutations of Cys-17 and Ala-271 in the human histamine H_2 receptor determine the species selectivity of guanidine-type agonists and increase constitutive activity. *J. Pharmacol. Exp. Ther.* **321**, 975-982, doi:10.1124/jpet.107.120519 (2007).

39. Katritch, V., Fenalti, G., Abola, E. E., Roth, B. L., Cherezov, V. & Stevens, R. C. Allosteric sodium in class A GPCR signaling. *Trends Biochem. Sci.* **39**, 233-244, doi:10.1016/j.tibs.2014.03.002 (2014).

3. BRET- and fluorescence anisotropy-based assays for real-time monitoring of ligand binding to M_2 muscarinic acetylcholine receptors

Note: Prior to the submission of this thesis, the content of this chapter was published in collaboration with partners:

Grätz, L.; Laasfeld, T; Allikalt, A.; Gruber, C. G.; Pegoli, A.; Tahk, M.-J.; Tsernant, M.-L.; Keller, M.; Rinken, A. BRET- and fluorescence anisotropy-based assays for real-time monitoring of ligand binding to M_2 muscarinic acetylcholine receptors. *Biochim. Biophys. Acta Mol. Cell Res.* **1868**, 118930, doi:10.1016/j.bbamcr.2020.118930 (2021).

The following experimental work was performed by co-authors:

T. Laasfeld:	Global analysis of data from FA experiments
Dr. A. Allikalt:	Generation of budded baculoviruses; establishment of the FA binding assay for **3.2**; FA binding experiments with **3.2**
C. Gruber:	Synthesis of the fluorescent ligands **3.1**, **3.4**, **3.6**-**3.8** (not shown)
Dr. A. Pegoli:	Synthesis of the fluorescent ligands **3.3** and **3.5** (not shown)
PD Dr. M. Keller:	Synthesis of the fluorescent ligand **3.2** (not shown)
M.-L. Tsernant:	Radioligand saturation binding experiments on baculoviruses
M.-J. Tahk:	Generation of budded baculoviruses; FA binding experiments with **3.2**

3.1 Introduction

A particularly important step in the development of novel ligands for GPCRs is to characterize them in terms of their binding properties. Representing an attractive alternative to radioligand binding assays,[1] fluorescence-based techniques have gained popularity in this context during the last decade.[2,3] Classical radioligand binding experiments have to be performed in a heterogeneous manner, i.e. the receptor-bound ligand has to be separated from the unbound ligand,[4] precluding equilibrium conditions during the measurement. In contrast, most of the fluorescence-based techniques can be used in homogeneous assay setups ("mix-and-read"[5]) to assess ligand binding at equilibrium and in kinetic analyses. Furthermore, the use of radiolabeled compounds has some practical and financial drawbacks, especially with respect to handling and waste management. Several different fluorescence-based readouts are available to study ligand binding to GPCRs,[2,3,6] including fluorescence anisotropy (FA),[7-10] fluorescence correlation spectroscopy,[11,12] and (time-resolved) Förster or bioluminescence resonance energy transfer ((TR)-FRET[13-16] or BRET[17-21]).

For BRET binding assays (see Figure 3.1A), the small luciferase NanoLuc® (NLuc)[22] is fused to the N-terminus of the investigated GPCR.[21,23] Additionally, a suitable fluorescent ligand, whose excitation spectrum must overlap with the bioluminescence spectrum of NLuc ($\lambda_{max} \approx 460$ nm[22]), is needed as a BRET acceptor. Once the luciferase substrate is added and the fluorescent ligand binds to the luciferase-tagged receptor, the fluorescent ligand can emit photons after the occurrence of BRET, which strongly depends on the proximity of the donor and the acceptor, as well as their relative orientation. The energy transfer efficiency correlates directly with the amount of receptor-bound ligand and can be easily quantified.

On the other hand, the FA binding assay (see Figure 3.1B) measures the change in rotational mobility of the fluorescent ligand upon binding to a receptor.[24] The sample is excited with linearly polarized light to induce a photoselection of fluorophores, i.e. fluorophores with excitation dipoles oriented parallel to the excitation plane are preferably excited. A free fluorescent ligand can rotate quickly due to its small size, leading to a strongly depolarized emission (low FA). In contrast, when the fluorescent ligand is bound to a receptor, its rotational freedom decreases due to the larger size of the ligand-receptor complex, which results in a fluorescence emission with preserved polarization (high FA).[24,25] It is important to note that the ratio of receptor-bound and free ligand must change during ligand binding to observe a significant difference in FA signal.[5] This is best achieved when both ligand and receptor concentrations are similar to the expected ligand affinity values.[24]

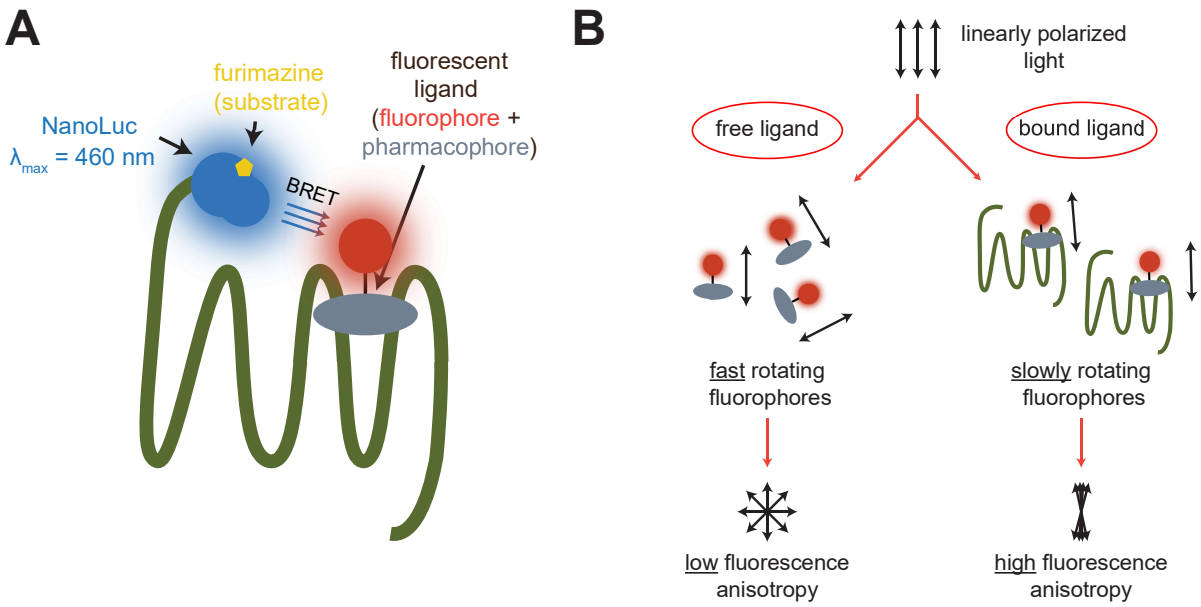

Figure 3.1: Schematic illustration of the assay principles used in this study. (**A**) BRET binding assay: A GPCR (here: M_2R) is N-terminally tagged with NLuc to monitor ligand binding using the phenomenon of BRET. Once a fluorescent ligand is bound, the proximity-dependent energy transfer from the luciferase to the bound ligand can be quantified. (**B**) FA binding assay: The sample is excited with linearly polarized light. Binding of the fluorescent ligand to the receptor causes a decrease in rotational freedom of the ligand, subsequently increasing the anisotropy of the fluorescent ligand emission.

In this study, we directly compared a BRET-based and an FA-based receptor binding assay. We explored the performance of both assays with an emphasis on kinetic measurements and the determination of affinities of the same labeled and unlabeled ligands. Furthermore, we wanted to study their practicality and limitations. For this purpose, the human M_2 muscarinic acetylcholine receptor (M_2R) was used as a model GPCR. Muscarinic acetylcholine receptors (MRs), which comprise five subtypes (M_1R-M_5R), represent an important family within the rhodopsin-like (class A) GPCRs.[26] MRs are interesting targets for drug discovery, as they are involved in several processes in both the central nervous system (e.g. modulation of cognition and memory)[27,28] and in the periphery (e.g. heart rate regulation and smooth muscle contraction).[29,30]

Recently, a set of differently fluorescence-labeled dibenzodiazepinone (DIBA)-type high-affinity M_2R ligands was described,[31,32] comprising probes that were designed for a potential use in BRET- and FA-based binding assays (e.g. **3.1** and **3.2**, Figure 3.2).[31]

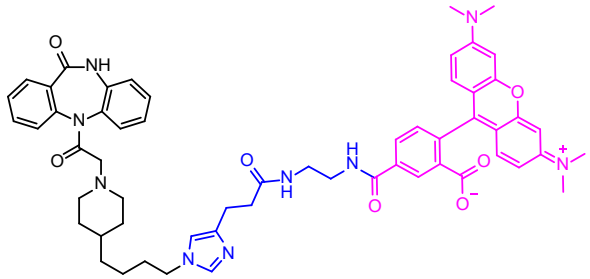

3.1, UR-CG072

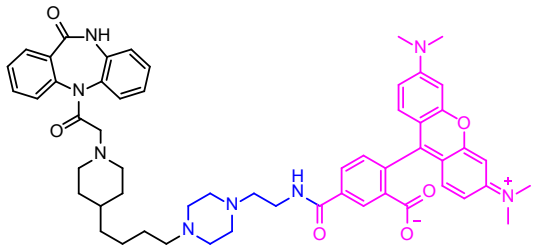

3.2, UR-MK342

Figure 3.2: Structures of the TAMRA-labeled DIBA-derived MR ligands **3.1** and **3.2**. The linker moieties, being the only structural difference between **3.1** and **3.2**, are highlighted in blue. The TAMRA label is highlighted in magenta.

When choosing a suitable ligand for fluorescence-based techniques, it is mandatory to consider the general properties of the fluorophores, such as their quantum yield or propensity for non-specific interactions, as these might significantly influence the outcome of the measurements. As mentioned previously, for the BRET assay, it is also crucial to consider the spectral characteristics of the fluorescent ligand, e.g. peak excitation wavelength, as an overlap of its excitation spectrum with the bioluminescence spectrum of the luciferase is required.[23] In contrast, the spectral properties are not as limiting for a potential use in the FA assay. The suitability of a fluorophore for the FA assay is primarily dependent on its fluorescence lifetime. If the fluorescence lifetime is much longer than the rotational correlation time of the ligand-receptor complex or shorter than that of the free ligand (low ns region),[24] the change of FA signal will become difficult to detect. As the fluorophore TAMRA (5-carboxytetramethylrhodamine) has previously been reported to be compatible with both BRET-[18-21,33] and FA-based assays,[10,34-36] we decided to use the TAMRA-labeled DIBA-derived MR ligands **3.1** (UR-CG072) and **3.2** (UR-MK342) (see Figure 3.2)[31] for a direct comparison of BRET- and FA-based binding assays at the M_2R, an approach not described to date.

3.2 Materials and methods

3.2.1 Materials

Dulbecco's Modified Eagle's Medium (DMEM), L-glutamine, ExCell 420 Serum-Free Medium for Insect Cells (ExCell), fetal calf serum (FCS), Pluronic F-127 and HEPES were purchased from Sigma-Aldrich (Munich, Germany). Trypsin/EDTA (0.05%/0.02%) was from Biochrom (Berlin, Germany). Bovine serum albumin (BSA) was purchased from SERVA Electrophoresis (Heidelberg, Germany). Leibovitz' L-15 medium (L-15) and geneticin (G418) were from Fisher Scientific (Nidderau, Germany). Furimazine (Nano-Glo® Live Cell Substrate) was purchased from Promega (Mannheim, Germany). Dithiothreitol (DTT), $MgCl_2$, KCl, $CaCl_2$ and NaCl used for the preparation of washing/assay buffer in FA and radioligand saturation binding experiments on BBVs were from AppliChem (Darmstadt, Germany) and Complete EDTA-free Protease Inhibitor Cocktail was from Roche Diagnostics (Mannheim, Germany).

Atropine sulfate (atr) was from Sigma-Aldrich (Munich, Germany) or Merck (Darmstadt, Germany). Carbachol (CCh), iperoxo iodide (iper), N-methyl scopolamine bromide (NMS), scopolamine hydrobromide and W84 dibromide (W84) were purchased from Sigma-Aldrich (Munich, Germany). Oxotremorine sesquifumarate (oxo) was from Tocris Bioscience (Bristol, UK). The radioligand [^{3}H]NMS was purchased from American Radiolabeled Chemicals Inc. (St. Louis, MO, USA; specific activity = 80 Ci/mmol) or PerkinElmer (Waltham, MA, USA; specific activity = 84 Ci/mmol). Stock solutions of the unlabeled ligands were prepared in millipore H_2O, except for W84, which was dissolved in DMSO (Merck Millipore, Darmstadt, Germany). Stock solutions of all fluorescent ligands were prepared in DMSO, and aliquots were stored at -80 °C.

The pcDNA3.1 vector was from Thermo Fisher (Nidderau, Germany) and the pFastBac1 vector from Gibco (Nidderau, Germany). The plasmid encoding the human M_2 receptor (M_2R) was purchased from the cDNA Resource Center (Rolla, MO, USA), whereas the plasmid containing the sequence of NanoLuc® (NLuc) was obtained from Promega (Mannheim, Germany).

3.2.2 Generation of stably transfected HEK293T cells and mammalian cell culture

The vector encoding the N-terminally NLuc-tagged M_2R (NLuc-M_2R) was generated by standard PCR techniques and Gibson Assembly. Therefore, the previously described pcDNA3.1 NLuc-hH_4R[17] was linearized upstream and downstream of the receptor-encoding sequence (note: this resulted in a linearized vector containing the sequence for NLuc but not for any receptor), and the gene of the human M_2R (*CHRM2*) was amplified through PCR creating overlaps with the linearized vector at both ends. After a restriction digest with *Dpn*I, NEBuilder HiFi DNA Assembly MasterMix (New England Biolabs, Frankfurt, Germany) was used according to the

manufacturer's protocol to generate the pcDNA3.1 NLuc-M_2R. The generated construct was verified by sequencing (Eurofins Genomics, Ebersberg, Germany).

HEK293T cells were a kind gift from Prof. Dr. Wulf Schneider (Institute for Medical Microbiology and Hygiene, University Hospital Regensburg, Germany) and were routinely cultivated in DMEM, supplemented with 2 mM L-glutamine and 10% FCS, in a water-saturated atmosphere (37 °C, 5% CO_2). To generate stable transfectants, cells were seeded in a 6-well plate (Sarstedt, Nümbrecht, Germany) at a density of $3 \cdot 10^5$ cells/mL one day before transfection. Cells were transfected with 2 µg of pcDNA3.1 NLuc-M_2R using X-tremeGENE™ HP transfection reagent (Roche Diagnostics, Mannheim, Germany) according to the manufacturer's protocol. After two days, the transfected cells were detached by trypsinization, centrifuged (500 *g*, 5 min) and seeded on a 150 mm-cell culture dish (Sarstedt, Nümbrecht, Germany). Geneticin (G418) was added immediately at a final concentration of 1 mg/mL. The medium was changed regularly for 2-3 weeks until stable colonies were visible. After a subsequent clonal selection for receptor expression (determined by the maximal BRET ratio induced by a high concentration of fluorescent ligand **3.5**), cultivation of the clone with the highest receptor expression was continued using a G418 concentration of 600 µg/mL. The cells were regularly tested for mycoplasma infection using the Venor GeM Mycoplasma Detection Kit (Minerva Biolabs, Berlin, Germany) and were negative.

3.2.3 Sf9 insect cells and budded baculoviruses (BBVs)

3.2.3.1 Generation of high-titer baculoviruses displaying the M_2R

The cDNA of the human M_2R was subcloned into the pFastBac1 vector using *Xba*I and *Xho*I restriction sites and transformed into DH10Bac competent cells (Invitrogen, Carlsbad, CA, USA) to obtain recombinant bacmid DNA.

Subsequently, the baculoviruses of passages P0, P1 and P2 were produced as described.[37] The produced P2 baculoviruses were titrated based on the increase in Sf9 cell diameter upon infection using the ICSE (image-based cell-size estimation) method.[38] High-titer baculoviruses in the passage P3 were obtained by infecting 110 mL of a Sf9 cell culture ($1.5 \cdot 10^6$ cells/ml) at a low multiplicity of infection (MOI = 0.1). The baculovirus suspension P3 was then again obtained as described.[37] FCS was added at a final concentration of 2% to the baculovirus suspension to enhance stability. Additionally, the P3 baculovirus was titrated to confirm a high titer for sufficient protein expression.

3.2.3.2 Preparation of BBVs displaying the M_2R

To prepare BBVs displaying the M_2R on their envelope, a Sf9 cell suspension (density: $2 \cdot 10^6$ cells/mL) was infected with a high-titer P3 baculovirus at an MOI of 1. The receptor preparation was collected after 4-5 days when the cell viability had dropped below ≈ 30% by centrifugation at 1600 *g* for 15 min to remove the remaining Sf9 cells. The supernatant containing the virus particles was pooled and centrifuged at 48 000 *g* for 40 min. The sediment was washed once with 500 µL of ice-cold buffer (consisting of 0.1% Pluronic F-127, 11 mM Na-HEPES (pH 7.4), 1 mM $MgCl_2$, 5 mM KCl, 1 mM $CaCl_2$, 135 mM NaCl and Complete EDTA-free Protease Inhibitor Cocktail (used according to manufacturer's protocol)), resuspended in 500 µL of ice-cold buffer and homogenized using a 1 mL syringe (Norm-Ject-F, B. Braun Melsungen AG, Melsungen, Germany) with a 0.3 mm diameter needle (Sterican, Braun Melsungen AG, Melsungen, Germany). The baculovirus suspension was stored in aliquots at -90 °C until further use.

3.2.4 Radioligand saturation binding assay

Radioligand saturation binding experiments with [^{3}H]NMS (specific activity = 80 Ci/mmol; American Radiolabeled Chemicals Inc., St. Louis, MO, USA) at intact, suspended HEK293T cells stably expressing the NLuc-M_2R, were performed according to a previously described protocol for CHO-M_2 cells[39] with minor modifications – in detail: cells were detached from the cell culture flasks by trypsinization. After centrifugation (400 *g* for 5 min), the cells were resuspended in L-15 with 1% BSA and the cell density was adjusted to $1.25 \cdot 10^6$ cells/mL. The experiments were performed in a final volume of 200 µL in clear 96-well plates (Brand, Wertheim, Germany). The wells were pre-filled with 20 µL of L-15 containing [^{3}H]NMS (10-fold more concentrated than the final assay concentration) and 20 µL of L-15 (for total binding) or L-15 containing atropine (non-specific binding, 1000-fold excess over the respective radioligand concentration). 160 µL of the concentration-adjusted cell suspension were added to all wells and the plate was shaken at 23 °C (room temperature) for 3 h. The bound radioactivity was then collected using a Brandel Harvester (Brandel, Gaithersburg, MD, USA) with GF/C filter mats (0.26 mm; Whatman, Maidstone, UK), which were pretreated with 0.3% polyethyleneimine. After harvesting, the filters were washed once with cold PBS and punched out. Punched out filters were then transferred into clear 96-well plates (PerkinElmer, Rodgau, Germany), 200 µL of Rotiszint eco plus (Carl Roth, Karlsruhe, Germany) were added and the plates were sealed using a transparent sealing tape (permanent seal for microplates, PerkinElmer, prod. no. 1450-461). The plates were vigorously shaken for 3 h. Before measuring the radioactivity (in dpm) with a MicroBeta2 plate counter (PerkinElmer, Rodgau, Germany), the plates were kept in the dark for at least 60 min.

Radioligand saturation binding assays on BBVs displaying the M_2R were performed following a protocol for BBVs displaying the dopamine D_1 receptor[40] with the following minor modifications: The assay buffer consisted of 0.1% Pluronic F-127, 11 mM Na-HEPES (pH 7.4), 1 mM $MgCl_2$, 5 mM KCl, 1 mM $CaCl_2$, 135 mM NaCl and Complete EDTA-free Protease Inhibitor Cocktail (used according to manufacturer's protocol). Right before the experiment, the assay buffer was supplemented with 0.1 mg/mL BSA and 1 mM DTT. [^{3}H]NMS (specific activity = 84 Ci/mmol; PerkinElmer, Waltham, MA, USA) was used as a radioligand and non-specific binding was assessed in the presence of 50 µM of 4-DAMP (1,1-dimethyl-4-diphenylacetoxypiperidinium iodide, Research Biochemicals Inc., Natick, MA, USA).

3.2.5 BRET binding assay

BRET binding assays were performed as described previously[17] with minor modifications – in detail: HEK293T cells stably expressing the NLuc-M_2R were detached at 80-90% confluency from the cell culture flasks by trypsinization and centrifuged (500 *g*, 5 min). After resuspension and adjustment of the cell density in L-15 supplemented with 5% FCS and 10 mM HEPES (pH 7.4), $1 \cdot 10^5$ cells were seeded in a volume of 70 µL (saturation/competition binding experiments) or 80 µL (kinetic experiments) per well into white 96-well plates (Brand, Wertheim, Germany) and incubated in a water-saturated atmosphere overnight (37 °C, no additional CO_2). On the day of the experiment, serial dilutions of the respective fluorescent ligands and competitors were prepared in assay buffer consisting of L-15 supplemented with 10 mM HEPES (pH 7.4) and 2% BSA (the latter added to reduce adsorption to the plate material and polypropylene vessels). Serial dilutions for saturation and competition binding experiments were prepared 10-fold more concentrated than the final assay concentration. For saturation binding experiments, 10 µL of assay buffer (total binding) or assay buffer containing atropine (non-specific binding, 500-fold excess over the respective concentration of fluorescent ligand) were added to the cells, followed by the addition of 10 µL of a dilution of the respective fluorescent ligand (varying concentrations). After an incubation time of 60 min (fluorescent ligands **3.1**, **3.3**-**3.6**) or 90 min (fluorescent ligands **3.2**, **3.7**, **3.8**) at 27 °C, 10 µL of the luciferase substrate furimazine (Nano-Glo® Live Cell Substrate, pre-diluted 1:1000 before use) were added. Cells were equilibrated for 5 min inside the plate reader (pre-warmed to 27 °C), and luminescence intensities were measured.

For competition binding experiments, 10 µL of the respective dilution of the competitor (varying concentrations) and 10 µL of a solution of **3.1** (c_{final} = 2 nM) were added to the cells. A positive control (100% value) containing only fluorescent ligand and no competitor, as well as a solvent control (0% value) were included in every experiment. After an incubation period of 60 min, 10 µL of furimazine (Nano-Glo® Live Cell Substrate, pre-diluted 1:1000 before use) were added, and the measurement was performed as described above. To perform competition binding

experiments in kinetic mode, the pre-diluted luciferase substrate (1:1000 before use) was added simultaneously with the respective competitive ligand. After an equilibration for 5 min, the fluorescent ligand was added, and the measurement was started immediately.

For kinetic measurements, 10 µL of assay buffer (total binding) or a solution of atropine (non-specific binding, c_{final} = 2 µM), and 10 µL of furimazine (Nano-Glo® Live Cell Substrate, pre-diluted 1:1000 before use) were added to the cells. Samples were equilibrated inside the plate reader (pre-warmed to 27 °C) for 5 min. To start the association, a solution of the fluorescent ligands **3.1** or **3.2** (V = 50 µL, c_{final} = 2 nM) was added using the injector module of the plate reader, and the luminescence and fluorescence signals were measured for 60 min (**3.1**) or 90 min (**3.2**) (ligand association). Subsequently, dissociation was started by injecting 50 µL of a solution of atropine (c_{final} = 2 µM) and the measurement was continued for maximal 4 h (final well volume: 200 µL).

BRET measurements were performed at 27 °C using a TECAN GENiosPro or a TECAN InfiniteLumi plate reader (Tecan Austria GmbH, Grödig, Austria). Bioluminescence intensity was detected using a 460 ± 35 nm band-pass (460/35BP) filter (InfiniteLumi) or a 460 ± 50 nm band-pass (460/50BP) filter (GENiosPro). The emission of the fluorescent ligand was detected using a 610 nm long-pass filter (610LP). The integration times for equilibrium measurements were set to 100 ms (460/35BP filter or 460/50BP filter) and 1000 ms (610LP filter). For all kinetic measurements (InfiniteLumi), the integration time for the detection through the blue channel (460/35BP filter) was changed to 500 ms to reduce noise.

3.2.6 FA binding assay

FA binding experiments were performed as previously described[41,42] with some modifications to account for the specific properties of the M_2R and the used fluorescent ligands. All dilutions were prepared in FA assay buffer (consisting of 0.1% Pluronic F-127, 11 mM Na-HEPES (pH 7.4), 1 mM $MgCl_2$, 5 mM KCl, 1 mM $CaCl_2$, 135 mM NaCl and Complete EDTA-free Protease Inhibitor Cocktail (used according to manufacturer's protocol)). Previously prepared baculoviruses, displaying the M_2R on their envelope, were thawed, resuspended and triturated ten times in a 1 mL syringe with a 0.3 mm diameter needle to reduce the number of conglomerates and avoid sedimentation during the measurement. For saturation binding experiments, 10 µL of solutions of the fluorescent ligands (c_{final}(**3.1**) = 0.5 nM and 2.5 nM; c_{final}(**3.2**) = 1 nM and 8 nM) were added to black, half area, flat bottom polystyrene NBS (non-binding surface) 96-well plates (Corning Inc., NY, USA, Product No. 3993). 30 µL of a solution of atropine for **3.1** or scopolamine for **3.2** were added to the wells specified for non-specific binding (c_{final} = 8 µM). FA assay buffer was added to each well to reach a volume of 60 µL inside each well before the addition of baculoviruses.

Two-fold serial dilutions of the baculovirus suspension were prepared in assay buffer in 2 mL Axygen 96-well polypropylene plates (Corning Inc., NY, USA, Product Number P-DW-20-C), and the binding reactions were started by the addition of 40 µL of the respective dilution of baculovirus suspension to the 96-well plate (final well volume: 100 µL). In addition, blank wells containing the same final volume and the same amount of baculovirus but no fluorescent ligand, atropine or scopolamine, were prepared for each baculovirus dilution.

For FA competition binding experiments, serial dilutions of the competitive ligands were prepared on the 96-well plate in 50 µL of FA assay buffer before the addition of 20 µL of FA assay buffer (neat) and 10 µL of a solution of **3.1** (c_{final} = 1 nM). To initiate the reaction, 20 µL of the 2-fold diluted baculovirus stock suspension (subsequently: V(BBV_{stock}) per well: 10 µL) were added to each well. Blank wells were prepared similarly as for FA saturation binding experiments.

All FA measurements were performed in duplicate using a Synergy NEO plate reader (BioTek, Winooski, VA, USA) with polarizing excitation (530 nm, bandwidth 30 nm) and dual emission (590 nm, bandwidth 35 nm) filters with a dichroic mirror allowing the simultaneous detection of parallelly and perpendicularly polarized fluorescence emission. All measurements were performed at 27 °C. For extended measurements (> 3 h), a glass lid was placed on top of the microplate to avoid excessive evaporation.

3.2.7 Data analysis

3.2.7.1 Analysis of data from radioligand saturation binding experiments

Total and non-specific binding data from radioligand saturation binding experiments were analyzed simultaneously using the “one site-total and non-specific binding” fit (GraphPad Prism 8.0, GraphPad Software Inc., San Diego, CA, USA), i.e. total binding was analyzed by an equation describing hyperbolic binding and non-specific binding by linear regression. Specific binding data from radioligand saturation binding experiments (in dpm for experiments at HEK293T NLuc-M_2R cells, in cpm for experiments on BBVs displaying the M_2R), were analyzed using an equation describing hyperbolic binding (“one site-specific binding”, Prism 8.0). The obtained K_d values were transformed into pK_d values, for which means and SEMs were calculated.

3.2.7.2 Analysis of data from the BRET binding assay

All data from BRET binding experiments were analyzed using GraphPad Prism 8.0. The raw BRET ratio was calculated as described in Chapter 2 using the following formula:

$$raw\ BRET\ ratio = \frac{emission\ (fluorescent\ acceptor, 610\mathrm{LP})}{emission\ (bioluminescent\ donor, 460\mathrm{BP})}$$

, with the numerator representing the emission of the fluorescent acceptor detected through the 610 nm long-pass filter and the denominator representing the donor luminescence detected through the 460 nm band-pass filter. All calculated values were baseline-corrected by subtracting the BRET ratio of a buffer control, yielding “corrected BRET ratios”.

For saturation binding experiments, specific binding data were analyzed using a one-site binding model (“one site-specific binding”, Prism 8.0) yielding K_d values. Total and non-specific binding were fitted simultaneously applying the “one site-total and nonspecific binding” fit (Prism 8.0). The K_d values were transformed into pK_d values, for which means and SEMs were calculated.

Data from kinetic experiments were normalized to the corrected BRET ratio right before the addition of fluorescent ligand (0% value) and the corrected BRET ratio after reaching a plateau (100% value). “Extra sum-of-squares F tests” ($p < 0.05$ was considered significant) were carried out to test whether monoexponential or biexponential models correlated better with the experimental data for both association and dissociation (Prism 8.0).

The association rate constant under the assumption of a monophasic reaction ($k_{on(mono)}$) was calculated according to the equation:

$$k_{\mathrm{on(mono)}} = \frac{k_{\mathrm{obs(mono)}} - k_{\mathrm{off(mono)}}}{c(ligand)}$$

, where $k_{obs(mono)}$ represents the observed association rate constant for a monophasic reaction and $k_{off(mono)}$ the dissociation rate constant for a monophasic reaction; c(ligand) represents the used concentration of fluorescent ligand **3.1** (here: c(**3.1**) = 2 nM).

The calculation of the kinetically derived dissociation constant ($K_d^{kinetic}$) under the assumption of a monophasic binding reaction (for **3.1**) was performed using the following equation:

$$K_{\mathrm{d}}^{\mathrm{kinetic}} = \frac{k_{\mathrm{off(mono)}}}{k_{\mathrm{on(mono)}}}$$

BRET competition binding data were normalized to a solvent control (0% value) and a positive control containing fluorescent ligand but no competitor (100% value). Normalized data were subsequently fitted by a four-parameter logistic equation to obtain pIC_{50} values, which were transformed into pK_i values using the Cheng-Prusoff equation.[43] Means and SEMs were calculated for the pK_i values.

3.2.7.3 Analysis of data from the FA binding assay

All FA data were processed using the Aparecium 2.0 software (available at http://www.gpcr.ut.ee/aparecium.html). Data fitting was performed either by GraphPad Prism 8.0 or by a modified version of IQMTools/SBToolbox2 (IntiQuan, Basel, Switzerland). All fitting was performed using the root-mean-square error loss function. For all global fitting procedures, the "simulated annealing"-based Nelder-Mead simplex optimization algorithm[44,45] was used with a starting temperature of 1000, temperature reduction factor of 0.2 and 1000 iterations per temperature.

The following equations were used to calculate the fluorescence anisotropy (FA) and total fluorescence intensity (TFI) from the measurements:

$$FA = \frac{(I_{II} - I_{\perp})}{(I_{II} + 2 \times I_{\perp})}$$

$$TFI = I_{II} + 2 \times I_{\perp}$$

, where I_{II} represents the fluorescence intensity parallel and $I_{\perp}$ the fluorescence intensity perpendicular to the plane of polarization of the excitation light. Parallel and perpendicular fluorescence intensities of blank wells, containing the same amount of baculovirus suspension without the other assay components, were subtracted from the corresponding intensity values prior to FA and TFI calculation.

During data preparation with the Aparecium software, the measurement time points were corrected for each well individually, accounting for the delay between the addition of the baculovirus preparations and the starting point of the first plate read. Additionally, the measurement time points were corrected for time shifts introduced by measurement delay for each well and kinetic cycle.

FA saturation binding experiments were analyzed using a reported global model implemented in Prism 8.0 assuming a single binding site for the fluorescent ligand, the possibility of non-specific binding, and a change in quantum yield upon binding.[46] Since this model only allowed fitting FA values, the relative quantum yield values used for subsequent calculations were obtained by pooling the results from kinetic global fitting (see below).

For kinetic global fitting of saturation binding experiments with the fluorescent ligand **3.1**, a kinetic version of the single binding site model with the possibility of non-specific binding and a change in quantum yield upon binding was developed and used (for details, see Appendix: *Global kinetic modeling of FA binding experiments with the fluorescent MR ligand **3.1**,* pp.151-155). All kinetic datapoints obtained from all baculovirus stock volumes and the two studied fluorescent ligand concentrations, as well as both the TFI and FA signals were fitted simultaneously. Physically reasonable constraints (e.g. intrinsic anisotropy of all states of the fluorescence ligand has to remain between 0 and 0.4) were applied for parameters where possible. The preference for mono- or biexponential models to describe the dissociation curves was assessed in the same manner as for the BRET assay. The fast and slow dissociation rate constants describing the dissociation of the fluorescent ligand **3.2** were obtained by applying the biexponential decay model in Prism 8.0.

The described model and constraints were also used for global fitting of competition binding experiments. Global fitting was performed for each individual experiment with each competitive ligand to obtain pK_i values. Some parameters, such as association and dissociation rate constants of the fluorescent ligand, were not fitted for these experiments but locked to the values obtained from the kinetic global fit of saturation binding experiments (described above). A fit analysis was performed for all FA experiments with at least 15 individual fitting procedures to obtain uncertainty estimates. Alternatively, the Cheng-Prusoff equation was used to calculate the pK_i values based on the pIC_{50} values,[43] which were obtained as described above for the BRET assay.

The correlation of pK_i values obtained from different assays was analyzed by Deming regression. Squared Pearson correlation coefficients (R^2) were calculated using Prism 8.0. All errors represent SEMs unless stated otherwise. Whenever necessary, error propagation was performed as described in Chapter 2.

3.3 Results and discussion

3.3.1 Determination of the binding affinities of 3.1 and 3.2 in BRET and FA binding assays

HEK293T cells stably expressing the M_2R, N-terminally fused to NLuc (NLuc-M_2R), were generated to study ligand binding properties in the BRET assay. In the case of the FA assay, we generated budded baculoviruses (BBVs)[47] displaying the wild-type M_2R on the viral envelope. BBVs have successfully served as receptor sources in radioligand binding[40,48,49] and FA binding assays[41,42,46,50,51] for several GPCRs. They turned out to be especially useful for the latter, as BBVs possess some major advantages over cell membranes. For example, baculovirus particles in suspension are uniform in shape and size and are stable over a long time making them suitable for longer measurements.[24]

To check whether attachment of the luciferase to the receptor or the display of the M_2R on a viral envelope alters the binding behavior of the orthosteric MR ligand NMS, we conducted radioligand saturation binding experiments with the radioligand [^{3}H]NMS at intact, suspended HEK293T NLuc-M_2R cells (Figure 3.3A) and on BBVs displaying the M_2R (Figure 3.3B). The radioligand was able to bind to both the NLuc-tagged receptor expressed in HEK293T cells and the wild-type receptors displayed on the viral envelope in a saturable manner. [^{3}H]NMS retained the high M_2R affinity at the HEK293T NLuc-M_2R cells (pK_d ± SEM = 9.77 ± 0.09 (N = 3)) and at the virus-displayed receptor (pK_d ± SEM = 9.08 ± 0.08 (N = 3)). The obtained pK_d values were in good agreement with previously published M_2R binding data of [^{3}H]NMS measured at wild-type M_2 receptors expressed in CHO cells.[31,52,53] This is especially remarkable considering the obvious differences of the used expression systems (e.g. membrane composition or membrane potential). Since high-affinity [^{3}H]NMS binding was conserved in both receptor expression systems, they were both considered to be suitable for the following BRET and FA experiments.

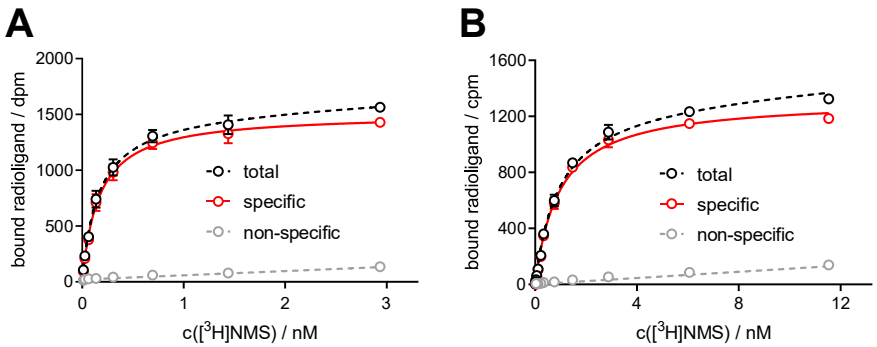

Figure 3.3: Binding isotherms from radioligand saturation binding experiments at intact, suspended HEK293T cells stably expressing the NLuc-M_2R (**A**) or on BBVs displaying the M_2R on their envelope (**B**). Non-specific binding was assessed in the presence of atropine (**A**, 1000-fold excess over the respective concentration of radioligand) or 50 µM 4-DAMP (**B**). Data represent means (total and non-specific binding) or calculated values (specific binding) ± errors of one representative experiment from a set of three independent experiments, each performed in triplicate (**A**) or duplicate (**B**). Error bars of total and non-specific binding represent the SEM, whereas error bars of specific binding represent propagated errors.

Next, the binding of the fluorescent ligands **3.1** and **3.2** was investigated in the BRET and FA assay. For the BRET assay, classical saturation binding setups could be used, i.e. the fluorescent ligand was added at increasing concentrations to a constant amount of adherent recombinant cells. Both ligands showed saturable binding and a very low non-specific signal (see Figure 3.4A and 3.4B; pK_d ± SEM (BRET) for **3.1** and **3.2** = 8.97 ± 0.03 and 9.32 ± 0.16, cf. Table 3.1). However, the observation of a low non-specific signal in the BRET assay must be interpreted with caution. Due to the distance-dependence, significant BRET can only be detected once the fluorescent ligand is bound to the luciferase-tagged receptor. On the contrary, when the ligand interacts non-specifically, e.g., with other structures, such as cell surface proteins, almost no BRET can take place and the non-specific binding of the ligand is potentially underestimated. Fortunately, since the fluorescent ligands **3.1** and **3.2** also showed low non-specific binding in flow cytometry-based saturation binding experiments,[31] binding to other cellular compartments is not a concern.

A different approach had to be pursued for the determination of fluorescent ligand affinities in the FA assay. Using the fluorescent ligand in excess, as in conventional saturation binding experiments, would consequently also increase the concentration of unbound ligand in the well, resulting in a smaller change in FA. Therefore, the experiment was conducted vice versa by performing a saturation of two fixed fluorescent ligand concentrations with different volumes of baculovirus stock suspension, corresponding to different receptor concentrations.[46] The used ligand and receptor concentrations were close to the expected affinity of the fluorescent ligands to obtain maximal changes in FA values. Increasing the amount of baculovirus stock resulted in an increase of FA signal for both fluorescent ligands at both applied ligand concentrations (see Figure 3.4C and 3.4D). Once free ligand was depleted at higher receptor concentrations, the total FA signal reached a plateau (cf. Figure 3.4C and 3.4D). Interestingly, the total fluorescence

intensity (TFI) signal elicited by ligand **3.1** decreased upon receptor binding indicating a change in quantum yield (cf. Appendix Figure A9C and A9D). The relative quantum yield of receptor-bound **3.1** compared to free ligand was determined to be 0.73 ± 0.02, which significantly affects the measured FA values. For ligand **3.2** however, the quantum yield change was negligible and had no effect on the FA values (data not shown). Fitting the obtained data using a previously described algorithm,[46] in which ligand depletion and a possible change in quantum yield during ligand binding are considered, enabled the determination of apparent binding affinities for the fluorescent ligands (pK_d ± SEM (FA) for **3.1** and **3.2** = 9.36 ± 0.02 and 9.30 ± 0.11, cf. Table 3.1) as well as an estimation of the number of ligand-specific binding sites in the used baculovirus stocks (R_{stock}). The R_{stock} value for **3.1** was found to be 35 ± 6 nM for **3.1** and 55 ± 7 nM for **3.2**. Both values were determined using the same stock of baculoviruses.

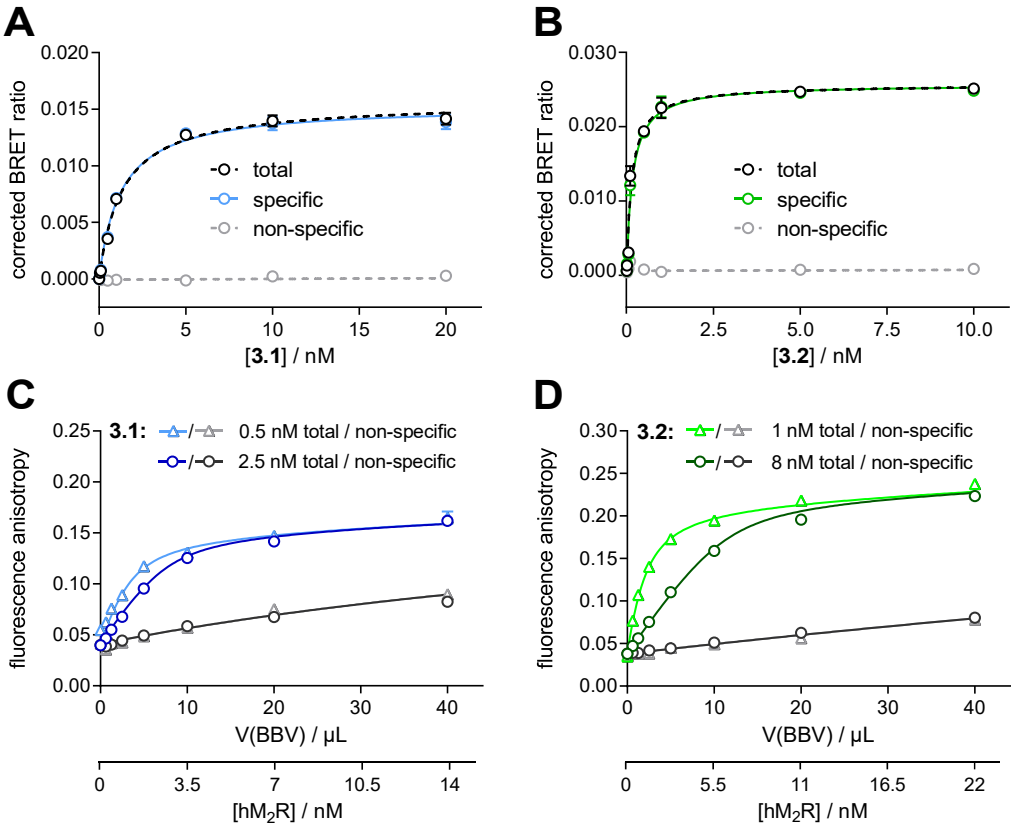

Figure 3.4: Binding isotherms from BRET-based (**A**, **B**) and FA-based (**C**, **D**) saturation binding experiments with **3.1** (**A**, **C**, blue lines) and **3.2** (**B**, **D**, green lines). (**A**, **B**) BRET-based saturation binding experiments with **3.1** (**A**) and **3.2** (**B**) were performed at HEK293T cells, stably expressing the NLuc-M_2R, measured after 60 min incubation. Non-specific binding was determined in the presence of a 500-fold excess of atropine over the respective concentration of fluorescent ligand. (**C**, **D**) Binding curves of **3.1** (**C**, c = 0.5 nM and 2.5 nM) and **3.2** (**D**, c = 1 nM and 8 nM) from FA binding experiments, performed at increasing concentrations of the M_2R displayed on BBVs applying incubation times of 60 min (**3.1**) or 120 min (**3.2**). Non-specific binding was determined in the presence of an excess of atropine (for **3.1**) or scopolamine (for **3.2**) (c = 8 µM). Ligand-specific receptor concentration values were obtained from the global fitting of the data and are depicted on a second x-axis below the graphs. Data represent means (total and non-specific binding) or calculated values (specific binding in **A** and **B**) ± errors of a representative experiment from a set of three to four independent experiments performed in triplicate (BRET) or duplicate (FA). Error bars of total and non-specific binding represent the SEM, error bars of specific binding in **A** and **B** represent propagated errors.

The affinities of **3.1** and **3.2**, resulting from the BRET and the FA assay (cf. Table 3.1), were in good agreement with the recently reported M_2R affinities of **3.1** and **3.2** obtained from radioligand competition binding experiments (pK_i = 8.75 and 9.62, respectively) and flow cytometric saturation binding experiments (pK_d = 8.36 and 8.86, respectively).[31]

Here, **3.2** elicited higher BRET and FA signals compared to **3.1**, even though both ligands carry the same fluorescence label (TAMRA). As mentioned earlier, BRET is in general a strongly distance-dependent and dipole-dipole orientation-dependent measure. Therefore, this observation suggested differences in the orientation and proximity of the two fluorescent ligands towards the luciferase-tagged N-terminus of the receptor, which can most likely be attributed to the structural differences in **3.1** and **3.2**, i.e. their dissimilar linker moieties. As ligand **3.1** showed a decrease in quantum yield upon binding to the receptor in the FA assay, the lower BRET signal observed for **3.1** might also be attributed to a decreased quantum yield in the receptor-bound state. Another possible explanation is that some fraction of the total receptor pool is not accessible for **3.1**, but accessible for **3.2**, leading to a smaller BRET ratio for **3.1** at the plateau. This hypothesis would also explain the differences in the determined R_{stock} values for the two ligands.

To test the limitations of the BRET assay, we performed BRET saturation binding experiments with other fluorescent DIBA-type MR ligands (**3.3**-**3.8**), which are structurally similar to **3.1** and **3.2**, but are labeled with different fluorophores (Figure 3.5A).[31,32] Notably, the excitation spectra of ligands **3.3** and **3.6** show only limited overlap with the NLuc spectrum (see Appendix Figure A7). Nevertheless, saturable M_2R binding of all probes could be observed in the BRET assay with good signal-to-background ratios (Figure 3.5B). The obtained pK_d values were in the same range as the $pK_{d/i}$ values from canonical assay formats, such as radioligand competition binding (cf. Table 3.1).[31,32] These results showed that, in principle, various types of fluorophores can be used in the BRET assay. Even fluorophores, which exhibit only a small spectral overlap with the luciferase, can be used in the BRET binding assay, although this is likely to be under the condition that they possess a high quantum yield to compensate the lack of spectral overlap, e.g. indolinium-type cyanine dyes as present in ligand **3.3**.[32]

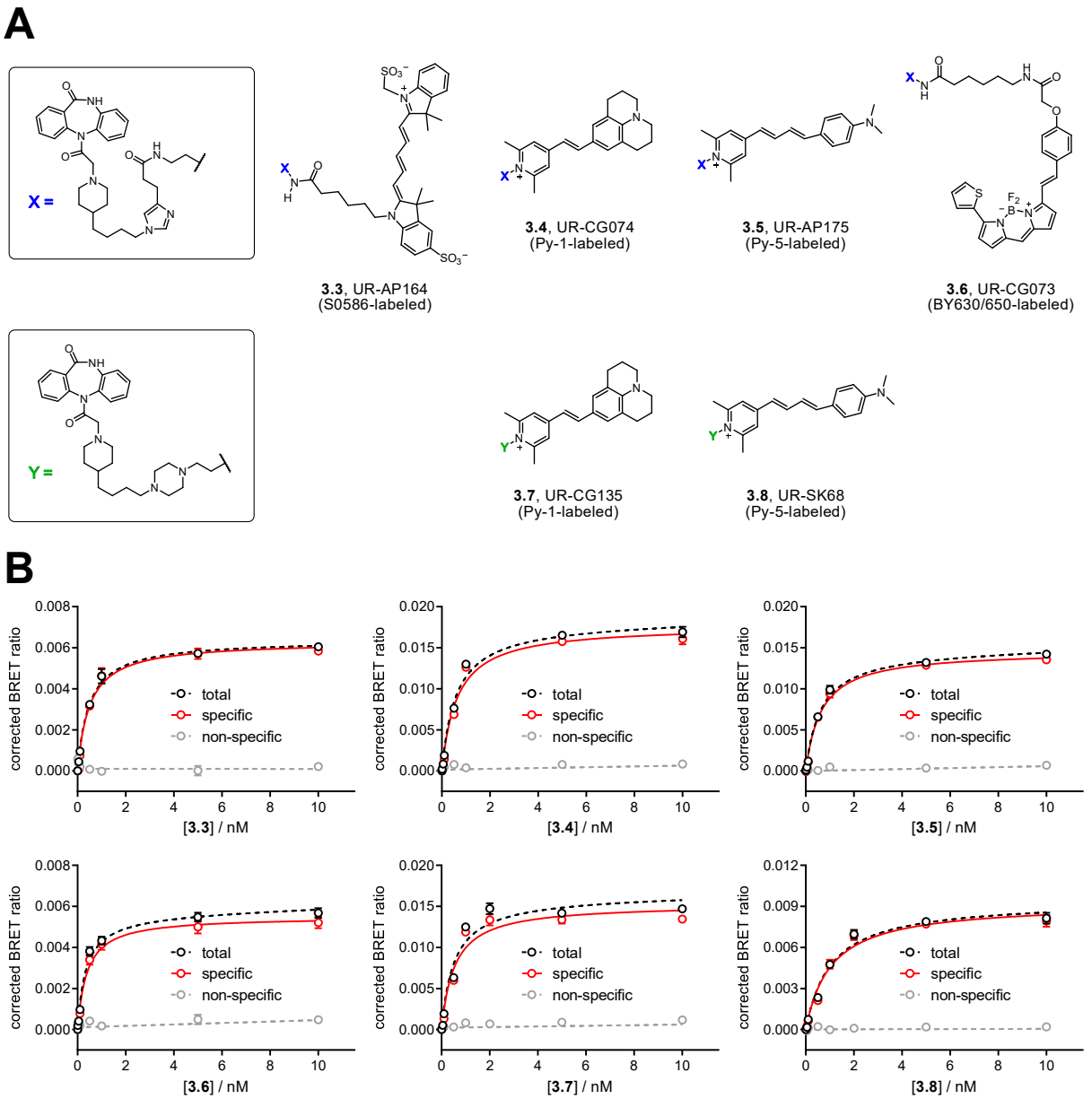

Figure 3.5: BRET saturation binding experiments with MR ligands **3.3**-**3.8** bearing different fluorescence labels. (**A**) Structures of the fluorescently labeled DIBA-derived MR ligands **3.3**-**3.8**. (**B**) Binding isotherms from BRET saturation binding experiments with **3.3**-**3.8** at HEK293T cells stably expressing the NLuc-M_2R. Non-specific binding was assessed in the presence of a 500-fold excess of atropine (over the respective concentration of fluorescent ligand). Data represent means (total and non-specific binding) or calculated values (specific binding) ± errors of a representative experiment from a set of at least three independent experiments, each performed in triplicate. Error bars of total and non-specific binding represent the SEM. Error bars of specific binding represent propagated errors.

Table 3.1: Equilibrium dissociation constants (pK_d values) of the fluorescently labeled MR ligands **3.1**-**3.8** obtained from BRET and FA binding assays.

Compound	BRET binding assay		FA binding assay		Flow cytometry	Radioligand comp. binding
	pK_d[a]	*N*	pK_d[b]	*N*	pK_d	pK_i
3.1	8.97 ± 0.03	4	9.36 ± 0.02	3	8.36[c]	8.75[c]
3.2	9.32 ± 0.16	4	9.30 ± 0.11	3	8.86[c]	9.62[c]
3.3	9.06 ± 0.09	4	n.d.	---	8.35[d]	9.10[d]
3.4	9.21 ± 0.04	4	n.d.	---	8.70[c]	8.87[c]
3.5	9.22 ± 0.07	4	n.d.	---	8.74[c]	9.04[c]
3.6	9.61 ± 0.11	4	n.d.	---	8.41[c]	9.16[c]
3.7	9.12 ± 0.08	3	n.d.	---	9.19[c]	9.02[c]
3.8	9.19 ± 0.14	3	n.d.	---	n.d.	8.52[d]

[a]Determined by BRET saturation binding experiments at intact HEK293T cells stably expressing the NLuc-M_2R; data represent means ± SEM from *N* independent experiments performed in triplicate. [b]Determined by FA saturation binding experiments on BBVs displaying the M_2R on their envelope, which were analyzed according to Veiksina *et al.*[46]; data represent means ± SEM from *N* independent experiments performed in duplicate. [c]Gruber *et al.*[31] [d]She *et al.*[32] n.d.: not determined.

3.3.2 Association and dissociation kinetics of ligands 3.1 and 3.2

As both the BRET and FA assay enable the real-time measurement of ligand binding with a high temporal resolution, we investigated the association/dissociation of **3.1** and **3.2** to/from the M_2R (see Figure 3.6).

Notably, the observed kinetic curves of **3.1** and **3.2** (association and dissociation) from the two assays showed similar shapes (see Figure 3.6), indicating the measurement of the same processes during ligand binding. Compound **3.1** displayed a faster association to the M_2R than **3.2** in the BRET assay (Figure 3.6A) and in the FA assay (Figure 3.6B). In dissociation experiments, **3.1** was displaced completely from the M_2R within 2-3 h, whereas a slower dissociation from the M_2R (≈ 50% after 4 h) was observed for **3.2**, independent from the assay used. One major drawback of the BRET assay, when using the standard substrate furimazine, is its temporal limitation due to the depletion of the luciferase substrate. Potentially, this could be overcome to some extent by using extended live cell substrates.[54] In contrast, the FA assay is not limited in this aspect, as there is no need for a substrate and the used baculovirus particles are stable in solution for a long time without a noticeable change in FA signal.[46] This property allowed the measurement of the dissociation of **3.2** for an extended period revealing that the binding of **3.2** was fully reversible after approx. 20 h (data not shown).

Interestingly, the small structural difference in the linker moiety between the two studied fluorescent ligands **3.1** and **3.2** (cf. Figure 3.2) caused a marked difference in their dissociation behavior.

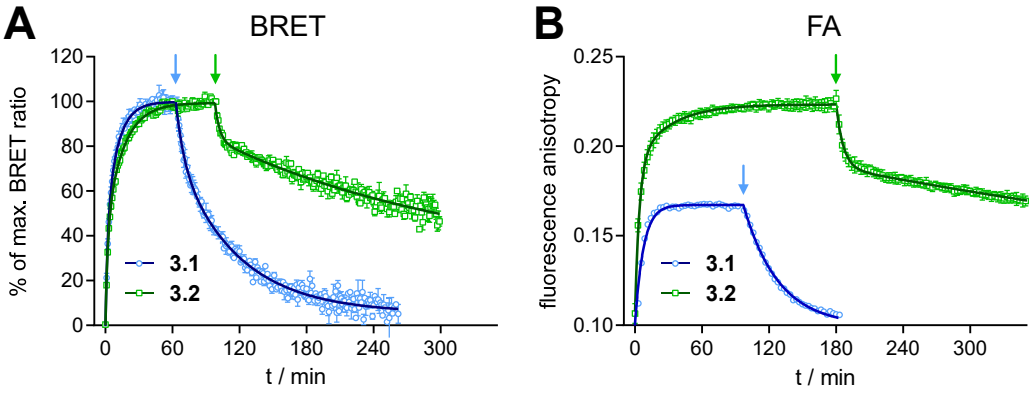

Figure 3.6: Association and dissociation kinetics of **3.1** and **3.2** at the M_2R determined in BRET (**A**) and FA (**B**) binding assays at 27 °C. (**A**) BRET binding experiments were performed at HEK293T cells stably expressing the NLuc-M_2R. Association was started by the addition of **3.1** or **3.2** (c = 2 nM). Dissociation was initiated after 60 min (**3.1**) or 90 min (**3.2**) by the addition of an excess of atropine (c = 2 µM). (**B**) FA binding experiments were performed on BBVs displaying the M_2R on the viral envelope. Association was started by the addition of 40 µL of the baculovirus stock to wells containing **3.1** (c = 2.5 nM) or **3.2** (c = 8 nM). Dissociation was initiated after 95 min (**3.1**) or 180 min (**3.2**) by the addition of an excess of atropine (for **3.1**) or scopolamine (for **3.2**) (c = 8 µM). Data represent calculated values (**A**) or means (**B**) ± errors of a representative experiment of three independent experiments, each performed in triplicate (BRET) or duplicate (FA). Error bars in (**A**) represent propagated errors, error bars in (**B**) the SEM.

In the case of the BRET assay, monoexponential and biexponential association/dissociation models were used for the quantitative analysis of the binding kinetics of **3.1** and **3.2** and compared in terms of their suitability to describe the experimental data (see Appendix Figure A8). The biexponential equations resulted in significantly better fits than the monoexponential equations for the association and dissociation of both ligands ($p < 0.0001$, extra sum-of-squares F test). The preference for the biexponential model was particularly obvious for **3.2** (see Appendix Figure A8C and A8D). However, there was a comparatively small difference (≈ 10-fold) between the fast and slow observed association (and dissociation) rate constants for **3.1** (cf. Table 3.2), which potentially indicates only a small deviation of the measured kinetic data from monophasic association and dissociation (see Appendix Figure A8A and A8B). Thus, we additionally determined monophasic rate constants for **3.1** and calculated a kinetically derived dissociation constant ($pK_d^{kinetic}$) under the assumption of monophasic behavior as an approximation. The obtained value ($pK_d^{kinetic}$(**3.1**) = 9.08 ± 0.12) was not different from the affinity constant from equilibrium experiments ($pK_d^{(equilibrium)}$(**3.1**) = 8.97 ± 0.03, cf. Table 3.2), which corroborated our hypothesis.

Table 3.2: Dissociation constants and kinetic constants of the investigated fluorescent MR ligands **3.1** and **3.2** obtained from BRET and FA binding experiments.

	BRET binding assay		FA binding assay	
	3.1	**3.2**	**3.1**	**3.2**
$k_{obs(fast)}$[a] [min^{-1}]	0.419 ± 0.009[a] (0.27 ± 0.06)	0.346 ± 0.045[a] (0.48 ± 0.02)	n.a.	n.a.
$k_{obs(slow)}$[a] [min^{-1}]	0.048 ± 0.006[a]	0.052 ± 0.003[a]	n.a.	n.a.
$k_{obs(mono)}$[b] [min^{-1}]	0.084 ± 0.017[b]	n.a.	n.a.	n.a.
$k_{off(fast)}$[c] [min^{-1}]	0.197 ± 0.016[c] (0.19 ± 0.02)	0.146 ± 0.019[c] (0.35 ± 0.03)	n.a.	0.195 ± 0.011[c] (0.28 ± 0.03)
$k_{off(slow)}$[c] [min^{-1}]	0.019 ± 0.0003[c]	0.005 ± 0.001[c]	n.a.	0.002 ± 0.0004[c]
$k_{off(mono)}$[d,e] [min^{-1}]	0.025 ± 0.001[d]	n.a.	0.043 ± 0.005[e]	n.a.
$k_{on(mono)}$[f,g] [nM^{-1} min^{-1}]	0.030 ± 0.008[f]	n.a.	0.032 ± 0.001[g]	n.a.
p$K_d^{kinetic}$, [h]	9.08 ± 0.12[h]	n.a.	n.a.	n.a.
pK_d^{global}, [i]	n.a.	n.a.	9.12 ± 0.04[i]	n.a.
p$K_d^{equilibrium}$, [k]	8.97 ± 0.03[k]	9.32 ± 0.16[k]	9.36 ± 0.02[k]	9.30 ± 0.11[k]

[a-i]Determined by kinetic BRET binding experiments performed at HEK293T cells stably expressing the NLuc-M_2R or by kinetic FA experiments performed on BBVs displaying the M_2R on the viral envelope. All given kinetic parameters originate from three independent kinetic experiments performed in triplicate (BRET) or duplicate (FA). [a]Observed association rate constant (k_{obs}) ± SEM describing the fast and slow component of the association of **3.1** or **3.2** (c = 2 nM) to the NLuc-M_2R obtained by applying a fit for biexponential association to data from BRET binding experiments; values in parentheses indicate the fraction of the fast component. [b]Observed association rate constant ($k_{obs(mono)}$) ± SEM from BRET binding experiments assuming a monophasic association for **3.1** (c = 2 nM). [c]Dissociation rate constant (k_{off}) ± SEM describing the fast and slow component of the dissociation of **3.1** or **3.2** obtained by applying a fit for biexponential decay to data from BRET or FA binding experiments; values in parentheses indicate the fraction of the fast component. [d,e]Dissociation rate constant ($k_{off(mono)}$) ± SEM describing the (monophasic) dissociation of **3.1** obtained [d] by applying a fit for monoexponential decay to data from BRET binding experiments or [e] by global analysis of FA binding experiments. [f,g]Association rate constant ($k_{on(mono)}$) assuming a monophasic association for **3.1**, [f] calculated using $k_{obs(mono)}$, $k_{off(mono)}$, and the used concentration of **3.1** (c = 2 nM) ($k_{on(mono)}$ = ($k_{obs(mono)}$ - $k_{off(mono)}$) / c(ligand)) or [g] obtained by global analysis of FA experiments; for [f], the indicated error is the propagated error, whereas the error of [g] represents the SEM. [h]Kinetically derived dissociation constant ($K_d^{kinetic}$ = $k_{off(mono)}$ / $k_{on(mono)}$; transformed into a p$K_d^{kinetic}$ value) ± propagated error from BRET experiments, assuming monophasic behavior for **3.1**. [i]Dissociation constant obtained by global analysis (pK_d^{global}) ± SEM from kinetic FA experiments. [k]Equilibrium dissociation constants (p$K_d^{equilibrium}$) ± SEM obtained from saturation binding experiments; values were taken from Table 3.1 and were renamed as p$K_d^{equilibrium}$ for clarification. n.a. not applicable.

In contrast to the BRET assay, simple exponential functions are not sufficient to accurately describe the association kinetics of a ligand determined in the FA assay. This can be caused by the ligand depletion, which is present due to the assay setup, and a change of the quantum yield upon binding, as it was observed for **3.1**. However, global kinetic modeling takes both effects into account and allows the simultaneous consideration of both the FA and TFI values for all tested receptor and fluorescent ligand concentrations, which results in a greater accuracy of kinetic constants.[55] Therefore, we used the datasets generated during the experiments described in section 3.3.1 (note: measurements were performed in kinetic mode) to obtain the global parameters describing the binding of the fluorescent ligands (for **3.1**: see Figure 3.7 and Appendix Figure A9). The biexponential equations, which were found to be the preferred model for the binding of **3.1** in the BRET assay, can theoretically arise due to many different effects. However, proposing a mechanistic model that would explain the biphasic behavior was not feasible based on the data from FA experiments. As the analysis of the data from BRET binding experiments with **3.1** based on a monophasic model yielded pK_d values in the same range as the equilibrium experiments, we instead used a single binding site model for the global analysis of the association of **3.1** in FA experiments. Furthermore, the dissociation kinetics of **3.1** could be reasonably explained by a monophasic model, which supported the applicability of the single binding site model in this case. In total, the global model can describe the general changes of FA and TFI over time and for the different receptor and ligand concentrations with sufficient accuracy (Figure 3.7 and Appendix Figure A9). The dissociation constant of **3.1** derived from global analysis (pK_d^{global}(**3.1**) = 9.12 ± 0.04) was found to match the dissociation constants from BRET and FA measurements at equilibrium (cf. Table 3.2). In contrast to **3.1**, compound **3.2** showed an apparent biphasic behaviour for association and dissociation in the FA assay (see Figure 3.6B), similar to the BRET assay results. Therefore, global analysis using a single binding site model was not applicable. As neither the global model nor exponential equations were suited for fitting the association kinetics of **3.2**, no reliable estimates of association rate constants could be calculated. In contrast, for dissociation kinetics, the conditions for first order reactions are generally fulfilled, which allowed calculating dissociation rate constants for **3.2** (cf. Table 3.2). The determined fast and slow dissociation rate constants differed by ≈ 100-fold (cf. Table 3.2), which further confirmed the assumption of a biphasic behavior for **3.2**.

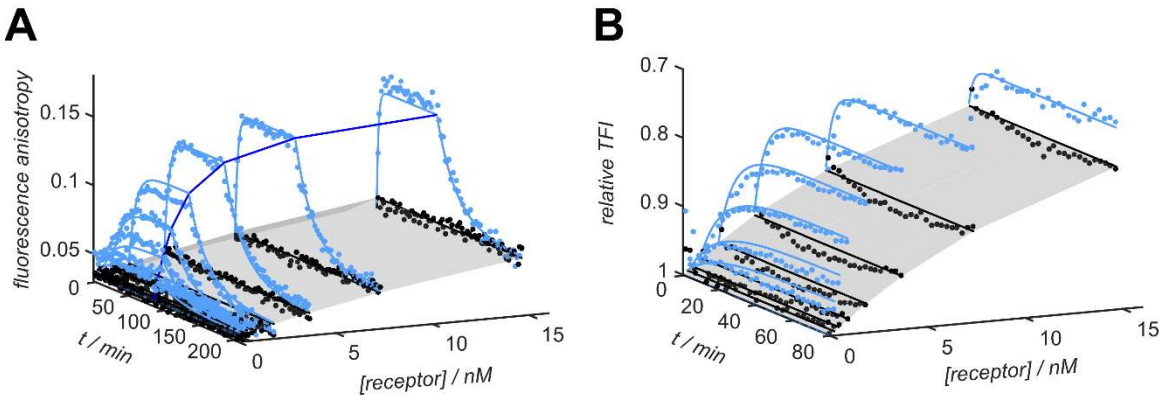

Figure 3.7: Time-dependent change of FA (**A**) and TFI (**B**) upon binding of **3.1** (c = 0.5 nM) to different concentrations of the M_2R displayed on BBVs. Graphs show representative results from one of three independent experiments performed in duplicate. The global fit of the data from FA experiments using the single binding site model under consideration of ligand depletion and the change in quantum yield is indicated by the light blue lines (total binding) and grey surface (non-specific binding). The dark blue line in **A** indicates the timepoint, where the dissociation was initiated by the addition of atropine (c = 8 µM). The relative TFI axis was inverted for visualization purposes. (for details, see Appendix: *Global kinetic modeling of FA binding experiments with the fluorescent MR ligand **3.1**,* pp.151-155*)*.

3.3.3 Competition binding experiments with 3.1 and reported MR ligands

Next, we wanted to investigate whether both methods were equally suited for determining M_2R affinities of unlabeled MR ligands. For this purpose, we performed competition binding experiments with several MR ligands (for structures, see Appendix Figure A11) covering different qualities of action (agonists vs. antagonists, orthosteric vs. allosteric ligands) over a wide affinity range. **3.1** was used as the fluorescent probe because it showed reversible M_2R binding (cf. Figure 3.6) and monophasic dissociation (FA) or dissociation kinetics close to monophasic behavior (BRET).

The real-time feature of both assays enabled the time-dependent monitoring of competition binding experiments with **3.1** and the unlabeled ligands (representative experiments with **3.1** and NMS in Figure 3.8). Steady signal intensities, indicating equilibrium, were reached after approximately 40 min.

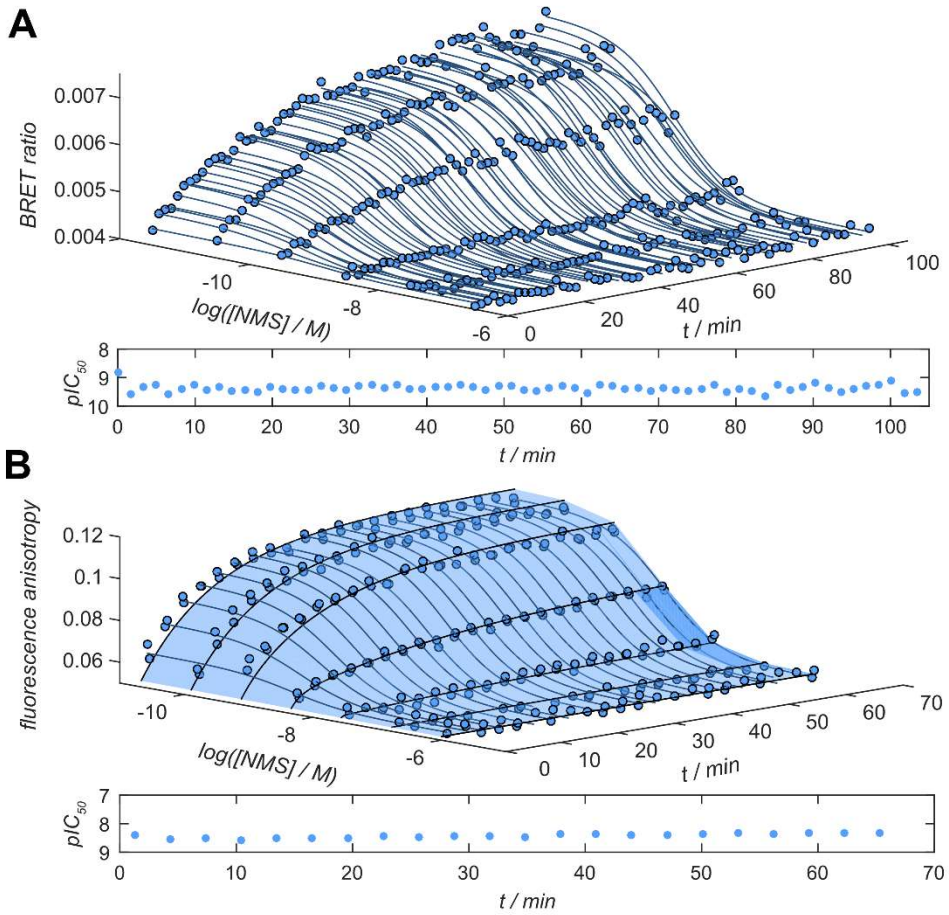

Figure 3.8: Time-dependence of the displacement of **3.1** (c = 2 nM (**A**) or c = 1 nM (**B**)) with increasing concentrations of NMS obtained from BRET (**A**) or FA (**B**) competition binding experiments. Data shown in **A** represent means ± SEM of a representative experiment performed in triplicate. In **B**, the duplicates of a representative experiment are shown. The global fit of a single binding site model to the data from FA experiments (**B**) is indicated by the light blue surface. The changes in pIC_{50} values over time are shown in separate boxes below the respective graphs.

All tested compounds could displace the fluorescent ligand **3.1** completely from the M_2R in both assays (Figure 3.9). M_2R affinities (pK_i values), calculated according to the Cheng-Prusoff equation,[43] are summarized in Table 3.3. It should be noted that the application of the Cheng-Prusoff equation requires the competition of both ligands for the same binding site.[43] As previously reported, fluorescent M_2R ligands, that have a closely related structure to **3.1** (same pharmacophore, different fluorophore), showed dualsteric binding to the M_2R and were fully competitive with the allosteric M_2R modulator W84.[32] Thus, the same behavior was assumed for **3.1** and a pK_i value was also calculated for W84.

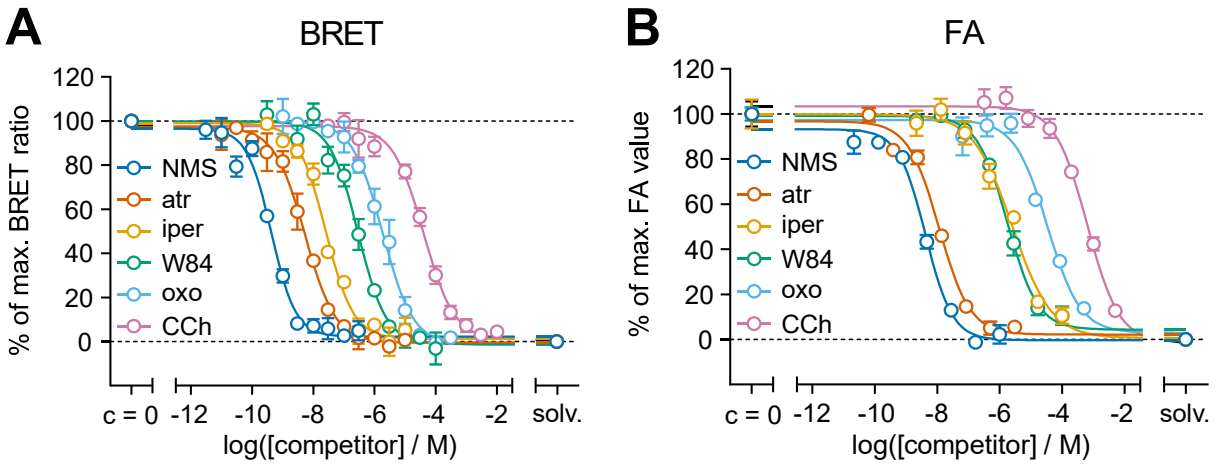

Figure 3.9: Displacement curves from BRET (**A**) and FA (**B**) competition binding experiments at the M_2R performed with **3.1** (c = 2 nM (**A**), and 1 nM (**B**), respectively) and reported orthosteric and allosteric M_2R ligands. BRET-based experiments (**A**) were performed at HEK293T cells stably expressing the NLuc-M_2R. FA measurements (**B**) were performed on BBVs displaying the M_2R on their envelope ($V(BBV_{stock})$ = 10 µL, $c(M_2R) \approx 3.5$ nM). Presented curves originate from values after an incubation time of 60 min. Data represent means ± SEM from at least four independent experiments, each performed in triplicate (**A**), or means ± SEM of one representative experiment from at least three independent experiments performed in duplicate (**B**). solv.: solvent control.

As described above, when performing the FA assay, the fluorescent ligand must be used in a similar concentration range as the receptor to reliably detect changes in FA after ligand binding, which consequently leads to ligand depletion. Together with the changing quantum yield of **3.1** upon binding to the receptor, this potentially precludes the calculation of accurate pK_i values using the Cheng-Prusoff equation. A global model takes these effects into account and represents a more rigorous and correct way to calculate ligand affinity constants in the FA assay. Therefore, we applied global fitting of a single binding site model to the data from FA competition binding experiments (see Figure 3.8B) and compared the results with the ones obtained by applying the Cheng-Prusoff equation. Surprisingly, a very good correlation (R^2 = 0.99) with a regression slope not significantly different from unity (0.97 ± 0.07) was found between the pK_i values from the global analysis and the pK_i values that were calculated from pIC_{50} values according to the Cheng-Prusoff equation (see Appendix Figure A12). This can be explained by a mutual compensation of the occurring ligand depletion and the decrease in quantum yield under these particular assay conditions. Consequently, the Cheng-Prusoff equation can be used as a reasonable simplification for the calculation of pK_i values when using the presented FA M_2R competition binding assay. However, it must be pointed out that such a simplification may not be true for other assay conditions or when studying other fluorescent ligands or receptors.

Table 3.3: Binding data (pK_i values) of reported orthosteric and allosteric MR ligands obtained from BRET-based and FA-based competition binding experiments using **3.1** as a fluorescent probe.

Compound	BRET comp. binding		FA comp. binding			Radioligand comp. binding
	pK_i[a]	*N*	pK_i[b]	pK_i (global analysis)[c]	*N*	p$K_{i/A}$[d]
carbachol	4.85 ± 0.06	5	3.79 ± 0.17	3.48 ± 0.03	3	4.96-5.92[56-59]
oxotremorine	6.19 ± 0.08	4	5.10 ± 0.05	5.17 ± 0.09	4	6.02[60], 7.04[32]
iperoxo	8.03 ± 0.07	4	6.15 ± 0.14	6.29 ± 0.03	4	7.49-9.15[58,61-64]
atropine	8.74 ± 0.06	5	8.42 ± 0.15	8.28 ± 0.04	3	8.30-9.04[53,56,60,64-68]
NMS	9.83 ± 0.07	4	8.82 ± 0.09	8.84 ± 0.06	3	9.37-10.04[32,61,68-70]
W84	7.07 ± 0.03	4	6.46 ± 0.25	6.53 ± 0.07	5	6.55-8.08[61,64,68]

[a]Determined by BRET competition binding experiments with **3.1** (c = 2 nM) at HEK293T cells stably expressing the NLuc-M_2R; pK_i values were calculated according to the Cheng-Prusoff equation[43] from pIC_{50} values determined after 60 min of incubation time (c(**3.1**) = 2 nM, K_d = 1.07 nM); data represent means ± SEM from *N* independent experiments, each performed in triplicate. [b,c]Determined by FA competition binding experiments with **3.1** (c = 1 nM) on BBVs displaying the M_2R. [b]pK_i values were calculated according to the Cheng-Prusoff equation[43] from pIC_{50} values determined after 60 min of incubation time (c(**3.1**) = 1 nM, K_d^{global} = 0.76 nM). [c]pK_i values were obtained by global analysis of the data from FA experiments. [d]Reported pK_i values (except for W84) obtained from radioligand competition binding experiments with the radiolabeled antagonist [^{3}H]NMS in different mammalian expression systems. For the allosteric M_2R modulator W84, pK_A values calculated according to the allosteric ternary complex model are shown[61,64,68].

The affinities of the MR ligands, determined with the BRET and the FA assay, were compared with each other and literature data (cf. Table 3.3 and Figure 3.10). For the latter, only results from radioligand competition binding studies with the standard MR radioligand [^{3}H]NMS in different mammalian receptor expression systems were included. For the allosteric M_2R modulator W84, a direct correlation of the pK_i values was only tested between the BRET and the FA assay, as the orthosteric radioligand [^{3}H]NMS and W84 were shown to address distinct binding sites,[39] precluding the calculation of a pK_i value for W84. Generally, the M_2R affinities, covering a broad range, correlated very well between the two studied assays (see Figure 3.10A, R^2 = 0.94) as well as between the BRET assay and radioligand binding data (literature values, see Figure 3.10C, R^2 = 0.997) and between the FA assay and radioligand binding data (see Figure 3.10B, R^2 = 0.94).

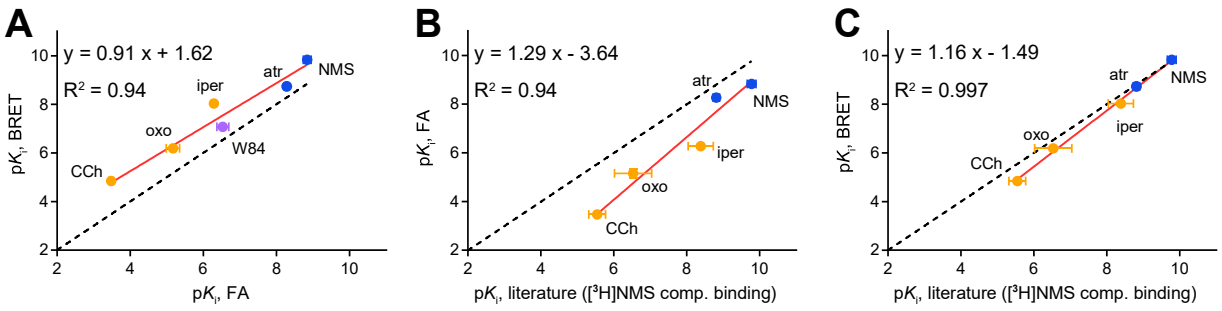

Figure 3.10: Correlation plots of affinities (pK_i values) of reported MR ligands measured in different test systems. (**A**) Comparison of pK_i values determined by BRET competition binding experiments and pK_i values obtained from FA competition binding experiments. (**B**) Comparison of pK_i values determined in the FA competition binding assay and pK_i values from literature (determined by radioligand competition binding experiments with [^{3}H]NMS. (**C**) Comparison of pK_i values determined by BRET competition binding experiments and pK_i values from literature (determined by radioligand competition binding experiments with [^{3}H]NMS). Investigated agonists are presented as orange symbols, antagonists as blue symbols and the allosteric modulator W84 as a purple symbol. Solid red lines indicate Deming regression, whereas black dashed lines would represent a perfect agreement between the datasets. Error bars represent the SEM.

The largest discrepancies were found for the investigated agonists (carbachol, oxotremorine and iperoxo): the pK_i values from the FA assay were consistently lower than the pK_i values from BRET or radioligand competition binding assays. This might be attributed to the differences in the used expression systems. Whereas mammalian G proteins are present in HEK293T cells (BRET assay), they are absent in BBVs (FA assay), if no additional co-transfection was performed. Consequently, active receptor conformations of the M_2R, generally representing the high-affinity receptor state in terms of agonist binding,[71,72] cannot be stabilized by G proteins in the Sf9/BBV expression system. This results in lower apparent pK_i values for agonists in the FA assay (note: the M_2R was additionally reported to couple only weakly, if at all, to insect G proteins[73,74]).

3.4 Conclusion

To the best of our knowledge, this study represents the first direct comparison of FA and BRET binding assays at the same target using the same fluorescent probes, here shown for the M_2R. The assays both allow for real-time measurements of ligand binding, even though they are based on different technical concepts. In this study, both fluorescence-based assays proved to be attractive alternatives to canonical binding assays, e.g. radioligand binding assays, as the affinities of fluorescently labeled and unlabeled receptor ligands could be reliably determined with a similar throughput.

However, both methods exhibit some distinct advantages and disadvantages (cf. Table 3.4). To set up a BRET assay, the receptor of interest must be genetically modified, which potentially alters the receptor's behavior. In contrast, the FA assay can be performed with unmodified receptors. Moreover, a luciferase substrate is needed for the BRET assay to monitor ligand binding, limiting the duration of the experiments. The BRET assay is mainly performed at whole live cells, whereas the FA assay is preferentially performed using membranes (here: receptors displayed on viral envelopes). The difference in receptor source might cause discrepancies in apparent ligand affinities, e.g. because of differences in membrane composition, membrane potential or the absence of G proteins. However, the BRET binding assay should in general also be feasible with luciferase-tagged receptors displayed on baculoviruses, which might allow the effect of different expression systems to be studied more directly in the future. The requirement of an external light source for the FA assay could, in contrast to the bioluminescence-based BRET assay, lead to photobleaching of the fluorescent ligands. In conjunction with the limitations concerning the fluorescence lifetime, this narrows the portfolio of fluorophores suitable for FA. Furthermore, the complexity of the data analysis for FA experiments requires specialized software and training.

Nevertheless, both methods are superior to radioligand binding assays regarding the measurement of binding kinetics. They can be performed in a homogeneous manner without any separation or washing steps, allowing for higher throughput, and possess a better temporal resolution, which gives more detailed information about the binding behavior. For this study specifically, the acquired kinetic data suggested a complex binding mechanism of both ligands at the M_2R, especially for **3.2**. Since this was consistent in both assays, the observation is unlikely to be caused by any assay system artifacts (e.g. different assay principles, receptor sources or equipment). These observations need to be investigated in more detail in future studies. Hypothetically, effects of allosteric sites,[75-77] the presence of multiple receptor populations arising from oligomerization[78,79] or multi step binding mechanisms,[80] which have all previously been observed in MR binding studies, might be involved.

Table 3.4: Advantages and disadvantages of the BRET binding assay and the FA binding assay

	BRET binding assay	FA binding assay
Pros	- homogeneous and easy-to-perform real-time assay - broad set of usable fluorophores - (preferentially) live cell-based assay that is closer to physiological conditions - simple data analysis - no external light source needed	- homogeneous and easy-to-perform real-time assay - can be studied at both modified and wild type receptors - measurements over longer time periods possible - possibility of a direct determination of the receptor concentration - works for all receptors if a suitable fluorescent ligand is available
Cons	- receptors must be genetically modified - luciferase tag might alter ligand binding - must be optimized for every receptor - requirement for a luciferase substrate - duration of experiments is limited by substrate depletion - potential underestimation of non-specific binding	- smaller set of usable fluorophores (fluorescence lifetime as limiting factor) - receptors might behave differently in (viral) membranes - more complex data analysis - external light source might bleach the fluorophore - high non-specific binding can distort the assay results

3.5 References

1. Paton, W. D. & Rang, H. P. The uptake of atropine and related drugs by intestinal smooth muscle of the guinea-pig in relation to acetylcholine receptors. *Proc. R. Soc. Lond. B Biol. Sci.* **163**, 1-44, doi:10.1098/rspb.1965.0058 (1965).

2. Sridharan, R., Zuber, J., Connelly, S. M., Mathew, E. & Dumont, M. E. Fluorescent approaches for understanding interactions of ligands with G protein coupled receptors. *Biochim. Biophys. Acta Biomembr.* **1838**, 15-33, doi:10.1016/j.bbamem.2013.09.005 (2014).

3. Stoddart, L. A., White, C. W., Nguyen, K., Hill, S. J. & Pfleger, K. D. Fluorescence- and bioluminescence-based approaches to study GPCR ligand binding. *Br. J. Pharmacol.* **173**, 3028-3037, doi:10.1111/bph.13316 (2016).

4. Sykes, D. A., Stoddart, L. A., Kilpatrick, L. E. & Hill, S. J. Binding kinetics of ligands acting at GPCRs. *Mol. Cell. Endocrinol.* **485**, 9-19, doi:10.1016/j.mce.2019.01.018 (2019).

5. Nosjean, O., Souchaud, S., Deniau, C., Geneste, O., Cauquil, N. & Boutin, J. A. A simple theoretical model for fluorescence polarization binding assay development. *J. Biomol. Screen.* **11**, 949-958, doi:10.1177/1087057106294841 (2016).

6. Hoffmann, C., Castro, M., Rinken, A., Leurs, R., Hill, S. J. & Vischer, H. F. Ligand residence time at G-protein–coupled receptors—why we should take our time to study it. *Mol. Pharmacol.* **88**, 552-560, doi:10.1124/mol.115.099671 (2015).

7. Allen, M., Reeves, J. & Mellor, G. High throughput fluorescence polarization: a homogeneous alternative to radioligand binding for cell surface receptors. *J. Biomol. Screen.* **5**, 63-69, doi:10.1177/108705710000500202 (2000).

8. Banks, P., Gosselin, M. & Prystay, L. Fluorescence polarization assays for high throughput screening of G protein-coupled receptors. *J. Biomol. Screen.* **5**, 159-168, doi:10.1177/108705710000500308 (2000).

9. Kecskés, M., Kumar, T. S., Yoo, L., Gao, Z.-G. & Jacobson, K. A. Novel Alexa Fluor-488 labeled antagonist of the A_{2A} adenosine receptor: application to a fluorescence polarization-based receptor binding assay. *Biochem. Pharmacol.* **80**, 506-511, doi:10.1016/j.bcp.2010.04.027 (2010).

10. Veiksina, S., Kopanchuk, S. & Rinken, A. Fluorescence anisotropy assay for pharmacological characterization of ligand binding dynamics to melanocortin 4 receptors. *Anal. Biochem.* **402**, 32-39, doi:10.1016/j.ab.2010.03.022 (2010).

11. Corriden, R., Kilpatrick, L. E., Kellam, B., Briddon, S. J. & Hill, S. J. Kinetic analysis of antagonist-occupied adenosine-A_3 receptors within membrane microdomains of individual cells provides evidence of receptor dimerization and allosterism. *FASEB J.* **28**, 4211-4222, doi:10.1096/fj.13-247270 (2014).

12. Grime, R. L., Goulding, J., Uddin, R., Stoddart, L. A., Hill, S. J., Poyner, D. R., Briddon, S. J. & Wheatley, M. Single molecule binding of a ligand to a G-protein-coupled receptor in real time using fluorescence correlation spectroscopy, rendered possible by nano-encapsulation in styrene maleic acid lipid particles. *Nanoscale* **12**, 11518-11525, doi:10.1039/d0nr01060j (2020).

13. Emami-Nemini, A., Roux, T., Leblay, M., Bourrier, E., Lamarque, L., Trinquet, E. & Lohse, M. J. Time-resolved fluorescence ligand binding for G protein–coupled receptors. *Nat. Protoc.* **8**, 1307-1320, doi:10.1038/nprot.2013.073 (2013).

14. Schiele, F., Ayaz, P. & Fernández-Montalván, A. A universal homogeneous assay for high-throughput determination of binding kinetics. *Anal. Biochem.* **468**, 42-49, doi:10.1016/j.ab.2014.09.007 (2015).

15. Tahtaoui, C., Parrot, I., Klotz, P., Guillier, F., Galzi, J. L., Hibert, M. & Ilien, B. Fluorescent pirenzepine derivatives as potential bitopic ligands of the human M1 muscarinic receptor. *J. Med. Chem.* **47**, 4300-4315, doi:10.1021/jm040800a (2004).

16. Valenzuela-Fernández, A. n., Palanche, T., Amara, A., Magerus, A., Altmeyer, R., Delaunay, T., Virelizier, J.-L., Baleux, F., Galzi, J.-L. & Arenzana-Seisdedos, F. Optimal inhibition of X4 HIV isolates by the CXC chemokine stromal cell-derived factor 1α requires interaction with cell surface heparan sulfate proteoglycans. *J. Biol. Chem.* **276**, 26550-26558, doi:10.1074/jbc.M100411200 (2001).

17. Bartole, E., Grätz, L., Littmann, T., Wifling, D., Seibel, U., Buschauer, A. & Bernhardt, G. UR-DEBa242: a Py-5-labeled fluorescent multipurpose probe for investigations on the histamine H_3 and H_4 receptors. *J. Med. Chem.* **63**, 5297-5311, doi:10.1021/acs.jmedchem.0c00160 (2020).

18. Hoare, B. L., Bruell, S., Sethi, A., Gooley, P. R., Lew, M. J., Hossain, M. A., Inoue, A., Scott, D. J. & Bathgate, R. A. D. Multi-component mechanism of H2 relaxin binding to RXFP1 through NanoBRET kinetic analysis. *iScience* **11**, 93-113, doi:10.1016/j.isci.2018.12.004 (2019).

19. Sakyiamah, M. M., Nomura, W., Kobayakawa, T. & Tamamura, H. Development of a NanoBRET-based sensitive screening method for CXCR4 ligands. *Bioconjug. Chem.* **30**, 1442-1450, doi:10.1021/acs.bioconjchem.9b00182 (2019).

20. Soave, M., Stoddart, L. A., Brown, A., Woolard, J. & Hill, S. J. Use of a new proximity assay (NanoBRET) to investigate the ligand-binding characteristics of three fluorescent ligands to the human β_1-adrenoceptor expressed in HEK-293 cells. *Pharmacol. Res. Perspect.* **4**, e00250, doi:10.1002/prp2.250 (2016).

21. Stoddart, L. A., Johnstone, E. K. M., Wheal, A. J., Goulding, J., Robers, M. B., Machleidt, T., Wood, K. V., Hill, S. J. & Pfleger, K. D. G. Application of BRET to monitor ligand binding to GPCRs. *Nat. Methods* **12**, 661-663, doi:10.1038/nmeth.3398 (2015).

22. Hall, M. P., Unch, J., Binkowski, B. F., Valley, M. P., Butler, B. L., Wood, M. G., Otto, P., Zimmerman, K., Vidugiris, G., Machleidt, T., Robers, M. B., Benink, H. A., Eggers, C. T., Slater, M. R., Meisenheimer, P. L., Klaubert, D. H., Fan, F., Encell, L. P. & Wood, K. V. Engineered luciferase reporter from a deep sea shrimp utilizing a novel imidazopyrazinone substrate. *ACS Chem. Biol.* **7**, 1848-1857, doi:10.1021/cb3002478 (2012).

23. Stoddart, L. A., Kilpatrick, L. E. & Hill, S. J. NanoBRET approaches to study ligand binding to GPCRs and RTKs. *Trends Pharmacol. Sci.* **39**, 136-147, doi:10.1016/j.tips.2017.10.006 (2018).

24. Rinken, A., Lavogina, D. & Kopanchuk, S. Assays with detection of fluorescence anisotropy: challenges and possibilities for characterizing ligand binding to GPCRs. *Trends Pharmacol. Sci.* **39**, 187-199, doi:10.1016/j.tips.2017.10.004 (2018).

25. Jameson, D. M. & Ross, J. A. Fluorescence polarization/anisotropy in diagnostics and imaging. *Chem. Rev.* **110**, 2685-2708, doi:10.1021/cr900267p (2010).

26. Caulfield, M. P. & Birdsall, N. J. International Union of Pharmacology. XVII. Classification of muscarinic acetylcholine receptors. *Pharmacol. Rev.* **50**, 279-290 (1998).

27. Kruse, A. C., Kobilka, B. K., Gautam, D., Sexton, P. M., Christopoulos, A. & Wess, J. Muscarinic acetylcholine receptors: novel opportunities for drug development. *Nat. Rev. Drug Discov.* **13**, 549-560, doi:10.1038/nrd4295 (2014).

28. Langmead, C. J., Watson, J. & Reavill, C. Muscarinic acetylcholine receptors as CNS drug targets. *Pharmacol. Ther.* **117**, 232-243, doi:10.1016/j.pharmthera.2007.09.009 (2008).

29. Caulfield, M. P. Muscarinic receptors—characterization, coupling and function. *Pharmacol. Ther.* **58**, 319-379, doi:10.1016/0163-7258(93)90027-b (1993).

30. Eglen, R. M., Hegde, S. S. & Watson, N. Muscarinic receptor subtypes and smooth muscle function. *Pharmacol. Rev.* **48**, 531-565 (1996).

31. Gruber, C. G., Pegoli, A., Müller, C., Grätz, L., She, X. & Keller, M. Differently fluorescence-labelled dibenzodiazepinone-type muscarinic acetylcholine receptor ligands with high M_2R affinity. *RSC Med. Chem.* **11**, 823-832, doi:10.1039/d0md00137f (2020).

32. She, X., Pegoli, A., Gruber, C. G., Wifling, D., Carpenter, J., Hübner, H., Chen, M., Wan, J., Bernhardt, G., Gmeiner, P., Holliday, N. D. & Keller, M. Red-emitting dibenzodiazepinone derivatives as fluorescent dualsteric probes for the muscarinic acetylcholine M_2 receptor. *J. Med. Chem.* **63**, 4133-4154, doi:10.1021/acs.jmedchem.9b02172 (2020).

33. Kilpatrick, L. E., Friedman-Ohana, R., Alcobia, D. C., Riching, K., Peach, C. J., Wheal, A. J., Briddon, S. J., Robers, M. B., Zimmerman, K., Machleidt, T., Wood, K. V., Woolard, J. & Hill, S. J. Real-time analysis of the binding of fluorescent $VEGF_{165}$a to VEGFR2 in living cells: effect of receptor tyrosine kinase inhibitors and fate of internalized agonist-receptor complexes. *Biochem. Pharmacol.* **136**, 62-75, doi:10.1016/j.bcp.2017.04.006 (2017).

34. Ito, K., Murayama, Y., Kurokawa, Y., Kanamaru, S., Kokabu, Y., Maki, T., Mikawa, T., Argunhan, B., Tsubouchi, H., Ikeguchi, M., Takahashi, M. & Iwasaki, H. Real-time tracking reveals catalytic roles for the two DNA binding sites of Rad51. *Nat. Commun.* **11**, doi:10.1038/s41467-020-16750-3 (2020).

35. Qi, J., Kizjakina, K., Robinson, R., Tolani, K. & Sobrado, P. A fluorescence polarization binding assay to identify inhibitors of flavin-dependent monooxygenases. *Anal. Biochem.* **425**, 80-87, doi:10.1016/j.ab.2012.03.002 (2012).

36. Shapiro, A. B., Comita-Prevoir, J. & Sylvester, M. 5-Carboxytetramethylrhodamine-ampicillin fluorescence anisotropy-based assay of *Escherichia coli* penicillin-binding protein 2 transpeptidase inhibition. *ACS Infect. Dis.* **5**, 863-872, doi:10.1021/acsinfecdis.8b00351 (2019).

37. Veiksina, S., Tahk, M., Laasfeld, T., Link, R., Kopanchuk, S. & Rinken, A. Fluorescence anisotropy-based assay for characterization of ligand binding dynamics to GPCRs. The case of Cy3B-labelled ligands binding to MC4 receptors in budded baculoviruses. In *G Protein-Coupled Receptor Screening Assays: Methods and Protocols, 2nd Edition, In press* (2020).

38. Laasfeld, T., Kopanchuk, S. & Rinken, A. Image-based cell-size estimation for baculovirus quantification. *Biotechniques* **63**, 161-168, doi:10.2144/000114595 (2017).

39. Pegoli, A., She, X., Wifling, D., Hubner, H., Bernhardt, G., Gmeiner, P. & Keller, M. Radiolabeled dibenzodiazepinone-type antagonists give evidence of dualsteric binding at the M_2 muscarinic acetylcholine receptor. *J. Med. Chem.* **60**, 3314-3334, doi:10.1021/acs.jmedchem.6b01892 (2017).

40. Allikalt, A. & Rinken, A. Budded baculovirus particles as a source of membrane proteins for radioligand binding assay: The case of dopamine D_1 receptor. *J. Pharmacol. Toxicol. Methods* **86**, 81-86, doi:10.1016/j.vascn.2017.04.004 (2017).

41. Allikalt, A., Kopanchuk, S. & Rinken, A. Implementation of fluorescence anisotropy-based assay for the characterization of ligand binding to dopamine D_1 receptors. *Eur. J. Pharmacol.* **839**, 40-46, doi:10.1016/j.ejphar.2018.09.008 (2018).

42. Link, R., Veiksina, S., Rinken, A. & Kopanchuk, S. Characterization of ligand binding to melanocortin 4 receptors using fluorescent peptides with improved kinetic properties. *Eur. J. Pharmacol.* **799**, 58-66, doi:10.1016/j.ejphar.2017.01.040 (2017).

43. Cheng, Y. & Prusoff, W. H. Relationship between the inhibition constant (K_i) and the concentration of inhibitor which causes 50 per cent inhibition (I_{50}) of an enzymatic reaction. *Biochem. Pharmacol.* **22**, 3099-3108, doi:10.1016/0006-2952(73)90196-2 (1973).

44. Kirkpatrick, S., Gelatt, C. D. & Vecchi, M. P. Optimization by simulated annealing. *Science* **220**, 671-680, doi:10.1126/science.220.4598.671 (1983).

45. Nelder, J. A. & Mead, R. A simplex method for function minimization. *Comput. J.* **7**, 308-313, doi:10.1093/comjnl/7.4.308 (1965).

46. Veiksina, S., Kopanchuk, S. & Rinken, A. Budded baculoviruses as a tool for a homogeneous fluorescence anisotropy-based assay of ligand binding to G protein-coupled receptors: the case of melanocortin 4 receptors. *Biochim. Biophys. Acta Biomembr.* **1838**, 372-381, doi:10.1016/j.bbamem.2013.09.015 (2014).

47. Mäkelä, A. R. & Oker-Blom, C. The baculovirus display technology - an evolving instrument for molecular screening and drug delivery. *Comb. Chem. High Throughput Screen.* **11**, 86-98, doi:10.2174/138620708783744525 (2008).

48. Loisel, T. P., Ansanay, H., St-Onge, S., Gay, B., Boulanger, P., Strosberg, A. D., Marullo, S. & Bouvier, M. Recovery of homogeneous and functional β_2-adrenergic receptors from extracellular baculovirus particles. *Nat. Biotechnol.* **15**, 1300-1304, doi:10.1038/nbt1197-1300 (1997).

49. Masuda, K., Itoh, H., Sakihama, T., Akiyama, C., Takahashi, K., Fukuda, R., Yokomizo, T., Shimizu, T., Kodama, T. & Hamakubo, T. A combinatorial G protein-coupled receptor reconstitution system on budded baculovirus: evidence for $G\alpha_i$ and $G\alpha_o$ coupling to a human leukotriene B_4 receptor *J. Biol. Chem.* **278**, 24552-24562, doi:10.1074/jbc.M302801200 (2003).

50. Link, R., Veiksina, S., Tahk, M. J., Laasfeld, T., Paiste, P., Kopanchuk, S. & Rinken, A. The constitutive activity of melanocortin-4 receptors in cAMP pathway is allosterically modulated by zinc and copper ions. *J. Neurochem.* **153**, 346-361, doi:10.1111/jnc.14933 (2019).

51. Tõntson, L., Kopanchuk, S. & Rinken, A. Characterization of 5-HT_{1A} receptors and their complexes with G-proteins in budded baculovirus particles using fluorescence anisotropy of Bodipy-FL-NAN-190. *Neurochem. Int.* **67**, 32-38, doi:10.1016/j.neuint.2014.01.012 (2014).

52. Dörje, F., Wess, J., Lambrecht, G., Tacke, R., Mutschler, E. & Brann, M. R. Antagonist binding profiles of five cloned human muscarinic receptor subtypes. *J. Pharmacol. Exp. Ther.* **256**, 727-733 (1991).

53. Keller, M., Tränkle, C., She, X., Pegoli, A., Bernhardt, G., Buschauer, A. & Read, R. W. M_2 subtype preferring dibenzodiazepinone-type muscarinic receptor ligands: effect of chemical homo-dimerization on orthosteric (and allosteric?) binding. *Bioorg. Med. Chem.* **23**, 3970-3990, doi:10.1016/j.bmc.2015.01.015 (2015).

54. Dale, N. C., Johnstone, E. K. M., White, C. W. & Pfleger, K. D. G. NanoBRET: the bright future of proximity-based assays. *Front. Bioeng. Biotechnol.* **7**, 56, doi:10.3389/fbioe.2019.00056 (2019).

55. Otto, M. R., Lillo, M. P. & Beechem, J. M. Resolution of multiphasic reactions by the combination of fluorescence total-intensity and anisotropy stopped-flow kinetic experiments. *Biophys. J.* **67**, 2511-2521, doi:10.1016/s0006-3495(94)80741-6 (1994).

56. Cheng, K., Khurana, S., Chen, Y., Kennedy, R. H., Zimniak, P. & Raufman, J.-P. Lithocholylcholine, a bile acid/acetylcholine hybrid, is a muscarinic receptor antagonist. *J. Pharmacol. Exp. Ther.* **303**, 29-35, doi:10.1124/jpet.102.036376 (2002).

57. Dei, S., Angeli, P., Bellucci, C., Buccioni, M., Gualtieri, F., Marucci, G., Manetti, D., Matucci, R., Romanelli, M. N., Scapecchi, S. & Teodori, E. Muscarinic subtype affinity and functional activity profile of 1-methyl-2-(2-methyl-1,3-dioxolan-4-yl)pyrrolidine and 1-methyl-2-(2-methyl-1,3-oxathiolan-5-yl)pyrrolidine derivatives. *Biochem. Pharmacol.* **69**, 1637-1645, doi:10.1016/j.bcp.2005.03.009 (2005).

58. Fish, I., Stößel, A., Eitel, K., Valant, C., Albold, S., Huebner, H., Möller, D., Clark, M. J., Sunahara, R. K., Christopoulos, A., Shoichet, B. K. & Gmeiner, P. Structure-based design and discovery of new M_2 receptor agonists. *J. Med. Chem.* **60**, 9239-9250, doi:10.1021/acs.jmedchem.7b01113 (2017).

59. Matucci, R., Bellucci, C., Martino, M. V., Nesi, M., Manetti, D., Welzel, J., Bartz, U., Holze, J., Tränkle, C., Mohr, K., Mazzolari, A., Vistoli, G., Dei, S., Teodori, E. & Romanelli, M. N. Carbachol dimers with primary carbamate groups as homobivalent modulators of muscarinic receptors. *Eur. J. Pharmacol.* **883**, 173183, doi:10.1016/j.ejphar.2020.173183 (2020).

60. Nelson, C. P., Nahorski, S. R. & Challiss, R. A. J. Constitutive activity and inverse agonism at the M_2 muscarinic acetylcholine receptor. *J. Pharmacol. Exp. Ther.* **316**, 279-288, doi:10.1124/jpet.105.094383 (2006).

61. Antony, J., Kellershohn, K., Mohr-Andrä, M., Kebig, A., Prilla, S., Muth, M., Heller, E., Disingrini, T., Dallanoce, C., Bertoni, S., Schrobang, J., Trankle, C., Kostenis, E., Christopoulos, A., Höltje, H. D., Barocelli, E., Amici, M., Holzgrabe, U. & Mohr, K. Dualsteric GPCR targeting: a novel route to binding and signaling pathway selectivity. *FASEB J.* **23**, 442-450, doi:10.1096/fj.08-114751 (2008).

62. Bock, A., Chirinda, B., Krebs, F., Messerer, R., Bätz, J., Muth, M., Dallanoce, C., Klingenthal, D., Tränkle, C., Hoffmann, C., De Amici, M., Holzgrabe, U., Kostenis, E. & Mohr, K. Dynamic ligand binding dictates partial agonism at a G protein–coupled receptor. *Nat. Chem. Biol.* **10**, 18-20, doi:10.1038/nchembio.1384 (2014).

63. Bock, A., Merten, N., Schrage, R., Dallanoce, C., Bätz, J., Klöckner, J., Schmitz, J., Matera, C., Simon, K., Kebig, A., Peters, L., Müller, A., Schrobang-Ley, J., Tränkle, C., Hoffmann, C., De Amici, M., Holzgrabe, U., Kostenis, E. & Mohr, K. The allosteric vestibule of a seven transmembrane helical receptor controls G-protein coupling. *Nat. Commun.* **3**, 1044, doi:10.1038/ncomms2028 (2012).

64. Schmitz, J., van der Mey, D., Bermudez, M., Klöckner, J., Schrage, R., Kostenis, E., Tränkle, C., Wolber, G., Mohr, K. & Holzgrabe, U. Dualsteric muscarinic antagonists–orthosteric binding pose controls allosteric subtype selectivity. *J. Med. Chem.* **57**, 6739-6750, doi:10.1021/jm500790x (2014).

65. Buckley, N. J., Bonner, T. I., Buckley, C. M. & Brann, M. R. Antagonist binding properties of five cloned muscarinic receptors expressed in CHO-K1 cells. *Mol. Pharmacol.* **35**, 469-476 (1989).

66. Huang, F., Buchwald, P., Browne, C. E., Farag, H. H., Wu, W. M., Ji, F., Hochhaus, G. & Bodor, N. Receptor binding studies of soft anticholinergic agents. *AAPS PharmSci* **3**, E30, doi:10.1208/ps030430 (2001).

67. She, X., Pegoli, A., Mayr, J., Hübner, H., Bernhardt, G., Gmeiner, P. & Keller, M. Heterodimerization of dibenzodiazepinone-type muscarinic acetylcholine receptor ligands leads to increased M_2R affinity and selectivity. *ACS Omega* **2**, 6741-6754, doi:10.1021/acsomega.7b01085 (2017).

68. Tränkle, C., Weyand, O., Voigtländer, U., Mynett, A., Lazareno, S., Birdsall, N. J. & Mohr, K. Interactions of orthosteric and allosteric ligands with [^{3}H]dimethyl-W84 at the common allosteric site of muscarinic M_2 receptors. *Mol. Pharmacol.* **64**, 180-190, doi:10.1124/mol.64.1.180 (2003).

69. Dei, S., Bellucci, C., Buccioni, M., Ferraroni, M., Guandalini, L., Manetti, D., Martini, E., Marucci, G., Matucci, R., Nesi, M., Romanelli, M. N., Scapecchi, S. & Teodori, E. Synthesis, affinity profile, and functional activity of muscarinic antagonists with a 1-methyl-2-(2,2-alkylaryl-1,3-oxathiolan-5-yl)pyrrolidine structure. *J. Med. Chem.* **50**, 1409-1413, doi:10.1021/jm061374r (2007).

70. Del Bello, F., Barocelli, E., Bertoni, S., Bonifazi, A., Camalli, M., Campi, G., Giannella, M., Matucci, R., Nesi, M., Pigini, M., Quaglia, W. & Piergentili, A. 1,4-Dioxane, a suitable scaffold for the development of novel M_3 muscarinic receptor antagonists. *J. Med. Chem.* **55**, 1783-1787, doi:10.1021/jm2013216 (2012).

71. De Lean, A., Stadel, J. M. & Lefkowitz, R. J. A ternary complex model explains the agonist-specific binding properties of the adenylate cyclase-coupled β-adrenergic receptor. *J. Biol. Chem.* **255**, 7108-7117 (1980).

72. Gether, U. Uncovering molecular mechanisms involved in activation of G protein-coupled receptors. *Endocr. Rev.* **21**, 90-113, doi:10.1210/edrv.21.1.0390 (2000).

73. Parker, E. M., Kameyama, K., Higashijima, T. & Ross, E. M. Reconstitutively active G protein-coupled receptors purified from baculovirus-infected insect cells. *J. Biol. Chem.* **266**, 519-527 (1991).

74. Uustare, A., Näsman, J., Åkerman, K. E. O. & Rinken, A. Characterization of M_2 muscarinic receptor activation of different G protein subtypes. *Neurochem. Int.* **44**, 119-124, doi:10.1016/s0197-0186(03)00103-7 (2004).

75. Birdsall, N. J. & Lazareno, S. Allosterism at muscarinic receptors: ligands and mechanisms. *Mini-Rev. Med. Chem.* **5**, 523-543, doi:10.2174/1389557054023251 (2005).

76. Gregory, K. J., Hall, N. E., Tobin, A. B., Sexton, P. M. & Christopoulos, A. Identification of orthosteric and allosteric site mutations in M_2 muscarinic acetylcholine receptors that contribute to ligand-selective signaling bias. *J. Biol. Chem.* **285**, 7459-7474, doi:10.1074/jbc.M109.094011 (2010).

77. Jakubík, J. & El-Fakahany, E. E. Current advances in allosteric modulation of muscarinic receptors. *Biomolecules* **10**, 325, doi:10.3390/biom10020325 (2020).

78. Marsango, S., Ward, R. J., Alvarez-Curto, E. & Milligan, G. Muscarinic receptor oligomerization. *Neuropharmacology* **136**, 401-410, doi:10.1016/j.neuropharm.2017.11.023 (2018).

79. Redka, D. S., Heerklotz, H. & Wells, J. W. Efficacy as an intrinsic property of the M_2 muscarinic receptor in its tetrameric state. *Biochemistry* **52**, 7405-7427, doi:10.1021/bi4003869 (2013).

80. Jakubík, J., Randáková, A., Zimčík, P., El-Fakahany, E. E. & Doležal, V. Binding of N-methylscopolamine to the extracellular domain of muscarinic acetylcholine receptors. *Sci. Rep.* **7**, doi:10.1038/srep40381 (2017).

4. Insertion of NanoLuc into the second extracellular loop as a complementary strategy to establish BRET binding assays for GPCRs

The following experimental work was performed by others:

C. Müller:	Synthesis of the fluorescent ligand **4.1** (not shown); radioligand competition binding experiments with **4.1**
Dr. A. Pegoli:	Synthesis of the fluorescent ligands **3.5**, **4.2** and **4.3** (not shown)
C. Gruber:	Synthesis of the fluorescent ligands **3.1** and **3.4** (not shown)
PD Dr. M. Keller:	Synthesis of BIBO3304 and BIBP3226 (not shown)
L. Schindler:	Radioligand saturation binding experiments at the NTS_1R(T227) and AT_1R(S186)

4.1 Introduction

G protein-coupled receptors (GPCRs) represent one of the largest protein families with more than 800 members encoded in the human genome.[1] All GPCRs share many structural features, as they all consist of an extracellular N-terminus, an intracellular C-terminus and seven transmembrane domains, which are connected by three extracellular (ECL1-3) and three intracellular loops (ICL1-3).[2,3] Due to their abundant expression in humans and their involvement in various (patho)physiological processes, GPCRs represent the most important target structure for therapy and drug discovery.[4,5] A mandatory step in the development of novel drug candidates is the assessment of their binding properties to the target. In addition to the determination of affinities, the investigation of the kinetics of ligand binding is of particular interest.[6-8] In the last decades, fluorescence-based techniques emerged as alternative or complementary methods to the widely used radioligand binding assays, as they offer distinct advantages, e.g. in terms of handling, safety and costs of waste disposal.[9-11] Especially, methods exploiting resonance energy transfer (BRET or (TR-)FRET) gained popularity because of their high throughput capability, the low influence of non-specific binding and the possibility of performing kinetic measurements in real time without any separation steps.[12-14] Stoddart *et al.* introduced a procedure to quantify binding of a fluorescent ligand based on BRET by fusing the very brightly blue light-emitting NanoLuc® (NLuc, $\lambda_{max} \approx 460$ nm)[15] to the N-terminus of a receptor of interest to serve as a bioluminescent donor.[16] Prerequisites for this technique to give robust results are an overlap of the excitation spectrum of the fluorescent ligand (acceptor) with the emission spectrum of the luciferase (donor), an appropriate distance (approx. < 10 nm) between donor and acceptor and their correct orientation towards each other.[13] However, although this technique has been used successfully for the determination of binding affinities and binding kinetics at several GPCRs across different classes,[17-22] we realized that it was not universally applicable for all receptors. While exploring possible reasons, we noticed that receptors, for which this approach failed, had comparatively long N-termini (> 40 amino acids). Therefore, it was the aim of this study to get a better understanding whether the N-terminus of the receptor affects the applicability of the approach described by Stoddart *et al.* based on an N-terminally NLuc-tagged receptor.[16] Furthermore, we wanted to develop an alternative strategy for those receptors, for which the N-terminal fusion of NLuc did not result in functioning BRET binding assays. The neuropeptide Y Y_1 receptor (Y_1R) was first taken as a model receptor to address these questions due to its rather long N-terminus (44 amino acids) and an N-terminally NLuc-tagged Y_1R was generated to test the original approach.[16] Due to the lack of a specific BRET signal, we examined the insertion of NLuc into unstructured regions within the ECL2 and ECL3 of the Y_1R, which ultimately enabled BRET binding experiments at this receptor.

The presented approach was then transferred to the neurotensin receptor 1 (NTS_1R) comprising an N-terminus of 67 amino acids. Furthermore, the applicability was tested at two receptors with slightly shorter N-termini, the angiotensin II receptor type 1 (AT_1R) and the M_1 muscarinic acetylcholine receptor (M_1R). For both receptors, the N-terminal fusion of NLuc resulted in specific BRET upon addition of a fluorescently labeled ligand, but the assays were either compromised by low signal-to-background (S/B) ratios or gave ligand affinities inconsistent with reference data from canonical assays. Besides the determination of the affinities of fluorescently labeled and unlabeled ligands to their target, we performed a detailed analysis of the binding kinetics of the fluorescent ligands with a focus on the NTS_1R and the AT_1R.

4.2 Materials and methods

4.2.1 Materials

Dulbecco's Modified Eagle's Medium (DMEM), L-glutamine, fetal calf serum (FCS), HEPES and Triton X-100 were from Sigma-Aldrich (Munich, Germany). Trypsin/EDTA (0.05%/0.02%) was from Biochrom (Berlin, Germany). Leibovitz' L-15 medium (L-15) and geneticin (G418) were from Fisher Scientific (Nidderau, Germany). Bovine serum albumin (BSA) and bacitracin were from SERVA Electrophoresis (Heidelberg, Germany). Furimazine (Nano-Glo® Live Cell Substrate) was purchased from Promega (Mannheim, Germany). The pcDNA3.1 vector was from Thermo Fisher (Nidderau, Germany).

Alcuronium chloride (alc), atropine sulfate (atr), carbachol (CCh), iperoxo iodide (iper), N-methyl scopolamine bromide (NMS) and pirenzepine dihydrochloride (pir) were from Sigma-Aldrich (Munich, Germany). BMS193885, oxotremorine sesquifumarate (oxo), PD160170 and SR142948 (SR) were from Tocris Bioscience (Bristol, UK). Candesartan (can) and losartan potassium salt (los) were kindly provided by Hexal AG (Holzkirchen, Germany). Neurotensin(8-13) (NT(8-13)) and porcine neuropeptide Y (pNPY) were from SynPeptide (Shanghai, China), whereas angiotensin II (ang II) was from Bachem (Bubendorf, Switzerland). The radioligand [^{3}H]NMS (specific activity = 80 Ci/mmol) was purchased from American Radiolabeled Chemicals Inc. (St. Louis, MO, USA). The syntheses of UR-MK299 and the radioligand [^{3}H]UR-MK299 as well as the syntheses of the radioligands [^{3}H]UR-MK292 and [^{3}H]UR-MK300 were reported elsewhere.[23,24] Stock solutions of the fluorescent ligands were prepared in DMSO (Merck Millipore, Darmstadt, Germany) and stored in aliquots at -80 °C. Stock solutions of angiotensin II and NT(8-13) were prepared in a mixture of ethanol and 50 mM HCl (30:70). Stock solutions of the other competitive ligands were prepared in H_2O or in DMSO, whenever the compound was insoluble in H_2O.

4.2.2 Generation of plasmids

Plasmids containing the sequences of the investigated human GPCRs (neuropeptide Y Y_1 receptor (Y_1R), neurotensin receptor 1 (NTS_1R), angiotensin II receptor type 1 (AT_1R) and M_1 muscarinic acetylcholine receptor (M_1R)) were purchased from the cDNA Resource Center (Rolla, MO, USA). The vector encoding NanoLuc® (NLuc) was obtained from Promega (Mannheim, Germany). All constructs in this study were generated using standard PCR and restriction techniques. The vectors encoding the N-terminally NLuc-tagged receptors (Nterm) were prepared by exchanging the receptor sequence in the previously described pcDNA3.1 NLuc-hH_4R[17] by the respective GPCR of interest. The pcDNA3.1 Y_1R(Δ1-31) encoding NLuc fused to the N-terminus of a truncated Y_1 receptor (lacking amino acids 1-31) was obtained

analogously. For the constructs with the luciferase being located within the ECLs, NLuc was integrated into the receptor sequence downstream of the indicated amino acids (e.g. pcDNA3.1 Y_1R(Y192): after the tyrosine in position 192). A short flexible linker sequence consisting of Gly and Ser was used to connect the luciferase to the receptor at both the 5' and 3' ends. The quality of all generated plasmids was verified by sequencing (Eurofins Genomics, Ebersberg, Germany).

4.2.3 Cell culture and generation of stable transfectants

HEK293T cells (kind gift from Prof. Dr. Wulf Schneider, Institute for Medical Microbiology and Hygiene, University of Regensburg, Germany) were cultivated in DMEM supplemented with 2 mM L-glutamine and 10% FCS at 37 °C in a water-saturated atmosphere (containing 5% CO_2). One day before transfection, the cells were seeded at a density of $3 \cdot 10^5$ cells/mL in 6-well plates (Sarstedt, Nümbrecht, Germany). On the following day, cells were transfected with 2 µg of the respective cDNA using X-tremeGENE^{TM} HP (Roche Diagnostics, Mannheim, Germany) as the transfection reagent (used according to manufacturer's protocol). After two days, the transfected cells were detached by trypsinization, centrifuged (500 *g*, 5 min) and seeded on a 150 mm-cell culture dish (Sarstedt, Nümbrecht, Germany) in DMEM containing 10% FCS and G418 at a final concentration of 1 mg/mL. The medium was changed on a regular basis for 2-3 weeks until stable growth of cell colonies was observed. The culture of the stable transfectants was continued using G418 at a concentration of 600 µg/mL. All cells were regularly tested for mycoplasma infection using the Venor GeM Mycoplasma Detection Kit (Minerva Biolabs, Berlin, Germany) and were negative.

4.2.4 Radioligand binding experiments

Radioligand saturation binding experiments at intact, suspended HEK293T cells stably expressing the Y_1R(Nterm), the Y_1R(Δ1-31), the Y_1R(Y192), the M_1R(Nterm) or the M_1R(G176) were performed according to a procedure described for CHO cells[25] (also cf. Chapter 3) with the following minor modifications: After reaching approx. 80% confluency, the cells were detached from the cell culture flask by trypsinization. After centrifugation (400 *g*, 6 min), the cells were resuspended in L-15 medium with 1% BSA and the cell density was adjusted to $1.25 \cdot 10^6$ (for the Y_1R constructs and the M_1R(G176)) or $1.25 \cdot 10^5$ (for the M_1R(Nterm)) cells/mL. [^{3}H]UR-MK299[23] or [^{3}H]NMS were used as radioligands for experiments at the Y_1R constructs or M_1R constructs, respectively. Non-specific binding was assessed in the presence of either BIBO3304 (for the Y_1R constructs, 500-fold excess over each concentration of radioligand) or atropine (for the M_1R constructs, 1000-fold excess over each concentration of radioligand). The wells were pre-filled with 20 µL of L-15 containing the respective radioligand (10-fold more concentrated than the

final assay concentration) and 20 µL of L-15 (total binding) or L-15 containing the suitable competitive ligand (non-specific binding). 160 µL of the concentration-adjusted cell suspension were added to the wells and the plate was incubated under gentle shaking at 23 °C for 90 min (for the Y_1R constructs) or 3 h (for the M_1R constructs), respectively. The following steps were performed as described in Chapter 3.

Saturation binding experiments at the NTS_1R(T227) and the AT_1R(S186) were essentially conducted following a described protocol[24] with modifications – in detail: saturation binding was investigated with [^{3}H]UR-MK300 at intact HEK293T cells stably expressing the NTS_1R(T227) and with [^{3}H]UR-MK292 at intact HEK293T cells stably expressing the AT_1R(S186). Experiments were performed at room temperature (rt) in white 96-well plates with clear bottom (Corning Inc., Tewksbury, MA, USA). One day before the experiment, the plates were treated with poly-D-lysine hydrobromide (Sigma-Aldrich, Munich, Germany) for 10 min. Subsequently, the plates were washed once with PBS and left to dry overnight at rt. Dulbecco's PBS (D-PBS) with Ca^{2+} and Mg^{2+} (1.8 mM $CaCl_2$, 2.68 mM KCl, 1.47 mM KH_2PO_4, 3.98 mM $MgSO_4$, 136.9 mM NaCl and 8.06 mM Na_2HPO_4), supplemented with 1% BSA and 100 µg/mL of the protease inhibitor bacitracin, served as binding buffer. Washing steps were performed using D-PBS at rt (prior to the incubation) or ice-cold (after incubation). Cells were seeded one day before the experiment in 100 µL of DMEM with 2 mM L-glutamine and 10% FCS at a density of $1 \cdot 10^5$ cells/well. On the day of the experiment, the culture medium was carefully removed using a multi-channel pipette (Transferpette S-12, Brand, Wertheim, Germany), the cells were washed once with D-PBS (200 µL) and covered with binding buffer (160 µL). For the assessment of total binding, 20 µL of binding buffer and 20 µL of binding buffer containing the radioligand (10-fold more concentrated than the final concentration) were added. Non-specific binding was determined in the presence of NT(8-13) (for the NTS_1R(T227)) or angiotensin II (for the AT_1R(S186)) in 500-fold excess over the respective concentration of the radioligand by adding binding buffer (20 µL) containing the competitor (10-fold more concentrated than the final concentration) and binding buffer (20 µL) containing the radioligand (10-fold more concentrated than the final concentration). The plates were then gently shaken at rt for 2 h. After incubation, the liquid was carefully removed using a multi-channel pipette, the cells were washed twice with ice-cold D-PBS (200 µL) and treated with a lysis solution (urea (8 M), acetic acid (3 M) and Triton X-100 (1%) in water) (25 µL). The plates were shaken for 20 min, a liquid scintillator (Ultima Gold (PerkinElmer, Waltham, MA, USA)) (200 µL) was added, and the plates were sealed with a transparent sealing tape (permanent seal for microplates, PerkinElmer, prod. no. 1450−461). Complete mixing of scintillator and lysis solution was achieved by turning the plates upside down multiple times. The plates were kept in the dark for at least 30 min prior to the measurement of the radioactivity (dpm) with a MicroBeta2 plate counter (PerkinElmer, Rodgau, Germany).

Specific binding data from saturation binding experiments (in dpm) were plotted against the free radioligand concentration and fitted by an equation describing hyperbolic binding ("one site-specific binding", GraphPad Prism 8.0, GraphPad Software Inc., San Diego, CA, USA) yielding K_d and B_{max} values. The free radioligand concentration was calculated as described by subtracting the concentration of specifically bound radioligand from the total radioligand concentration.[24] Total and non-specific binding were analyzed simultaneously using the "one site-total and non-specific binding" model in Prism 8.0. The number of binding sites per cell was calculated from the B_{max} values as described.[24] Error propagation was performed as described in Chapter 2, whenever necessary.

Radioligand competition binding experiments with [^{3}H]UR-MK292 at intact CHO-AT_1-$G\alpha_{16}$-mtAEQ cells were performed as described.[24] Obtained data were analyzed by a four-parameter logistic equation (Prism 8.0) yielding pIC_{50} values. These were transformed into pK_i values using the Cheng-Prusoff equation,[26] for which the mean and SEM was calculated.

4.2.5 BRET binding assay at intact HEK293T cells

BRET binding experiments were essentially performed as described[17] with the following minor modifications: one day prior to the experiment, HEK293T cells stably expressing the respective NLuc-receptor fusion construct were detached from the cell culture dish by trypsinization, centrifuged (500 *g*, 5 min) and resuspended in L-15 with 5% FCS and 10 mM HEPES (pH 7.4). After adjusting the cell density to $1.4 \cdot 10^6$ cells/mL, the cells were seeded in a volume of 70 µL per well into white 96-well plates (Brand, Wertheim, Germany) and incubated overnight in a water-saturated atmosphere (37 °C, no additional CO_2). On the day of the experiment, serial dilutions of the fluorescent ligands and the competitors (all 10-fold more concentrated than the final assay concentration) were prepared in assay buffer consisting of L-15 medium with 10 mM HEPES (pH 7.4) and 2% BSA.

For saturation binding experiments, 10 µL of assay buffer (total binding) or assay buffer containing the suitable competitive ligand (for the assessment of non-specific binding, for the Y_1R: BIBO3304 in a 500-fold excess; for the NTS_1R: SR142948 in a 100-fold excess; for the AT_1R: candesartan in a 100-fold excess; for the M_1R: atropine in a 500-fold excess; the excess always refers to the respective concentration of fluorescent ligand used) were added to the wells. Subsequently, 10 µL of a solution of the investigated fluorescent ligand (in varying concentrations) were added. After an incubation period of 60 min at 27 °C, 10 µL of the substrate furimazine (Nano-Glo® Live Cell Substrate, pre-diluted 1:1000 before use) were added and after an equilibration time of 5 min inside the plate reader (pre-warmed to 27 °C), the measurement was initiated.

For competition binding experiments at the Y_1R(Y192), the Y_1R(Q291), the NTS_1R(T227) and the M_1R(G176), 10 µL of a solution of the investigated competitive ligand (varying concentrations) and 10 µL of a solution of the suitable fluorescent ligand (for the Y_1R(Y192)/Y_1R(Q291): c_{final}(**4.1**) = 0.5 nM; for the NTS_1R(T227): c_{final}(**4.2**) = 5 nM; for the M_1R(G176): c_{final}(**3.5**) = 5 nM) were added. For competition binding experiments at the AT_1R(S186), the same volumes were used but the cells were preincubated with the competitor for 30 min before the addition of the fluorescent ligand **4.3** (c_{final} = 10 nM). A positive control containing only fluorescent ligand and no competitor (100% value), as well as a solvent control (0% value) were included in every experiment. After an incubation period of 60 min at 27°C, 10 µL of furimazine (Nano-Glo® Live Cell Substrate, pre-diluted 1:1000 before use) were added to the cells and after an equilibration for 5 min, the measurement was started.

For kinetic saturation and competition binding experiments, 10 µL of the substrate furimazine (Nano-Glo® Live Cell Substrate, pre-diluted 1:1000 before use) and 10 µL of assay buffer (total binding) or assay buffer containing the suitable competitive ligand (non-specific binding and competition binding experiments) were added to the cells. After a short equilibration (5 min), 10 µL of the solution of the investigated fluorescent ligand were added to the cells (final concentrations of the fluorescent ligands in competition binding experiments: see above) and the measurement was started immediately. For kinetic competition binding experiments at the AT_1R(S186), the cells were preincubated with the competitive ligand for 30 min as described above prior to the addition of the substrate and the fluorescent ligand **4.3**.

For recording association and dissociation kinetics, 20 µL of assay buffer (total binding) or assay buffer containing the suitable competitive ligand (non-specific binding, for the Y_1R(Y192): BIBP3226, c_{final} = 500 nM; for the NTS_1R(T227): SR142948, c_{final} = 2.5 µM; for the AT_1R(S186): candesartan, c_{final} = 2.5 µM; for the M_1R(G176): atropine, c_{final} = 5 µM) were added to the cells. After the addition of 10 µL of furimazine (Nano-Glo® Live Cell Substrate, pre-diluted 1:1000 before use), cells were equilibrated inside the thermostated plate reader (27 °C) for 5 min and the measurement was started. After the first cycle (t = 0 min), 50 µL of assay buffer containing the fluorescent ligands **4.1** (Y_1R(Y192), c_{final} = 0.5 nM), **4.2** (NTS_1R(T227), c_{final} = 10 nM), **4.3** (AT_1R(S186), c_{final} = 10 nM) or **3.5** (M_1R(G176), c_{final} = 5 nM) were added via the injector module. Dissociation was initiated by the addition of 50 µL of assay buffer containing the suitable competitive ligand (for the Y_1R(Y192): BIBP3226, c_{final} = 500 nM; NTS_1R(T227): SR142948, c_{final} = 2.5 µM; AT_1R(S186): candesartan, c_{final} = 2.5 µM; M_1R(G176): atropine, c_{final} = 5 µM).

All BRET measurements were performed at a temperature of 27 °C using a TECAN GENiosPro or a TECAN InfiniteLumi plate reader (Tecan Austria GmbH, Grödig, Austria). The bioluminescence of the luciferase was detected using a 460 ± 50 nm band-pass (460/50BP, GENiosPro) filter or a 460 ± 35 nm band-pass (460/35BP, InfiniteLumi) filter. The emission originating from the fluorescent ligand was detected through a 610 nm long-pass (610LP) filter with both readers. Integration times for equilibrium experiments were set to 100 ms for both channels except for experiments at the Y_1R(Y192), where a longer integration time (300 ms) was used for both channels. Kinetic saturation and competition binding experiments were monitored using an integration time of 1000 ms for the 610LP filter to reduce noise.

For the determination of on-off-kinetics, the following integration times (460BP / 610LP) were used: Y_1R(Y192): 1000 ms / 1000 ms, NTS_1R(T227) and AT_1R(S186): 100 ms / 500 ms, M_1R(G176): 1000 ms / 1000 ms.

Data analysis was performed using GraphPad Prism 8.0. The “raw BRET ratio” was calculated by dividing the emission detected through the 610LP filter by the emission detected through the 460BP filter, as described in Chapters 2 and 3. A baseline correction was performed for all values by subtracting the BRET ratio of a buffer control, yielding “corrected BRET ratios”. For saturation binding experiments, total and non-specific binding were fitted simultaneously applying a one site binding model (“one site-total and non-specific binding”; Prism 8.0), which fits total binding by a hyperbolic curve and non-specific binding by linear regression. Specific binding was fitted by an equation describing hyperbolic binding (“one site-specific binding”, Prism 8.0), yielding K_d values. These were transformed into pK_d values, for which means and SEMs were calculated.

For competition binding experiments, the data were normalized to the BRET ratio obtained for a solvent control (0% value) and the BRET ratio obtained for wells containing fluorescent ligand but no competitor (100% value). The normalized data were then fitted by a four-parameter logistic equation (Prism 8.0). The obtained pIC_{50} values were subsequently transformed into pK_i values by the Cheng-Prusoff equation[26] and means and SEMs were calculated for the pK_i values.

Kinetic data were normalized to the BRET ratio before the addition of a fluorescent ligand (0%) and the maximal BRET ratio obtained after association reached a plateau (100%). The data from combined association and dissociation experiments were then analyzed by an “association then dissociation” fit (Prism 8.0) yielding estimates for k_{on}, k_{off} and $K_d^{kinetic}$ values for each independent experiment. The obtained $K_d^{kinetic}$ values were transformed into p$K_d^{kinetic}$ values for every experiment. Means and SEMs were calculated for the respective p$K_d^{kinetic}$ values. Wherever applicable, error propagation was performed as described in Chapter 2.

4.2.6 Preparation of HEK293T cell homogenates

Cell homogenates of HEK293T cells stably expressing the AT_1R(S186) or the NTS_1R(T227) were prepared as described[27] with the following minor modifications: after cell lysis and the centrifugation of the lysate (23 000 rpm, 45 min, 4 °C, Optima-L70-Preparative Ultracentrifuge, Beckmann Coulter, Munich, Germany), the pellet was resuspended in ice-cold binding buffer (50 mM Tris-HCl, 1 mM EDTA, pH 7.4) and homogenized using a 1 mL syringe (Injekt-F, B. Braun Melsungen AG, Melsungen, Germany) and a needle with 0.4 mm diameter (BD Microlance, Becton Dickinson, Heidelberg, Germany). The protein concentration was determined by the Bradford method and aliquots of the homogenates were stored at -80 °C until further use.

4.2.7 BRET binding assay at HEK293T cell homogenates

To perform kinetic BRET saturation binding experiments at cell homogenates of HEK293T cells stably expressing the AT_1R(S186) or the NTS_1R(T227), the respective homogenate was thawed and centrifuged (16 000 *g*, 4 °C, 10 min). The pellet was resuspended in ice-cool binding buffer and the protein concentration was adjusted to 1.5 µg/µL (AT_1R(S186)) or 0.9 µg/µL (NTS_1R(T227)). 10 µL of the concentration-adjusted cell homogenates were added to each well in a white 96-well plate (Brand, Wertheim, Germany) together with 60 µL of binding buffer. The assay was performed as described above following the protocol for BRET saturation binding experiments at intact cells using a Tecan GENiosPro plate reader. The integration times were set to 100 ms (460/50BP filter) and 500 ms (610LP filter). The data analysis was performed as described above for BRET saturation binding experiments at intact cells.

4.3 Results and discussion

4.3.1 Search for a strategy to establish a BRET binding assay at the Y_1R

The approach to establish a BRET binding assay described by Stoddart *et al.*[16] was pursued for the Y_1R and NLuc was fused to its N-terminus (Y_1R(Nterm)). However, no specific signal was detectable in BRET saturation binding experiments (Figure 4.1B) with the high-affinity fluorescent Y_1R ligand UR-CM138 (**4.1**; for structure, see Figure 4.2). Membrane expression of the tagged receptor could be proven by radioligand saturation binding experiments with [^{3}H]UR-MK299[23] (see Appendix Figure A13A). Furthermore, the retained ability of the radioligand to bind to the modified receptor with high affinity (see Appendix Table A1) ruled out an abrogation of receptor binding upon fusion with the luciferase. At this point, we hypothesized that shortening the N-terminal domain of the Y_1R might lead to a BRET signal and saturable binding of the fluorescent ligand **4.1**, since the efficiency of BRET is strongly dependent on the distance between donor and acceptor.[13] As a model system to test this hypothesis, we utilized a Y_1R deletion mutant described by Lindner *et al.*,[28] lacking the first 31 amino acids. We removed those same amino acids from the N-terminus and fused NLuc to Asp32 via a short Gly/Ser linker yielding the construct Y_1R(Δ1-31). Although the ability of this mutant to bind NPY was slightly impaired,[28] it still represented the mutant that allows the greatest possible proximity between NLuc and the fluorophore. Interestingly, **4.1** was now able to elicit a specific and saturable signal in a BRET-based saturation binding experiment at the luciferase-tagged truncated Y_1R (see Figure 4.1B) with a comparably high S/B ratio of 12.77 ± 0.17 (see Appendix Figure A14 and Table A2). However, the determined equilibrium dissociation constant (pK_d ± SEM (**4.1**, Y_1R(Δ1-31) = 8.54 ± 0.05, cf. Table 4.1) was found to be inconsistent with the previously obtained results from radioligand competition binding studies at the wild-type Y_1R (pK_i ± SEM = 9.95 ± 0.01, cf. Table 4.1), although the radioligand [^{3}H]UR-MK299 still showed saturable binding and a high affinity to the truncated and modified receptor (see Appendix Figure A13B and Table A1).

In 2018, the structure of the human Y_1R was published in complex with UR-MK299 (PDB-ID: 5ZBQ),[29] which represents the parent compound of the used fluorescent ligand **4.1**. The crystal structure showed that the diphenylacetic acid moiety, which served as the attachment point for the fluorophore in **4.1** (see Figure 4.2), is pointing towards the extracellular region of the receptor (see Figure 4.1A). However, the N-terminus of the Y_1R is comparably long in size (44 amino acids) and, even though this region of the receptor was not fully resolved, seems to be directed away from the ligand binding pocket. This might be an explanation why the N-terminal fusion of NLuc did not yield specific BRET (Figure 4.1B). The distance could apparently be reduced by truncation of the N-terminus, which resulted in a higher BRET signal, but compromised the binding of **4.1** to the receptor.

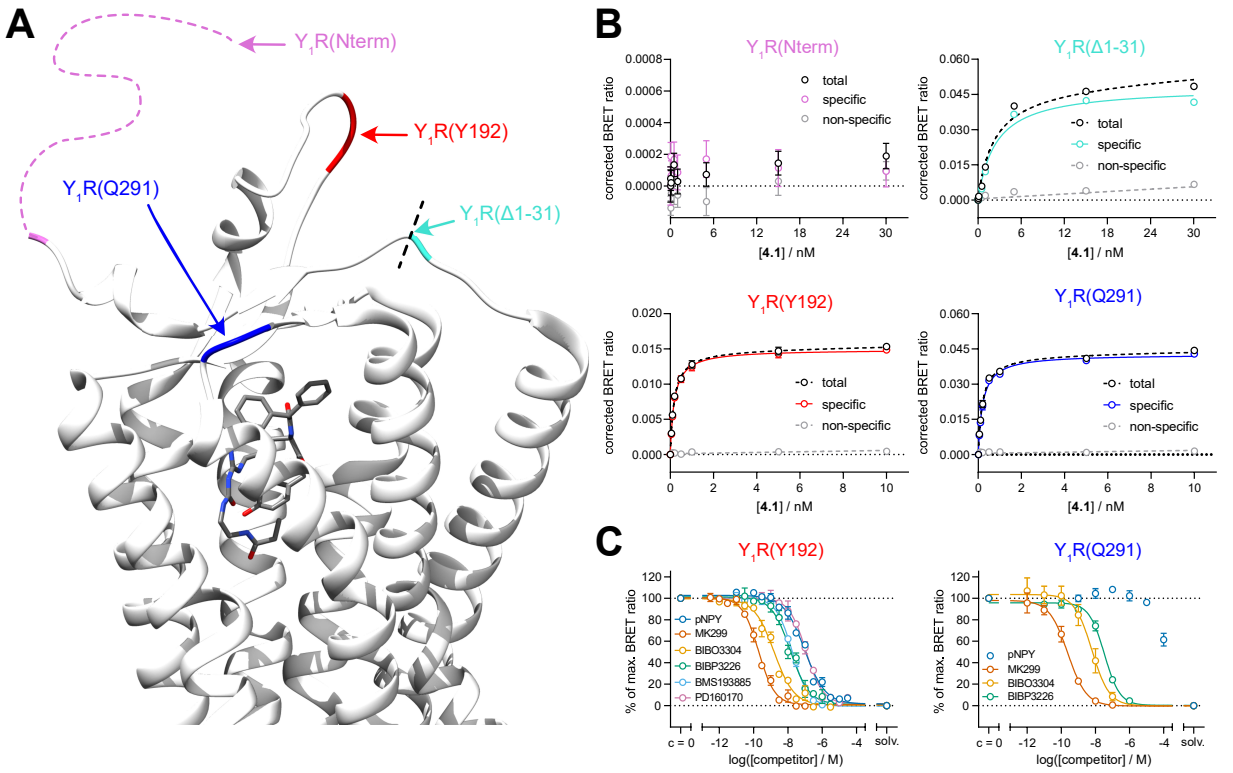

Figure 4.1: Influence of different attachment and insertion sites of NLuc at the Y_1R on BRET-based binding. (**A**) Crystal structure of the Y_1R in complex with UR-MK299 (PDB-ID: 5ZBQ).[29] Receptor sites addressed by attachment or insertion of NLuc are indicated by different colors; the N-terminus was artificially extended for the illustration as it was not completely resolved in the structure. Structure visualization was done with UCSF Chimera.[30] (**B**) Binding isotherms from BRET saturation binding experiments with **4.1** at HEK293T cells stably expressing the Y_1R(Nterm), the Y_1R(Δ1-31), the Y_1R(Y192) or the Y_1R(Q291). Non-specific binding was determined in the presence of a 500-fold excess of BIBO3304 (over the respective concentration of **4.1**). Data are shown as means (total and non-specific binding) or calculated values (specific binding) ± errors of one representative experiment from a set of three to four independent experiments, each performed in triplicate. Error bars of total and non-specific binding represent the SEM, the error bars of specific binding represent propagated errors. (**C**) Displacement curves from BRET competition binding experiments with **4.1** (c = 0.5 nM) and reported Y_1R ligands at HEK293T cells stably expressing the Y_1R(Y192) or the Y_1R(Q291). Data are shown as means ± SEM from at least three independent experiments, each performed in triplicate. solv.: solvent control.

Making use of the structure of the Y_1R, we therefore pursued a different strategy: to get the luciferase in a more favorable position towards the fluorescent ligand, we inserted NLuc into unstructured regions within the second (ECL2) or third extracellular loop (ECL3) of the receptor after Tyr192 (Y_1R(Y192)) or Gln291 (Y_1R(Q291)), respectively. In BRET saturation binding experiments, **4.1** showed saturable binding at both the Y_1R(Y192) and the Y_1R(Q291) (see Figure 4.1B). In contrast to the Y_1R(Δ1-31), the dissociation constants for **4.1** (pK_d ± SEM (**4.1**, Y_1R(Y192)) = 9.62 ± 0.05; pK_d ± SEM (**4.1**, Y_1R(Q291)) = 9.54 ± 0.07) were now both in very good agreement with the results from radioligand competition binding experiments at unmodified Y_1 receptors (cf. Table 4.1). The obtained BRET was more efficient for the Y_1R(Q291), which might be explained by the closer proximity of ECL3 to the binding pocket of the receptor.

Interestingly, the S/B ratio obtained for the Y_1R(Y192) was comparatively high considering the low number of receptors per cell estimated by radioligand saturation binding experiments (≈ 2500 receptors/cell, Appendix Figure A13C). This proves the sensitivity of the BRET-based approach in general, which has already been shown by establishing NLuc-based BRET binding assays at endogenously expressed receptors (e.g. adenosine A_{2B} receptors) by means of genome editing.[31]

Table 4.1: Equilibrium dissociation constants (pK_d values) of the fluorescent Y_1R ligand **4.1** obtained from BRET saturation binding experiments.

Compound	Receptor (construct)	pK_d (BRET)[a]	*N*	pK_i (radioligand comp. binding)[b]
4.1	Y_1R(wild-type)	n.a.	---	9.95 ± 0.01
	Y_1R(Nterm)	n.a.	---	n.d.
	Y_1R(Δ1-31)	8.54 ± 0.05	3	n.d.
	Y_1R(Y192)	9.62 ± 0.05	4	n.d.
	Y_1R(Q291)	9.54 ± 0.07	4	n.d.

[a]Determined by BRET saturation binding experiments at intact HEK293T cells stably expressing the respective receptor construct. Data represent means ± SEM from *N* independent experiments performed in triplicate. [b]Determined by radioligand competition binding experiments with [^{3}H]UR-MK299 (c = 0.15 nM; K_d = 0.044 nM) at SK-N-MC cells endogenously expressing the Y_1R. Experiments were performed as described elsewhere.[23] Value represents the mean ± SEM from three independent experiments performed in triplicate. n.a. not applicable. n.d. not determined.

BRET competition binding experiments were performed with **4.1** and different structurally diverse Y_1R ligands (for structures, see Appendix A15) at the Y_1R(Y192) and the Y_1R(Q291) (see Figure 4.1C). The obtained affinities (pK_i values) of the antagonists UR-MK299, BIBO3304, BIBP3226, BMS193885 and PD160170 were in very good agreement with data reported in literature (cf. Table 4.2 for the Y_1R(Y192) and Appendix Table A3 for the Y_1R(Q291)). Interestingly, the agonist pNPY was not able to displace the fluorescent tracer **4.1** from the Y_1R(Q291) (Figure 4.1C, right). Apparently, the insertion of the luciferase into the ECL3 of the Y_1R had a negative impact and disrupted the binding of pNPY. At the Y_1R(Y192), pNPY was able to displace **4.1** from the receptor with a pK_i of 7.49 ± 0.08 (Table 4.2). This is in accordance with data found in literature for competition binding experiments performed in buffers containing physiological concentrations of sodium ions.[29,32,33]

Table 4.2: Binding data (pK_i values) of standard Y_1R ligands from BRET competition binding experiments with the fluorescent ligand **4.1** at the Y_1R(Y192).

Receptor construct	Compound	pK_i (BRET)[a]	*N*	pK_i (literature)[b]
Y_1R(Y192)	pNPY	7.49 ± 0.08	5	7.78-9.75[23,29,32-34]
	UR-MK299	10.20 ± 0.06	6	10.11[23]
	BIBO3304	9.31 ± 0.11	5	8.76-9.60[29,32,34]
	BIBP3226	8.38 ± 0.11	5	8.14-9.00[23,29,34-36]
	BMS193885	8.23 ± 0.01	4	7.66-8.48[29,37,38]
	PD160170	7.45 ± 0.05	5	7.30[39], 7.32[40]

[a]Determined by BRET competition binding experiments with **4.1** (c = 0.5 nM, K_d = 0.24 nM) at intact HEK293T cells stably expressing the Y_1R(Y192). Data represent means ± SEM from *N* independent experiments, each performed in triplicate. [b]Reference binding data (pK_i values) from literature, which were obtained from radioactivity-based or fluorescence-based competition binding experiments at the Y_1R devoid of the NLuc tag.

4.3.2 Transfer of the novel strategy to other GPCRs (NTS_1R, AT_1R, M_1R)

Next, we investigated if the presented strategy, i.e. the insertion of NLuc into the extracellular loop region of a GPCR, might be generally applicable to establish BRET binding assays at GPCRs with "long" N-termini. Therefore, the approach was transferred to the NTS_1R, which comprises an even longer N-terminus (67 amino acids) than the Y_1R. Furthermore, the angiotensin II receptor type 1 (AT_1R) with an N-terminus of 27 amino acids, and the M_1 muscarinic acetylcholine receptor (M_1R), whose N-terminal domain has 24 amino acids, were investigated. Structural information was available for all three receptors,[41-43] which allowed educated guessing of potential insertion sites by detecting unstructured regions within the extracellular loops and estimating the distance between the luciferase and the binding pocket (for snake plots of all generated constructs, see Appendix Figure A16). The NT(8-13) based NTS_1R ligand **4.2**,[44] the angiotensin II-derived AT_1R ligand **4.3** and the DIBA-derived MR ligand **3.5**[45] were used as fluorescent ligands (see Figure 4.2). All used ligands carried the fluorescence label Py-5 (**4.4**), as it was previously shown to be suitable for a combination with NLuc in BRET binding assays.[17]

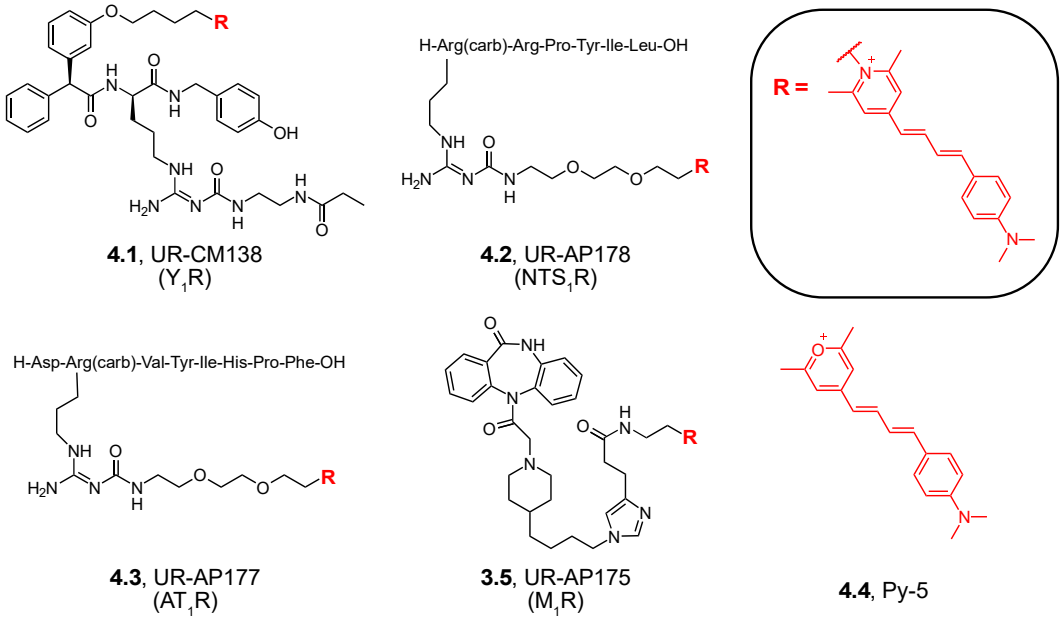

Figure 4.2: Structures of the investigated fluorescent ligands (**3.5**, **4.1**-**4.3**) and the labeling reagent Py-5 (**4.4**).

By analogy with the results for the Y_1R, no specific binding of **4.2** was observed in BRET saturation binding experiments at the N-terminally NLuc-tagged NTS_1 receptor (NTS_1R(Nterm), see Figure 4.3A). This observation additionally suggested that the length and orientation of the N-terminus of a given receptor play an important role in whether the N-terminal fusion of NLuc[16] results in a functioning BRET binding assay. According to our novel strategy, NLuc was inserted into the ECL2 of the NTS_1R after Thr227 (NTS_1R(T227)). Membrane localization and retained binding properties of the receptor-luciferase fusion protein were again confirmed by radioligand saturation binding. The radioligand [^{3}H]UR-MK300 bound to the modified NTS_1 receptor in a saturable manner with an affinity not more than half a log unit below the pK_d values obtained at unmodified receptors (see Appendix Figure A13D and Table A1).[24] In contrast to the NTS_1R(Nterm), a specific BRET signal could be observed in BRET saturation binding experiments with **4.2** at the NTS_1R(T227), stably expressed in HEK293T cells. Notably, several insertion sites located within the N-terminus and extracellular loops of the NTS_1R were analyzed (see Appendix Figure A17) but only the NTS_1R(T227) led to a specific signal and an affinity of **4.2** comparable with literature-described values (pK_d ± SEM (**4.2**, NTS_1R(T227)) = 8.32 ± 0.08, cf. Table 4.3).[44] Similarly, BRET competition binding experiments with **4.2** yielded pK_i values for the reference agonist NT(8-13) and the antagonist SR142948 (for structures, see Appendix Figure A15) with no more than half an order of magnitude difference from data described in literature (cf. Table 4.4).

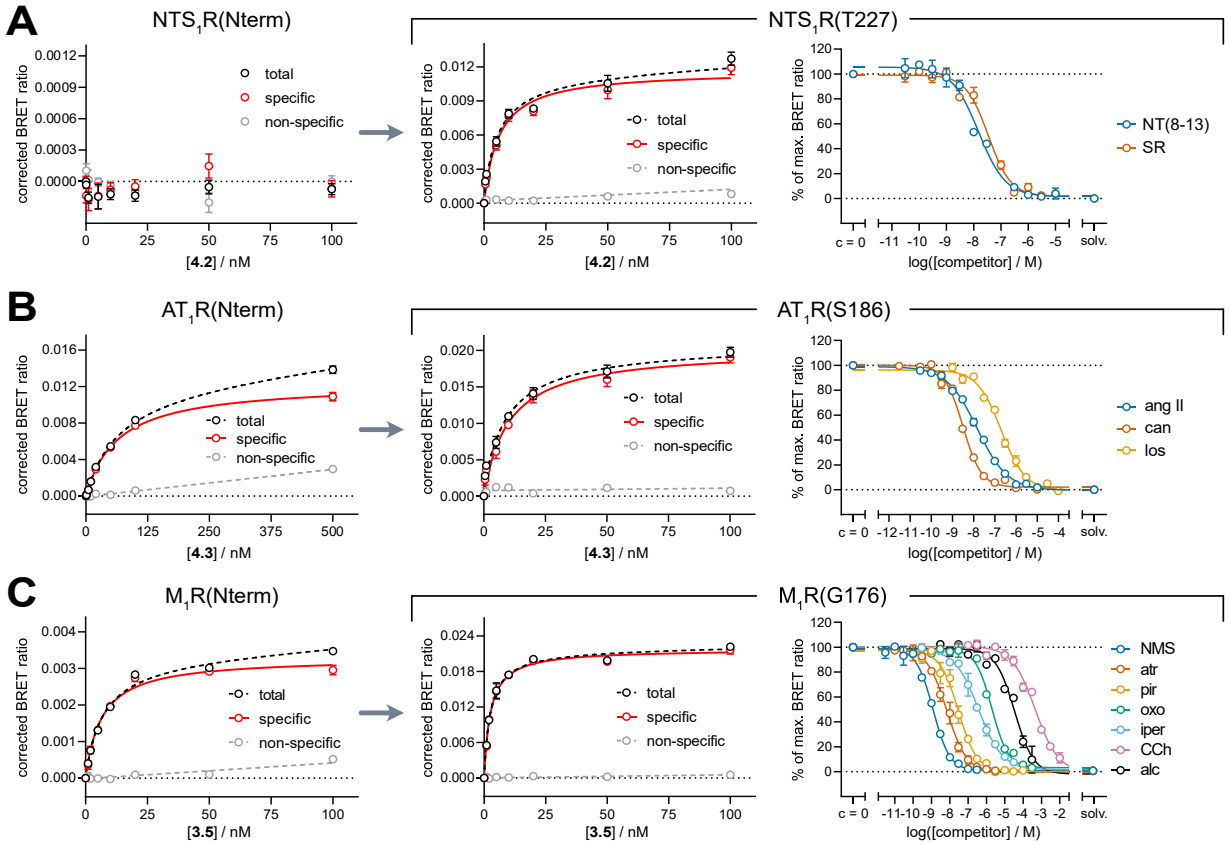

Figure 4.3: BRET binding experiments at the NTS_1R (**A**), the AT_1R (**B**) and the M_1R (**C**). In the left and middle section of the figure, binding isotherms from saturation binding experiments with the fluorescent ligands **4.2** (**A**), **4.3** (**B**) or **3.5** (**C**) at HEK293T cells stably expressing the N-terminally NLuc-tagged receptors (NTS_1R(Nterm) in **A**, AT_1R(Nterm) in **B** or M_1R(Nterm) in **C**) or the respective receptor constructs with NLuc inserted into the second extracellular loop (NTS_1R(T227) in **A**, AT_1R(S186) in **B** or M_1R(G176) in **C**) are shown. Non-specific binding was assessed in the presence of an excess of SR142948 (**A**, 100-fold excess), candesartan (**B**, 100-fold excess) or atropine (**C**, 500-fold excess) (for all experiments: excess over the concentration of the fluorescent ligand). Data are shown as means (total and non-specific binding) or calculated values (specific binding) ± errors of one representative experiment from a set of at least three independent experiments, each performed in triplicate. Error bars of total and non-specific binding represent the SEM, whereas error bars of specific binding represent propagated errors. In the right section of the figure, displacement curves from BRET competition binding experiments with the fluorescent ligands **4.2** (**A**, c = 5 nM), **4.3** (**B**, c = 10 nM) or **3.5** (**C**, c = 5 nM) and standard ligands at the respective receptor construct, stably expressed in HEK293T cells, are shown. Data represent means ± SEM from at least four independent experiments, each performed in triplicate. solv.: solvent control.

We extended our approach to the AT_1R and the M_1R, which both have shorter N-terminal sequences (AT_1R: 27 amino acids, M_1R: 24 amino acids).

As a BRET binding assay for the N-terminally NLuc-tagged AT_1R (AT_1R(Nterm)) has been reported,[16] we expected that BRET saturation binding experiments with the angiotensin II-derived ligand **4.3** would yield a concentration-dependent and saturable specific BRET signal (see Figure 4.3B). Interestingly, the pK_d value for ligand **4.3** at the AT_1R(Nterm) (pK_d ± SEM (**4.3**, AT_1R(Nterm)) = 7.24 ± 0.07) was not comparable with results from radioligand competition binding experiments at unmodified receptors (cf. Table 4.3). As the ECL2 was the insertion site for both the Y_1R and the NTS_1R, which showed the most convincing results, we followed this approach for the AT_1R as well by introducing NLuc after Ser186 (AT_1R(S186)). Ligand **4.3** showed saturable binding to the modified receptor but, in comparison to the N-terminally tagged variant,[16] bound with higher affinity (pK_d ± SEM (**4.3**, AT_1R(S186)) = 8.04 ± 0.08). Although being more in line with the data from radioligand competition binding experiments at unmodified AT_1 receptors, the obtained value was still slightly lower (cf. Table 4.3). The CHO cells used for the radioligand competition binding experiments were stably cotransfected with the $G\alpha_{16}$ subunit, which stabilizes the present AT_1Rs in an active receptor conformation, thus favoring agonist binding.[46] This presumably led to a higher affinity estimate for **4.3**, a compound derived from the endogenous AT_1R agonist angiotensin II. The same explanation also holds true for the discrepancy between the pK_d value of the radiolabeled agonist [^{3}H]UR-MK292 from radioligand saturation binding experiments at the AT_1R(S186) and the previously reported results from experiments at CHO-AT_1R cells stably coexpressing $G\alpha_{16}$ (see Appendix Figure A13E and Table A1).[24] Another indication supporting this hypothesis are the BRET competition binding experiments with **4.3** and the agonist angiotensin II or the antagonists candesartan and losartan (Figure 4.3B, right panel; for structures, see Appendix Figure A15). The determined pK_i values were in very good agreement with previously reported radioligand competition binding data (cf. Table 4.4), especially when comparing with affinities determined at cells devoid of the stably coexpressed $G\alpha_{16}$ subunit.[47-50]

BRET saturation binding experiments with the fluorescent ligand **3.5** at the N-terminally NLuc-tagged M_1 receptor (M_1R(Nterm)) resulted in a specific BRET signal (Figure 4.3C) and a pK_d value of 8.22 ± 0.06 (cf. Table 4.3), which was well comparable with results from radioligand competition binding experiments at unmodified receptors.[45] Applying our novel strategy, NLuc was inserted into the ECL2 of the M_1R after Gly176 (M_1R(G176)). Compared to the results at the M_1R(Nterm), a clear increase in S/B ratio (see Figure 4.3C, Appendix Figure A14 and Table A2) was observed. At the same time, the pK_d value originating from BRET saturation binding experiments at the M_1R(G176) (pK_d ± SEM (**3.5**, M_1R(G176)) = 8.65 ± 0.04) matched well with

the results at the M_1R(Nterm) and with the pK_i value from radioligand competition binding experiments (cf. Table 4.3).[45]

The marked increase in S/B ratio can however not be explained by an increased membrane expression of the M_1R(G176). By performing radioligand saturation binding experiments with [^{3}H]NMS at both M_1R constructs (see Appendix Figure A13F and A13G), it could be estimated that there were ≈ 40-fold more M_1 receptor-specific binding sites in the HEK293T M_1R(Nterm) cells (≈ 650 000 specific binding sites/cell) than in the HEK293T M_1R(G176) cells (≈ 16 000 specific binding sites/cell). Therefore, a more favorable position of the luciferase with respect to the bound fluorescent ligand is more likely to be responsible for the higher S/B ratio. The increase in S/B ratio by inserting NLuc into the ECL2 of the M_1R could additionally be confirmed by BRET saturation binding experiments with the related TAMRA-labeled MR ligand **3.1** and the Py-1-labeled MR ligand **3.4** (see Appendix Figure A18 and Table A4).

BRET competition binding experiments at the M_1R(G176) with **3.5** and several reference ligands yielded pK_i values in good agreement with reported data from literature (cf. Table 4.4). Even the allosteric modulator alcuronium could still bind to the M_1R(G176) (see Figure 4.3C).

Table 4.3: Equilibrium dissociation constants (pK_d values) of the investigated fluorescent ligands **3.5**, **4.2** and **4.3** obtained from BRET saturation binding experiments.

Compound	Receptor (construct)	pK_d (BRET)[a]	*N*	pK_i (radioligand comp. binding)
4.2	NTS_1R(wild-type)	n.a.	---	8.89[b], 9.12[b]
	NTS_1R(Nterm)	n.a.	---	n.d.
	NTS_1R(T227)	8.32 ± 0.08	4	n.d.
4.3	AT_1R(wild-type)	n.a.	---	8.69 ± 0.04[c]
	AT_1R(Nterm)	7.24 ± 0.07	3	n.d.
	AT_1R(S186)	8.04 ± 0.08	5	n.d.
3.5	M_1R(wild-type)	n.a.	---	8.31[d]
	M_1R(Nterm)	8.22 ± 0.06	5	n.d.
	M_1R(G176)	8.65 ± 0.04	4	n.d.

[a]Determined by BRET saturation binding experiments at intact HEK293T cells stably expressing the indicated receptor construct. Data represent means ± SEM from *N* independent experiments performed in triplicate. [b]Keller *et al.*[24] [c]Determined by radioligand competition binding experiments with [^{3}H]UR-MK292 (c = 1 nM, K_d = 0.94 nM) at intact CHO-AT_1-$G_{\alpha16}$-mtAEQ cells. Value represents mean ± SEM from two independent experiments performed in triplicate. [d]Gruber *et al.*[45] n.a. not applicable. n.d. not determined.

Table 4.4: Binding data (pK_i values) of standard NTS_1R, AT_1R and M_1R ligands from BRET competition binding experiments with **4.2** (NTS_1R(T227)), **4.3** (AT_1R(S186)) or **3.5** (M_1R(G176)) at the indicated receptor construct.

Receptor construct	Compound	pK_i (BRET)[a]	*N*	pK_i (literature)[b]
NTS_1R(T227)	NT(8-13)	8.24 ± 0.16	4	8.27-9.85[24,44,51-53]
	SR142948	7.93 ± 0.12	4	8.05-8.99[24,44,51,54]
AT_1R(S186)	angiotensin II	8.15 ± 0.07	5	7.61-9.62[24,47-50]
	candesartan	8.82 ± 0.04	5	8.46-10.28[24,43,47-49]
	losartan	7.06 ± 0.05	4	7.23-8.00[24,43,47,49,50]
M_1R(G176)	carbachol	3.89 ± 0.09	6	3.46-4.52[55-60]
	oxotremorine	6.00 ± 0.11	5	5.48-5.86[56,58,60]
	iperoxo	7.00 ± 0.07	6	6.46[57]
	atropine	8.60 ± 0.09	6	8.50-9.70[56,61-66]
	NMS	9.41 ± 0.03	5	9.49-10.22[56,63,67]
	pirenzepine	7.91 ± 0.10	6	6.85-8.29[56,61,64,65,68]

[a]Determined by BRET competition binding experiments with **4.2** (NTS_1R(T227), c = 5 nM, K_d = 4.82 nM), **4.3** (AT_1R(S186), c = 10 nM, K_d = 9.02 nM) or **3.5** (M_1R(G176), c = 5 nM, K_d = 2.23 nM) at intact HEK293T cells stably expressing the indicated receptor construct. Data represent means ± SEM from *N* independent experiments, each performed in triplicate. [b]Reference binding data (pK_i values) from literature determined by radioactivity-based or fluorescence-based competition binding experiments at the respective receptors devoid of the NLuc tag.

4.3.3 Investigation of the binding kinetics at the generated constructs

One of the most useful characteristics of the BRET binding assay is the possibility to record the association and dissociation of fluorescent ligands in real time. Therefore, kinetic BRET binding experiments were conducted to obtain more information about the binding behavior of the fluorescent ligands **4.1**-**4.3** and **3.5** at their target receptor/NLuc fusion proteins (see Figure 4.4 and Table 4.5).

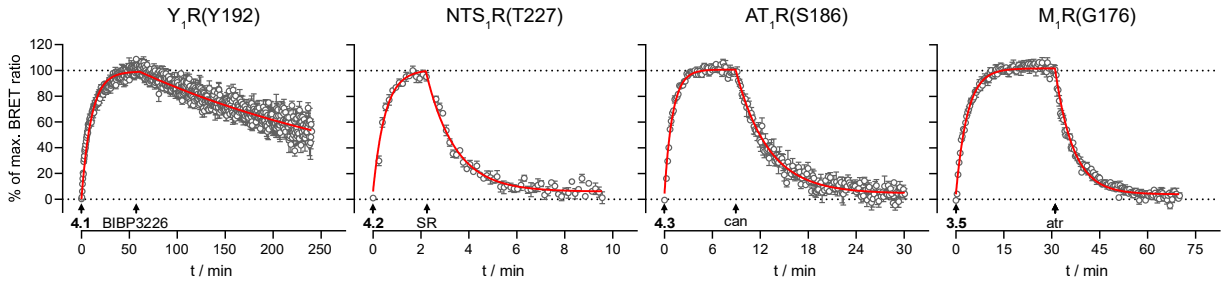

Figure 4.4: Association and dissociation kinetics (specific binding) of the fluorescent ligands **4.1** (Y_1R(Y192), c = 0.5 nM), **4.2** (NTS_1R(T227)), c = 10 nM), **4.3** (AT_1R(S186), c = 10 nM) and **3.5** (M_1R(G176), c = 5 nM) from kinetic BRET binding experiments at intact HEK293T cells stably expressing the respective construct (note: differing time scales). Association was initiated by the addition of the respective fluorescent ligand. Dissociation was initiated at the indicated timepoints by the addition of BIBP3226 (Y_1R(Y192), c = 500 nM), SR142948 (NTS_1R(T227)), c = 2.5 µM), candesartan (AT_1R(S186), c = 2.5 µM) or atropine (M_1R(G176), c = 5 µM). Data represent calculated values ± propagated errors and are representative of three independent experiments, each performed in triplicate.

The fluorescent Y_1R ligand **4.1** (c = 0.5 nM) showed an association to the Y_1R(Y192) within 60 min and very slow dissociation kinetics (≈ 40% were displaced after 4 h). The slow dissociation kinetics are presumably also responsible for the deviation of the kinetically derived dissociation constant ($pK_d^{kinetic}$) from the results from equilibrium experiments (cf. Table 4.5). However, as described above, the slow dissociation of **4.1** from the receptor did not preclude the complete displacement of the fluorescent ligand in competition binding experiments and the determination of valid pK_i values in good agreement with data from literature (cf. Table 4.2).

Association of the fluorescent NTS_1R ligand **4.2** (c = 10 nM) occurred rapidly within 2 min and the ligand could be displaced completely from the NTS_1R(T227) within 10 min (see Figure 4.4). This finding was consistent with previous results from confocal microscopy experiments with similar fluorescent ligands.[44] The fluorescent ligands **4.3** (c = 10 nM) and **3.5** (c = 5 nM) both showed a moderate association rate to their respective targets. After addition of a competitive ligand, both compounds could be displaced completely from their receptors within the observed time period (see Figure 4.4). The determined $pK_d^{kinetic}$ values were matching the respective pK_d values from equilibrium saturation binding experiments.

Table 4.5: Kinetic constants of the fluorescent ligands **4.1**-**4.3** and **3.5** obtained from BRET-based binding experiments.

Receptor construct	Compound	k_{off} [min^{-1}][a]	k_{on} [nM^{-1} min^{-1}][b]	p$K_d^{kinetic}$, [c]	p$K_d^{equilibrium}$, [d]
Y_1R(Y192)	**4.1**	0.004 ± 0.0005	0.143 ± 0.005	10.62 ± 0.07	9.62 ± 0.05
NTS_1R(T227)	**4.2**	0.830 ± 0.051	0.120 ± 0.012	8.16 ± 0.07	8.32 ± 0.08
AT_1R(S186)	**4.3**	0.236 ± 0.008	0.077 ± 0.005	8.51 ± 0.04	8.04 ± 0.08
M_1R(G176)	**3.5**	0.178 ± 0.002	0.022 ± 0.007	8.04 ± 0.15	8.65 ± 0.04

[a-c]Determined by kinetic BRET binding experiments with **4.1** (c = 0.5 nM), **4.2** (c = 10 nM), **4.3** (c = 10 nM) and **3.5** (c = 5 nM) at intact HEK293T cells stably expressing the indicated receptor construct; all kinetic parameters originate from three independent experiments performed in triplicate. [a]Dissociation rate constant (k_{off}) ± SEM. [b]Association rate constant (k_{on}) ± SEM. [c]Kinetically derived dissociation constant ($K_d^{kinetic}$), which was transformed into the pK_d value for each independent experiment; indicated values represent means ± SEM of the p$K_d^{kinetic}$ values. [d]Equilibrium dissociation constants from BRET saturation binding experiments; values were taken from Tables 4.1 and 4.3, respectively, and renamed as p$K_d^{equilibrium}$ for clarification.

Interestingly, the association kinetics of ligands **4.2** and **4.3**, when observing them for a longer time, showed a peak followed by a decrease in signal without the addition of a competitive ligand. In contrast, the kinetic traces of the antagonists **4.1** at the Y_1R(Y192) and **3.5** at the M_1R(G176) both reached a stable plateau (see Figure 4.5A). The qualitative curve shapes were independent of the used ligand concentration (see Appendix Figure A19 for exemplary kinetic traces of BRET saturation binding experiments). Similar effects were reported for BRET binding assays at the receptor tyrosine kinase VEGFR2 and were explained by agonist-dependent internalization of the receptor and subsequent dissociation of the ligand-receptor complex.[69,70] Furthermore, immunostaining studies at the NTS_1R and the AT_1R indicated that agonist binding can cause internalization and that the ligand and the receptor are then located in different compartments within the cells.[71,72] As the fluorescent ligands **4.2** and **4.3** are both putative agonists at their target, we assumed that this uncoupling of the ligand and the receptor after internalization was responsible for the observed signal decay in our BRET-based binding assay. To investigate this assumption, BRET saturation binding experiments were performed at cell homogenates of HEK293T cells stably expressing the NTS_1R(T227) or the AT_1R(S186), as receptor internalization cannot occur in cell homogenates. The fluorescent ligands **4.2** and **4.3** bound in a saturable manner to the homogenates and after association, the BRET signal was now stable over a longer period of time (see Appendix Figure A20). This indicates that the signal decay in Figure 4.5A was caused by internalization processes. It should be noted that the determined pK_d values for **4.2** and **4.3** at the cell homogenates differed by around two log units from the results obtained using intact cells (cf. Appendix Table A5), presumably due to the uncoupling of the heterotrimeric G protein from the receptor in homogenates, which consequently resulted in a lower agonist affinity to the free receptor.[73,74]

The above-mentioned experiments hinted at a dissociation of receptor and fluorescent ligand after internalization. We hypothesized that it should be possible to abolish the remaining signal at any given timepoint by addition of a competitor, since the residual BRET should originate from fluorescent ligands binding to receptors at the cell surface. Therefore, further kinetic BRET binding experiments were performed in analogy to the experiments depicted in Figure 4.4. However, dissociation of the fluorescent ligands **4.2** or **4.3** was now initiated after different timepoints, when BRET already began to decrease (Figure 4.5B and 4.5C). Independent on the timepoint of dissociation initiation, both fluorescent ligands could be displaced completely from the NTS_1R(T227) or the AT_1R(S186) and each timepoint showed similar dissociation kinetics. Therefore, we concluded that the detected BRET signal originated from the ligand-bound receptors at the membrane and not from internalized receptors, which further confirmed the assumption that the receptor and the ligand dissociated after internalization.

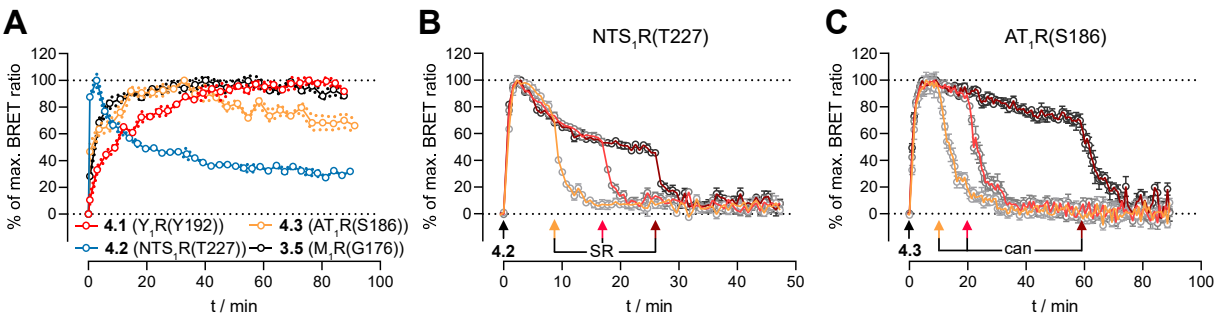

Figure 4.5: (**A**) Comparison of the association kinetics (specific binding) of the fluorescent ligands **4.1** (Y_1R(Y192), c = 0.5 nM), **4.2** (NTS_1R(T227), c = 5 nM), **4.3** (AT_1R(S186), c = 5 nM) and **3.5** (M_1R(G176), c = 5 nM) from BRET binding experiments at intact HEK293T cells stably expressing the respective construct. (**B**, **C**) Dissociation of **4.2** (c = 10 nM) from the NTS_1R(T227) (**B**) or **4.3** (c = 10 nM) from the AT_1R(S186) (**C**). Dissociation was initiated after different timepoints (indicated by differently colored arrows) by the addition of SR142948 (**B**, c = 2.5 µM) or candesartan (**C**, c = 2.5 µM). Data represent calculated values ± propagated errors. Data shown are representative of at least three independent experiments, each performed in triplicate. Data in **A** were sampled from kinetic saturation binding experiments performed at the respective construct (see Appendix Figure A19).

As expected, following the time course of BRET competition binding experiments at the NTS_1R(T227) and the AT_1R(S186) with **4.2** and **4.3** resulted in similar kinetic traces (see Appendix Figure A21A-E). However, despite the steady signal decrease over time, the pIC_{50} values of the investigated competitive ligands determined at different time points, stabilized quickly (maximum: 45 min for losartan and angiotensin II) (see Appendix Figure A21F and A21G), suggesting equilibrium.

4.4 Conclusion

Here we present a complementary approach to establish BRET binding assays for GPCRs by inserting the bioluminescent donor NLuc into the ECL2 of the receptor instead of fusing it to the N-terminus. This strategy proved especially useful for receptors with longer N-termini (exceeding 40 amino acids), e.g. the Y_1R and the NTS_1R, as BRET-based binding assays with a specific signal and retained affinity of the fluorescent ligand were only possible with the herein presented approach. The strategy was also applicable to receptors with shorter N-terminal domains. For those receptors, when compared to the N-terminal fusion of NLuc, our approach resulted in an affinity estimate for the fluorescent ligand more in line with literature-described data, and/or a marked increase in S/B ratio because of a more favorable orientation/proximity of the luciferase towards the fluorescent acceptor. BRET competition binding experiments at all receptor constructs yielded affinity values comparable with literature-described data for several standard ligands. Kinetic BRET binding experiments with the agonistic ligands **4.2** and **4.3** at the NTS_1R(T227) and the AT_1R(S186), respectively, delivered association curves, which did not end in plateaus, but showed a decline after a peak was reached. This could be explained by receptor internalization, occurring in live cells, as plateau-reaching association curves could be obtained by BRET saturation binding experiments with **4.2** and **4.3** at cell homogenates.

The herein presented approach should be of high value for the establishment of BRET binding assays for receptors, for which an N-terminal NLuc fusion delivers no or insufficient BRET upon addition of a fluorescent ligand.

4.5 References

1. Fredriksson, R., Lagerström, M. C., Lundin, L.-G. & Schiöth, H. B. The G-protein-coupled receptors in the human genome form five main families. Phylogenetic analysis, paralogon groups, and fingerprints. *Mol. Pharmacol.* **63**, 1256-1272, doi:10.1124/mol.63.6.1256 (2003).

2. Venkatakrishnan, A. J., Deupi, X., Lebon, G., Tate, C. G., Schertler, G. F. & Babu, M. M. Molecular signatures of G-protein-coupled receptors. *Nature* **494**, 185-194, doi:10.1038/nature11896 (2013).

3. Peeters, M. C., van Westen, G. J. P., Li, Q. & Ijzerman, A. P. Importance of the extracellular loops in G protein-coupled receptors for ligand recognition and receptor activation. *Trends Pharmacol. Sci.* **32**, 35-42, doi:10.1016/j.tips.2010.10.001 (2011).

4. Santos, R., Ursu, O., Gaulton, A., Bento, A. P., Donadi, R. S., Bologa, C. G., Karlsson, A., Al-Lazikani, B., Hersey, A., Oprea, T. I. & Overington, J. P. A comprehensive map of molecular drug targets. *Nat. Rev. Drug Discov.* **16**, 19-34, doi:10.1038/nrd.2016.230 (2017).

5. Hauser, A. S., Attwood, M. M., Rask-Andersen, M., Schiöth, H. B. & Gloriam, D. E. Trends in GPCR drug discovery: new agents, targets and indications. *Nat. Rev. Drug Discov.* **16**, 829-842, doi:10.1038/nrd.2017.178 (2017).

6. Hoffmann, C., Castro, M., Rinken, A., Leurs, R., Hill, S. J. & Vischer, H. F. Ligand residence time at G-protein–coupled receptors—why we should take our time to study it. *Mol. Pharmacol.* **88**, 552-560, doi:10.1124/mol.115.099671 (2015).

7. Swinney, D. C., Haubrich, B. A., Van Liefde, I. & Vauquelin, G. The role of binding kinetics in GPCR drug discovery. *Curr. Top. Med. Chem.* **15**, 2504-2522, doi:10.2174/1568026615666150701113054 (2015).

8. Zhang, R. & Monsma, F. Binding kinetics and mechanism of action: toward the discovery and development of better and best in class drugs. *Expert Opin. Drug Discov.* **5**, 1023-1029, doi:10.1517/17460441.2010.520700 (2010).

9. Sridharan, R., Zuber, J., Connelly, S. M., Mathew, E. & Dumont, M. E. Fluorescent approaches for understanding interactions of ligands with G protein coupled receptors. *Biochim. Biophys. Acta Biomembr.* **1838**, 15-33, doi:10.1016/j.bbamem.2013.09.005 (2014).

10. Stoddart, L. A., White, C. W., Nguyen, K., Hill, S. J. & Pfleger, K. D. Fluorescence- and bioluminescence-based approaches to study GPCR ligand binding. *Br. J. Pharmacol.* **173**, 3028-3037, doi:10.1111/bph.13316 (2016).

11. Zhang, R. & Xie, X. Tools for GPCR drug discovery. *Acta Pharmacol. Sin.* **33**, 372-384, doi:10.1038/aps.2011.173 (2012).

12. Emami-Nemini, A., Roux, T., Leblay, M., Bourrier, E., Lamarque, L., Trinquet, E. & Lohse, M. J. Time-resolved fluorescence ligand binding for G protein–coupled receptors. *Nat. Protoc.* **8**, 1307-1320, doi:10.1038/nprot.2013.073 (2013).

13. Stoddart, L. A., Kilpatrick, L. E. & Hill, S. J. NanoBRET approaches to study ligand binding to GPCRs and RTKs. *Trends Pharmacol. Sci.* **39**, 136-147, doi:10.1016/j.tips.2017.10.006 (2018).

14. Tahtaoui, C., Parrot, I., Klotz, P., Guillier, F., Galzi, J. L., Hibert, M. & Ilien, B. Fluorescent pirenzepine derivatives as potential bitopic ligands of the human M1 muscarinic receptor. *J. Med. Chem.* **47**, 4300-4315, doi:10.1021/jm040800a (2004).

15. Hall, M. P., Unch, J., Binkowski, B. F., Valley, M. P., Butler, B. L., Wood, M. G., Otto, P., Zimmerman, K., Vidugiris, G., Machleidt, T., Robers, M. B., Benink, H. A., Eggers, C. T., Slater, M. R., Meisenheimer, P. L., Klaubert, D. H., Fan, F., Encell, L. P. & Wood, K. V. Engineered luciferase reporter from a deep sea shrimp utilizing a novel imidazopyrazinone substrate. *ACS Chem. Biol.* **7**, 1848-1857, doi:10.1021/cb3002478 (2012).

16. Stoddart, L. A., Johnstone, E. K. M., Wheal, A. J., Goulding, J., Robers, M. B., Machleidt, T., Wood, K. V., Hill, S. J. & Pfleger, K. D. G. Application of BRET to monitor ligand binding to GPCRs. *Nat. Methods* **12**, 661-663, doi:10.1038/nmeth.3398 (2015).

17. Bartole, E., Grätz, L., Littmann, T., Wifling, D., Seibel, U., Buschauer, A. & Bernhardt, G. UR-DEBa242: a Py-5-labeled fluorescent multipurpose probe for investigations on the histamine H_3 and H_4 receptors. *J. Med. Chem.* **63**, 5297-5311, doi:10.1021/acs.jmedchem.0c00160 (2020).

18. Fernández-Dueñas, V., Qian, M., Argerich, J., Amaral, C., Risseeuw, M. D. P., Van Calenbergh, S. & Ciruela, F. Design, synthesis and characterization of a new series of fluorescent metabotropic glutamate receptor type 5 negative allosteric modulators. *Molecules* **25**, 1532, doi:10.3390/molecules25071532 (2020).

19. Grätz, L., Tropmann, K., Bresinsky, M., Müller, C., Bernhardt, G. & Pockes, S. NanoBRET binding assay for histamine H_2 receptor ligands using live recombinant HEK293T cells. *Sci. Rep.* **10**, 13288, doi:10.1038/s41598-020-70332-3 (2020).

20. Hoare, B. L., Bruell, S., Sethi, A., Gooley, P. R., Lew, M. J., Hossain, M. A., Inoue, A., Scott, D. J. & Bathgate, R. A. D. Multi-component mechanism of H2 relaxin binding to RXFP1 through NanoBRET kinetic analysis. *iScience* **11**, 93-113, doi:10.1016/j.isci.2018.12.004 (2019).

21. Kozielewicz, P., Bowin, C. F., Turku, A. & Schulte, G. A NanoBRET-based binding assay for Smoothened allows real-time analysis of ligand binding and distinction of two binding sites for BODIPY-cyclopamine. *Mol. Pharmacol.* **97**, 23-34, doi:10.1124/mol.119.118158 (2020).

22. Zhao, P., Liang, Y.-L., Belousoff, M. J., Deganutti, G., Fletcher, M. M., Willard, F. S., Bell, M. G., Christe, M. E., Sloop, K. W., Inoue, A., Truong, T. T., Clydesdale, L., Furness, S. G. B., Christopoulos, A., Wang, M.-W., Miller, L. J., Reynolds, C. A., Danev, R., Sexton, P. M. & Wootten, D. Activation of the GLP-1 receptor by a non-peptidic agonist. *Nature* **577**, 432-436, doi:10.1038/s41586-019-1902-z (2020).

23. Keller, M., Weiss, S., Hutzler, C., Kuhn, K. K., Mollereau, C., Dukorn, S., Schindler, L., Bernhardt, G., König, B. & Buschauer, A. N^{ω}-Carbamoylation of the argininamide moiety: an avenue to insurmountable NPY Y_1 receptor antagonists and a radiolabeled selective high-affinity molecular tool ([^{3}H]UR-MK299) with extended residence time. *J. Med. Chem.* **58**, 8834-8849, doi:10.1021/acs.jmedchem.5b00925 (2015).

24. Keller, M., Kuhn, K. K., Einsiedel, J., Hübner, H., Biselli, S., Mollereau, C., Wifling, D., Svobodová, J., Bernhardt, G., Cabrele, C., Vanderheyden, P. M. L., Gmeiner, P. & Buschauer, A. Mimicking of arginine by functionalized N^{ω}-carbamoylated arginine as a new broadly applicable approach to labeled bioactive peptides: high affinity angiotensin, neuropeptide Y, neuropeptide FF, and neurotensin receptor ligands as examples. *J. Med. Chem.* **59**, 1925-1945, doi:10.1021/acs.jmedchem.5b01495 (2016).

25. Pegoli, A., She, X., Wifling, D., Hubner, H., Bernhardt, G., Gmeiner, P. & Keller, M. Radiolabeled dibenzodiazepinone-type antagonists give evidence of dualsteric binding at the M_2 muscarinic acetylcholine receptor. *J. Med. Chem.* **60**, 3314-3334, doi:10.1021/acs.jmedchem.6b01892 (2017).

26. Cheng, Y. & Prusoff, W. H. Relationship between the inhibition constant (K_I) and the concentration of inhibitor which causes 50 per cent inhibition (I_{50}) of an enzymatic reaction. *Biochem. Pharmacol.* **22**, 3099-3108, doi:10.1016/0006-2952(73)90196-2 (1973).

27. Bartole, E., Littmann, T., Tanaka, M., Ozawa, T., Buschauer, A. & Bernhardt, G. [^{3}H]UR-DEBa176: a 2,4-diaminopyrimidine-type radioligand enabling binding studies at the human, mouse, and rat histamine H_4 Receptors. *J. Med. Chem.* **62**, 8338-8356, doi:10.1021/acs.jmedchem.9b01342 (2019).

28. Lindner, D., Walther, C., Tennemann, A. & Beck-Sickinger, A. G. Functional role of the extracellular N-terminal domain of neuropeptide Y subfamily receptors in membrane integration and agonist-stimulated internalization. *Cell. Signal.* **21**, 61-68, doi:10.1016/j.cellsig.2008.09.007 (2009).

29. Yang, Z., Han, S., Keller, M., Kaiser, A., Bender, B. J., Bosse, M., Burkert, K., Kögler, L. M., Wifling, D., Bernhardt, G., Plank, N., Littmann, T., Schmidt, P., Yi, C., Li, B., Ye, S., Zhang, R., Xu, B., Larhammar, D., Stevens, R. C., Huster, D., Meiler, J., Zhao, Q., Beck-Sickinger, A. G., Buschauer, A. & Wu, B. Structural basis of ligand binding modes at the neuropeptide Y Y_1 receptor. *Nature* **556**, 520-524, doi:10.1038/s41586-018-0046-x (2018).

30. Pettersen, E. F., Goddard, T. D., Huang, C. C., Couch, G. S., Greenblatt, D. M., Meng, E. C. & Ferrin, T. E. UCSF Chimera-a visualization system for exploratory research and analysis. *J. Comput. Chem.* **25**, 1605-1612, doi:10.1002/jcc.20084 (2004).

31. White, C. W., Johnstone, E. K. M., See, H. B. & Pfleger, K. D. G. NanoBRET ligand binding at a GPCR under endogenous promotion facilitated by CRISPR/Cas9 genome editing. *Cell. Signal.* **54**, 27-34, doi:10.1016/j.cellsig.2018.11.018 (2019).

32. Liu, M., Richardson, R. R., Mountford, S. J., Zhang, L., Tempone, M. H., Herzog, H., Holliday, N. D. & Thompson, P. E. Identification of a cyanine-dye labeled peptidic ligand for Y_1R and Y_4R, based upon the neuropeptide Y C-terminal analogue, BVD-15. *Bioconjug. Chem.* **27**, 2166-2175, doi:10.1021/acs.bioconjchem.6b00376 (2016).

33. Richardson, R. R., Groenen, M., Liu, M., Mountford, S. J., Briddon, S. J., Holliday, N. D. & Thompson, P. E. Heterodimeric analogues of the potent Y1R antagonist 1229U91, lacking one of the pharmacophoric C-terminal structures, retain potent Y1R affinity and show improved selectivity over Y4R. *J. Med. Chem.* **63**, 5274-5286, doi:10.1021/acs.jmedchem.0c00027 (2020).

34. Keller, M., Erdmann, D., Pop, N., Pluym, N., Teng, S., Bernhardt, G. & Buschauer, A. Red-fluorescent argininamide-type NPY Y_1 receptor antagonists as pharmacological tools. *Bioorg. Med. Chem.* **19**, 2859-2878, doi:10.1016/j.bmc.2011.03.045 (2011).

35. Keller, M., Bernhardt, G. & Buschauer, A. [^{3}H]UR-MK136: a highly potent and selective radioligand for neuropeptide Y Y_1 receptors. *ChemMedChem* **6**, 1566-1571, doi:10.1002/cmdc.201100197 (2011).

36. Rudolf, K., Eberlein, W., Engel, W., Wieland, H. A., Willim, K. D., Entzeroth, M., Wienen, W., Beck-Sickinger, A. G. & Doods, H. N. The first highly potent and selective non-peptide neuropeptide Y Y_1 receptor antagonist: BIBP3226. *Eur. J. Pharmacol.* **271**, R11-R13, doi:10.1016/0014-2999(94)90822-2 (1994).

37. Antal-Zimanyi, I., Bruce, M. A., Leboulluec, K. L., Iben, L. G., Mattson, G. K., McGovern, R. T., Hogan, J. B., Leahy, C. L., Flowers, S. C., Stanley, J. A., Ortiz, A. A. & Poindexter, G. S. Pharmacological characterization and appetite suppressive properties of BMS-193885, a novel and selective neuropeptide Y_1 receptor antagonist. *Eur. J. Pharmacol.* **590**, 224-232, doi:10.1016/j.ejphar.2008.06.032 (2008).

38. Poindexter, G. S., Bruce, M. A., LeBoulluec, K. L., Monkovic, I., Martin, S. W., Parker, E. M., Iben, L. G., McGovern, R. T., Ortiz, A. A., Stanley, J. A., Mattson, G. K., Kozlowski, M., Arcuri, M. & Antal-Zimanyi, I. Dihydropyridine neuropeptide Y Y_1 receptor antagonists. *Bioorg. Med. Chem. Lett.* **12**, 379-382, doi:10.1016/S0960-894X(01)00761-2 (2002).

39. Wielgosz-Collin, G., Duflos, M., Pinson, P., Le Baut, G., Renard, P., Bennejean, C., Boutin, J. & Boulanger, M. 8-Amino-5-nitro-6-phenoxyquinolines: potential non-peptidic neuropeptide Y receptor ligands. *J. Enzyme Inhib. Med. Chem.* **17**, 449-453, doi:10.1080/1475636021000005758 (2002).

40. Wright, J., Bolton, G., Creswell, M., Downing, D., Georgic, L., Heffner, T., Hodges, J., MacKenzie, R. & Wise, L. 8-Amino-6-(arylsulphonyl)-5-nitroquinolines: novel nonpeptide neuropeptide Y1 receptor antagonists. *Biorg. Med. Chem. Lett.* **6**, 1809-1814, doi:10.1016/0960-894X(96)00319-8 (1996).

41. Thal, D. M., Sun, B., Feng, D., Nawaratne, V., Leach, K., Felder, C. C., Bures, M. G., Evans, D. A., Weis, W. I., Bachhawat, P., Kobilka, T. S., Sexton, P. M., Kobilka, B. K. & Christopoulos, A. Crystal structures of the M1 and M4 muscarinic acetylcholine receptors. *Nature* **531**, 335-340, doi:10.1038/nature17188 (2016).

42. White, J. F., Noinaj, N., Shibata, Y., Love, J., Kloss, B., Xu, F., Gvozdenovic-Jeremic, J., Shah, P., Shiloach, J., Tate, C. G. & Grisshammer, R. Structure of the agonist-bound neurotensin receptor. *Nature* **490**, 508-513, doi:10.1038/nature11558 (2012).

43. Zhang, H., Unal, H., Gati, C., Han, Gye W., Liu, W., Zatsepin, Nadia A., James, D., Wang, D., Nelson, G., Weierstall, U., Sawaya, Michael R., Xu, Q., Messerschmidt, M., Williams, Garth J., Boutet, S., Yefanov, Oleksandr M., White, Thomas A., Wang, C., Ishchenko, A., Tirupula, Kalyan C., Desnoyer, R., Coe, J., Conrad, Chelsie E., Fromme, P., Stevens, Raymond C., Katritch, V., Karnik, Sadashiva S. & Cherezov, V. Structure of the angiotensin receptor revealed by serial femtosecond crystallography. *Cell* **161**, 833-844, doi:10.1016/j.cell.2015.04.011 (2015).

44. Keller, M., Mahuroof, S. A., Hong Yee, V., Carpenter, J., Schindler, L., Littmann, T., Pegoli, A., Hübner, H., Bernhardt, G., Gmeiner, P. & Holliday, N. D. Fluorescence labeling of neurotensin(8–13) via arginine residues gives molecular tools with high receptor affinity. *ACS Med. Chem. Lett.* **11**, 16-22, doi:10.1021/acsmedchemlett.9b00462 (2020).

45. Gruber, C. G., Pegoli, A., Müller, C., Grätz, L., She, X. & Keller, M. Differently fluorescence-labelled dibenzodiazepinone-type muscarinic acetylcholine receptor ligands with high M_2R affinity. *RSC Med. Chem.* **11**, 823-832, doi:10.1039/D0MD00137F (2020).

46. De Lean, A., Stadel, J. M. & Lefkowitz, R. J. A ternary complex model explains the agonist-specific binding properties of the adenylate cyclase-coupled β-adrenergic receptor. *J. Biol. Chem.* **255**, 7108-7117 (1980).

47. Bhuiyan, M. A., Ishiguro, M., Hossain, M., Nakamura, T., Ozaki, M., Miura, S. & Nagatomo, T. Binding sites of valsartan, candesartan and losartan with angiotensin II receptor 1 subtype by molecular modeling. *Life Sci.* **85**, 136-140, doi:10.1016/j.lfs.2009.05.001 (2009).

48. Le, M. T., Vanderheyden, P. M., Szaszák, M., Hunyady, L. & Vauquelin, G. Angiotensin IV is a potent agonist for constitutive active human AT_1 receptors. Distinct roles of the N- and C-terminal residues of angiotensin II during AT_1 receptor activation. *J. Biol. Chem.* **277**, 23107-23110, doi:10.1074/jbc.C200201200 (2002).

49. Verheijen, I., Fierens, F. L., Debacker, J. P., Vauquelin, G. & Vanderheyden, P. M. Interaction between the partially insurmountable antagonist valsartan and human recombinant angiotensin II type 1 receptors. *Fundam. Clin. Pharmacol.* **14**, 577-585, doi:10.1111/j.1472-8206.2000.tb00443.x (2000).

50. Wingler, L. M., McMahon, C., Staus, D. P., Lefkowitz, R. J. & Kruse, A. C. Distinctive activation mechanism for angiotensin receptor revealed by a synthetic nanobody. *Cell* **176**, 479-490, doi:10.1016/j.cell.2018.12.006 (2019).

51. Lang, C., Maschauer, S., Hübner, H., Gmeiner, P. & Prante, O. Synthesis and evaluation of a ^{18}F-labeled diarylpyrazole glycoconjugate for the imaging of NTS1-positive tumors. *J. Med. Chem.* **56**, 9361-9365, doi:10.1021/jm401491e (2013).

52. Lundquist & Dix, T. A. Synthesis and human neurotensin receptor binding activities of neurotensin(8−13) analogues containing position 8 α-azido-*N*-alkylated derivatives of ornithine, lysine, and homolysine. *J. Med. Chem.* **42**, 4914-4918, doi:10.1021/jm9903444 (1999).

53. Schindler, L., Bernhardt, G. & Keller, M. Modifications at Arg and Ile give neurotensin(8–13) derivatives with high stability and retained NTS_1 receptor affinity. *ACS Med. Chem. Lett.* **10**, 960-965, doi:10.1021/acsmedchemlett.9b00122 (2019).

54. Gully, D., Labeeuw, B., Boigegrain, R., Oury-Donat, F., Bachy, A., Poncelet, M., Steinberg, R., Suaud-Chagny, M. F., Santucci, V., Vita, N., Pecceu, F., Labbé-Jullié, C., Kitabgi, P., Soubrié, P., Le Fur, G. & Maffrand, J. P. Biochemical and pharmacological activities of SR 142948A, a new potent neurotensin receptor antagonist. *J. Pharmacol. Exp. Ther.* **280**, 802-812 (1997).

55. Abdul-Ridha, A., López, L., Keov, P., Thal, D. M., Mistry, S. N., Sexton, P. M., Lane, J. R., Canals, M. & Christopoulos, A. Molecular determinants of allosteric modulation at the M_1 muscarinic acetylcholine receptor. *J. Biol. Chem.* **289**, 6067-6079, doi:10.1074/jbc.M113.539080 (2014).

56. Dong, G. Z., Kameyama, K., Rinken, A. & Haga, T. Ligand binding properties of muscarinic acetylcholine receptor subtypes (m1-m5) expressed in baculovirus-infected insect cells. *J. Pharmacol. Exp. Ther.* **274**, 378-384 (1995).

57. Fish, I., Stößel, A., Eitel, K., Valant, C., Albold, S., Huebner, H., Möller, D., Clark, M. J., Sunahara, R. K., Christopoulos, A., Shoichet, B. K. & Gmeiner, P. Structure-based design and discovery of new M_2 receptor agonists. *J. Med. Chem.* **60**, 9239-9250, doi:10.1021/acs.jmedchem.7b01113 (2017).

58. Jakubík, J., Bacáková, L., El-Fakahany, E. E. & Tucek, S. Positive cooperativity of acetylcholine and other agonists with allosteric ligands on muscarinic acetylcholine receptors. *Mol. Pharmacol.* **52**, 172-179, doi:10.1124/mol.52.1.172 (1997).

59. Matucci, R., Bellucci, C., Martino, M. V., Nesi, M., Manetti, D., Welzel, J., Bartz, U., Holze, J., Tränkle, C., Mohr, K., Mazzolari, A., Vistoli, G., Dei, S., Teodori, E. & Romanelli, M. N. Carbachol dimers with primary carbamate groups as homobivalent modulators of muscarinic receptors. *Eur. J. Pharmacol.* **883**, 173183, doi:10.1016/j.ejphar.2020.173183 (2020).

60. Richards, M. H. & van Giersbergen, P. L. Human muscarinic receptors expressed in A9L and CHO cells: activation by full and partial agonists. *Br. J. Pharmacol.* **114**, 1241-1249, doi:10.1111/j.1476-5381.1995.tb13339.x (1995).

61. Buckley, N. J., Bonner, T. I., Buckley, C. M. & Brann, M. R. Antagonist binding properties of five cloned muscarinic receptors expressed in CHO-K1 cells. *Mol. Pharmacol.* **35**, 469-476 (1989).

62. Christopoulos, A., Pierce, T. L., Sorman, J. L. & El-Fakahany, E. E. On the unique binding and activating properties of xanomeline at the M_1 muscarinic acetylcholine receptor. *Mol. Pharmacol.* **53**, 1120-1130 (1998).

63. Fruchart-Gaillard, C., Mourier, G., Marquer, C., Ménez, A. & Servent, D. Identification of various allosteric interaction sites on M_1 muscarinic receptor using ^{125}I-Met35-oxidized muscarinic toxin 7. *Mol. Pharmacol.* **69**, 1641-1651, doi:10.1124/mol.105.020883 (2006).

64. Huang, F., Buchwald, P., Browne, C. E., Farag, H. H., Wu, W. M., Ji, F., Hochhaus, G. & Bodor, N. Receptor binding studies of soft anticholinergic agents. *AAPS PharmSci* **3**, E30, doi:10.1208/ps030430 (2001).

65. Keller, M., Tränkle, C., She, X., Pegoli, A., Bernhardt, G., Buschauer, A. & Read, R. W. M_2 Subtype preferring dibenzodiazepinone-type muscarinic receptor ligands: effect of chemical homo-dimerization on orthosteric (and allosteric?) binding. *Bioorg. Med. Chem.* **23**, 3970-3990, doi:10.1016/j.bmc.2015.01.015 (2015).

66. Keov, P., López, L., Devine, S. M., Valant, C., Lane, J. R., Scammells, P. J., Sexton, P. M. & Christopoulos, A. Molecular mechanisms of bitopic ligand engagement with the M_1 muscarinic acetylcholine receptor. *J. Biol. Chem.* **289**, 23817-23837, doi:10.1074/jbc.M114.582874 (2014).

67. Del Bello, F., Barocelli, E., Bertoni, S., Bonifazi, A., Camalli, M., Campi, G., Giannella, M., Matucci, R., Nesi, M., Pigini, M., Quaglia, W. & Piergentili, A. 1,4-Dioxane, a suitable scaffold for the development of novel M_3 muscarinic receptor antagonists. *J. Med. Chem.* **55**, 1783-1787, doi:10.1021/jm2013216 (2012).

68. Esqueda, E. E., Gerstin, E. H., Jr., Griffin, M. T. & Ehlert, F. J. Stimulation of cyclic AMP accumulation and phosphoinositide hydrolysis by M_3 muscarinic receptors in the rat peripheral lung. *Biochem. Pharmacol.* **52**, 643-658, doi:10.1016/0006-2952(96)00339-5 (1996).

69. Kilpatrick, L. E., Friedman-Ohana, R., Alcobia, D. C., Riching, K., Peach, C. J., Wheal, A. J., Briddon, S. J., Robers, M. B., Zimmerman, K., Machleidt, T., Wood, K. V., Woolard, J. & Hill, S. J. Real-time analysis of the binding of fluorescent $VEGF_{165}$a to VEGFR2 in living cells: effect of receptor tyrosine kinase inhibitors and fate of internalized agonist-receptor complexes. *Biochem. Pharmacol.* **136**, 62-75, doi:10.1016/j.bcp.2017.04.006 (2017).

70. Peach, C. J., Kilpatrick, L. E., Woolard, J. & Hill, S. J. Comparison of the ligand-binding properties of fluorescent VEGF-A isoforms to VEGF receptor 2 in living cells and membrane preparations using NanoBRET. *Br. J. Pharmacol.* **176**, 3220-3235, doi:10.1111/bph.14755 (2019).

71. Hein, L., Meinel, L., Pratt, R. E., Dzau, V. J. & Kobilka, B. K. Intracellular trafficking of angiotensin II and its AT_1 and AT_2 receptors: evidence for selective sorting of receptor and ligand. *Mol. Endocrinol.* **11**, 1266-1277, doi:10.1210/mend.11.9.9975 (1997).

72. Vandenbulcke, F., Nouel, D., Vincent, J. P., Mazella, J. & Beaudet, A. Ligand-induced internalization of neurotensin in transfected COS-7 cells: differential intracellular trafficking of ligand and receptor. *J. Cell Sci.* **113**, 2963-2975 (2000).

73. Park, P. S. H., Lodowski, D. T. & Palczewski, K. Activation of G protein-coupled receptors: beyond two-state models and tertiary conformational changes. *Annu. Rev. Pharmacol. Toxicol.* **48**, 107-141, doi:10.1146/annurev.pharmtox.48.113006.094630 (2008).

74. Samama, P., Cotecchia, S., Costa, T. & Lefkowitz, R. J. A mutation-induced activated state of the β_2-adrenergic receptor. Extending the ternary complex model. *J. Biol. Chem.* **268**, 4625-4636 (1993).

5. Towards a split luciferase-based assay for the time-dependent and quantitative analysis of GRK2 recruitment to GPCRs

5.1 Introduction

G protein-coupled receptors (GPCRs) represent the largest family of membrane receptors and transduce various stimuli from the cellular environment, e.g. light, extracellular neurotransmitter or hormone release, into the cell.[1] GPCR signaling occurs via two major pathways: as their name already indicates, one of them is mediated by heterotrimeric G proteins, while the other is based on the recruitment of β-arrestins to the receptor.[2] Heterotrimeric G proteins consist of an α-subunit as well as of a β- and a γ-subunit, the last two of which are present as a tightly associated complex.[3,4] Upon receptor stimulation, a nucleotide exchange from GDP to GTP in the Gα subunit leads to the dissociation of the receptor/G protein complex and also to a release of the Gβγ dimer from the Gα subunit.[5] Both can then activate or inhibit different effector proteins, e.g. adenylate cyclases,[6] phospholipase C-β (PLC-β)[7] or potassium channels.[8] On the other hand, GPCR activation leads to the phosphorylation of serine and tyrosine residues at intracellular parts of the receptor, mainly mediated by G protein-coupled receptor kinases (GRKs) or second messenger-dependent kinases, such as protein kinases A or C.[9,10] The phosphorylated receptors, especially in the case of GRK-mediated phosphorylation,[11,12] have a high affinity for β-arrestins, which, in the first instance, prevent the coupling and activation of G proteins by sterical hindrance.[9,13] Furthermore, β-arrestins can promote (clathrin-dependent) receptor endocytosis[14] and can even initiate or regulate downstream signaling events, e.g. by helping proteins of the ERK signaling cascade to interact.[15,16]

GRKs, belonging to the family of AGC kinases (named after protein kinases A, G and C), comprise seven subtypes in humans.[17] These are subdivided into three subfamilies based on sequence homology: the GRK1 subfamily (GRK1 and GRK7), the GRK2 subfamily comprising GRK2 and GRK3, and the GRK4 subfamily containing GRK4, GRK5 and GRK6.[18,19] GRK2, GRK3, GRK5 and GRK6 are ubiquitously expressed in various tissues of the human body.[20,21] In contrast, expression and action of GRK1 (rhodopsin kinase) and GRK7 is restricted to the visual system, and GRK4 shows a tissue-specific expression in testes, kidneys and the cerebellum.[13,20] For this study, investigations were limited to GRK2 as it is ubiquitously expressed and was shown to target a broad range of GPCRs.[20] It has been shown previously, e.g. by means of BRET[22-28] and FRET[29] that stimulation of different GPCRs leads to the translocation of GRK2 from the cytoplasm to the membrane-bound receptor.[30] Membrane targeting of GRK2 is thereby mediated by its C-terminal pleckstrin homology (PH) domain, with which it binds to anionic phospholipids[31,32] and interacts with the free, membrane-associated Gβγ dimer[33,34] being available after receptor activation and dissociation of the heterotrimeric G protein. In terms of measuring GRK2 recruitment to GPCRs, literature reports either showed final concentration-response curves of agonists or merely the observation of recruitment kinetics for a single agonist concentration.[22,24,26,27,29]

In order to perform a more detailed and simultaneous analysis of the concentration- and time-dependent recruitment of GRK2 to a GPCR, an approach based on the split luciferase complementation technique was pursued.[35,36] For this purpose, GRK2 and the investigated GPCR were tagged with complementary, catalytically inactive fragments of the luciferase NanoLuc® (NLuc).[35] The agonist-induced recruitment of GRK2 to the receptor brings the two luciferase fragments into close proximity, leading to refolding of a functional enzyme capable of catalyzing a bioluminescent reaction.[36] We chose the blue light-emitting luciferase NLuc ($\lambda_{max} \approx$ 460 nm),[37] as the short maturation time after the reversible complementation and its bright bioluminescence allow for real-time measurements at live cells.[35]

Using the developed split luciferase-based assay, we determined and compared the kinetics of GRK2 recruitment to three different GPCRs, the M_1 and M_5 muscarinic acetylcholine receptors (M_1R, M_5R) and the neurotensin receptor 1 (NTS_1R). For standard ligands of these GPCRs, kinetic time courses of GRK2 recruitment were determined. Furthermore, the effect of the selective GRK2/3 inhibitor Takeda compound101 (cmpd101)[38] on GRK2 recruitment was investigated.

5.2 Materials and methods

5.2.1 Materials

Dulbecco's Modified Eagle's Medium (DMEM), L-glutamine, fetal calf serum (FCS) and HEPES were purchased from Sigma-Aldrich (Munich, Germany). Trypsin/EDTA (0.05%/0.02%) was purchased from Biochrom (Berlin, Germany). Leibovitz' L-15 medium (L-15) and geneticin (G418) were from Fisher Scientific (Nidderau, Germany), whereas zeocin was from InvivoGen (Toulouse, France). Furimazine (Nano-Glo® Live Cell Substrate) was purchased from Promega (Mannheim, Germany). The pcDNA3.1 and pcDNA4 vectors were from Thermo Fisher (Nidderau, Germany).

Carbachol, iperoxo iodide, atropine sulfate and N-methyl scopolamine bromide (NMS) were from Sigma-Aldrich (Munich, Germany). NT(8-13) was from SynPeptide (Shanghai, China), whereas SR142948 and the GRK2/3 inhibitor Takeda compound101 (cmpd101) were from Tocris Bioscience (Bristol, UK). Structures of the investigated compounds can be found in the Appendix (Figure A22). The stock solution of NT(8-13) was prepared in a mixture of ethanol and 50 mM HCl (30:70). The other stock solutions were prepared in millipore H_2O or DMSO (Merck, Millipore, Darmstadt) for SR142948 and cmpd101.

5.2.2 Generation of plasmids

All plasmids were generated by standard PCR and restriction techniques within the respective vector backbones. The receptor constructs M_1R-NLucC, M_5R-NLucC and NTS_1R-NLucC encoding the respective human receptor C-terminally fused to the smaller luciferase fragment (NLucC) were described recently[39] and were subcloned into the pcDNA3.1 vector backbone. The sequence for GRK2 (obtained by mRNA isolation from MCF-7 cells and following reverse transcription[39]) was subcloned into the pcDNA4 vector backbone. To generate the pcDNA4 GRK2-NLucN, the sequence encoding the larger luciferase fragment (NLucN, obtained from Promega (Mannheim, Germany)) was attached C-terminally to the sequence of GRK2 via a flexible linker sequence (-GSSGGGGSGGGGSGGGG-). The quality of all plasmids was verified by sequencing (Eurofins Genomics, Ebersberg, Germany).

5.2.3 Cell culture and generation of stable transfectants

HEK293T cells were a kind gift from Prof. Dr. Wulf Schneider (Institute for Medical Microbiology and Hygiene, University Hospital Regensburg, Germany) and were maintained in DMEM, supplemented with 2 mM L-glutamine and 10% FCS, at 37 °C in a water-saturated atmosphere containing 5% CO_2. To generate stable transfectants, cells were seeded at a density of $3 \cdot 10^5$ cells/mL in a 6-well plate (Sarstedt, Nümbrecht, Germany). On the following day, cells were

transfected with 2 µg of the pcDNA4 GRK2-NLucN (also encoding a zeocin resistance gene) using the X-tremeGENE™ HP transfection reagent (Roche Diagnostics, Mannheim, Germany) according to the manufacturer's protocol. After two days of incubation, the cells were detached by trypsinization, centrifuged (500 *g*, 5 min), and seeded on a 150 mm-cell culture dish (Sarstedt, Nümbrecht, Germany). The cells were allowed to attach and zeocin was added at a final concentration of 400 µg/mL to select for stable transfectants. The medium was exchanged in regular intervals until a growth of stable colonies could be observed, and the cell culture was continued with a reduced zeocin concentration of 100 µg/mL. After subsequent transfection with the plasmid encoding one of the GPCR-NLucC constructs (also encoding a neomycin resistance gene), cells stably expressing both fusion proteins were obtained as described above in the presence of 100 µg/mL zeocin and 1 mg/mL G418. Cultivation of the stable double transfectants was then continued using 100 µg/mL zeocin and 600 µg/mL G418. Cells were tested regularly for mycoplasma infection using the Venor GeM Mycoplasma Detection Kit (Minerva Biolabs, Berlin, Germany) and were negative.

5.2.4 Split luciferase-based GRK2 recruitment assay

One day before the experiment, cells stably expressing GRK2-NLucN and the respective GPCR-NLucC construct, were detached from the culture flask (≈ 80% confluency) by trypsinization and centrifuged (500 *g*, 5 min). The cell pellet was resuspended in L-15 medium supplemented with 5% FCS and 10 mM HEPES (pH 7.4). After adjusting the cell density to $1.25 \cdot 10^6$ cells/mL, 80 µL of the cell suspension were added to each well of a white 96-well plate (Brand, Wertheim, Germany) and the plates were incubated overnight at 37 °C in a water-saturated atmosphere (no additional CO_2).

For the investigation of agonists, 10 µL of the luciferase substrate furimazine (Nano-Glo® Live Cell Substrate, pre-diluted 1:100 before use) were added to each well and the plate was equilibrated for 5 min within the plate reader (pre-warmed to 37 °C), followed by measurement of the basal luminescence for 15 min (30 plate reads). 10 µL of a serial dilution of the investigated agonist (prepared in L-15 and pre-warmed to 37 °C) were added and the measurement of luminescence was continued for 45 min (90 plate reads). A solvent control (0% value) and a 100% control (M_1R, M_5R: carbachol, NTS_1R: NT(8-13); used in a concentration yielding the maximal response) were included in every experiment for normalization of the data.

For the investigation of antagonists, 10 µL of a serial dilution of the investigated antagonist were added and cells were preincubated at 37 °C for 20 min followed by the addition of 10 µL of the substrate furimazine (Nano-Glo® Live Cell Substrate, pre-diluted 1:100 before use). After 5 min of equilibration inside the plate reader and measuring the basal luminescence as described above, 10 µL of a pre-warmed solution (37 °C) of the reference agonist (M_1R, M_5R: carbachol,

NTS_1R: NT(8-13)) were added to the cells in a concentration approximately corresponding to its EC_{80} value (M_1R: c_{final} = 100 µM; M_5R: c_{final} = 3 µM; NTS_1R: c_{final} = 5 nM). The measurement was continued as described above for the agonist mode. Again, a solvent control (0% value) and a positive control (100% value), containing the agonist in the above-mentioned concentrations but no antagonist, were included for normalization purposes.

To investigate the effects of the GRK2/3 inhibitor cmpd101 on GRK2 recruitment, cells were preincubated with the indicated concentrations of cmpd101 at 37 °C for 30 min. After the addition of furimazine and equilibration inside the plate reader, concentration-response curves of the respective agonists carbachol (M_1R, M_5R) or NT(8-13) (NTS_1R) were recorded as described above. A concentration-response curve of the agonist in the absence of cmpd101 was included in every experiment as a control.

All measurements were performed at 37 °C using an EnSpire plate reader (PerkinElmer, Rodgau, Germany) with an integration time of 100 ms per well. All data were analyzed using GraphPad Prism 8.0 (GraphPad Software Inc., San Diego, CA, USA). The detected luminescence values were corrected for inter-well variability by dividing each value by the mean of the last five datapoints obtained right before agonist addition. Subsequently, potential effects of the signal decay of NLuc[37] were corrected by dividing all luminescence values by the values of the buffer control and the areas under the corrected curves (AUC) were calculated. Data (AUC) from agonist mode were normalized to the response of the solvent control (0% value) and the maximal response (100% value) induced by a high concentration of carbachol (M_1R, M_5R) or NT(8-13) (M_1R: c = 1 mM; M_5R: c = 10 µM; NTS_1R: c = 1 µM). The 100% value from experiments with cmpd101 was set to the maximal response induced by the respective agonist in the absence of cmpd101. Normalized data were then analyzed by a four-parameter logistic equation yielding pEC_{50} and E_{max} values. Data from experiments with antagonists (AUC) were normalized to the response of the solvent control (0% value) and the response detected in the absence of antagonist (100% value). Normalized data were then fitted by a four-parameter logistic equation yielding pIC_{50} values, which were transformed into pK_b values by the Cheng-Prusoff equation.[40]

5.3 Results and discussion

5.3.1 Assay principle and characterization of standard ligands

First, we had to decide where to attach which luciferase fragment at the receptor and GRK2. As it had been shown that tagging the C-terminus of the GPCR with the larger luciferase fragment (NLucN) can affect receptor function, e.g. for the M_5R,[39] we used the constructs with the smaller C-terminal fragment (NLucC) fused to the C-terminus of the receptor (M_1R-NLucC, M_5R-NLucC and NTS_1R-NLucC).[39] The complementary NLucN fragment was fused to the C-terminus of GRK2 (GRK2-NLucN), as C-terminal attachment of fluorescent proteins was reported to be tolerated by GRK2 with respect to its function.[29,41]

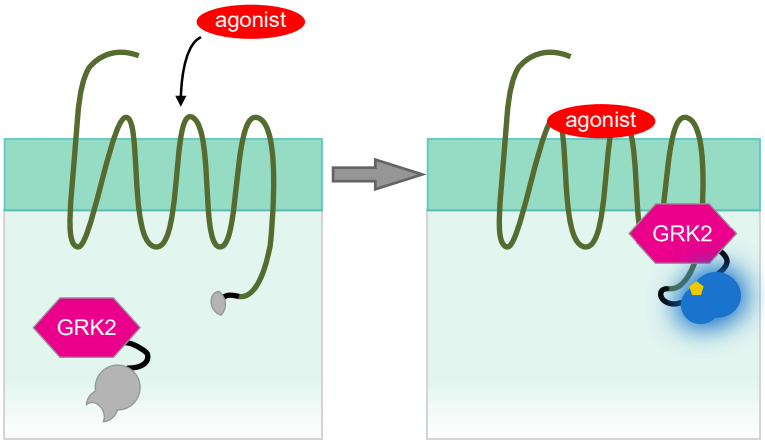

Figure 5.1: Schematic illustration of the assay principle. Activation of the receptor (e.g. by binding of an agonist) results in the translocation of GRK2 to the cell membrane. Upon binding of GRK2 to the receptor, the complementary luciferase fragments (C-terminal fragment fused to the C-terminus of the GPCR; N-terminal fragment fused to the C-terminus of GRK2) refold and the catalytical activity of the luciferase is reversibly restored.

Accordingly, HEK293T cells stably expressing GRK2-NLucN and one of the NLucC-tagged GPCRs (M_1R-NLucC, M_5R-NLucC or NTS_1R-NLucC) were generated. In these cells, agonist-mediated receptor stimulation should lead to an increase in luminescence signal upon recruitment of GRK2 to the receptor (Figure 5.1) due to restoration of the enzymatic activity of the luciferase. Making use of the possibility to perform live-cell measurements in real time (luciferase exhibits a short maturation time),[35,39] we investigated the time course of GRK2 recruitment upon agonist stimulation and potential differences between the investigated receptors.

As shown in Figure 5.2, the M_1R and the M_5R both showed a very rapid concentration-dependent increase in luminescence, which reached a peak immediately (approximately 1 min) after addition of the agonist carbachol. After reaching the peak, the luminescence signal showed a fast decline and a plateau, higher than the baseline level, was reached after 15-20 min, potentially reflecting a steady-state between association of GRK2 to and dissociation from the receptor.[23]

However, the NTS_1R showed a different behavior: depending on the applied concentration of the agonist NT(8-13), the peak of the signal occurred at different times (Figure 5.2). Additionally, the obtained responses appeared to be more stable than the signals detected for the M_1R and the M_5R indicating a more persistent interaction.

GPCRs can be categorized into class A and class B receptors according to the persistence of the receptor-β-arrestin complexes.[42] The M_1R and M_5R were shown to belong to the class A receptors,[39] which generally show a transient interaction with β-arrestins leading to a fast recycling of the receptors to the plasma membrane.[43] In contrast, the NTS_1R was classified as a class B receptor. These receptors show longer-lasting interactions with β-arrestins, resulting in the colocalization of β-arrestin and the receptor in endosomes[44,45] and a higher tendency towards lysosomal degradative pathways.[14] To the best of our knowledge, no such classification has been made for GPCRs in terms of their interaction with GRKs. However, the presented results suggested a differential interaction of receptors with GRKs as well, possibly being consistent with the β-arrestin-based classification.[42]

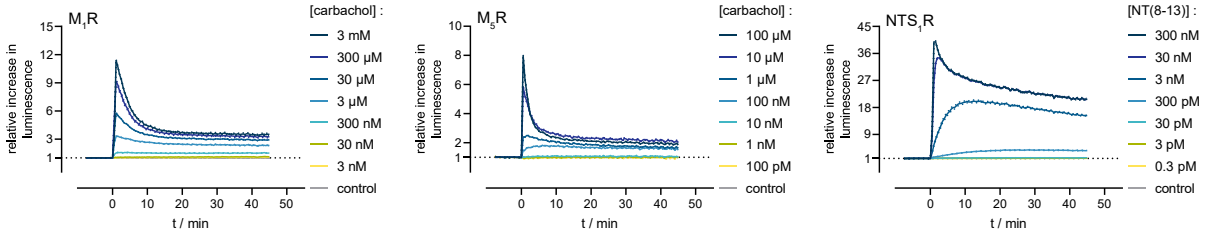

Figure 5.2: Time courses of the agonist-induced GRK2 recruitment to the M_1R-NLucC, the M_5R-NLucC or the NTS_1R-NLucC, monitored with the split luciferase-based GRK2 recruitment assay. Experiments were performed at HEK293T cells stably expressing GRK2-NLucN and the indicated GPCR-NLucC fusion proteins. The respective agonist was added in different concentrations at the timepoint t = 0 min. Data represent means ± SEM of one representative experiment from a set of at least three independent experiments, each performed in triplicate. For some datapoints, the error bars are the same size or smaller than the used symbols.

After the initial evaluation of the luminescence time courses, concentration-response curves were generated for different reference agonists by calculating the areas under the curves (see Figures 5.2 and 5.3A), allowing the determination of agonistic potencies (pEC_{50} values) and efficacies (E_{max} values). Furthermore, antagonists were characterized by quantifying the inhibition of the luminescence signal induced by an ≈ EC_{80} concentration of the agonists carbachol (M_1R, M_5R) or NT(8-13) (NTS_1R), yielding antagonistic potencies (pK_b values). The determined values are summarized in Table 5.1. Because only few pharmacological data of receptor agonists and antagonists are available resulting from the quantification of GRK2 recruitment to GPCRs, a comparison of the determined values with literature data is difficult.

However, assuming that GRK and β-arrestin recruitment assays should afford similar results, the determined parameters were compared with reported data determined in a split luciferase-based β-arrestin recruitment assay (Table 5.1).[39]

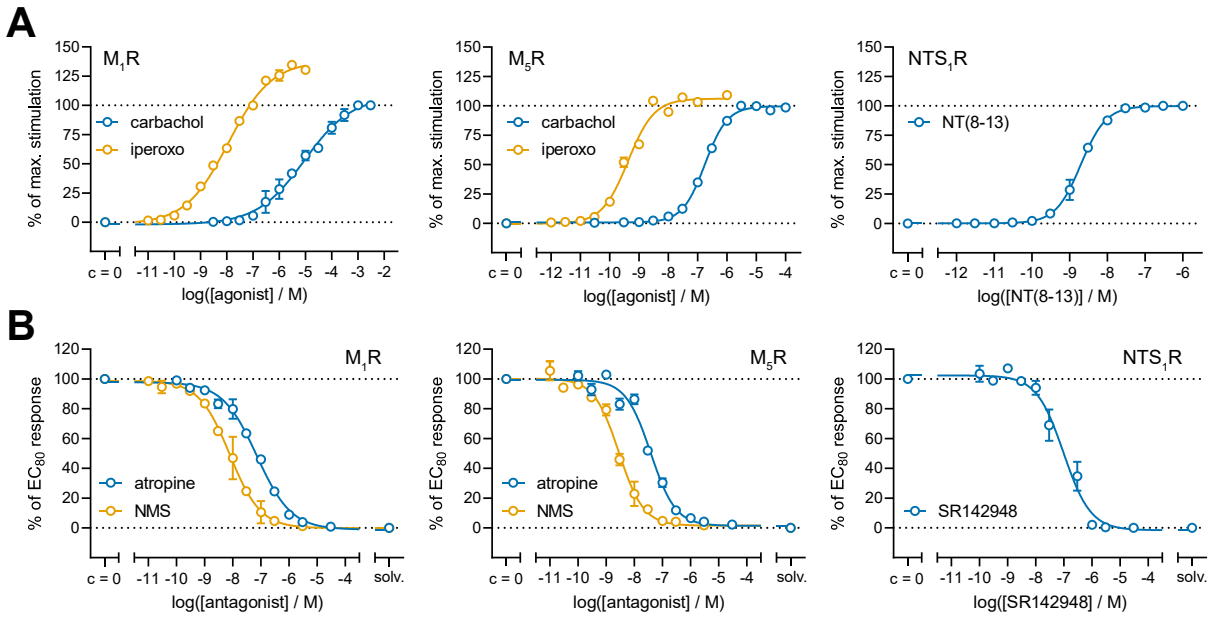

Figure 5.3: Characterization of reference ligands in the split luciferase-based GRK2 recruitment assay. Experiments were performed at HEK293T cells stably expressing GRK2-NLucN and the indicated GPCR, C-terminally fused to NLucC (M_1R-NLucC, M_5R-NLucC or NTS_1R-NLucC). (**A**) Investigation of reference M_1R, M_5R and NTS_1R agonists; data represent means ± SEM from at least four independent experiments performed in triplicate. (**B**) Inhibition of the response induced by the EC_{80} concentration of carbachol (M_1R: c = 100 µM; M_5R: c = 3 µM) or NT(8-13) (c = 5 nM) by reference antagonists; data represent means ± SEM from four independent experiments, each performed in triplicate. Corresponding pEC_{50} and E_{max} values (**A**) or pK_b values (**B**) are shown in Table 5.1. solv.: solvent control.

At the M_1R, the determined pEC_{50} values for the studied agonists carbachol and iperoxo were found to be in good agreement with results from a recently described β-arrestin2 recruitment assay based on the split NLuc system.[39] At the M_1R, iperoxo behaved as a superagonist (Figure 5.3A) as previously determined in the β-arrestin2 recruitment assay.[39] However, this is in contradiction to most literature data, where no superagonism could be observed for iperoxo at the M_1R in functional assays based on the detection of second messengers[46,47] or dynamic mass redistribution.[48] The pK_b values of the MR antagonists atropine and NMS were in accordance with the results from the β-arrestin recruitment assay[39] and with M_1R binding affinities determined in Chapter 4.

Surprisingly, pEC_{50} (and E_{max}) values of carbachol and iperoxo determined at the M_5R were inconsistent with the data from the β-arrestin2 recruitment assay.[39] However, they were in better agreement with data obtained from a split luciferase-based assay detecting the interaction between $G\alpha_q$ and PLC-β.[7] Although to a lesser extent, the same was also true for the pK_b values of the antagonists atropine and NMS.

In this context, it is worth mentioning that GRK2 was shown to directly interact with the $G\alpha_q$ subunit,[49] representing the preferred G protein for the M_1R and M_5R. Potentially, there are receptor-dependent differences in the extent or type of interaction between GRK2, the receptor and $G\alpha_q$. A stronger interaction of GRK2 with the $G\alpha_q$ subunit upon stimulation of the M_5R, compared to the M_1R, could possibly explain the high similarities between the potencies determined in the GRK2 recruitment assay and the potencies determined for the $G\alpha_q$ signaling pathway.

In the case of the NTS_1R, the potency of the reference agonist NT(8-13) was well comparable with the results from the β-arrestin2 recruitment assay.[39] For the standard NTS_1R antagonist SR142928, the determined pK_b value was slightly lower than the reported pK_b value (β-arrestin2 recruitment) (Table 5.1),[39] whereas it was in good agreement with the pK_i value from the BRET competition binding experiments described in Chapter 4.

Table 5.1: pEC_{50} and E_{max} values of reference M_1R, M_5R and NTS_1R agonists as well as pK_b values of M_1R, M_5R and NTS_1R antagonists determined in the split luciferase-based GRK2 recruitment assay.

Receptor construct	Compound	GRK2 recruitment					β-arrestin2 recruitment
		pEC_{50}[a]	E_{max}[b]	*N*	pK_b[c]	*N*	pEC_{50}/(pK_b)[d]
M_1R-NLucC	carbachol	5.00 ± 0.12	1.00	5	n.a.	---	4.73
	iperoxo	7.87 ± 0.04	1.40 ± 0.03	5	n.a.	---	7.74
	atropine	n.a.	n.a.	---	8.19 ± 0.04	4	(8.73)
	NMS	n.a.	n.a.	---	9.13 ± 0.10	4	(8.96)
M_5R-NLucC	carbachol	6.76 ± 0.02	1.00	5	n.a.	---	5.37
	iperoxo	9.33 ± 0.05	1.09 ± 0.03	5	n.a.	---	8.02
	atropine	n.a.	n.a.	---	8.69 ± 0.05	4	(9.02)
	NMS	n.a.	n.a.	---	9.80 ± 0.07	4	(9.32)
NTS_1R-NLucC	NT(8-13)	8.70 ± 0.06	1.00	4	n.a.	---	8.96
	SR142948	n.a.	n.a.	---	7.57 ± 0.11	4	(8.30)

[a]Determined in the split luciferase-based GRK2 recruitment assay at HEK293T cells stably expressing GRK2-NLucN and the respective GPCR-NLucC construct; data represent means ± SEM from *N* independent experiments, each performed in triplicate. [b]Efficacy normalized to the maximal response (E_{max} = 1.00) induced by carbachol (M_1R, M_5R) or NT(8-13) (NTS_1R); data represent means ± SEM from *N* independent experiments, each performed in triplicate. [c]Determined by inhibition of the response induced by carbachol (M_1R: c = 100 µM, EC_{50} = 10 µM; M_5R: c = 3 µM, EC_{50} = 173 nM) or NT(8-13) (c = 5 nM, EC_{50} = 2 nM) in the split luciferase-based GRK2 recruitment assay; data represent means ± SEM from *N* independent experiments, each performed in triplicate. [d]Littmann *et al.*[39] n.a.: not applicable.

5.3.2 Effect of the GRK2/3 inhibitor cmpd101 on GRK2 recruitment

In order to study the effect of the selective GRK2/3 inhibitor cmpd101[38] on the process of GRK2 recruitment, HEK293T cells stably co-expressing a C-terminally NLucC-tagged GPCR and the C-terminally NLucN-tagged GRK2, were preincubated with different concentrations of cmpd101 for 30 min prior to recording the concentration- and time-dependent bioluminescence signals upon stimulation with the agonists carbachol (M_1R, M_5R) or NT(8-13) (NTS_1R) (see Figure 5.4). The highest applied concentration of cmpd101 was 30 µM. At higher concentrations, cmpd101 can potentially affect M_1R and M_5R binding of carbachol as it was reported to displace the MR radioligand [^{3}H]NMS from both receptors at high concentrations (> 30 µM).[39]

Interestingly, different effects were observed depending on the investigated receptor:

At the M_1R, the GRK2/3 inhibitor decreased the maximal signal, but had no effect on the kinetics of GRK2 recruitment and only a slight effect on the determined potency of carbachol (see Figure 5.4A). In the case of the M_5R, cmpd101 caused a change in the kinetics of GRK2 recruitment, especially for high carbachol concentrations (see Figure 5.4B). The peak, which was observed immediately after agonist addition in the absence of cmpd101 (cf. Figure 5.2), was increasingly flattened in the presence of increasing concentrations of cmpd101 due to an elevation of the BRET signal measured after this peak. The shape of these time courses resembled the traces observed for low concentrations of carbachol at the M_5R in the absence of cmpd101 (cf. Figure 5.2). Furthermore, because all experiments were analyzed by calculating the area under the curve, the corresponding concentration-response curves of carbachol varied with respect to potency (pEC_{50}) and the upper curve plateau (efficacy, E_{max}). In contrast, recruitment of GRK2 to the NTS_1R was only marginally affected by the presence of cmpd101. Consequently, the corresponding concentration-response curves of NT(8-13) were highly similar (Figure 5.4C).

Different effects of cmpd101 on the recruitment of GRK2 to GPCRs have also been described in literature: for example, cmpd101 did not affect the concentration-dependent response in a BRET-based GRK2 recruitment assay at the dopamine D_2 receptor.[27] In contrast, cmpd101 decreased recruitment of GRK2 to the µ-opioid receptor in a BRET-based assay.[26] This observation led the authors to the conclusion that the µ-opioid receptor preferably interacts with GRK2 in its active conformation, as cmpd101 was reported to bind in the ATP binding site of the inactive kinase.[38,50] It should be mentioned that the possibility of comparing reported data with our results is limited, as kinetic data are missing in the respective articles (only the effect of cmpd101 on the concentration-response curve or on the signal measured upon stimulation with only one individual agonist concentration were provided).[26,27]

In analogy with a FRET-based study to investigate the interaction between GRK2 and the M_3R,[29] future studies should include GRK2 mutants. For example, kinase-deficient GRK2 variants (GRK2(K220R))[51] or mutants with a reduced affinity for the Gβγ dimer (GRK2(R587Q)),[33] which is involved in plasma membrane recruitment and the catalytic activity of GRK2,[34] might help to gain a better understanding about GRK2/GPCR interactions.

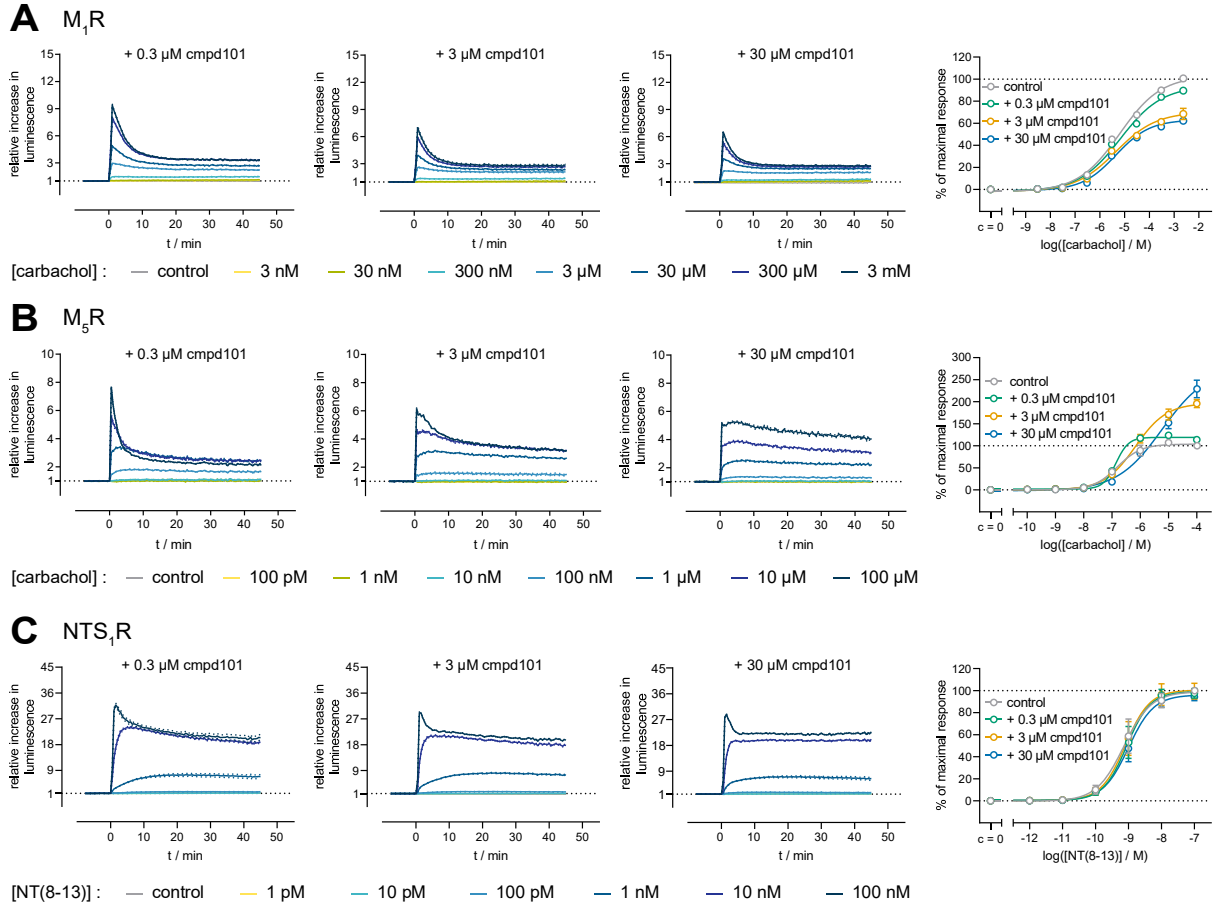

Figure 5.4: Effect of the GRK2/3 inhibitor cmpd101 on the recruitment of GRK2-NLucN to M_1R-NLucC (**A**), M_5R-NLucC (**B**) and NTS_1R-NLucC (**C**), measured with the split luciferase-based GRK2 recruitment assay. Experiments were performed at HEK293T cells stably expressing GRK2-NLucN and the indicated GPCR-NLucC fusion proteins. Cells were preincubated (37 °C, 30 min) with the GRK2/3 inhibitor cmpd101 used at the indicated concentrations, followed by the stimulation with different concentrations of the respective GPCR agonists (M_1R and M_5R: carbachol; NTS_1R: NT(8-13)). Shown are the effects of cmpd101 on the kinetics of GRK2 recruitment and on the resulting concentration-response curves of the agonists. Signal time courses represent means ± SEM being representative of two (M_1R) or three (M_5R, NTS_1R) independent experiments, each performed in triplicate. Data of the concentration-response curves represent means ± SEM from two (M_1R) or three (M_5R, NTS_1R) independent experiments, each performed in triplicate. For some datapoints, the error bars are the same size or smaller than the used symbols.

5.4 Conclusion

Here we present a split NLuc-based assay for the concentration- and time-dependent analysis of the recruitment of the G protein-coupled receptor kinase 2 (GRK2) to the M_1R, M_5R and NTS_1R. This approach revealed differences in the kinetics of GRK2 recruitment to the receptor: whereas the luminescence signals obtained for M_1R and M_5R activation decreased rapidly after a sharp initial peak, the signal obtained upon activation of the NTS_1R was more persistent (slow decline after the initial signal increase). The results suggested that GPCRs can potentially be classified according to their GRK2 recruitment behavior, in a similar manner as GPCRs have been grouped with regard to interactions with β-arrestins.[42] Furthermore, it was demonstrated that the developed assay is also useful for the characterization of GPCR agonists and antagonists. Experiments with the GRK2/3 inhibitor cmpd101 suggested different interactions between the investigated GPCRs and GRK2 in terms of GRK2 recruitment kinetics.

In future studies, the set of investigated GPCRs should be extended to verify a potential classification with respect to the kinetics of GRK2 recruitment. It would also be interesting to see whether pathway-biased ligands (in terms of G protein or β-arrestin recruitment) also show a bias with respect to GRK recruitment. Besides future studies including GRK2 mutants, the presented approach can also be transferred to other GRKs, such as GRK5 or GRK6. This may contribute to a better understanding of the role of various GRK subtypes, as recent studies suggested different functions of GRK2/3 on one side and GRK5/6 on the other side, promoting β-arrestin mediated GPCR endocytosis and β-arrestin dependent ERK signaling, respectively.[52-54]

5.5 References

1. Pierce, K. L., Premont, R. T. & Lefkowitz, R. J. Seven-transmembrane receptors. *Nat. Rev. Mol. Cell. Biol.* **3**, 639-650, doi:10.1038/nrm908 (2002).

2. Weis, W. I. & Kobilka, B. K. The molecular basis of G protein-coupled receptor activation. *Annu. Rev. Biochem* **87**, 897-919, doi:10.1146/annurev-biochem-060614-033910 (2018).

3. Hepler, J. R. & Gilman, A. G. G proteins. *Trends Biochem. Sci.* **17**, 383-387, doi:10.1016/0968-0004(92)90005-t (1992).

4. Offermanns, S. G-proteins as transducers in transmembrane signalling. *Prog. Biophys. Mol. Biol.* **83**, 101-130, doi:10.1016/s0079-6107(03)00052-x (2003).

5. Hilger, D., Masureel, M. & Kobilka, B. K. Structure and dynamics of GPCR signaling complexes. *Nat. Struct. Mol. Biol.* **25**, 4-12, doi:10.1038/s41594-017-0011-7 (2018).

6. Milde, M., Rinne, A., Wunder, F., Engelhardt, S. & Bünemann, M. Dynamics of $G\alpha_{i1}$ interaction with type 5 adenylate cyclase reveal the molecular basis for high sensitivity of G_i-mediated inhibition of cAMP production. *Biochem. J.* **454**, 515-523, doi:10.1042/bj20130554 (2013).

7. Littmann, T., Ozawa, T., Hoffmann, C., Buschauer, A. & Bernhardt, G. A split luciferase-based probe for quantitative proximal determination of $G\alpha_q$ signalling in live cells. *Sci. Rep.* **8**, 17179, doi:10.1038/s41598-018-35615-w (2018).

8. Whorton, M. R. & MacKinnon, R. X-ray structure of the mammalian GIRK2–βγ G-protein complex. *Nature* **498**, 190-197, doi:10.1038/nature12241 (2013).

9. Tobin, A. B. G-protein-coupled receptor phosphorylation: where, when and by whom. *Br. J. Pharmacol.* **153**, S167-S176, doi:10.1038/sj.bjp.0707662 (2008).

10. Patwardhan, A., Cheng, N. & Trejo, J. Post-translational modifications of G protein–coupled receptors control cellular signaling dynamics in space and time. *Pharmacol. Rev.* **73**, 120-151, doi:10.1124/pharmrev.120.000082 (2021).

11. Lohse, M. J., Benovic, J. L., Caron, M. G. & Lefkowitz, R. J. Multiple pathways of rapid β_2-adrenergic receptor desensitization. Delineation with specific inhibitors. *J. Biol. Chem.* **265**, 3202-3211 (1990).

12. Lohse, M., Benovic, J., Codina, J., Caron, M. & Lefkowitz, R. β-Arrestin: a protein that regulates β-adrenergic receptor function. *Science* **248**, 1547-1550, doi:10.1126/science.2163110 (1990).

13. Reiter, E. & Lefkowitz, R. J. GRKs and β-arrestins: roles in receptor silencing, trafficking and signaling. *Trends Endocrinol. Metab.* **17**, 159-165, doi:10.1016/j.tem.2006.03.008 (2006).

14. Moore, C. A. C., Milano, S. K. & Benovic, J. L. Regulation of receptor trafficking by GRKs and arrestins. *Annu. Rev. Physiol.* **69**, 451-482, doi:10.1146/annurev.physiol.69.022405.154712 (2007).

15. Gurevich, E. V. & Gurevich, V. V. Arrestins: ubiquitous regulators of cellular signaling pathways. *Genome Biol.* **7**, 236, doi:10.1186/gb-2006-7-9-236 (2006).

16. Peterson, Y. K. & Luttrell, L. M. The diverse roles of arrestin scaffolds in G protein–coupled receptor signaling. *Pharmacol. Rev.* **69**, 256-297, doi:10.1124/pr.116.013367 (2017).

17. Pearce, L. R., Komander, D. & Alessi, D. R. The nuts and bolts of AGC protein kinases. *Nat. Rev. Mol. Cell. Biol.* **11**, 9-22, doi:10.1038/nrm2822 (2010).

18. Gurevich, E. V., Tesmer, J. J. G., Mushegian, A. & Gurevich, V. V. G protein-coupled receptor kinases: more than just kinases and not only for GPCRs. *Pharmacol. Ther.* **133**, 40-69, doi:10.1016/j.pharmthera.2011.08.001 (2012).

19. Komolov, K. E. & Benovic, J. L. G protein-coupled receptor kinases: past, present and future. *Cell. Signal.* **41**, 17-24, doi:10.1016/j.cellsig.2017.07.004 (2018).

20. Sato, P. Y., Chuprun, J. K., Schwartz, M. & Koch, W. J. The evolving impact of G protein-coupled receptor kinases in cardiac health and disease. *Physiol. Rev.* **95**, 377-404, doi:10.1152/physrev.00015.2014 (2015).

21. Ribas, C., Penela, P., Murga, C., Salcedo, A., García-Hoz, C., Jurado-Pueyo, M., Aymerich, I. & Mayor, F. The G protein-coupled receptor kinase (GRK) interactome: role of GRKs in GPCR regulation and signaling. *Biochim. Biophys. Acta Biomembr.* **1768**, 913-922, doi:10.1016/j.bbamem.2006.09.019 (2007).

22. Hasbi, A., Devost, D., Laporte, S. A. & Zingg, H. H. Real-time detection of interactions between the human oxytocin receptor and G protein-coupled receptor kinase-2. *Mol. Endocrinol.* **18**, 1277-1286, doi:10.1210/me.2003-0440 (2004).

23. Jorgensen, R., Holliday, N. D., Hansen, J. L., Vrecl, M., Heding, A., Schwartz, T. W. & Elling, C. E. Characterization of G-protein coupled receptor kinase interaction with the neurokinin-1 receptor using bioluminescence resonance energy transfer. *Mol. Pharmacol.* **73**, 349-358, doi:10.1124/mol.107.038877 (2008).

24. Jorgensen, R., Kubale, V., Vrecl, M., Schwartz, T. W. & Elling, C. E. Oxyntomodulin differentially affects glucagon-like peptide-1 receptor β-arrestin recruitment and signaling through $G\alpha_s$. *J. Pharmacol. Exp. Ther.* **322**, 148-154, doi:10.1124/jpet.107.120006 (2007).

25. Matti, C., Salnikov, A., Artinger, M., D'Agostino, G., Kindinger, I., Uguccioni, M., Thelen, M. & Legler, D. F. ACKR4 recruits GRK3 prior to β-arrestins but can scavenge chemokines in the absence of β-arrestins. *Front. Immunol.* **11**, doi:10.3389/fimmu.2020.00720 (2020).

26. Miess, E., Gondin, A. B., Yousuf, A., Steinborn, R., Mösslein, N., Yang, Y., Göldner, M., Ruland, J. G., Bünemann, M., Krasel, C., Christie, M. J., Halls, M. L., Schulz, S. & Canals, M. Multisite phosphorylation is required for sustained interaction with GRKs and arrestins during rapid μ-opioid receptor desensitization. *Sci. Signal.* **11**, eaas9609, doi:10.1126/scisignal.aas9609 (2018).

27. Pack, T. F., Orlen, M. I., Ray, C., Peterson, S. M. & Caron, M. G. The dopamine D2 receptor can directly recruit and activate GRK2 without G protein activation. *J. Biol. Chem.* **293**, 6161-6171, doi:10.1074/jbc.RA117.001300 (2018).

28. Quoyer, J., Janz, J. M., Luo, J., Ren, Y., Armando, S., Lukashova, V., Benovic, J. L., Carlson, K. E., Hunt, S. W., 3rd & Bouvier, M. Pepducin targeting the C-X-C chemokine receptor type 4 acts as a biased agonist favoring activation of the inhibitory G protein. *Proc. Natl. Acad. Sci. U.S.A.* **110**, E5088-E5097, doi:10.1073/pnas.1312515110 (2013).

29. Wolters, V., Krasel, C., Brockmann, J. & Bünemann, M. Influence of $G\alpha_q$ on the dynamics of M_3-acetylcholine receptor-G-protein-coupled receptor kinase 2 interaction. *Mol. Pharmacol.* **87**, 9-17, doi:10.1124/mol.114.094722 (2015).

30. Barak, L. S., Warabi, K., Feng, X., Caron, M. G. & Kwatra, M. M. Real-time visualization of the cellular redistribution of G protein-coupled receptor kinase 2 and β-arrestin 2 during homologous desensitization of the substance P receptor. *J. Biol. Chem.* **274**, 7565-7569, doi:10.1074/jbc.274.11.7565 (1999).

31. DebBurman, S. K., Ptasienski, J., Benovic, J. L. & Hosey, M. M. G protein-coupled receptor kinase GRK2 is a phospholipid-dependent enzyme that can be conditionally activated by G protein βγ subunits. *J. Biol. Chem.* **271**, 22552-22562, doi:10.1074/jbc.271.37.22552 (1996).

32. Onorato, J. J., Gillis, M. E., Liu, Y., Benovic, J. L. & Ruoho, A. E. The β-adrenergic receptor kinase (GRK2) is regulated by phospholipids. *J. Biol. Chem.* **270**, 21346-21353, doi:10.1074/jbc.270.36.21346 (1995).

33. Carman, C. V., Barak, L. S., Chen, C., Liu-Chen, L. Y., Onorato, J. J., Kennedy, S. P., Caron, M. G. & Benovic, J. L. Mutational analysis of Gβγ and phospholipid interaction with G protein-coupled receptor kinase 2. *J. Biol. Chem.* **275**, 10443-10452, doi:10.1074/jbc.275.14.10443 (2000).

34. Pitcher, J. A., Inglese, J., Higgins, J. B., Arriza, J. L., Casey, P. J., Kim, C., Benovic, J. L., Kwatra, M. M., Caron, M. G. & Lefkowitz, R. J. Role of βγ subunits of G proteins in targeting the β-adrenergic receptor kinase to membrane-bound receptors. *Science* **257**, 1264-1267, doi:10.1126/science.1325672 (1992).

35. Dixon, A. S., Schwinn, M. K., Hall, M. P., Zimmerman, K., Otto, P., Lubben, T. H., Butler, B. L., Binkowski, B. F., Machleidt, T., Kirkland, T. A., Wood, M. G., Eggers, C. T., Encell, L. P. & Wood, K. V. NanoLuc complementation reporter optimized for accurate measurement of protein interactions in cells. *ACS Chem. Biol.* **11**, 400-408, doi:10.1021/acschembio.5b00753 (2016).

36. Hattori, M. & Ozawa, T. Split luciferase complementation for analysis of intracellular signaling. *Anal. Sci.* **30**, 539-544, doi:10.2116/analsci.30.539 (2014).

37. Hall, M. P., Unch, J., Binkowski, B. F., Valley, M. P., Butler, B. L., Wood, M. G., Otto, P., Zimmerman, K., Vidugiris, G., Machleidt, T., Robers, M. B., Benink, H. A., Eggers, C. T., Slater, M. R., Meisenheimer, P. L., Klaubert, D. H., Fan, F., Encell, L. P. & Wood, K. V. Engineered luciferase reporter from a deep sea shrimp utilizing a novel imidazopyrazinone substrate. *ACS Chem. Biol.* **7**, 1848-1857, doi:10.1021/cb3002478 (2012).

38. Thal, D. M., Yeow, R. Y., Schoenau, C., Huber, J. & Tesmer, J. J. G. Molecular mechanism of selectivity among G protein-coupled receptor kinase 2 inhibitors. *Mol. Pharmacol.* **80**, 294-303, doi:10.1124/mol.111.071522 (2011).

39. Littmann, T., Buschauer, A. & Bernhardt, G. Split luciferase-based assay for simultaneous analyses of the ligand concentration- and time-dependent recruitment of β-arrestin2. *Anal. Biochem.* **573**, 8-16, doi:10.1016/j.ab.2019.02.023 (2019).

40. Cheng, Y. & Prusoff, W. H. Relationship between the inhibition constant (K_i) and the concentration of inhibitor which causes 50 per cent inhibition (I_{50}) of an enzymatic reaction. *Biochem. Pharmacol.* **22**, 3099-3108, doi:10.1016/0006-2952(73)90196-2 (1973).

41. Schulz, R., Wehmeyer, A. & Schulz, K. Opioid receptor types selectively cointernalize with G protein-coupled receptor kinases 2 and 3. *J. Pharmacol. Exp. Ther.* **300**, 376-384, doi:10.1124/jpet.300.2.376 (2002).

42. Oakley, R. H., Laporte, S. A., Holt, J. A., Caron, M. G. & Barak, L. S. Differential affinities of visual arrestin, βarrestin1, and βarrestin2 for G protein-coupled receptors delineate two major classes of receptors. *J. Biol. Chem.* **275**, 17201-17210, doi:10.1074/jbc.M910348199 (2000).

43. Oakley, R. H., Laporte, S. A., Holt, J. A., Barak, L. S. & Caron, M. G. Association of beta-arrestin with G protein-coupled receptors during clathrin-mediated endocytosis dictates the profile of receptor resensitization. *J. Biol. Chem.* **274**, 32248-32257, doi:10.1074/jbc.274.45.32248 (1999).

44. Oakley, R. H., Laporte, S. A., Holt, J. A., Barak, L. S. & Caron, M. G. Molecular determinants underlying the formation of stable intracellular G protein-coupled receptor-beta-arrestin complexes after receptor endocytosis. *J. Biol. Chem.* **276**, 19452-19460, doi:10.1074/jbc.M101450200 (2001).

45. Zhang, J., Barak, L. S., Anborgh, P. H., Laporte, S. A., Caron, M. G. & Ferguson, S. S. Cellular trafficking of G protein-coupled receptor/β-arrestin endocytic complexes. *J. Biol. Chem.* **274**, 10999-11006, doi:10.1074/jbc.274.16.10999 (1999).

46. Holze, J., Bermudez, M., Pfeil, E. M., Kauk, M., Bödefeld, T., Irmen, M., Matera, C., Dallanoce, C., De Amici, M., Holzgrabe, U., König, G. M., Tränkle, C., Wolber, G., Schrage, R., Mohr, K., Hoffmann, C., Kostenis, E. & Bock, A. Ligand-specific allosteric coupling controls G-protein-coupled receptor signaling. *ACS Pharmacol. Transl. Sci.* **3**, 859-867, doi:10.1021/acsptsci.0c00069 (2020).

47. van der Westhuizen, E. T., Spathis, A., Khajehali, E., Jörg, M., Mistry, S. N., Capuano, B., Tobin, A. B., Sexton, P. M., Scammells, P. J., Valant, C. & Christopoulos, A. Assessment of the molecular mechanisms of action of novel 4-phenylpyridine-2-one and 6-phenylpyrimidin-4-one allosteric modulators at the M_1 muscarinic acetylcholine receptors. *Mol. Pharmacol.* **94**, 770-783, doi:10.1124/mol.118.111633 (2018).

48. Chen, X., Klöckner, J., Holze, J., Zimmermann, C., Seemann, W. K., Schrage, R., Bock, A., Mohr, K., Tränkle, C., Holzgrabe, U. & Decker, M. Rational design of partial agonists for the muscarinic M_1 acetylcholine receptor. *J. Med. Chem.* **58**, 560-576, doi:10.1021/jm500860w (2015).

49. Carman, C. V., Parent, J. L., Day, P. W., Pronin, A. N., Sternweis, P. M., Wedegaertner, P. B., Gilman, A. G., Benovic, J. L. & Kozasa, T. Selective regulation of $G\alpha_{q/11}$ by an RGS domain in the G protein-coupled receptor kinase, GRK2. *J. Biol. Chem.* **274**, 34483-34492, doi:10.1074/jbc.274.48.34483 (1999).

50. Homan, K. T. & Tesmer, J. J. G. Molecular basis for small molecule inhibition of G protein-coupled receptor kinases. *ACS Chem. Biol.* **10**, 246-256, doi:10.1021/cb5003976 (2015).

51. Kong, G., Penn, R. & Benovic, J. L. A β-adrenergic receptor kinase dominant negative mutant attenuates desensitization of the β_2-adrenergic receptor. *J. Biol. Chem.* **269**, 13084-13087 (1994).

52. Kim, J., Ahn, S., Ren, X.-R., Whalen, E. J., Reiter, E., Wei, H. & Lefkowitz, R. J. Functional antagonism of different G protein-coupled receptor kinases for β-arrestin-mediated angiotensin II receptor signaling. *Proc. Natl. Acad. Sci. U.S.A.* **102**, 1442-1447, doi:10.1073/pnas.0409532102 (2005).

53. Ren, X.-R., Reiter, E., Ahn, S., Kim, J., Chen, W. & Lefkowitz, R. J. Different G protein-coupled receptor kinases govern G protein and β-arrestin-mediated signaling of V2 vasopressin receptor. *Proc. Natl. Acad. Sci. U.S.A.* **102**, 1448-1453, doi:10.1073/pnas.0409534102 (2005).

54. Nobles, K. N., Xiao, K., Ahn, S., Shukla, A. K., Lam, C. M., Rajagopal, S., Strachan, R. T., Huang, T. Y., Bressler, E. A., Hara, M. R., Shenoy, S. K., Gygi, S. P. & Lefkowitz, R. J. Distinct phosphorylation sites on the β_2-adrenergic receptor establish a barcode that encodes differential functions of β-arrestin. *Sci. Signal.* **4**, ra51, doi:10.1126/scisignal.2001707 (2011).

6. Summary

The development of novel ligands for G protein-coupled receptors (GPCRs), representing important drug targets, requires the determination of ligand-receptor affinities. This has primarily been done by radioligand competition binding experiments. However, the use of radioligands is disadvantageous with respect to safety concerns, legal handling regulations and waste disposal. Thus, alternative and radioactivity-free methods for studying ligand-receptor binding are needed. Over the last decades, techniques using fluorescent ligands have emerged as a promising option. A recently reported luminescence-based binding assay makes use of the phenomenon of BRET (bioluminescence resonance energy transfer). The N-terminus of the receptor of interest was tagged with a small luciferase, which generates bioluminescence upon the addition of its substrate (e.g. furimazine). When a fluorescent ligand binds to the receptor, BRET can occur due to the close proximity of the luciferase and the fluorescent ligand. The BRET signal correlates with the amount of receptor-bound ligand and, in contrast to radioligand binding assays, ligand binding can be measured in real time with high temporal resolution.

The aim of this thesis was the development of BRET-based binding assays for different GPCRs as alternative methods to radioligand binding assays. First, a BRET-based binding assay was developed for the histamine H_2 receptor (H_2R). For this purpose, the H_2R, N-terminally fused to the NanoLuc® (NLuc), was stably expressed in HEK293T cells. Out of three differently labeled fluorescent H_2R ligands, which were investigated in BRET saturation binding experiments, the Py-1-labeled ligand **2.1** turned out to be the most favorable in terms of ligand affinity and signal-to-background (S/B) ratio. The receptor binding kinetics of **2.1** were studied in real time and competition binding experiments with **2.1** and several reported H_2R ligands afforded H_2R binding data in accordance with literature values.

Furthermore, a BRET-based binding assay was developed for the M_2 muscarinic acetylcholine receptor (M_2R). Two TAMRA-labeled M_2R ligands (**3.1** and **3.2**) were characterized by saturation binding, association and dissociation kinetic (in real time) and, for **3.1**, competition binding experiments with standard MR ligands. As the fluorophore TAMRA is also suited for fluorescence anisotropy (FA) studies, the BRET-based M_2R binding assay was compared with an FA-based real-time binding assay, also using **3.1** and **3.2** as probes. Both methods, representing different methodologies, yielded similar results (ligand binding affinities from saturation binding and competition binding studies). Kinetic data from both assays revealed a complex binding behavior for **3.1** and **3.2** (e.g. biphasic dissociation kinetics), being most pronounced for **3.2**.

In the case of the neuropeptide Y Y_1 receptor (Y_1R) or the neurotensin receptor 1 (NTS_1R), both exhibiting long N-termini, application of the reported concept (N-terminal fusion of the GPCR to NLuc) failed to establish BRET-based binding assays for these receptors. Obviously, their longer N-termini led to an increased distance or an unfavorable position of the luciferase relative to the fluorescent ligand, precluding efficient BRET.

Therefore, an alternative strategy was developed by inserting the luciferase into the second extracellular loop of the Y_1R and the NTS_1R. This novel approach resulted in feasible BRET binding assays. The same strategy, which is considered a widely applicable method, was applied to two other GPCRs with comparably short N-termini, the angiotensin II receptor type 1 (AT_1R) and the M_1 muscarinic acetylcholine receptor (M_1R). When compared with the N-terminally NLuc-tagged AT_1R and M_1R, insertion of NLuc into ECL2 of the receptors led to ligand affinities in better accordance with literature data, and/or higher S/B ratios.

Finally, a split luciferase-based assay was developed to assess the recruitment of the G protein coupled receptor kinase 2 (GRK2) to three different receptors. Besides the possibility of generating concentration-response curves, the novel assay allowed analyzing GRK2 recruitment in a time-dependent manner. It revealed different recruitment kinetics for the NTS_1R, which showed a more sustained interaction with GRK2, when compared with the M_1R and the M_5R, both showing a short-lasting interaction with GRK2. This suggested a potential classification of GPCRs based on their differential interaction with GRKs.

7. Appendix

7.1 Appendix to Chapter 2

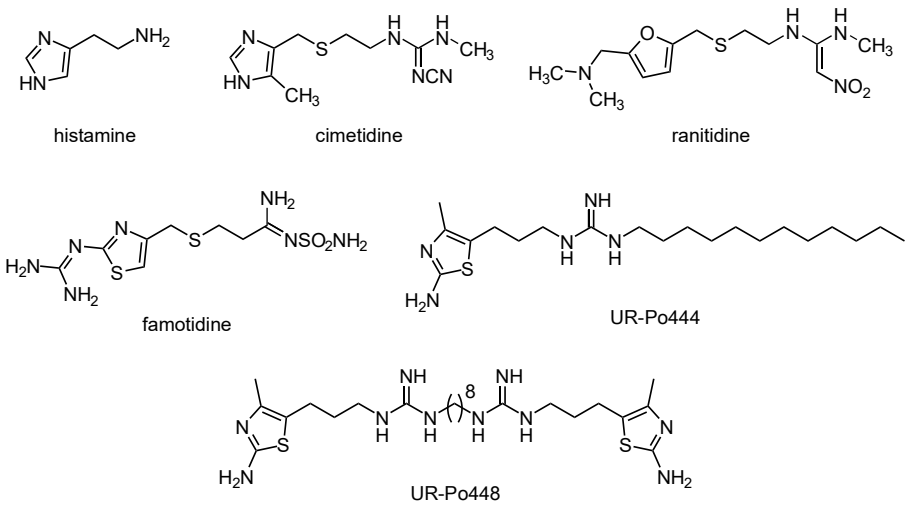

Figure A1: Structures of the H_2R ligands analyzed in Chapter 2.

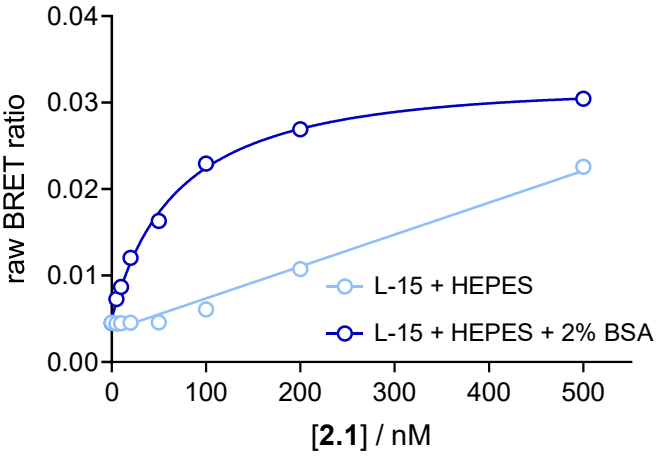

Figure A2: Effect of BSA on the total binding of the fluorescent ligand **2.1** in BRET-based binding experiments at intact HEK293T cells stably expressing the NLuc-H_2R. Serial dilutions of **2.1** were prepared in two different buffers: one buffer (light blue) consisted of L-15 medium with 10 mM HEPES (pH 7.4); the other buffer (dark blue) consisted of L-15 medium with 10 mM HEPES (pH 7.4) and 2% BSA. The dilutions of the fluorescent ligand **2.1** were added to the cells and after a preincubation at 27 °C for 60 min, total binding was assessed as described in Chapter 2. When using the dilution buffer devoid of BSA, no saturable binding could be observed for **2.1**, presumably due to adsorption of the fluorescent ligand to the plate material or the plastic vessels used for the dilutions. This could be prevented by the addition of 2% BSA. Shown data represent means ± SEM from a representative experiment performed in triplicate. For some datapoints, the error bars are shorter than the size of the symbol.

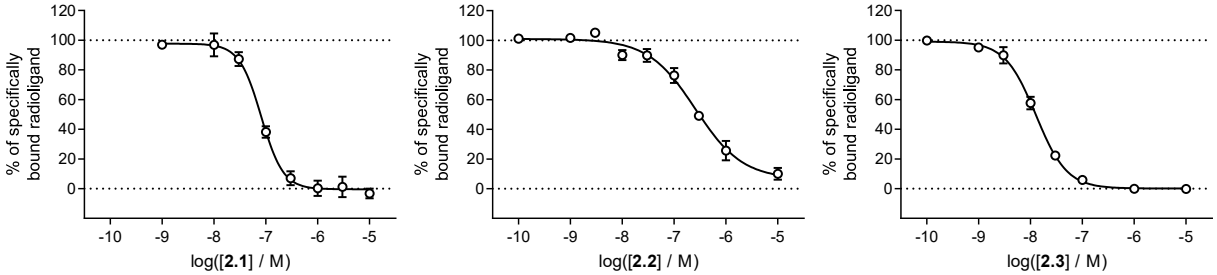

Figure A3: Displacement curves from radioligand competition binding experiments with the radioligand [^{3}H]UR-DE257[1] (c = 20 nM) and **2.1** (UR-KAT478), **2.2** (UR-KAT515) or **2.3** (UR-KAT514) using membrane preparations of Sf9 insect cells expressing the hH_2R-$G\alpha_s$ fusion protein. Data represent means ± SEM from at least three independent experiments, each performed in triplicate.

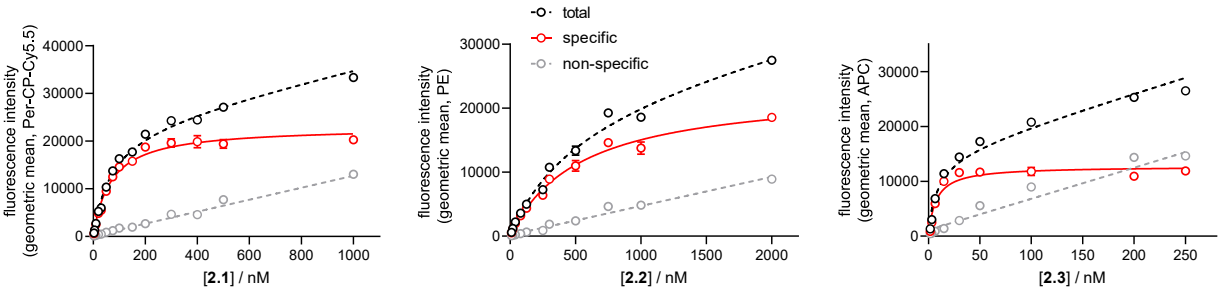

Figure A4: Representative isotherms from flow cytometric saturation binding experiments with the fluorescent ligands **2.1**-**2.3** at intact HEK293T-hH_2R-qs5-HA cells. Non-specific binding was determined in the presence of famotidine (300-fold excess over the respective concentration of fluorescent ligand). Used laser lines/emission filters: **2.1**, 488 nm/670 ± 65 nm (Per-CP-Cy5.5 channel), **2.2**, 488 nm/585 ± 21 nm (PE channel); **2.3**, 633 nm/660 ± 10 nm (APC channel). Data represent means (total and non-specific binding) or calculated values (specific binding) ± errors of a representative experiment from a set of three independent experiments, each performed in duplicate. Error bars of total and non-specific binding represent the SEM. Error bars of specific binding represent propagated errors.

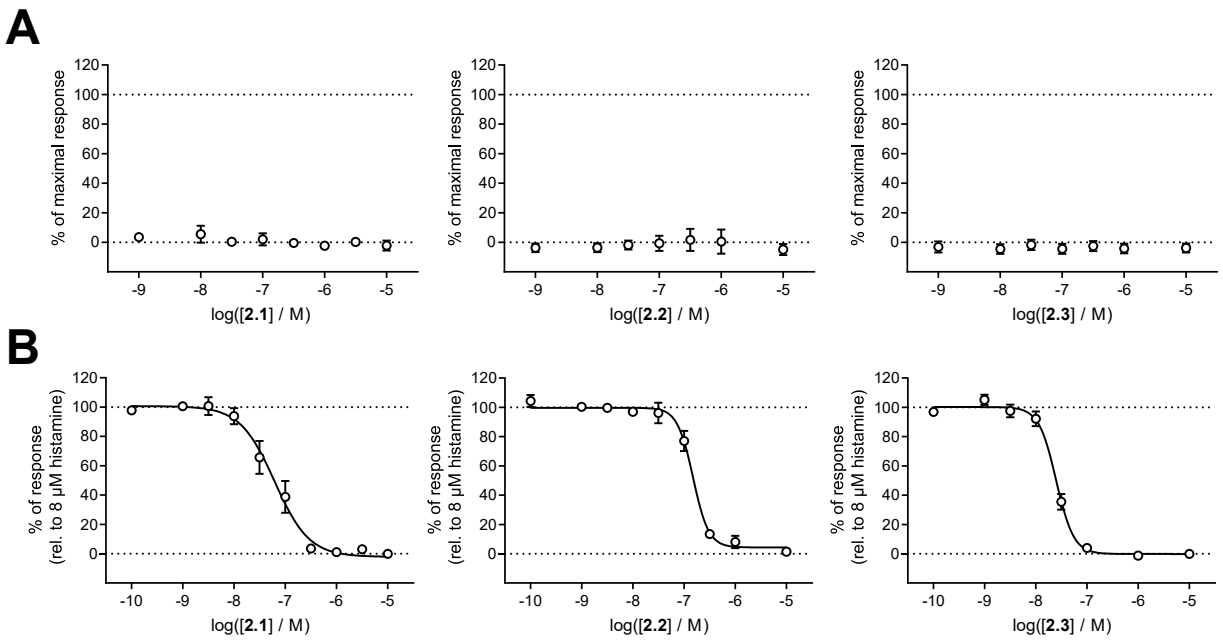

Figure A5: Functional characterization of the fluorescence-labeled H_2R ligands **2.1**-**2.3** in a split luciferase-based β-arrestin2 recruitment assay performed at HEK293T-ARRB2-hH_2R cells. (**A**) Agonist mode. Graphs display the compound-induced recruitment of β-arrestin2. Data represent means ± SEM from at least three independent experiments performed in triplicate. (**B**) Antagonist mode. Graphs display the inhibition of the response induced by the EC_{80} concentration of histamine (c = 8 µM). Data shown represent means ± SEM from at least three independent experiments, each performed in triplicate.

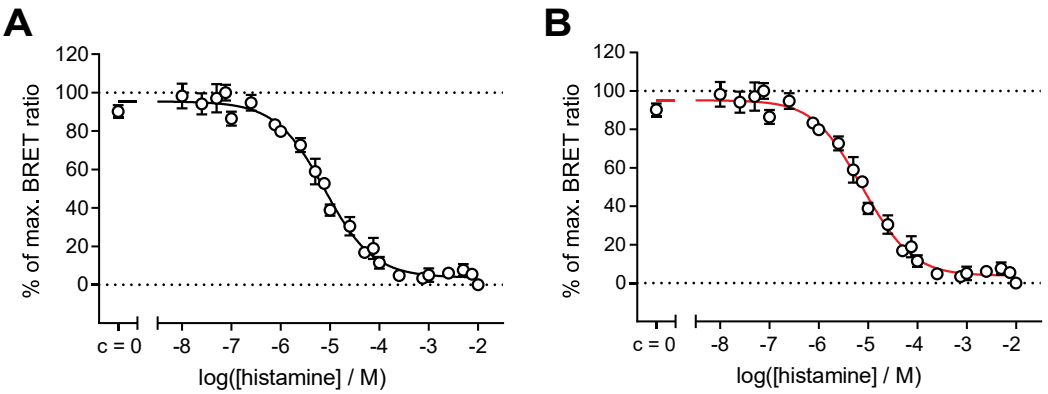

Figure A6: Representative displacement curve from a BRET competition binding experiment with **2.1** (c = 50 nM) and histamine at HEK293T cells, stably expressing the NLuc-H_2R. Data represent means ± SEM of a representative experiment from a set of two independent experiments performed in triplicate. Data shown in **A** and **B** originate from the same experiment. In **A**, the obtained data were analyzed using a monophasic fit, whereas a biphasic fit was used instead in **B**.

7.2 Appendix to Chapter 3

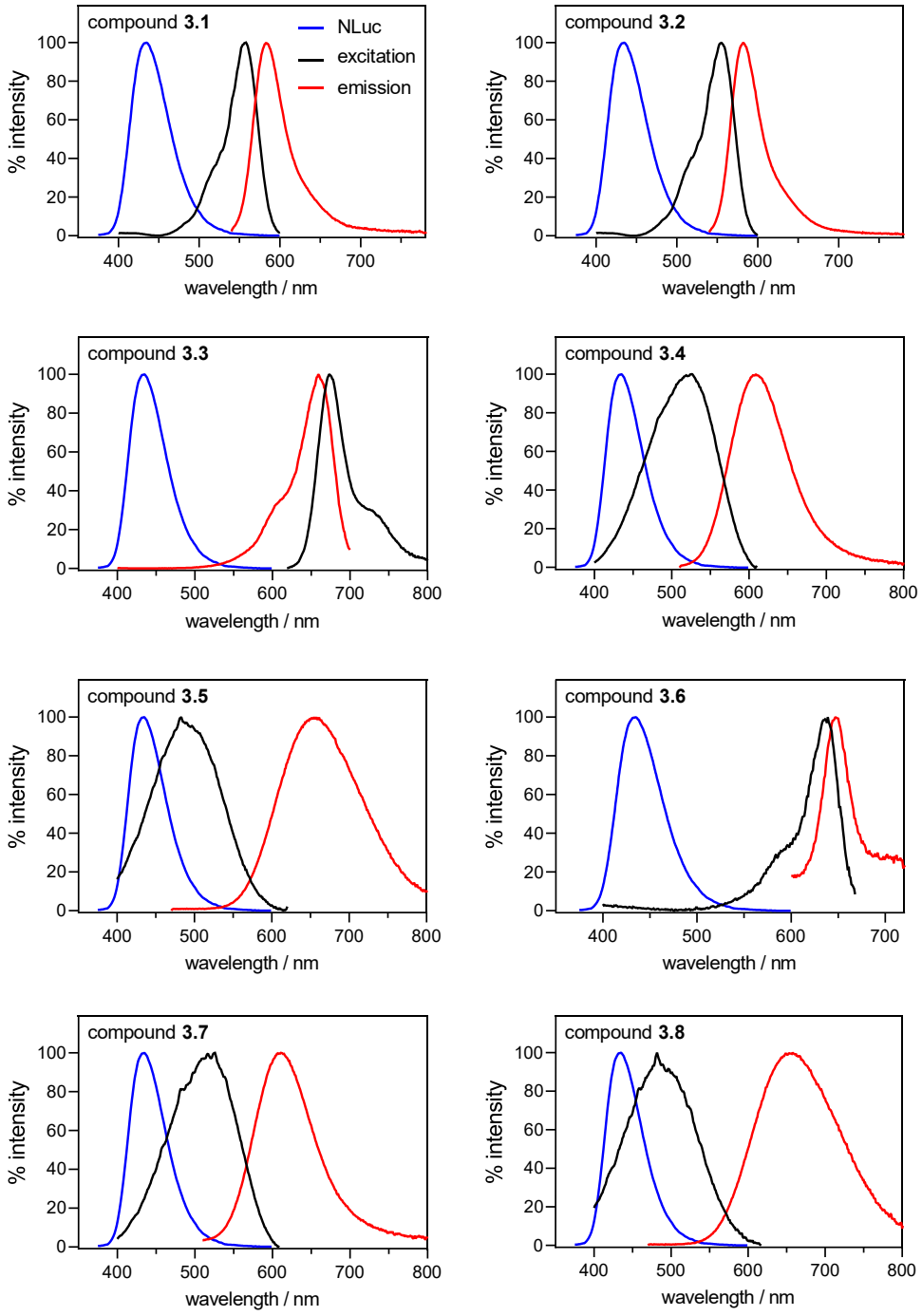

Figure A7: Overlay of the bioluminescence spectrum of NLuc with the excitation and corrected emission spectra of the investigated fluorescent MR ligands **3.1**-**3.8**. Data of excitation and emission spectra were taken from She *et al.*[2] and Gruber *et al.*[3], respectively, and represent the spectra recorded in PBS + 1% BSA. The bioluminescence spectrum of NLuc was recorded according to a described procedure[4] using HEK293T cells transiently transfected with the NLuc-M_2R.

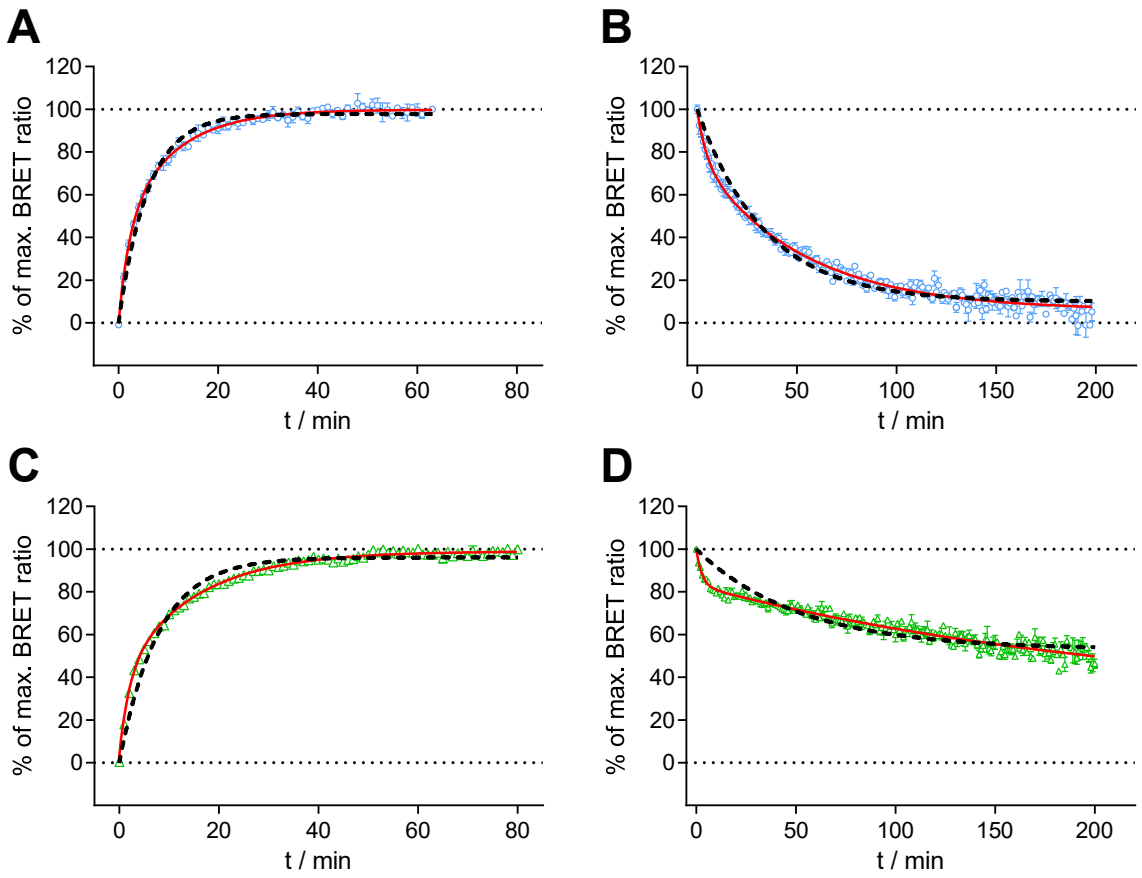

Figure A8: Heterogeneity of association and dissociation curves from kinetic BRET binding experiments at the NLuc-M_2R, stably expressed in HEK293T cells. Association and dissociation curves of **3.1** (blue symbols, **A** and **B**; c = 2 nM) and **3.2** (green symbols, **C** and **D**; c = 2 nM) from representative experiments, performed in triplicate, are depicted. Data are shown as calculated values ± propagated errors. Monophasic fits are indicated by dashed black lines, biphasic fits as solid red lines.

Global kinetic modeling of FA binding experiments with the fluorescent MR ligand 3.1

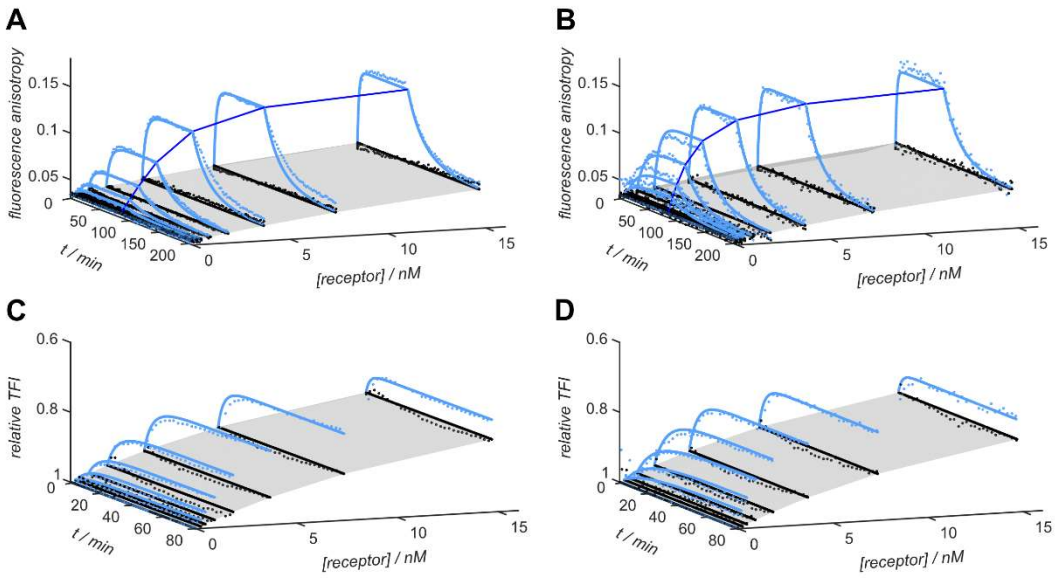

Figure A9: Time-dependent changes in FA and relative TFI upon binding of **3.1** to increasing concentrations of the M_2R displayed on BBVs. The concentration of **3.1** was 2.5 nM (**A**, **C**) or 0.5 nM (**B**, **D**). Graphs show representative results of one of three independent experiments performed in duplicate. The global fit of the single binding site model under consideration of the change in relative quantum yield is indicated by the light blue lines (total binding) and grey surface (non-specific binding). The dark blue line (**A**, **B**) indicates the timepoint, when the dissociation was started by the addition of atropine (c = 8 µM). TFI was modeled only for the association kinetics due to the appearance of non-continuous changes to the TFI signal upon addition of the competitive ligand. The relative TFI axis was inverted for visualization purposes.

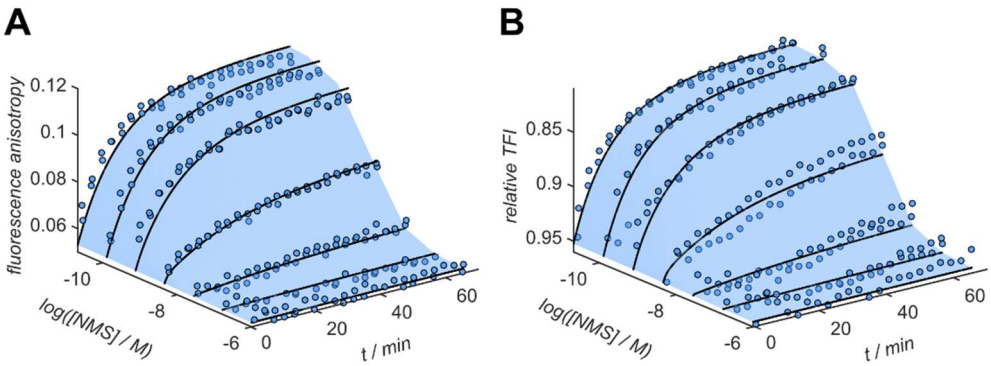

Figure A10: Time-dependent changes in FA (**A**) and relative TFI (**B**) in competition binding experiments with **3.1** (c = 1 nM) and NMS. The used volume of baculovirus stock was 10 µL. Graphs show results of one representative experiment from a set of three independent experiments performed in duplicate. The global fit using the single binding site model under consideration of the change in relative quantum yield is indicated by the light blue surface for both the change in FA (**A**) and relative TFI (**B**).

Model for the global analysis of FA binding experiments with **3.1**

The model, which should be used for the global kinetic modeling of FA experiments, must be defined by a set of differential equations, which describe the rates of concentration changes for all components present in the reaction. Additionally, the concentrations of the components (e.g. free fluorescent ligand, fluorescent ligand-receptor complex, non-specifically bound fluorescent ligand) must be linked with measurement parameters such as FA, TFI or both. Events, such as the initiation of the dissociation reaction, can be defined.

In the following section, the model used for the global analysis of the binding of **3.1** to the M_2R is given. It is composed of the following components:

R – free receptor; *L* – free fluorescent ligand; *C* – free competitive ligand
RL – fluorescent ligand-receptor complex; *RC* – competitive ligand-receptor complex
NBV – nonspecific binding sites on BBVs; *V* – added volume of BBVs
NBVL – nonspecific binding sites in complex with the fluorescent ligand

These components are involved in the following reversible chemical reactions:

R1 = *kf1**[*L*]*[*R*] – *kr1**[*RL*] , which describes the binding of the fluorescent ligand to the receptor. *kf1* represents the respective forward reaction rate constant and *kr1* the reverse reaction rate constant;

R2 = *kf2**[*C*]*[*R*]-*kr2**[*RC*] , which describes the binding of a competitive ligand to the receptor. *kf2* represents the respective forward reaction rate constant and *kr2* the reverse reaction rate constant.

R4 = *kf4**[*L*]*[*NBV*]-*kr4**[*NBVL*] , which describes the binding of the fluorescent ligand to nonspecific binding sites on BBVs. *kf4* represents the respective forward reaction rate constant and *kr4* the reverse reaction rate constant;

R5 = 1000**V* , which converts the volume of added baculovirus stock into the concentration of the receptor and non-specific binding sites. R5 is required for fitting R_{stock} (concentration of ligand-specific receptor binding sites in the stock solution) and NB_{stock} (concentration of non-specific binding sites (*NBV*) in the stock solution).

The differential equations describing the concentration changes within the system are defined as:

d[*C*]/dt = -R2

d[*L*]/dt = -R1-R4

d[*R*]/dt = -R1-R2+R5*R_{stock}

d[*RC*]/dt = R2

d[*RL*]/dt = R1

d[*NBV*]/dt = -R4+R5*NB_{stock}

d[*NBVL*]/dt = R4

d[*V*]/dt = -R5

In addition to the kinetic parameters, the following model parameters were used:

A_{free}	fluorescence anisotropy of the free fluorescent ligand
A_{RL}	fluorescence anisotropy of the fluorescent ligand-receptor complex (*RL*)
$A_{nonspecific}$	fluorescence anisotropy of the complex consisting of the fluorescent ligand bound to non-specific binding sites (*NBVL*)
R_{stock}	concentration of ligand-specific receptor binding sites (*R*) in the stock solution
NB_{stock}	concentration of non-specific binding sites (*NBV*) in the stock solution
QY_{RL}	relative quantum yield of the fluorescent ligand in the receptor-bound state (*RL*); the relative quantum yield of the free fluorescent ligand is considered to be equal to one.
QY_{NBVL}	relative quantum yield of the fluorescent ligand bound to non-specific binding sites (*NBVL*); the relative quantum yield of the free fluorescent ligand is considered to be equal to one.
Baseline	baseline of the fluorescence intensity level after time-dependent dulling of the fluorescent ligand
Dulling factor	monoexponential decay constant corresponding to the rate of time-dependent dulling of the fluorescent ligand

Screening parameter	specific screening parameter for total fluorescence intensity inside a particular well; should be fitted as a local parameter
TFI conversion factor	correlates total TFI to the used concentration of the fluorescent ligand; TFI value of 1 nM fluorescent ligand should be numerically equal to the TFI conversion factor.

The model also defines several variables, which relate the concentrations of the different binding states of the fluorescent ligand to the FA and TFI measurements.

$$\text{timefactor} = \textit{Baseline} + (1-\textit{Baseline})*e^{-\textit{Dulling factor}*\text{time}}$$

$$\text{TFI} = ([L]+[RL]*QY_{RL}+[NBVL]*QY_{NBVL})*\textit{TFI conversion factor}*\text{timefactor}*\textit{screening parameter}$$

$$\text{TFI}_{\text{relative}} = ([L]+[RL]*QY_{RL}+[NBVL]*QY_{NBVL})+10^{-9}$$

For the calculation of experimental $\text{TFI}_{\text{relative}}$ values, the following formula was used instead:

$$\text{TFI}_{\text{relative}} = \text{TFI}/(\textit{TFI conversion factor}*\text{timefactor}*\textit{screening parameter})$$

$$\text{FA} = ([L]*A_{free}+[RL]*A_{RL}*QY_{RL}+[NBVL]*A_{NBVL}*QY_{NBVL})/\text{TFI}_{\text{relative}}$$

Starting values of all parameters were defined in the Aparecium software before the global fitting and were set equal to the experimental conditions in the specific well.

Depending on the experimental design, different parameters can be accurately determined using this model. For example, FA saturation binding experiments allow the determination of *kf1* and *kr1* as well as A_{free}, A_{RL}, A_{NBVL}, QY_{RL} and QY_{NBVL}, whereas parameters that describe the competitive ligand, such as *kf2* and *kr2*, are not determined. In contrast, by applying the global model to FA competition binding experiments, *kf2* and *kr2* can be determined quite accurately. Therefore, only the parameters that can be determined from the particular experiment should remain without prior constraints during the fitting procedure.

For fitting FA saturation binding experiments, all model parameters were set free to take on different values, but only the ones that can be accurately determined were used for further analysis. The uncertainties were obtained by performing fit analysis (see Chapter 3).

The results from the global analysis of one representative FA saturation binding experiment with **3.1** at the M_2R are given in the following table:

parameter	value ± SD
pK_d	9.12 ± 0.04
Dulling factor	0.048 ± 0.024 min^{-1}
Baseline	0.88 ± 0.03
TFI conversion factor	27100 ± 900 nM^{-1}
QY_{NBVL}	0.36 ± 0.09
QY_{RL}	0.717 ± 0.006
NB_{stock}	5100 ± 1900 nM
R_{stock}	38.3 ± 1.8 nM
A_{free}	0.0343 ± 0.0001
A_{RL}	0.1580 ± 0.0014
A_{NBVL}	0.27 ± 0.09
kf1	0.0426 ± 0.0042 min^{-1} nM^{-1}
kr1	0.032 ± 0.001 min^{-1}
kf2	0.54 ± 0.18 min^{-1} nM^{-1}
kr2	16.2 ± 4.2 min^{-1}
kf4	9.6 ± 3.0 min^{-1} nM^{-1}

Similarly, a parameter estimation was performed for each FA competition binding experiment with **3.1**. The global fit of FA from a representative competition binding experiment with **3.1** and NMS is depicted in Figure 3.8 in Chapter 3 and the global fit of both FA and relative TFI is shown in Figure A10.

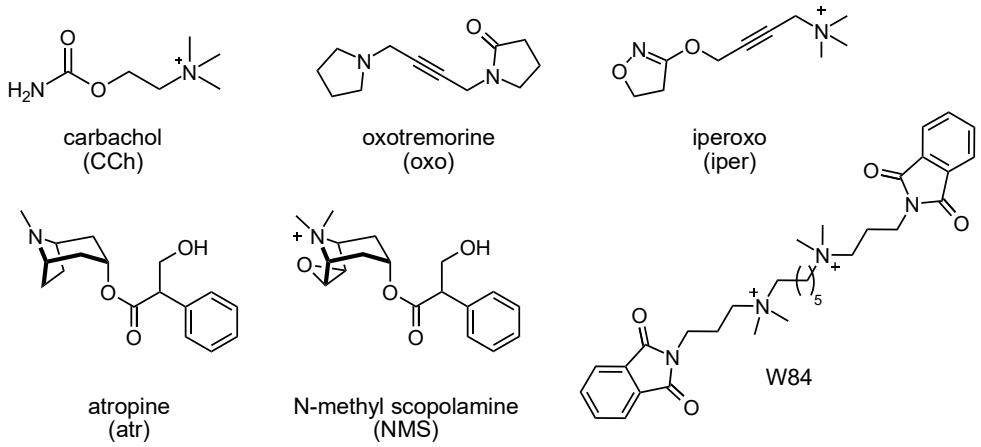

Figure A11: Structures of the orthosteric and allosteric unlabeled MR ligands used in Chapter 3.

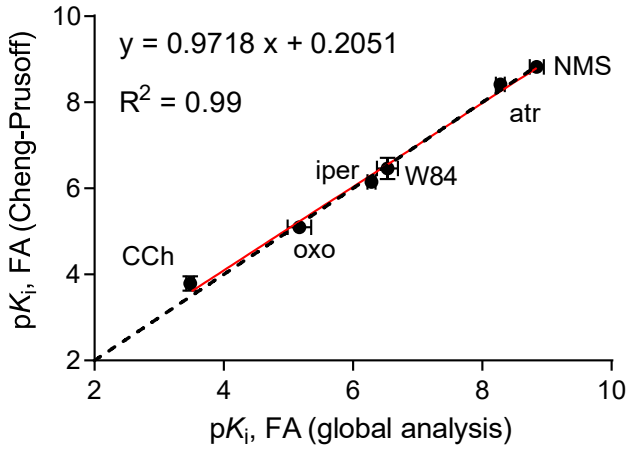

Figure A12: Correlation between pK_i values from FA competition binding experiments with **3.1** at the M_2R, obtained by the means of global analysis or the Cheng-Prusoff equation (without consideration of ligand depletion or the change of quantum yield upon binding of **3.1**).[5] The solid red line represents Deming regression, the dashed black line represents a perfect correlation. Error bars represent the SEM.

7.3 Appendix to Chapter 4

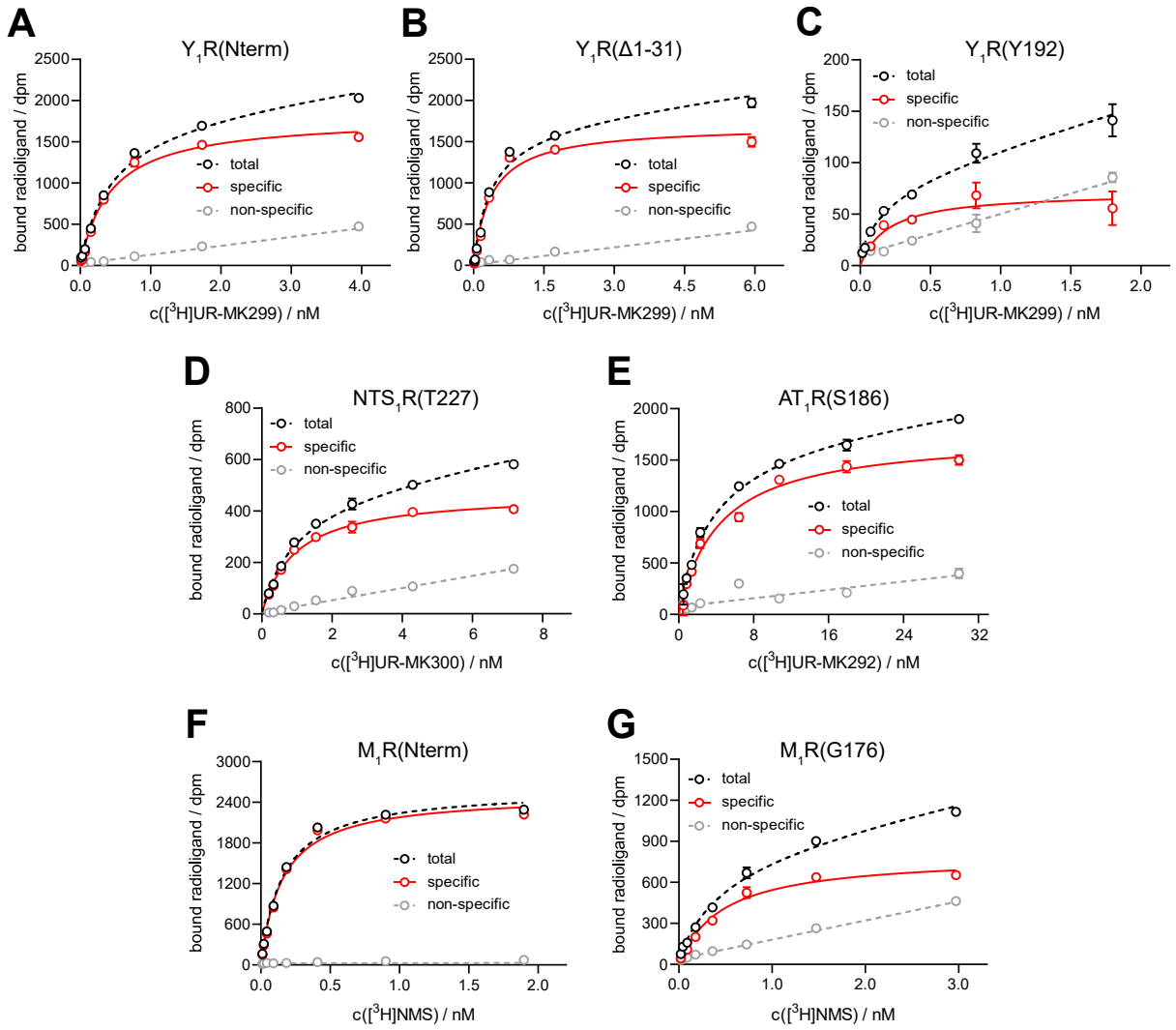

Figure A13: Binding isotherms from radioligand saturation binding experiments at intact, suspended HEK293T cells stably expressing the Y_1R(Nterm) (**A**), Y_1R(Δ1-31) (**B**), Y_1R(Y192) (**C**), NTS_1R(T227) (**D**), AT_1R(S186) (**E**), M_1R(Nterm) (**F**) or M_1R(G176) (**G**). [^{3}H]UR-MK299[6] (**A**-**C**), [^{3}H]UR-MK300[7] (**D**), [^{3}H]UR-MK292[7] (**E**) and [^{3}H]NMS (**F**, **G**) were used as radioligands. Non-specific binding was measured in the presence of an excess of BIBO3304 (**A**-**C**; 500-fold excess), NT(8-13) (**D**; 500-fold excess), angiotensin II (**E**, 500-fold excess) or atropine (**F**, **G**; 1000-fold excess). The excess always refers to the respective radioligand concentration. Data represent means (total and non-specific binding) or calculated values (specific binding) ± errors and are representative of three independent experiments, each performed in triplicate. Error bars of total and non-specific binding represent the SEM, whereas error bars of specific binding represent propagated errors. The corresponding pK_d values are listed in Table A1.

Table A1: Equilibrium dissociation constants (pK_d values) of the radioligands [^{3}H]UR-MK299, [^{3}H]UR-MK300, [^{3}H]UR-MK292 and [^{3}H]NMS from radioligand saturation binding experiments.

Radioligand	Receptor (construct)	pK_d	*N*
[^{3}H]UR-MK299	Y_1R(wild-type)	9.85[a], 10.36[a]	---
	Y_1R(Nterm)	9.28 ± 0.04[b]	3
	Y_1R(Δ1-31)	9.45 ± 0.01[b]	3
	Y_1R(Y192)	9.78 ± 0.08[b]	3
[^{3}H]UR-MK300	NTS_1R(wild-type)	9.24[c], 9.29[c]	---
	NTS_1R(T227)	8.81 ± 0.11[b]	3
[^{3}H]UR-MK292	AT_1R(wild-type)	9.03[c]	---
	AT_1R(S186)	8.30 ± 0.08[b]	3
[^{3}H]NMS	M_1R(wild-type)	9.77[d]	---
	M_1R(Nterm)	9.80 ± 0.01[b]	3
	M_1R(G176)	9.37 ± 0.13[b]	3

[a,c,d]Indicated pK_d values represent values from literature and were determined by radioligand saturation binding experiments at unmodified (wild-type) receptors. [a]Keller *et al.*[6] [b]Determined by radioligand saturation binding experiments at intact, suspended HEK293T cells stably expressing the respective construct. Data represent means ± SEM from *N* independent experiments, each performed in triplicate. [c]Keller *et al.*[7] [d]Gruber *et al.*[3].

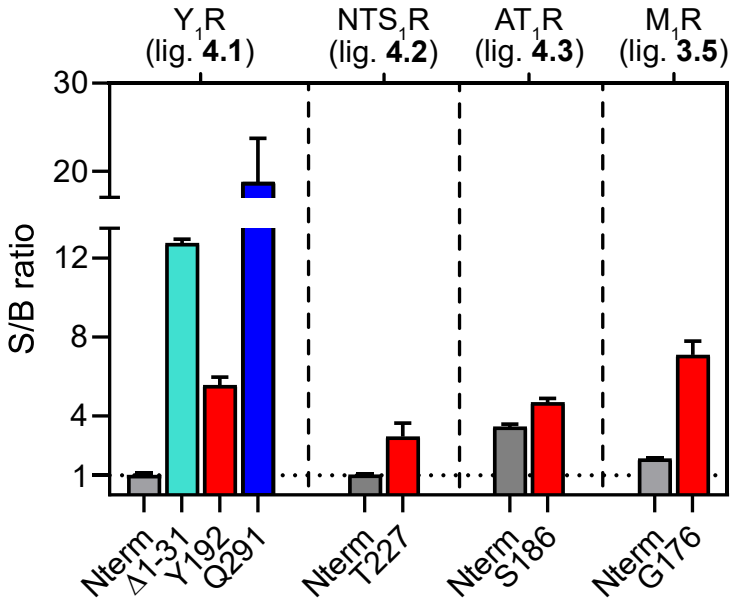

Figure A14: S/B ratios from BRET saturation binding experiments with **4.1** (Y_1R), **4.2** (NTS_1R), **4.3** (AT_1R) or **3.5** (M_1R) at HEK293T cells stably expressing the indicated receptor/NLuc fusion protein. S/B ratios were calculated by dividing the maximal BRET ratio (specific binding) by the BRET ratio of a solvent control. Data represent means ± SEM from three to five independent experiments, each performed in triplicate. The corresponding numerical values are listed in Table A2.

Table A2: S/B ratios from BRET saturation binding experiments with **4.1**, **4.2**, **4.3** or **3.5** at the indicated receptor construct, stably expressed in HEK293T cells. Shown values correspond to Figure A14. Data represent means ± SEM from *N* independent experiments, performed in triplicate.

Compound	Receptor construct	S/B ratio	*N*
4.1	Y_1R(Nterm)	1.03 ± 0.04	3
	Y_1R(Δ1-31)	12.77 ± 0.17	3
	Y_1R(Y192)	5.59 ± 0.38	4
	Y_1R(Q291)	18.81 ± 4.91	4
4.2	NTS_1R(Nterm)	1.06 ± 0.03	3
	NTS_1R(T227)	2.98 ± 0.66	4
4.3	AT_1R(Nterm)	3.48 ± 0.11	3
	AT_1R(S186)	4.71 ± 0.18	5
3.5	M_1R(Nterm)	1.87 ± 0.02	5
	M_1R(G176)	7.12 ± 0.66	4

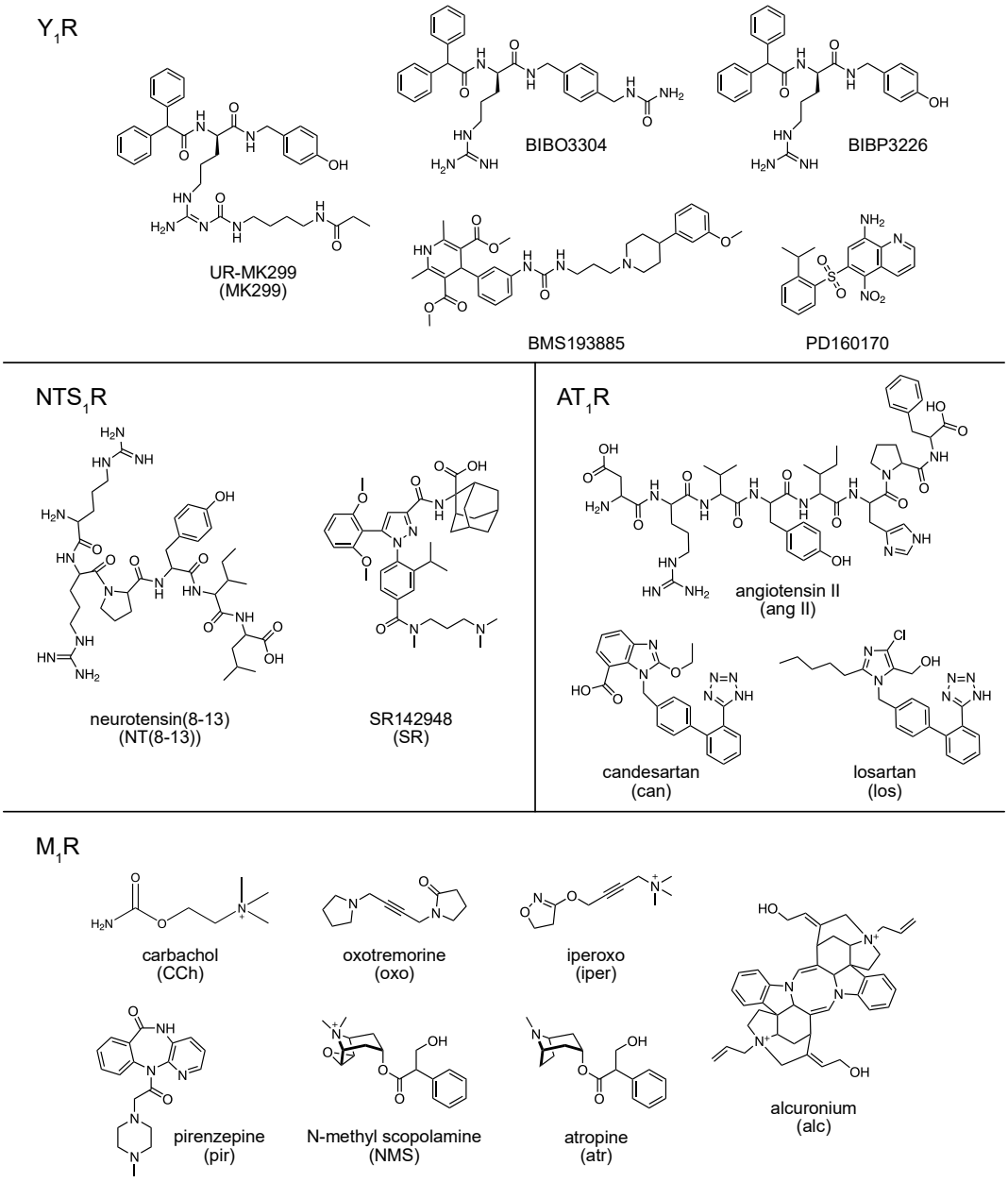

Figure A15: Structures of the competitive ligands used in Chapter 4.

Table A3: Binding data (pK_i values) of reported Y_1R antagonists from BRET competition binding experiments with **4.1** (c = 0.5 nM) at the Y_1R(Q291).

Compound	pK_i (BRET, Y_1R(Q291))[a]	*N*
UR-MK299	10.06 ± 0.07	3
BIBO3304	8.67 ± 0.23	3
BIBP3226	7.99 ± 0.10	3

[a]Determined by BRET competition binding experiments with **4.1** (c = 0.5 nM, K_d = 0.29 nM) at the Y_1R(Q291), stably expressed in HEK293T cells. Data represent means ± SEM from *N* independent experiments, each performed in triplicate.

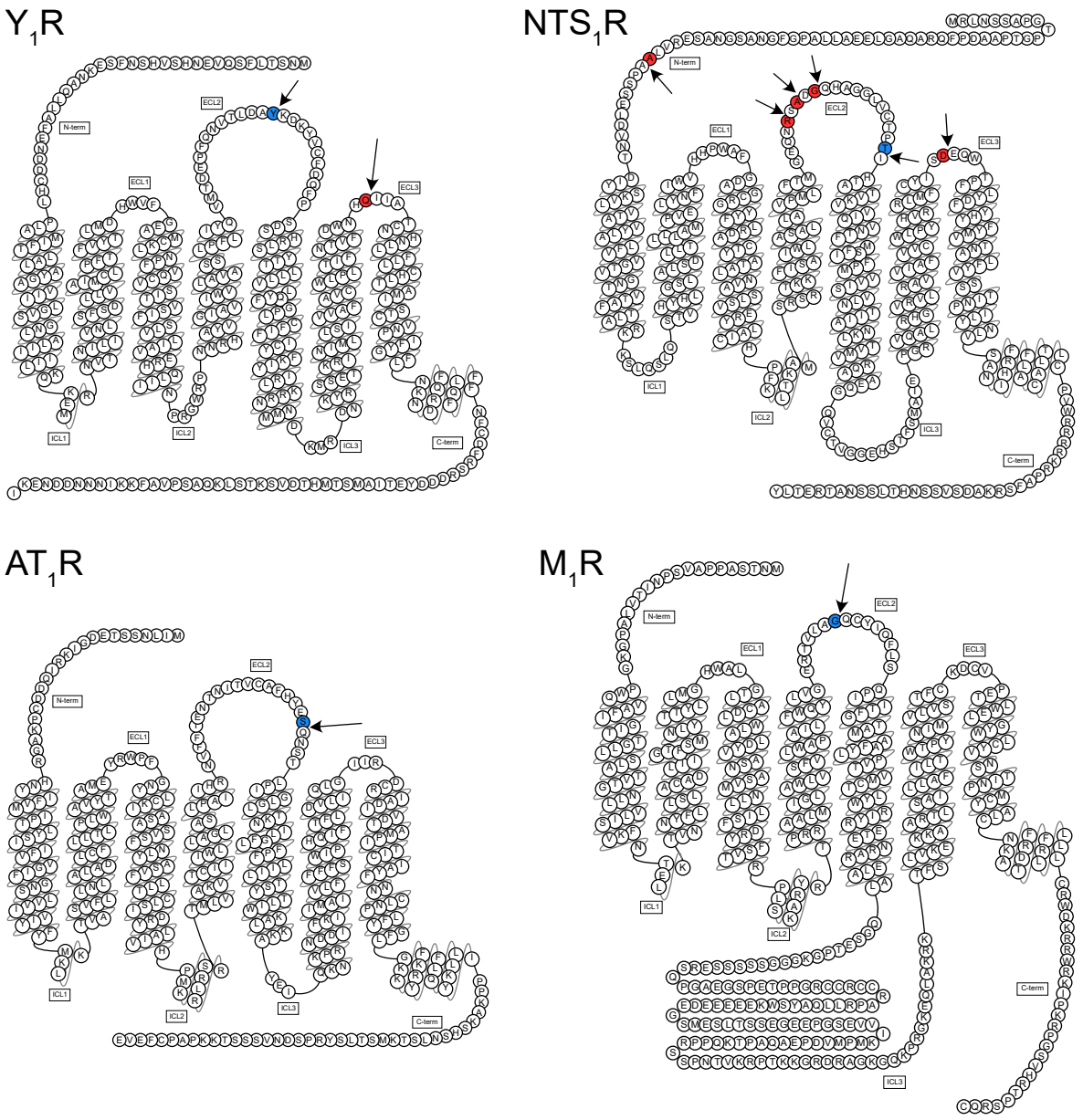

Figure A16: Snake plots illustrating the secondary structure of the Y_1R, NTS_1R, AT_1R and M_1R. Source files for the snake plots were obtained from GPCRdb.[8,9] Insertion of NLuc after the residues in blue yielded the receptor/NLuc fusion proteins, which resulted in working BRET binding assays (Y_1R(Y192), NTS_1R(T227), AT_1R(S186), M_1R(G176)). Constructs obtained by insertion of the luciferase after the red colored residues were omitted after an initial screening (see Figure 4.1 in Chapter 4 and Figure A17).

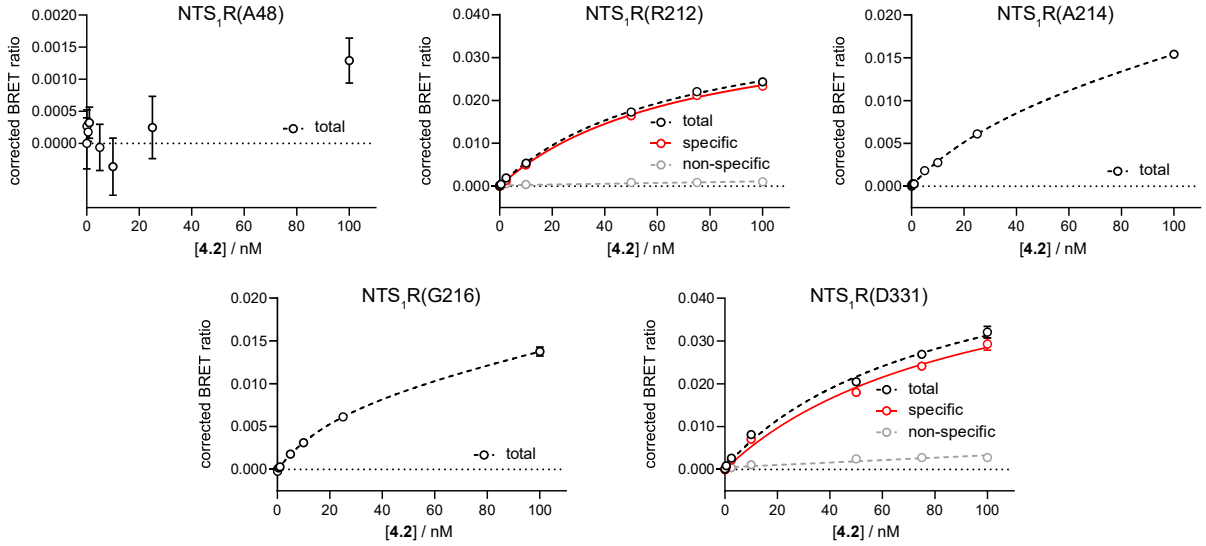

Figure A17: Exploration of other potential NLuc insertion sites at the NTS_1R. The insertion sites were located within the N-terminus (A48), the second extracellular loop (R212, A214, G216) or the third extracellular loop (D331) of the NTS_1R. For the NTS_1R(A48), the NTS_1R(A214) and the NTS_1R(G216), HEK293T cells were transiently transfected with 2 µg of cDNA encoding the respective receptor/NLuc fusion protein. After two days of incubation, the cells were seeded and total binding was assessed as described in Chapter 4 using the fluorescent NTS_1R ligand **4.2**. For the NTS_1R(R212) and the NTS_1R(D331), stable transfectants were generated and investigated in saturation binding experiments with **4.2** according to the procedures described in Chapter 4. Data are presented as means (total and non-specific binding) or calculated values (specific binding) ± errors of one representative experiment from a set of two to three independent experiments, each performed in triplicate. Error bars of total and non-specific binding represent the SEM, whereas error bars for specific binding represent propagated errors.

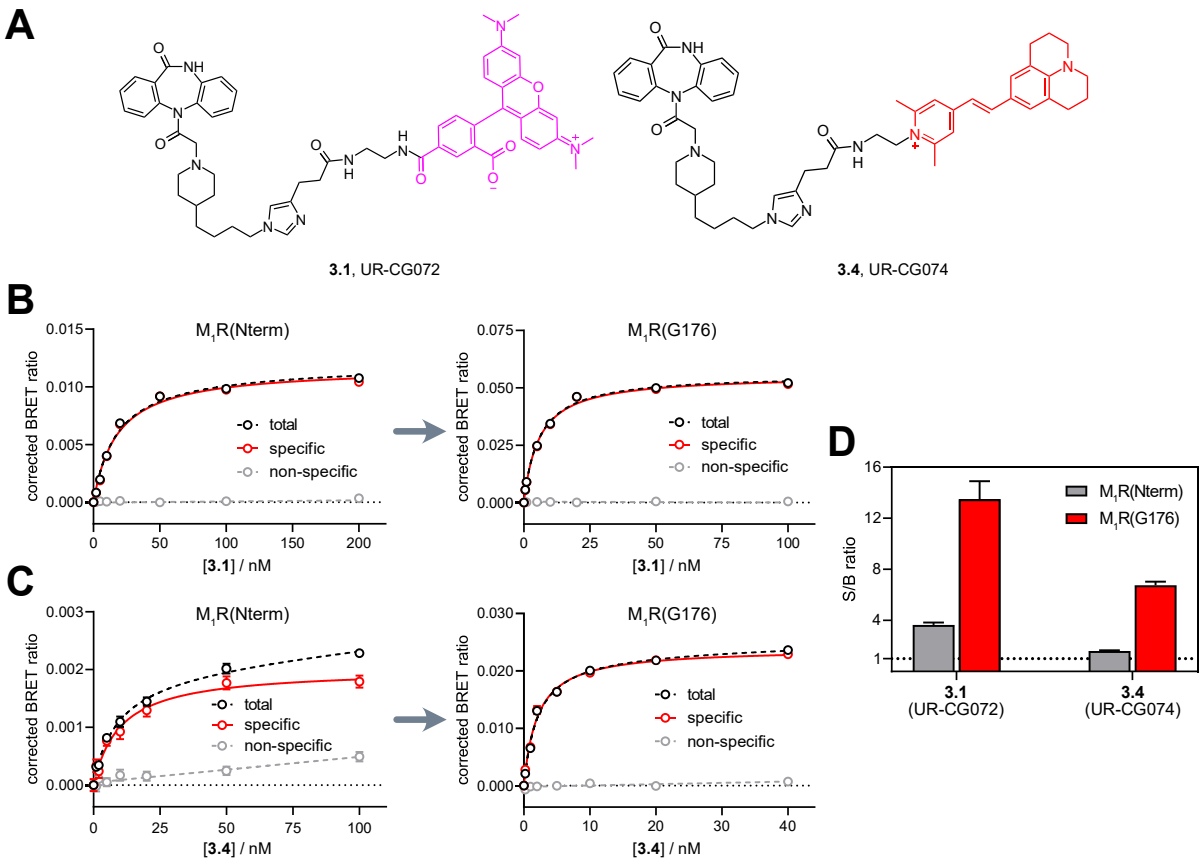

Figure A18: Characterization of the fluorescence-labeled MR ligands **3.1** and **3.4** in BRET binding experiments at the M_1R(Nterm) and the M_1R(G176). (**A**) Structures of the TAMRA-labeled MR ligand **3.1** (UR-CG072) and the Py-1-labeled MR ligand **3.4** (UR-CG074).[3] (**B**, **C**) Binding isotherms from BRET saturation binding experiments with **3.1** (**B**) and **3.4** (**C**) at the M_1R(Nterm) or the M_1R(G176), stably expressed in HEK293T cells. Non-specific binding was measured in the presence of a 500-fold excess of atropine (over the respective concentration of fluorescent ligand). Data represent means (total and non-specific binding) or calculated values (specific binding) ± errors of one representative experiment from a set of three independent experiments, each performed in triplicate. Error bars of total and non-specific binding represent the SEM, whereas error bars of specific binding represent propagated errors. Corresponding pK_d values are listed in Table A4. (**D**) S/B ratios from BRET saturation binding experiments with **3.1** and **3.4** at the M_1R(Nterm) (for **3.1**: 3.64 ± 0.19; for **3.4**: 1.60 ± 0.05) or the M_1R(G176) (for **3.1**: 13.51 ± 1.39; for **3.4**: 6.75 ± 0.28), stably expressed in HEK293T cells. Data represent means ± SEM from three independent experiments, performed in triplicate.

Table A4: Equilibrium dissociation constants (pK_d values) of the fluorescent ligands **3.1** and **3.4** from BRET saturation binding experiments at the M_1R(Nterm) and the M_1R(G176).

Compound	pK_d (BRET, M_1R(Nterm))[a]	*N*	pK_d (BRET, M_1R(G176))[a]	*N*	pK_i (radioligand comp. binding)[b]
3.1	7.68 ± 0.04	3	8.22 ± 0.03	3	8.21
3.4	8.04 ± 0.04	3	8.60 ± 0.06	3	8.15

[a]Determined by BRET saturation binding experiments at HEK293T cells, stably expressing the M_1R(Nterm) or the M_1R(G176). Data are given as means ± SEM from *N* independent experiments, each performed in triplicate. [b]Gruber *et al.*[3].

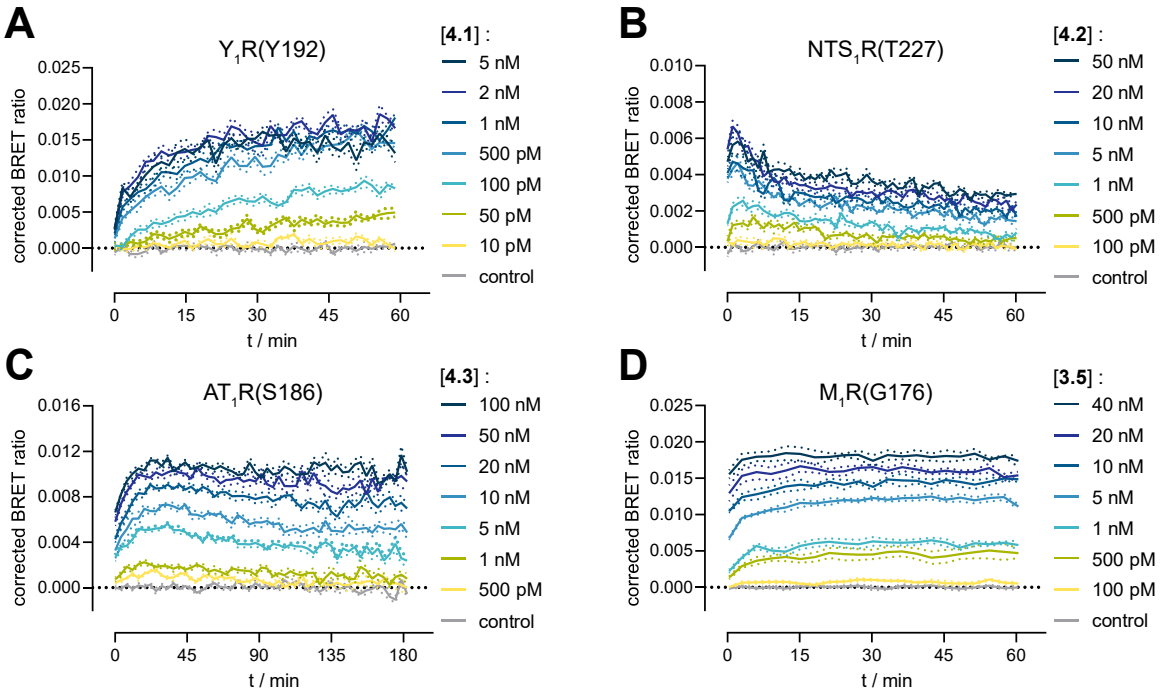

Figure A19: Kinetic traces of the specific binding of the fluorescent ligands **4.1** (Y_1R(Y192), **A**), **4.2** (NTS_1R(T227), **B**), **4.3** (AT_1R(S186), **C**) and **3.5** (M_1R(G176), **D**) obtained from (kinetic) BRET saturation binding experiments at intact HEK293T cells stably expressing the respective construct. The fluorescent ligands were added at the timepoint t = 0 min. Shown data represent calculated values ± propagated errors of a representative experiment from a set of at least three independent experiments, performed in triplicate.

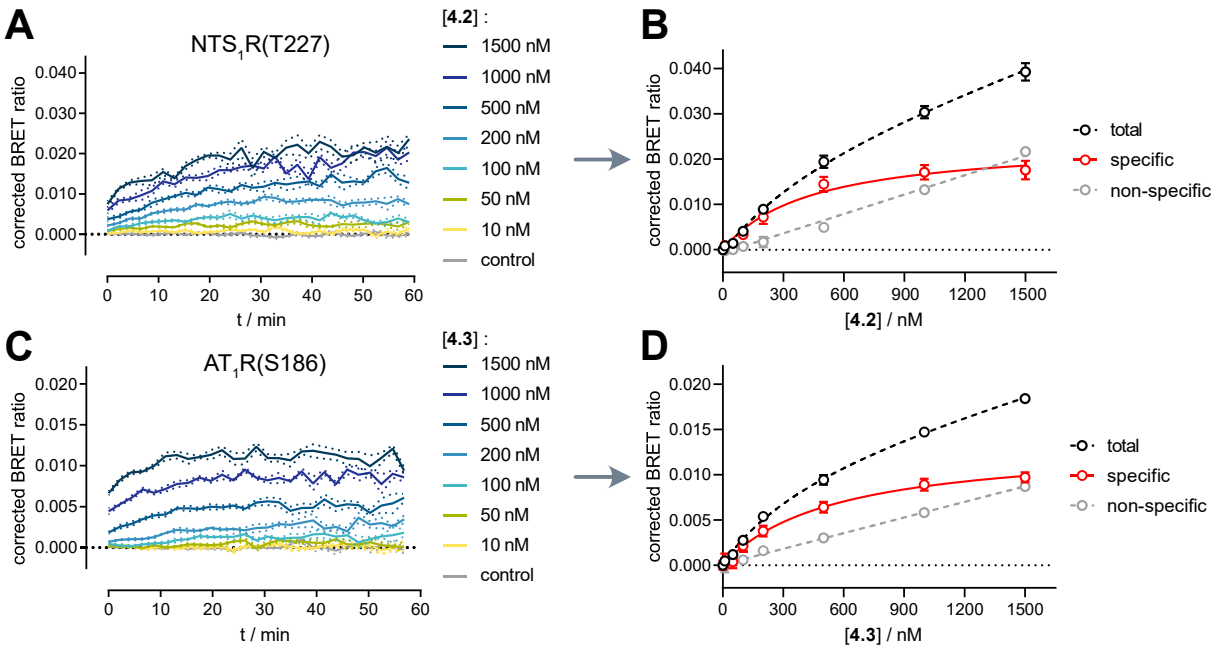

Figure A20: Saturation binding experiments with **4.2** or **4.3** at cell homogenates of HEK293T cells stably expressing the NTS_1R(T227) (**A**, **B**) or the AT_1R(S186) (**C**, **D**). (**A**, **C**) Kinetic traces of the specific binding of **4.2** to the NTS_1R(T227) (**A**) or **4.3** to the AT_1R(S186) (**C**) obtained from BRET saturation binding experiments at cell homogenates of HEK293T cells stably expressing the respective receptor/NLuc fusion protein. The fluorescent ligands **4.2** or **4.3** were added at the timepoint t = 0 min. Data are shown as calculated values ± propagated errors and are representative of two independent experiments, each performed in triplicate. (**B**, **D**) Binding isotherms of **4.2** (**B**) and **4.3** (**D**) corresponding to the kinetic traces in **A** and **C**. Shown data represent values after the last measurement point. Data are presented as means (total and non-specific binding) or calculated values (specific binding) ± errors of one representative experiment from a set of two independent experiments, each performed in triplicate. Error bars of total and non-specific binding represent the SEM. Error bars of specific binding represent propagated errors. Corresponding pK_d values are listed in Table A5.

Table A5: Equilibrium dissociation constants (pK_d values) of **4.2** and **4.3** obtained from BRET saturation binding experiments at cell homogenates of HEK293T cells expressing the NTS_1R(T227) or the AT_1R(S186).

Receptor construct	Compound	pK_d (cell homogenates)[a]	*N*	pK_d (intact cells)[b]	*N*
NTS_1R(T227)	**4.2**	6.24 ± 0.12	2	8.32 ± 0.08	4
AT_1R(S186)	**4.3**	6.17 ± 0.10	2	8.04 ± 0.08	5

[a]Determined by BRET saturation binding experiments at cell homogenates of HEK293T cells stably expressing the NTS_1R(T227) (for ligand **4.2**) or the AT_1R(S186) (for ligand **4.3**). Data represent means ± SEM from *N* independent experiments performed in triplicate. [b]Determined by BRET saturation binding experiments at intact HEK293T cells stably expressing the NTS_1R(T227) (for ligand **4.2**) or the AT_1R(S186) (for ligand **4.3**); values were taken from Table 4.3 in Chapter 4. Data are given as means ± SEM from *N* independent experiments performed in triplicate.

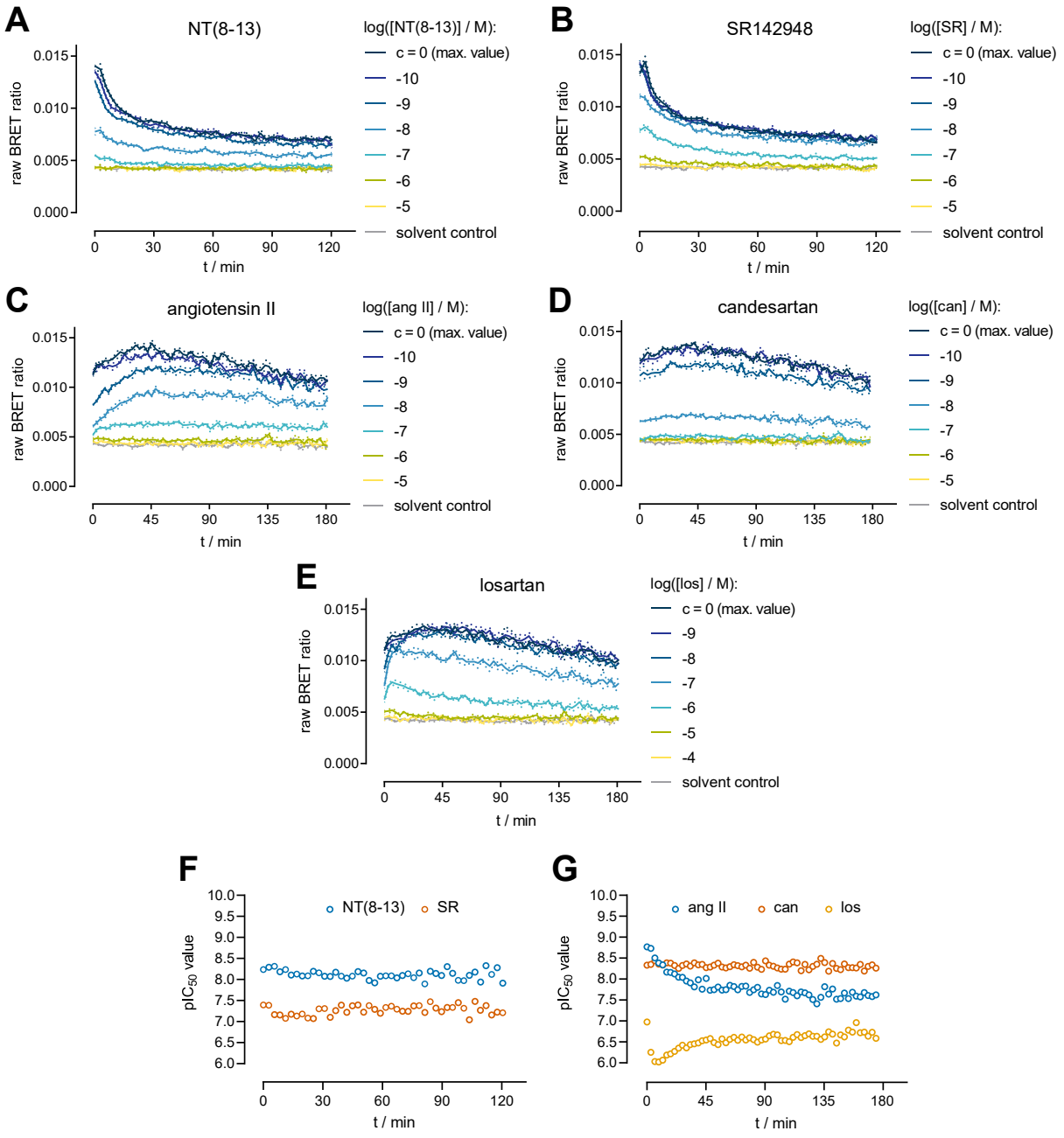

Figure A21: Kinetic traces from BRET competition binding experiments at the NTS_1R(T227) (**A**, **B**) or the AT_1R(S186) (**C**-**E**), stably expressed in HEK293T cells. **A** and **B** show exemplary kinetic competition binding experiments with the fluorescent ligand **4.2** (c = 5 nM) and NT(8-13) (**A**) or SR142948 (**B**) at the NTS_1R(T227). **C**-**E** show exemplary kinetic competition binding experiments with the fluorescent ligand **4.3** (c = 10 nM) and angiotensin II (**C**), candesartan (**D**) or losartan (**E**) at the AT_1R(S186). A solvent control (0% value) and a positive control (100% value, containing the fluorescent ligand **4.2** (**A**, **B**) or **4.3** (**C**-**E**) in the above-mentioned concentration but no competitor) were included in every experiment. The fluorescent ligands **4.2** (**A**, **B**) or **4.3** (**C**-**E**) were added at the timepoint t = 0 min. Data are presented as means ± SEM and are representative of at least two independent experiments performed in triplicate. (**F**, **G**) Time-dependent change of the pIC_{50} values for the investigated NTS_1R (**F**) and AT_1R (**G**) ligands determined after each plate read. Shown data are derived from the kinetic BRET competition binding experiments shown in **A**-**E**.

7.4 Appendix to Chapter 5

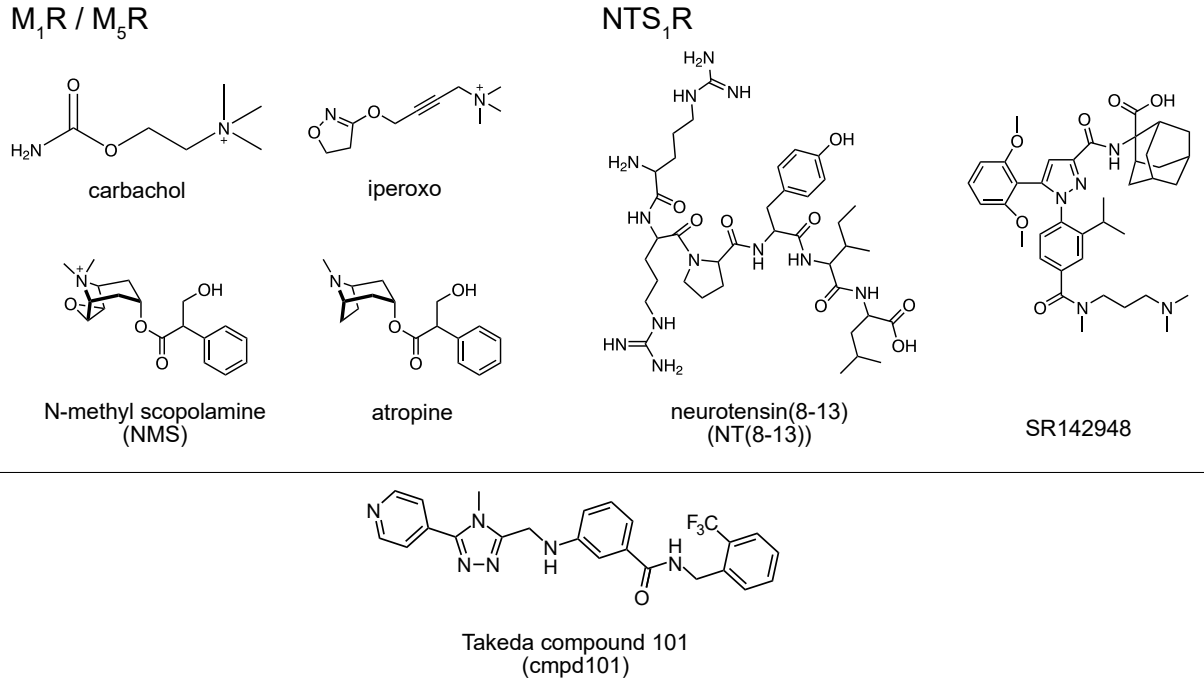

Figure A22. Structures of the compounds analyzed in Chapter 5.

7.5 Abbreviations

460/35BP	460 ± 35 nm band-pass filter
460/50BP	460 ± 50 nm band-pass filter
5-HT_{3A}	subunit A of the 5-hydroxytryptamin (serotonin) receptor type 3
610LP	610 nm long-pass filter
alc	alcuronium
AMP	adenosine monophosphate
ang II	angiotensin II
approx.	approximately
Asp	aspartate
AT_1R	angiotensin II receptor type 1
AT_1R(Nterm)	AT_1 receptor with NLuc fused to its N-terminus
AT_1R(S186)	AT_1 receptor with NLuc introduced after the serine in position 186 (ECL2)
ATP	adenosine triphosphate
atr	atropine
AUC	area under the curve
BBV	budded baculovirus
B_{max}	maximum number of binding sites
BRET	bioluminescence resonance energy transfer
BSA	bovine serum albumin
BY630/650	BODIPY 630/650 (fluorescent dye)
c	concentration
cAMP	3',5'-cyclic adenosine monophosphate
can	candesartan
CBG/CBR	engineered green/red click beetle luciferase from *Pyrophorus plagiophthalamus* (Germar, 1841)
CCh	carbachol
cDNA	complementary DNA (desoxyribonucleic acid)
c_{final}	final assay concentration
CHO	Chinese hamster ovary cells
Ci	Curie
CLuc	luciferase from *Cypridina noctiluca* (Kajiyama 1912)

cmpd101	Takeda compound 101
CNS	central nervous system
comp. binding	competition binding
cpm	counts per minute
Da	Dalton
DIBA	dibenzodiazepinone
DMEM	Dulbecco's Modified Eagle's Medium
DMSO	dimethyl sulfoxide
D_xR	dopamine receptor, x denotes the respective subtypes 1-5
D-PBS	Dulbecco's phosphate-buffered saline
dpm	disintegrations per minute
DTT	dithiothreitol
EC_{50}	concentration of an agonist that induces 50% of its maximal response
ECL	extracellular loop
EDTA	ethylenediaminetetraacetic acid
ELuc	engineered "emerald luciferase" from the click beetle *Pyrearinus termitilluminans* (Costa, 1982)
ELucN-ARRB2	fusion protein consisting of β-arrestin2 N-terminally fused to the N-terminal fragment of ELuc
E_{max}	maximal response of a compound in a functional assay
ERK	extracellular signal-regulated kinase
FA	fluorescence anisotropy
FCS	fetal calf serum
FLuc	firefly luciferase from *Photinus pyralis* (Linneaus, 1767)
FRET	Förster resonance energy transfer
G418	geneticin
$G\alpha_q$ or $G\alpha_{16}$	G alpha subunit q or 16
GDP	guanosine diphosphate
GF/C	glass microfiber, grade C (fine)
GFP	green fluorescent protein
GLuc	luciferase from *Gaussia princeps* (Scott, 1894)
Gln	glutamine
Gly	glycine

GPCR	G protein-coupled receptor
GRK	G protein-coupled receptor kinase
GRK2-NLucN	fusion protein consisting of GRK2 C-terminally fused to NLucN
$Gs\alpha_s$	G alpha subunit s, short isoform
GTP	guanosine triphosphate
h	hour(s)
HEK293T	human embryonic kidney cells
HEPES	2-[4-(2-hydroxyethyl)-1-piperazin-1-yl]ethanesulfonic acid
(h)H_xR	(human) histamine receptor; x denotes the respective subtypes 1-4
H_2R-ELucC	fusion protein consisting of the human histamine H_2 receptor C-terminally fused to the C-terminal fragment of ELuc
hH_2R-$Gs\alpha_s$	fusion protein consisting of the human histamine H_2 receptor and the short isoform of the $G\alpha_s$ subunit
IC_{50}	(a) inhibitor concentration, which displaces 50% of a labeled compound from the binding site (b) antagonist concentration, which suppresses 50% of an agonist induced response
ICL	intracellular loop
iper	iperoxo
K_b	equilibrium dissociation constant of a ligand determined in a functional assay
$K_d^{(equilibrium)}$	equilibrium dissociation constant determined in saturation binding experiments
K_d^{global}	equilibrium dissociation constant obtained by global analyis
$K_d^{kinetic}$	kinetically derived equilibrium dissociation constant
K_i	equilibrium dissociation constant of a ligand determined in competition binding experiments
k_{obs}	observed association rate constant
k_{off}	dissociation rate constant
k_{on}	association rate constant
λ_{max}	maximal emission wavelength (bioluminescence)
L	liter
L-15	Leibovitz' L-15 medium
los	losartan
M	molar (mol/L)

M_1R(G176)	M_1 muscarinic acetylcholine receptor with NLuc introduced after the glycine in position 176
M_1R-NLucC	M_1 muscarinic acetylcholine receptor C-terminally fused to the NLucC fragment
M_1R(Nterm)	M_1 muscarinic acetylcholine receptor with NLuc fused to its N-terminus
M_5R-NLucC	M_5 muscarinic acetylcholine receptor C-terminally fused to the NLucC fragment
MAP	mitogen-activated protein
max.	maximal
MCF-7	human breast adenocarcinoma cell line
min	minute(s)
MOI	multiplicity of infection
mol	mole(s)
mRNA	messenger RNA (ribonucleic acid)
M_xR	muscarinic acetylcholine receptor, x denotes the respective subtypes 1-5
NanoBiT®	NanoLuc® Binary Technology
NLuc	NanoLuc® luciferase
NLucC	C-terminal, smaller NLuc fragment (11 amino acids)
NLuc-H_2R	human H_2 receptor with NLuc fused to its N-terminus
NLuc-M_2R	M_2 receptor with NLuc fused to its N-terminus
NLucN	N-terminal, larger NLuc-fragment (159 amino acids)
NMS	N-methyl scopolamine
NT(8-13)	neurotensin (8-13)
NTS_1R	neurotensin receptor 1
NTS_1R(A48)	NTS_1 receptor with NLuc introduced after the alanine in position 48
NTS_1R(A214)	NTS_1 receptor with NLuc introduced after the alanine in position 214
NTS_1R(D331)	NTS_1 receptor with NLuc introduced after the aspartate in position 331
NTS_1R(G216)	NTS_1 receptor with NLuc introduced after the glycine in position 216
NTS_1R-NLucC	NTS_1 receptor C-terminally fused to the NLucC fragment
NTS_1R(Nterm)	NTS_1 receptor with NLuc fused to its N-terminus
NTS_1R(R212)	NTS_1 receptor with NLuc introduced after the arginine in position 212
NTS_1R(T227)	NTS_1 receptor with NLuc introduced after the threonine in position 227
oxo	oxotremorine

PBS	phosphate-buffered saline
PCR	polymerase chain reaction
pir	pirenzepine
PLC-β	phospholipase C-β
(p)NPY	(porcine) neuropeptide Y
PP_i	pyrophosphate
PPI	protein-protein interaction
r	distance
R^2	squared Pearson correlation coefficient
RET	resonance energy transfer
RLuc	luciferase from the sea pansy *Renilla reniformis* (Pallas, 1766)
RLuc8	RLuc mutant with increased light output and serum stability
RLuc8.6-535	RLuc8 mutant with green emission maximum
rpm	revolutions per minute
rt	room temperature
R_{stock}	concentration of ligand-specific receptor binding sites
s	second(s)
S/B ratio	signal-to-background ratio
SD	standard deviation
SEM	standard error of the mean
Ser	serine
Sf9	insect cell line from *Spopoptera frugiperda* (Smith, 1797)
SK-N-MC	human neuroblastoma cell line
solv.	solvent control
SR	SR142948
t	time
TFI	total fluorescence intensity
Thr	threonine
TR-FRET	time-resolved Förster resonance energy transfer
Tris	2-amino-2-(hydroxymethyl)propane-1,3-diol
Tyr	tyrosine
VEGFR2	vascular endothelial growth factor receptor 2

V	volume
$V(BBV_{stock})$	volume of the baculovirus stock suspension
v/v	volume per volume
Y_1R	neuropeptide Y Y_1 receptor
$Y_1R(\Delta 1\text{-}31)$	truncated Y_1 receptor, which lacks the first 31 amino acids, and has NLuc fused to the aspartate in position 32
Y_1R(Nterm)	Y_1 receptor with NLuc fused to its N-terminus
Y_1R(Y192)	Y_1 receptor with NLuc introduced after the tyrosine in position 192
Y_1R(Q291)	Y_1 receptor with NLuc introduced after the glutamine in position 291
YFP	yellow fluorescent protein

7.6 References

1. Baumeister, P., Erdmann, D., Biselli, S., Kagermeier, N., Elz, S., Bernhardt, G. & Buschauer, A. [^{3}H]UR-DE257: development of a tritium-labeled squaramide-type selective histamine H_2 receptor antagonist. *ChemMedChem* **10**, 83-93, doi:10.1002/cmdc.201402344 (2015).

2. She, X., Pegoli, A., Gruber, C. G., Wifling, D., Carpenter, J., Hübner, H., Chen, M., Wan, J., Bernhardt, G., Gmeiner, P., Holliday, N. D. & Keller, M. Red-emitting dibenzodiazepinone derivatives as fluorescent dualsteric probes for the muscarinic acetylcholine M_2 receptor. *J. Med. Chem.* **63**, 4133-4154, doi:10.1021/acs.jmedchem.9b02172 (2020).

3. Gruber, C. G., Pegoli, A., Müller, C., Grätz, L., She, X. & Keller, M. Differently fluorescence-labelled dibenzodiazepinone-type muscarinic acetylcholine receptor ligands with high M_2R affinity. *RSC Med. Chem.* **11**, 823-832, doi:10.1039/d0md00137f (2020).

4. Bartole, E., Grätz, L., Littmann, T., Wifling, D., Seibel, U., Buschauer, A. & Bernhardt, G. UR-DEBa242: a Py-5-labeled fluorescent multipurpose probe for investigations on the histamine H_3 and H_4 receptors. *J. Med. Chem.* **63**, 5297-5311, doi:10.1021/acs.jmedchem.0c00160 (2020).

5. Cheng, Y. & Prusoff, W. H. Relationship between the inhibition constant (K_I) and the concentration of inhibitor which causes 50 per cent inhibition (I_{50}) of an enzymatic reaction. *Biochem. Pharmacol.* **22**, 3099-3108, doi:10.1016/0006-2952(73)90196-2 (1973).

6. Keller, M., Weiss, S., Hutzler, C., Kuhn, K. K., Mollereau, C., Dukorn, S., Schindler, L., Bernhardt, G., König, B. & Buschauer, A. N$^{\omega}$-Carbamoylation of the argininamide moiety: an avenue to insurmountable NPY Y_1 receptor antagonists and a radiolabeled selective high-affinity molecular tool ([^{3}H]UR-MK299) with extended residence time. *J. Med. Chem.* **58**, 8834-8849, doi:10.1021/acs.jmedchem.5b00925 (2015).

7. Keller, M., Kuhn, K. K., Einsiedel, J., Hübner, H., Biselli, S., Mollereau, C., Wifling, D., Svobodová, J., Bernhardt, G., Cabrele, C., Vanderheyden, P. M. L., Gmeiner, P. & Buschauer, A. Mimicking of arginine by functionalized *N*$^{\omega}$-carbamoylated arginine as a new broadly applicable approach to labeled bioactive peptides: high affinity angiotensin, neuropeptide Y, neuropeptide FF, and neurotensin receptor ligands as examples. *J. Med. Chem.* **59**, 1925-1945, doi:10.1021/acs.jmedchem.5b01495 (2016).

8. Isberg, V., Mordalski, S., Munk, C., Rataj, K., Harpsøe, K., Hauser, A. S., Vroling, B., Bojarski, A. J., Vriend, G. & Gloriam, D. E. GPCRdb: an information system for G protein-coupled receptors. *Nucleic Acids Res.* **44**, D356-D364, doi:10.1093/nar/gkv1178 (2015).

9. Pándy-Szekeres, G., Munk, C., Tsonkov, T. M., Mordalski, S., Harpsøe, K., Hauser, A. S., Bojarski, A. J. & Gloriam, D. E. GPCRdb in 2018: adding GPCR structure models and ligands. *Nucleic Acids Res.* **46**, D440-D446, doi:10.1093/nar/gkx1109 (2017).

Ich erkläre hiermit an Eides statt, dass ich die vorliegende Arbeit ohne unzulässige Hilfe Dritter und ohne Benutzung anderer als der angegebenen Hilfsmittel angefertigt habe; die aus anderen Quellen direkt oder indirekt übernommenen Daten und Konzepte sind unter Angabe des Literaturzitats gekennzeichnet.

Teile der experimentellen Arbeiten wurden in Zusammenarbeit mit anderen Institutionen und Personen durchgeführt. Entsprechende Vermerke zu den Beiträgen der betreffenden Personen finden sich jeweils zu Beginn des entsprechenden Kapitels und unter „Acknowledgments“.

Weitere Personen waren an der inhaltlich-materiellen Herstellung der vorliegenden Arbeit nicht beteiligt. Insbesondere habe ich hierfür nicht die entgeltliche Hilfe eines Promotionsberaters oder anderer Personen in Anspruch genommen. Niemand hat von mir weder unmittelbar noch mittelbar geldwerte Leistungen für Arbeiten erhalten, die im Zusammenhang mit dem Inhalt der vorgelegten Dissertation stehen.

Die vorliegende Arbeit wurde bisher weder im In- noch im Ausland in gleicher oder ähnlicher Form einer anderen Prüfungsbehörde vorgelegt.

Regensburg, den _____

Lukas Grätz